INVESTIGATION OF THE WOOD/ PHENOL-FORMALDEHYDE ADHESIVE INTERPHASE MORPHOLOGY

By

Marie-Pierre G. Laborie

A Dissertation Submitted to the Faculty of Virginia Polytechnic Institute
and State University
in partial fulfillment of the requirements for the degree of

DOCTOR OF PHILOSOPHY
in
Wood Science and Forest Products

Approved by:

Charles E. Frazier, Chairman
Wolfgang G. Glasser
Frederick A. Kamke
Eva Marand
Thomas C. Ward
Alan Esker

February 1, 2002
Blacksburg, Virginia

Keywords: Wood /Adhesive Interphase, Glass transition, Cooperativity Analysis, Solid -State NMR

Copyright 2002, Marie-Pierre G. Laborie

INVESTIGATION OF THE WOOD/ PHENOL-FORMALDEHYDE INTERPHASE MORPHOLOGY

by

Marie-Pierre G. Laborie

C.E. Frazier, Chairman

Wood Science and Forest Products

ABSTRACT

This work addresses the morphology of the wood/ Phenol–Formaldehyde (PF) adhesive interphase using yellow-poplar. In this case, morphology refers to the scale or dimension of adhesive penetration into wood. The objective is to develop methods for revealing ever smaller levels of wood/resin morphology. Dynamic techniques that are commonly utilized in polymer blend studies are investigated as potential methods for probing the wood/ adhesive interphase morphology. These are Dynamic Mechanical Analysis (DMA) and solid state NMR using CP/MAS. PF resin molecular weight is manipulated to promote or inhibit resin penetration in wood, using a very low or a very high molecular weight PF resin.

With DMA, the influence of PF resin on wood softening is investigated. It is first demonstrated that the cooperativity analysis according to the Ngai coupling model of relaxation successfully applies to the *in-situ* lignin glass transition of yellow-poplar and spruce woods. No significant difference in intermolecular coupling is detected between the two woods.

It is then demonstrated that combining simple DMA measurements with the cooperativity analysis yields ample sensitivity to the interphase morphology. From simple DMA temperature scans, a low molecular weight PF (PF-Low) does not influence lignin glass transition temperature. However, the Ngai coupling model of relaxation indicates that intermolecular coupling is enhanced with the low molecular weight PF. This behavior is ascribed to the low molecular weight PF penetrating lignin on a nanometer scale and polymerizing in-situ.

On the other hand, a high molecular weight resin with a broad distribution of olecular weights (PF-High) lowers lignin glass transition temperature dramatically. This plasticizing effect is ascribed to a small fraction of the PF resin being low enough in molecular weight to penetrate lignin on a nanoscale, but being too dispersed for forming a crosslinked network.

With CP/MAS NMR, intermolecular cross-polarization experiments are found unsuitable to probe the angstrom scale morphology of the wood adhesive interphase. However, observing the influence of the PF resins on the spin lattice relaxation time in the rotating frame, $^{H}T_{1\rho}$, and the cross-polarization time (T_{CH}) is useful for probing the interphase morphology. None of the resins significantly affects the cross-polarization time, suggesting that angstrom scale penetration does not occur with a low nor a high molecular weight PF resin. However, the low molecular weight PF substantially modifies wood polymer $^{H}T_{1\rho}$, indicating that the nanometer scale environment of wood polymers is altered. On the other hand, the high molecular weight PF resin has no effect on wood $^{H}T_{1\rho}$. On average, the high molecular weight PF does not penetrate wood on a nanometer scale. Interestingly, the low molecular weight PF resin disrupts the spin coupling that is typical among wood components. Spin coupling between wood components is insensitive to the high molecular weight PF. Finally, it is noteworthy that the two PF resins have significantly different $T_{1\rho}$'s *in-situ.* The low molecular weight resin $T_{1\rho}$ lies within the range of wood relaxations, suggesting some degree of spin coupling. On the other hand, the $T_{1\rho}$ of the high molecular weight PF appears outside the range of wood relaxations. Spin coupling between the high molecular weight resin and wood components is therefore inefficient.

The CP/MAS NMR and DMA studies converge to identify nanometer scale penetration of the low molecular weight PF in wood. On the other hand, the high molecular weight PF resin forms separate domains from wood, although a very small fraction of the PF-High is able to penetrate wood polymers on a nanoscale.

Il faut bien quel qu'en soit le prix,
faire un peu de musique
avec cette vie unique.

Nicolas Bouvier

A ma mère,
Modèle d'un certain grain de folie,

A mon père,
Modèle du plus fort, du plus beau et surtout du plus intelligent,

A mes soeurs,
Modèles chacunes à leur façon,

ACKNOWLEDGEMENTS

When one starts a Ph.D., one has little appreciation of the road to follow. However, never can one find and follow its road without the guidance and support of teachers, colleagues and friends. I would like to spend some time thanking the teachers colleagues and friends that have been on my road and have helped me walk to its end.

Dr. Charles Frazier, my advisor and committee chair, has provided me with the scientific guidance and encouragement to find my personal interest in research. These five years of work in his group have been an astonishing experience. There have been the most fulfilling and thrilling hours of my student career but also some of the darkest hours. I am especially thankful of his patience and trust during the completion of part of this research on the other side of the Atlantic.

I would like to express my gratitude to my committee members, Dr. Wolfgang Glasser, Dr. Frederick Kamke, Dr. Eva Marand and Dr. Thomas Ward for assisting me and sharing their knowledge and enthusiasm in many occasions during the course of this work. I am especially indebted to Dr. Wolfgang Glasser for introducing me to Dr. Lennart Salmén. Without his kind support, the viscoelastic research presented in this dissertation may not have seen the day. Dr. Alan Esker has agreed to serve on my committee in several occasions. I am thankful for his time and constructive insight on my work.

The viscoelastic studies presented in this dissertation have been performed at the Swedish Research Institute for Pulp and Paper (STFI) in Stockholm. I am indebted to Dr. Lennart Salmén for sharing his time, facilities and expertise with me. The work of Lennart Salmén will remain for me a model of one's most thorough, rigorous and dedicated contribution to a particular aspect of wood science. I am also grateful to Ann-Mari Olsson and Joanna Hornatowska for their technical assistance and kindness. Working among Anna, Federica, Jesper, Martin, Maggan and Suzanne has been a wonderful experience.

The NMR studies have been performed in the department of Chemistry at Virginia Tech. The technical assistance of Tom Glass for the CP/MAS NMR studies is

gratefully acknowledged. Dr. Robert Schmidt and Dr. Reginald Mbachu at Dynea are also acknowledged for their assistance in molecular weight analysis.

Warm thanks also go to the students, staff and faculty in Wood Science and at the Center for Adhesive and Sealant Science. Nikki Robitaille has been my labmate and friend during my graduate career. It has been a pleasure to share many hard working hours and free time with her.

Friends and family, here and there, have been part of this work. In many occasions they have provided the moral support necessary for the completion of this work. Without the friends from all countries and cultures I have had a chance to appreciate, my stay in Blacksburg would not have been such a rich experience. I am especially indebted to Laurence who supported me in many ways during the writing period. I am also thankful for the friends at home that have remained my friends years and kilometers apart. I hope they will forgive my absence in those numerous occasions when one expects friends to be at one's side.

Last but not least, the project of earning a Ph.D. degree would never have come to my mind without the guidance, support and model of one of my former professors. Dr. Tony Pizzi has exerted a decisive influence on the course of my life. He first inspired "my fire" for wood science and chemistry through being my teacher, through his dedication to science and through his incredible enthusiasm. I cannot thank him enough for affecting so positively the course of my life.

TABLE OF CONTENTS

LIST OF FIGURES

LIST OF TABLES

I BACKGROUND

CHAPTER. I.1. INTRODUCTION

Adhesive penetration in wood is commonly categorized into *gross penetration* and *cell wall penetration*. *Adhesive gross penetration* results from the liquid adhesive flowing into the porous structure of wood. For c*ell wall penetration*, the adhesive enters the woody cell wall. *Adhesive gross penetration* and *cell wall penetration* are critical to joint performance [1], [3], [4]. A thorough understanding of adhesive penetration is therefore crucial to the wood adhesion field. In that purpose, one may want to establish a finer classification of adhesive penetration in wood. A categorization of adhesive penetration in wood is proposed below, based upon the scale of adhesive penetration. In the following classification, four scales of penetration are envisioned. These are:

- Macroscopic penetration (millimeters)
- Microscopic penetration (microns to tens of microns)
- Nanoscale penetration (nanometers to tens of nanometers)
- Angstrom scale penetration (up to tens of angstroms)

In its most simple approach, adhesive penetration can be associated with a 2 dimensional concept; the depth of adhesive penetration into the substrate. Visual inspection of a bondline provides a qualitative appreciation of the depth of penetration. It typically spans from fractions of millimeters to several millimeters. One may therefore coin this scale of penetration macroscopic penetration. Quantitative techniques have been developed to measure the depth of adhesive penetration. For instance, White et al. utilized Neutron Activation Analysis (NAA) on phenol-resorcinol-formaldehyde (PRF) adhesives tagged with bromine [8]. By measuring the cumulated bromine concentration throughout the cross-section of a joint with NAA, the authors were able to define a δ_{90} parameter; δ_{90} parameter that represents the distance from the bondline over which 90 % of the penetrated adhesive is found [8]. With this technique, White substantiated the hypothesis that the depth of adhesive penetration is influenced by adhesive parameters (viscosity), by substrate parameters (grain angle; earlywood or latewood) and by processing parameters (bonding pressure; open time) [1]. In addition, White correlated the depth of adhesive penetration with the joint fracture toughness [1].

A finer observation scale of adhesive domains can be defined by reference to wood anatomy.

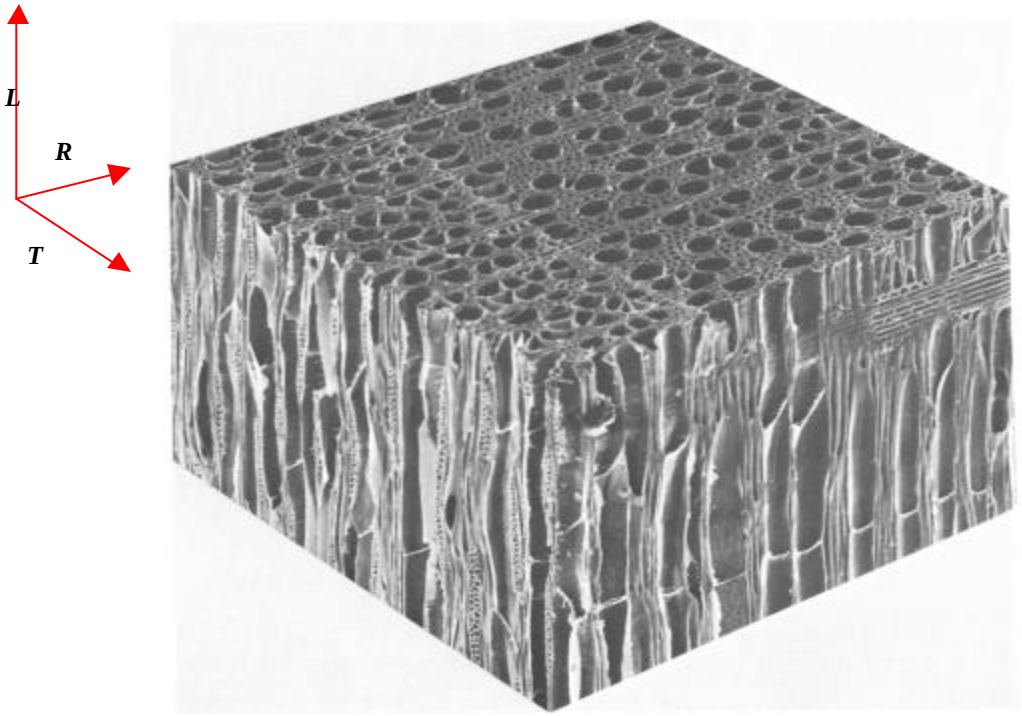

Figure I.1.1. Scanning Electron Micrograph of Yellow-poplar, (from [2])

Wood is an orthotropic material, in which arrays of cells are aligned along the longitudinal and radial directions (Figure I.1.1). Cells have a cavity in their center, the cell lumen, which is surrounded by the cell wall. Vessels, fibers and tracheids are aligned in the longitudinal direction while ray cells parallel the radial direction. For these cells, the lumen diameter spans from several microns to tens of microns and to a hundred microns when considering in turn fibers, tracheids and vessel elements. Cell lumen dimensions thus fall on the micron range. Perforations plates at the cell extremities and pits on the lateral cell walls constitute additional cavities between adjacent cells. Such cavities have diameters in the order of microns and may thus be termed “micropores”.

A microscopic porous network consequently imparts flow pathways within a solid wood block. It follows that adhesive penetration into cell lumens and “micropores” falls

into the dimensional domain of microscopic penetration. As expected, microscopic penetration is best evaluated with microscopic techniques. Optical microscopy, scanning and transmission electron microscopy (SEM/TEM) have been utilized with success to probe adhesive microscopic penetration [3], [5], [6]. Quantitative analysis of microscopic penetration has even been afforded by combining image analysis and fluorescence microscopy techniques [5]. In so doing, Jonson et al. evaluated that approximately 53 % of wood void volume is filled with Phenol-formaldehyde adhesives up to a penetration depth of 100 microns [5]. Adhesive variables (molecular weight distribution), substrate variables (wood surface direction, moisture content) and processing variables (adhesive cure method) influence microscopic penetration of adhesives in wood [5], [6]. Wood surface energy and adhesive surface tension are also important parameters of micron scale penetration [7].

In effect, the above classification of adhesive penetration into a macroscopic and a microscopic scales is a refinement of *adhesive gross penetration*, refinement based upon the observation scale of the adhesive domain. Similarly, *cell wall penetration* may be examined from the standpoint of the adhesive domain size.

Figure I.1.2 pictures the arrangement of the woody cell wall, in which individual layers have been removed up so as afford a visualization of their specific organization. The individual layers have a thickness on the order of the micron and display a distinct organization. For instance, cellulose microfibrils can be organized randomly (primary wall) or oriented at a particular angle (S_1, S_2 and S_3 layers). The width of the microfibrils ranges approximately from 10 to 40 nanometers. At this observation scale, the cell wall may still be viewed as a porous material. In fact, pore diameters within the cell wall have been estimated between 5 and 20 nanometers [9]. Adhesive penetration in such "nanopores" may therefore be classified as nanoscale penetration.

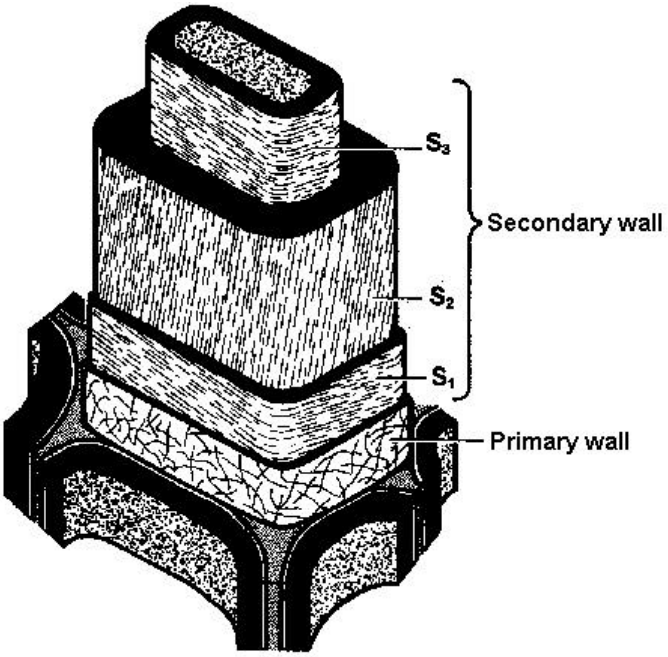

Figure I.1.2. Schematic of Wood Cell Wall Structure (from [2])

In order to detect adhesive penetration into the cell wall, sophisticated techniques are generally required. To date, the most successful methods for demonstrating cell wall penetration involve tagging of the adhesive. In 1971, Smith first combined SEM and Energy Dispersive Analysis of X-rays (EDAX) for assessing phenol-formaldehyde (PF) resin penetration into the cell wall [10]. In this pioneering approach to adhesive penetration, Smith brominated the PF resin and was able to detect the bromine element within the individual wood cell layers with SEM/EDAX. Smith also utilized light microscopy autoradiography on PF resin tagged with ^{14}C. For low moisture content Douglas-fir and Southern Pine (i.e. 2% moisture content), cell wall penetration was evidenced, albeit to a small degree [10]. While earlywood cells exhibited PF penetration in the S_3 and S_2 layers, adhesive penetration into latewood cells was restricted to the S_3 layer. In all cases, only those cells having their lumens filled with adhesive exhibited some degree of cell wall penetration, thus suggesting connectivity between adhesive "microphases" and adhesive in the cell wall. With higher initial moisture content of woods (20% moisture content), greater concentration of PF resin was evidenced in the

cell wall layers. Regardless of wood moisture content, no penetration into the middle lamella was found. Smith thus concluded in his study that penetration into the cell wall occurs outward from bulk adhesive "microphases" embedded into the cell lumens. Using the same techniques, Robison also detected penetration of an alkyd resin into the cell wall of Basswood [11]. In Robison study however, the penetrated resin was believed to remain uncured throughout the service life of the wood/coating system. Smith and Robison studies are therefore stringent evidence that commercial resins can penetrate, to some extent, the woody cell wall, thus revealing at least nanoscale penetration [10], [11].

Surprisingly then, for a series of polyethylene glycol (PEG) of various molecular weights, Tarkow estimated the limiting size for cell wall penetration to be 18-20 angstroms (i.e. corresponding to PEG-3000) [12]. Going back to Robison's work on alkyd resin, one should note that only the low molecular weight fraction of the alkyd resin (chain length below 16 angstroms) was believed to penetrate into the cell wall [11]. In Smith's study on the other hand, the PF resin was free of monomeric species and had an average degree of polymerization of six [10]. Suggested with these observations, is the possibility to further scale *cell wall penetration* down to a smaller level, namely that of angstrom scale penetration. Angstrom scale penetration shall now relate to the molecular scale morphology of wood polymers.

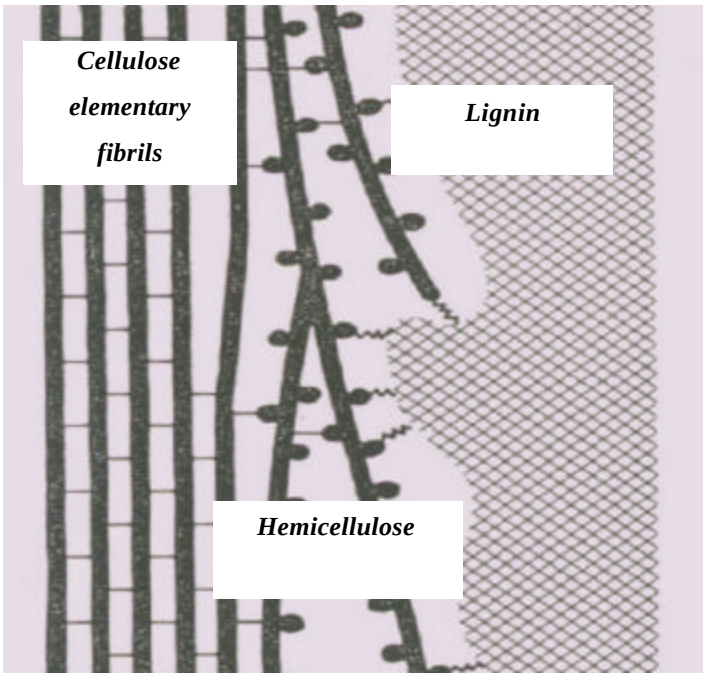

Figure I.1.3. Molecular Scale Morphology of Wood Polymers

Figure I.1.3 reveals that hemicelluloses are associated with cellulose elementary fibrils (through hydrogen bonding) but also with the lignin network (through covalent linkages). In other words, hemicellulose compatibilizes the ordered hydrophilic cellulose domains with the amorphous hydrophobic lignin network. If angstrom scale penetration occurs, it ought to take place in the amorphous matrix composed of lignin and hemicellulose. In fact, angstrom scale penetration entails to miscibility between polymers. In polymer blends, the free energy of mixing, ΔG, is governed by two parameters: entropy of mixing, ΔS, and enthalpy of mixing, ΔH (Equation *(I.1.1)*). On the one hand, the enthalpy is unfavorable to mixing unless specific interactions exist between the polymers. On the other hand, entropy is favorable to mixing but becomes less important as molecular weights increase. Therefore, for high molecular weight polymers, the entropic component vanishes and the enthalpic component dictates miscibility. However, for low molecular weight polymers, the balance between entropic and enthalpic components may yield a miscible blend ($\Delta G<0$).

(I.1.1) $$\Delta G = \Delta H - T\Delta S$$

For wood adhesives, a number of studies suggest that the low molecular weight fraction intimately mixes with wood polymers. Miscibility with wood polymers is generally referred to as swelling. Vinyl monomers have been reported to swell Basswood [13]. Swelling studies with isocyanates also suggest some degree of angstrom scale interactions [14]. In addition, Mantanis et al. demonstrated that benzyl alcohol, which crudely resembles the repeat units of Phenol-Formaldehyde (PF) resins is a powerful swelling agent for wood [15]. It is in fact not unexpected that swelling power relates to the molar volume and hydrogen donor capacity or basicity of the solvent [15]. Namely, the lower the molar volume and the greater the basicity, the faster the swelling rate and the greater the magnitude of the final swelling. Angstrom scale penetration is therefore likely to occur, to some extent, from the low molecular weight fractions of wood adhesives, especially those that are basic and have hydrogen bonding capabilities.

The perspective of observation scale of adhesive domains has granted a finer description of adhesive penetration in wood. The concepts of a*dhesive gross penetration* and *cell wall penetration* are now broken down into adhesive penetration at the macroscopic scale, microscopic scale, nanometer scale and angstrom scale. Along with a finer and finer scale of penetration, one easily pictures that the wood/adhesive region gradually evolves from an interface to a more and more diffuse interphase. In other words, with finer penetration scales, the proportion of intimate contacts between the woody material and the adhesive is increasing. Intimate contacts are essential to adhesion. The scale of the wood/adhesive interphase morphology shall therefore be critical to bond performance. Unfortunately, no technique is yet well developed for probing the solid wood/adhesive interphase morphology on the nanometer scale nor on the angstrom scale. Marcinko's work suggests some potential for dynamic approaches to successfully probe the wood adhesive interphase morphology on the smallest scales [150], [151]. Microscopic techniques lack the necessary resolution. Besides, visual techniques are limited in that only the presence or absence of the adhesive is determined. As exemplified in Robison's study with alkyd resins, the penetrated resin may remain uncured. Such a wood /adhesive interphase morphology differs drastically from that where *in-situ* polymerization yields adhesive interpenetration within the woody network.

Without doubt, these distinct morphologies yield different bond performances. An adhesive network cured *in-situ* can be expected to yield highly durable bonds. Uncured resin may provide a transition zone with increased toughness between wood and the cured resin phase. As a first step to the molecular scale engineering of wood bond performance, there is a need for methods that allow a finer characterization of the wood/adhesive interphase morphology.

- The primary objective of this research is to develop novel tools for probing the wood/adhesive interphase morphology on a finer scale, the nanometer scale and possibly the angstrom scale. Ideally, the novel tools shall give some insight on the state of the adhesive within the woody material.

Among other parameters, adhesive molecular size is critical to adhesive penetration, at least at all resolvable penetration scales.

- The second objective of this research is to investigate the molecular weight dependence of the wood/adhesive interphase morphology. Besides, this objective will be useful to probe the sensitivity of the novel morphological tools to be developed in this research.

In these objectives, dynamic methods utilized in miscible polymer blend studies hold some promise. Dynamic methods typically establish correspondence between the scale of intermolecular interactions and the domain size of molecular motions that is modified upon blending. For example, if in a polymer blend nanometer scale interactions develop, then the nanoscale molecular motions of the neat polymers are altered upon blending. By further probing different frequencies of motions i.e. different motional domains, a more complete understanding of polymer blend morphology is gained.

The first section of this dissertation provides some background on phenol-formaldehyde resins (PF), the resins to be utilized in this research. Also provided in the first section, is some background on selected dynamic techniques that are typically used in polymer blend studies and that may be suitable for probing the wood/PF interphase

morphology on the smallest scales. The second section evaluates novel methods for probing the morphology of the wood/PF interphase on the nanometer scale and the angstrom scale. In section III, the potential of these methods is illustrated by investigating the molecular weight dependence of the wood/PF interphase morphology. Conclusions are provided in section IV.

CHAPTER. I.2. PHENOL-FORMALDEHYDE RESINS

Phenol-Formaldehyde resins (PF) result from the polycondensation of phenol and formaldehyde. From a commercial standpoint, PF resins have been of prime importance since the early 1900's, when they appeared as the first synthetically produced polymers [16]. Empirical research and development has significantly contributed to the chemical engineering of PF properties. In fact, PF properties can be tailored for a variety of applications, including foundry resins, molding compounds and wood-based composite binders [26]. PF resins are weather durable. As a consequence they are utilized in exterior grade wood-based composites [17], [26]. Depending upon reagent ratios and catalyst type, two classes of adhesives have been developed. Resoles are produced from base catalyzed polymerization using excess formaldehyde. On the other hand, Novolacs are obtained from acid catalyzed polymerization using excess phenol. The manufacture of wood-based composites utilizes mainly resoles. Their chemistry and properties are reviewed below.

I.2.1 Synthesis of Resole Prepolymers

Resoles result from the polycondensation of phenol with excess formaldehyde in an aqueous alkaline medium. Typically P: F molar ratios lie in the 1:1.1-1:3 range [16]. Metal hydroxides of sodium and potassium are commonly used as catalysts. Ammonia and tertiary amines such as triethylamines can also catalyze PF condensation [19], [20]. Industrial resoles are usually manufactured by cooking the reagents from 1 to 8 hours at temperatures below 100°C [16]. In that process water is used as the solvent so that the final resole solid content lies in the 40 to 60% range [16]. Owing to the polyfunctionality of phenol, the chemistry of PF polymerization is very complex and a thorough characterization of resole molecular structures is still lacking. However, analytical techniques such as Nuclear Magnetic Resonance (NMR), Gel Permeation Chromatography (GPC) and Infra-Red (IR) spectroscopy have shed some light on the molecular structures and reaction mechanisms involved in PF synthesis. It is well established that PF synthesis is a step growth polymerization, which takes place in two stages [26]. Initially, formaldehyde adds to phenol thereby producing hydroxymethylated

phenols (HMP). Subsequently, HMP's undergo a condensation reaction, which causes chain growth and crosslinking.

I.2.1.1 Formation of Hydroxymethylated Phenols

When phenol is added to aqueous formaldehyde in the presence of a base, the phenolic hydroxyl group is readily deprotonated into a reactive phenoxide ion, which is resonance stabilized (Figure I.2.1).

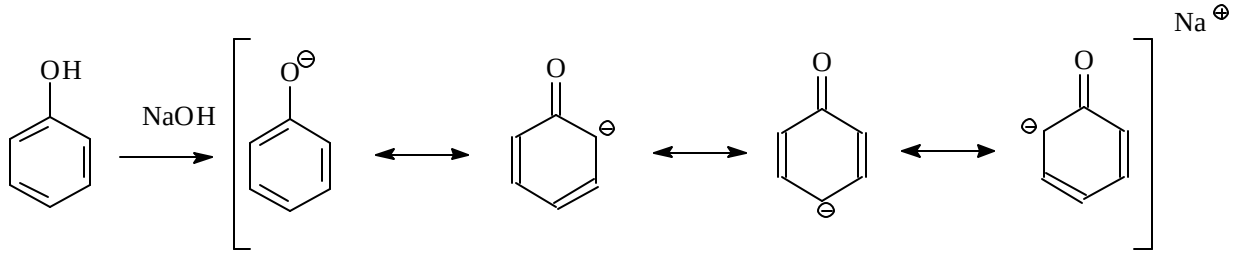

Figure I.2.1. Reactive Phenoxide Ion under Basic Conditions

The electron density in the phenoxide ion results in an electrophilic aromatic substitution with methylene glycol, the hydrated form of formaldehyde, both at the para and ortho positions (Figure I.2.2).

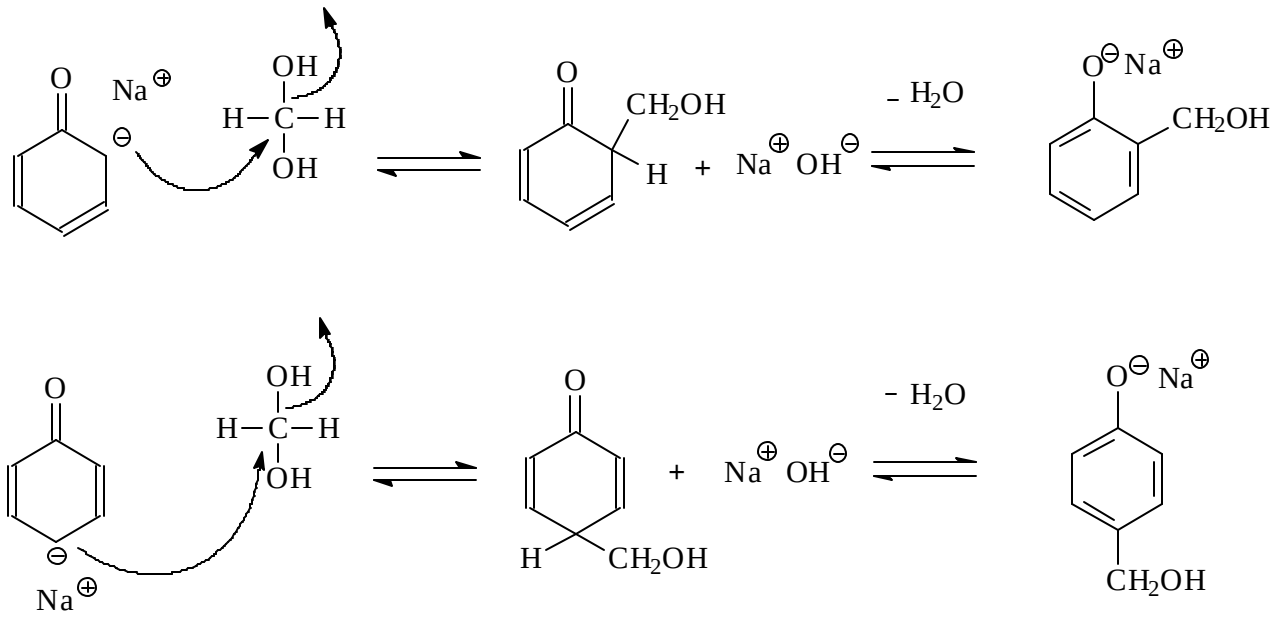

Figure I.2.2. Electrophilic Aromatic Substitution of Methylene Glycol on Phenol Ortho (top) and Para (bottom) Positions

The para position is believed to be more reactive than the ortho position [24]. However, because there are two ortho sites for one para site, ortho substitution predominates and proceeds at a faster rate than para substitution [26]. Generally, different catalytic mechanisms produce specific isomeric compositions of HMPs mixture [18], [26]. For instance, when metal hydroxides are utilized, a chelate ring mechanism, as first proposed by Caesar and Sachanen, favors ortho substitution (Figure I.2.3) [22].

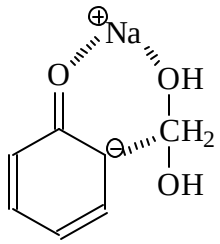

Figure I.2.3. Chelate Ring Intermediate in Sodium Hydroxide Based Catalysis

When ammonia and amine catalysts are utilized on the other hand, nitrogen containing intermediates are likely to form as illustrated in Figure I.2.4 [29].

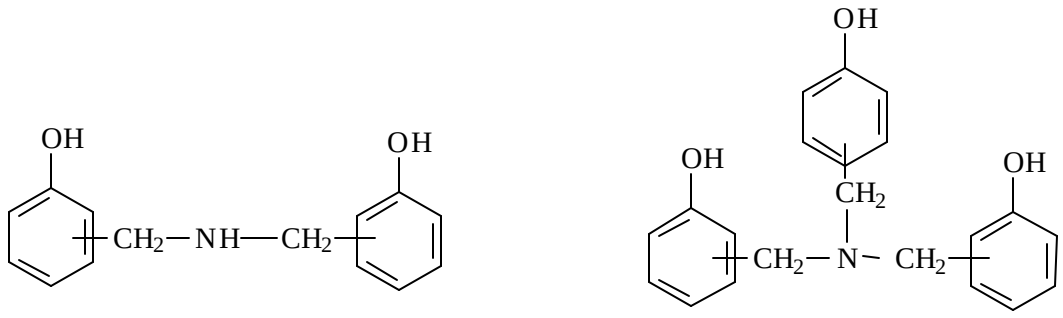

Figure I.2.4. Di(hydroxybenzylamine) (left) and Tri(hydroxybenzylamine) (right) Intermediates in Ammonia Based Catalysis of PF Polymerization

Regardless of catalytic mechanism, hydroxymethylation proceeds rapidly thereby yielding a high level of hydroxymethyl substitution prior to the slower condensation [21]. Typically the reaction mixture comprises mono-, di- and tri-substituted HMPs. In fact, electrophilic aromatic substitutions of formaldehyde on mono- and di-substituted HMPs proceed at a faster rate than the initial hydroxymethylation thereby yielding high proportions of difunctional and trifunctional derivatives [23]. At this stage of the polymerization, excess formaldehyde may also react with phenolic hydroxymethyl groups to produce substituted hemiformal moieties. Such molecular structures have been detected by solution NMR [25]. Figure I.2.5 illustrates some common hydroxymethylated derivatives present at the initial stage of PF polymerization. At this stage, HMPs are amenable for condensation reactions.

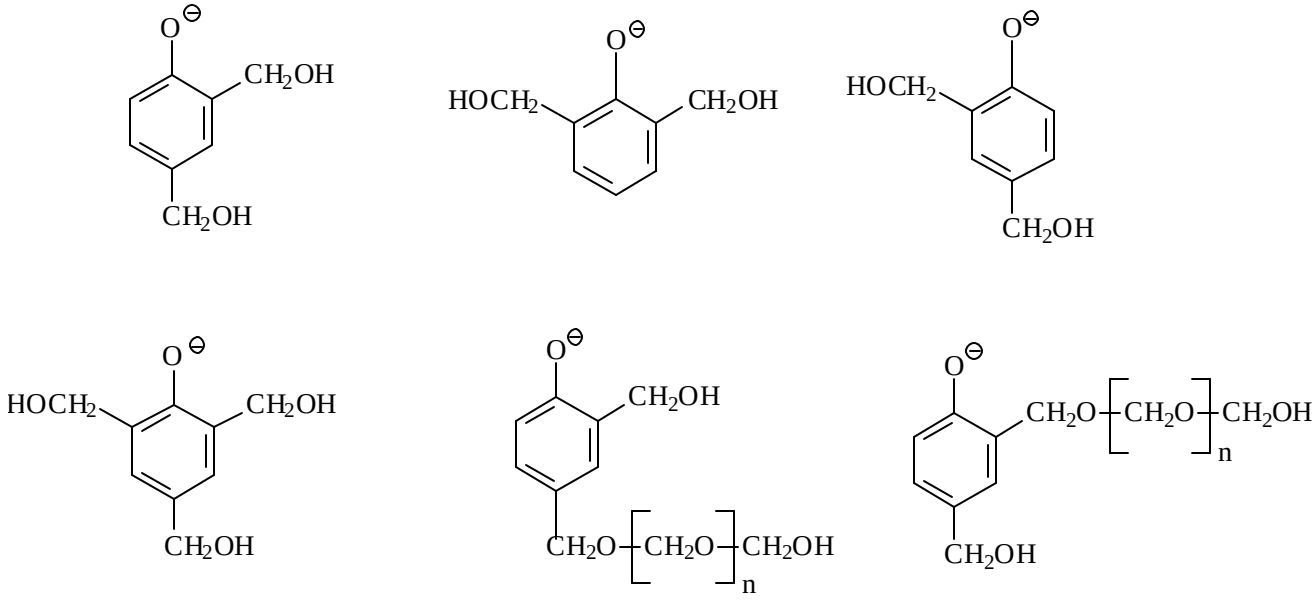

Figure I.2.5. HMP Derivatives

I.2.1.2 HMPs Condensation

The condensation of hydroxymethylated species is a step growth polymerization in that water is released. Jones first proposed the existence of quinone methide intermediates (Figure I.2.6) [30].

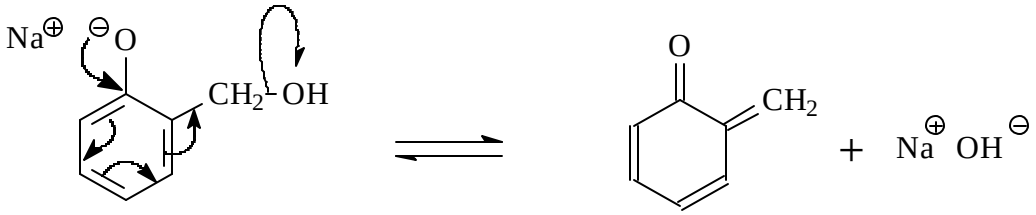

Figure I.2.6. Quinone Methide Formation from HMPs

Quinone methides are very reactive and will react with nucleophilic sites from another phenol or substituted phenol. In this subsequent electrophilic aromatic substitution, methylene bridges are generated (Figure I.2.7). Methylene bridges form

predominantly in the ortho-para and para-para positions, while ortho-ortho methylene bridges are more rarely formed [25].

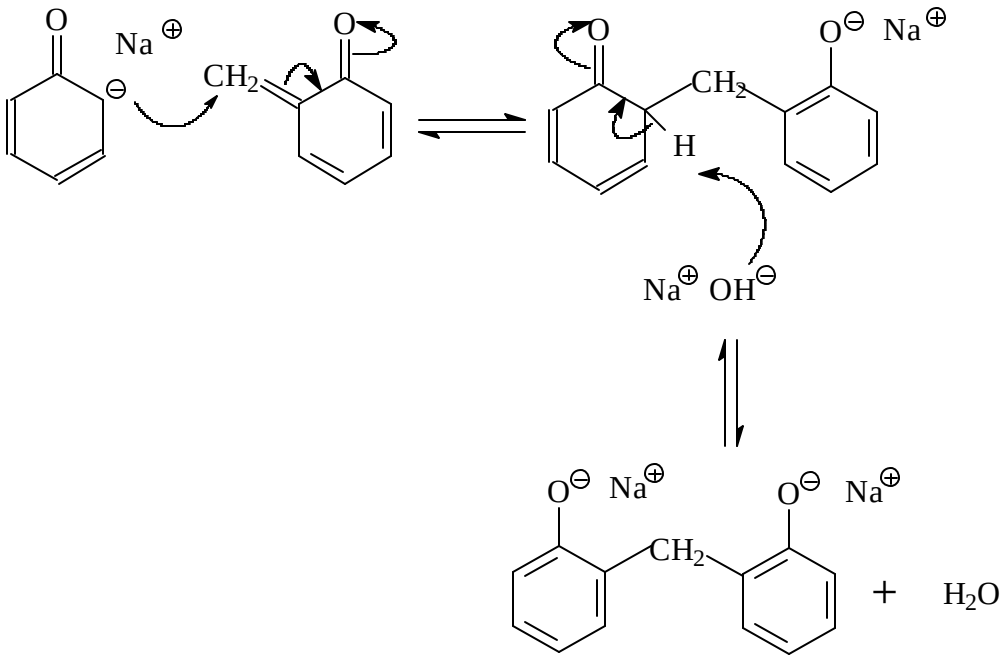

Figure I.2.7. Condensation Reactions via Quinone Methide Intermediates

It is also thought that HMP's hydroxymethyl groups can condense to form ether bridges. Methylene ether bridges may be obtained by the reaction of an hydroxymethyl group on a quinone methyde intermediate as illustrated in Figure I.2.8.

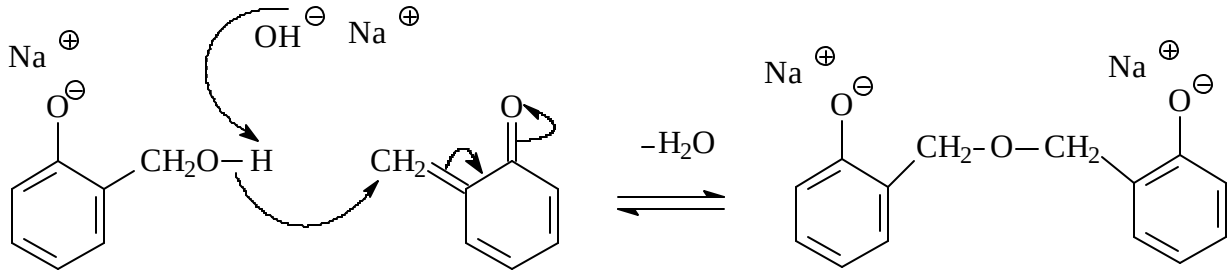

Figure I.2.8. Mechanism for Methylene Ether Bridge Formation

Dibenzyl ether bridge formation prevails under neutral or acidic conditions and requires temperatures as high as 130°C [23], [35]. Such conditions are not common in resole manufacture and methylene ether linkages are therefore scarce in commercial resoles. In addition, methylene ether bridges generally convert to the more stable methylene bridges upon additional heating [27]. Therefore, ether structures are likely to exist as an intermediate only during PF polymerization. Generally, PF condensation is stopped at this oligomeric stage; the so-called resitol or stage B resin has a pot life from 3 to 9 months [27]. Depending upon the end use of the resin, different synthesis procedures are implemented so as to deliver desirable properties. For instance, Oriented Strand Board (OSB) is manufactured with resoles that have a typical number average molecular weight of 200-500 g/ mole and viscosity of 100 to 500 mPa.s at 20°C. On the other hand, resoles destined for plywood manufacture are more advanced prepolymers with a characteristic number average molecular weight of 1000-2000 g/mol and viscosity up to 2000 mPa.s [17]. Consequently, the resin properties are easily controlled for specific applications.

I.2.2 Synthesis Conditions and Prepolymer Properties

A large number of studies have assessed PF properties on the basis of reaction conditions [17], [29]. In that matter, it has long been established that catalyst choice and reagent ratios significantly impact resitol characteristics. Likewise, cooking procedures have been empirically developed to respond to novel end use specifications [17]. Guidelines on PF synthesis/structure/properties relationships are presented below. However, the reader is directed to reference [29] for a detailed review.

I.2.2.1 Starting Reagents

I.2.2.1.1 Catalyst

The nature of the catalyst influences resitol isomeric structure and topology. For instance, preferential ortho substitution increases in the following sequence of catalysts KOH< NaOH< LiOH< BaOH< SrOH< CaOH< MgOH [20]. Ammonia-based catalysts are believed to favor more linear resitols [16]. Of significance also, is the catalyst impact on PF solubility. Sodium hydroxide for instance enhances PF solubility in water thus

lowering viscosity. Consequently more advanced resitols can be manufactured by increasing the sodium hydroxide content while maintaining adequate flow properties. Likewise, reagent dilution can be adjusted to permit more advanced resitols while maintaining adequate flow properties. Such practices are used in plywood PF resins, which have higher sodium hydroxide contents and lower resin solids than OSB resitols [17].

I.2.2.1.2 Reagent Ratio

PF resitol properties are largely governed by the initial F: P molar ratios [34], [35]. Generally, high F: P ratios produce highly branched resins whereas low F: P ratios favor more linear structures. So et al. utilized IR spectroscopy, GPC and NMR to obtain detailed information on PF characteristics as a function of F: P molar ratios [35]. As expected, higher F: P ratios were found to enhance hydroxymethylation and increase the degree of polymerization [35]. Similarly, hemiformal and ether bridge structures were directly related to the excess formaldehyde. More surprisingly, a synergy between F: P ratio and cure temperature on PF chemical structure was reported. Specifically, higher cure temperatures were required to convert methylene ether to methylene bridges when high F: P ratios were utilized [35]. While So et al. reported no F: P ratio influence on the resitol isomeric structure, another study suggests direct correlation between ortho substituted proportions and F: P molar ratio [34]. Namely, Holopainen and coworkers detected greater proportions of o-substitution, hemiformal species and p-p' methylene bridges with increasing F: P molar ratio [34]. The authors further confirmed greater degrees of polymerization with greater F: P molar ratios, whereas polydispersity exhibited the opposite trend. The study also assessed F: P ratio influence on resitol cure properties with Differential Scanning Calorimetry (DSC). It was found that hydroxymethylation and condensation reactions shift to more separate steps with increasing F: P molar ratios [34]. What clearly emerges from these studies is that the F: P ratio is a key factor to tailor PF topology, molecular weight, and curing properties.

I.2.2.1.3 Additives

In the production of industrial PF resins a variety of additives are utilized to modify the storage, application and cure properties of resitols. Methanol is commonly

added at the onset of the cook in order to control the polymerization exotherm. The addition of urea at the end of resitol cook is also a common practice of PF manufacturers [17]. Urea not only reduces the resin cost but also plays the role of free formaldehyde scavenger. Urea is also useful for lowering the preparation viscosity thereby allowing for more advanced resitols which require less cure to achieve their final properties [17]. Other additives include plasticizers, antifoams, starches and tackifiers [17].

I.2.2.2 Resin Cook Procedure

In the early 1960's, single-caustic charge cooks were developed to produce resitols for the plywood industry [17]. In a single-caustic charge cook, all reagents are fed into the reaction kettle and polymerized at a temperature nearing 90°C until a specific Gardner viscosity is achieved. The temperature is subsequently decreased to approximately 75°C permitting a better control of the polymerization. At the desired viscosity, the polymerization is quenched. Over the next decade, improvement of PF properties were brought by the development of double-caustic charge cooks. In these two-steps cooks, or split cooks, part of the catalyst is added initially and the polymerization is carried on to some degree before adding the remaining catalyst. It results from the split cook that a fraction of the resin is highly polymerized while there remains a low molecular weight fraction. The second caustic charge possibly activates unreacted phenol. Such split cooks are now common place for resins destined for plywood [17]. An alternative cooking procedure consists of adding formaldehyde continuously during the polymerization. Continuous addition of formaldehyde allows for a better control of the polymerization exotherm and plays an important role on the isomeric and topologic characteristics of PF prepolymers. Delayed addition of phenol is also customary for PF resins destined for particleboard [28].

I.2.2.3 Concluding Remarks

Owing to phenol polyfunctionality, PF polymerization is a complex process that yields a variety of isomeric structures and molecular sizes. While a complete understanding of PF chemistry is still lacking, empirical developments have been decisive to the molecular engineering of PF characteristics and properties on the basis of the reaction conditions. For example, OSB resins with their low molecular weights

contrast significantly from plywood resins obtained from split cooks and which display a bimodal distribution of molecular weights. The cure properties of such resins are therefore significantly different.

I.2.3 PF Resin Cure

PF resins achieve their final binding properties as a result of cure. For resoles, cure is exclusively heat induced and causes changes in the chemistry and in the physical properties of the material.

I.2.3.1 Cure Chemistry

The same condensation reactions as those generating PF prepolymers remain in action during PF cure. In other words, the bulk of PF cure proceeds via quinone methide intermediates. However, additional mechanisms become increasingly important as cure proceeds [31]. For instance, the conversion of methylene ether bridges into methylene bridges becomes predominant at temperatures greater than 160°C, which are typical of cure conditions [31]. During this reaction, formaldehyde is released. The decomposition of hemiformal moieties also generates free formaldehyde, which may be consumed in additional crosslinking mechanisms. In that matter, there is some controversy on PF crosslinking reactions. Zinke first proposed that part of the free formaldehyde generates crosslinks at the phenolic hydroxyl and methylene groups [32]. With the development of high-resolution NMR for solids (CP/MAS NMR) in the early 1980's, the involvement of the phenolic hydroxyl group and of free formaldehyde in crosslinking reactions has been further hypothesized [31], [33]. Maciel proposed 3 reactions accounting for the detection of ether structures at the phenolic hydroxyl site and for the detection of methine crosslinks in cured PF resins [31]. These involve the reaction of hydroxymethyl moieties with the phenolic hydroxyl group and reaction of free formaldehyde (and hydroxymethyl groups) with methylene carbons (Figure I.2.9) [31].

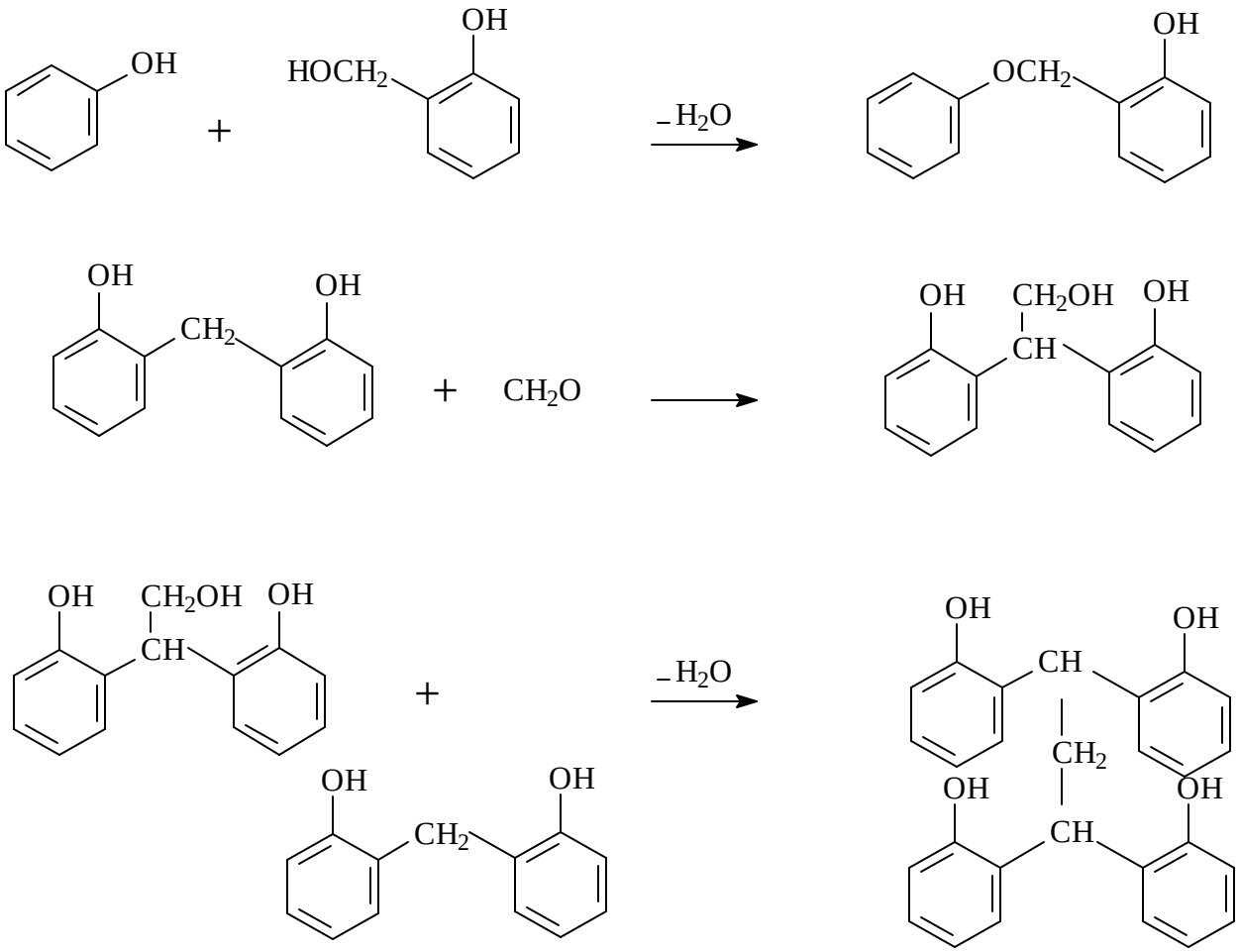

Figure I.2.9. Crosslinking Reactions Proposed by Maciel (after [31])

More recently, Solomon's group proposed an ether exchange reaction rather than a direct reaction of formaldehyde and phenolic hydroxyl from a solid state ^{13}C NMR study (Figure I.2.10) [33].

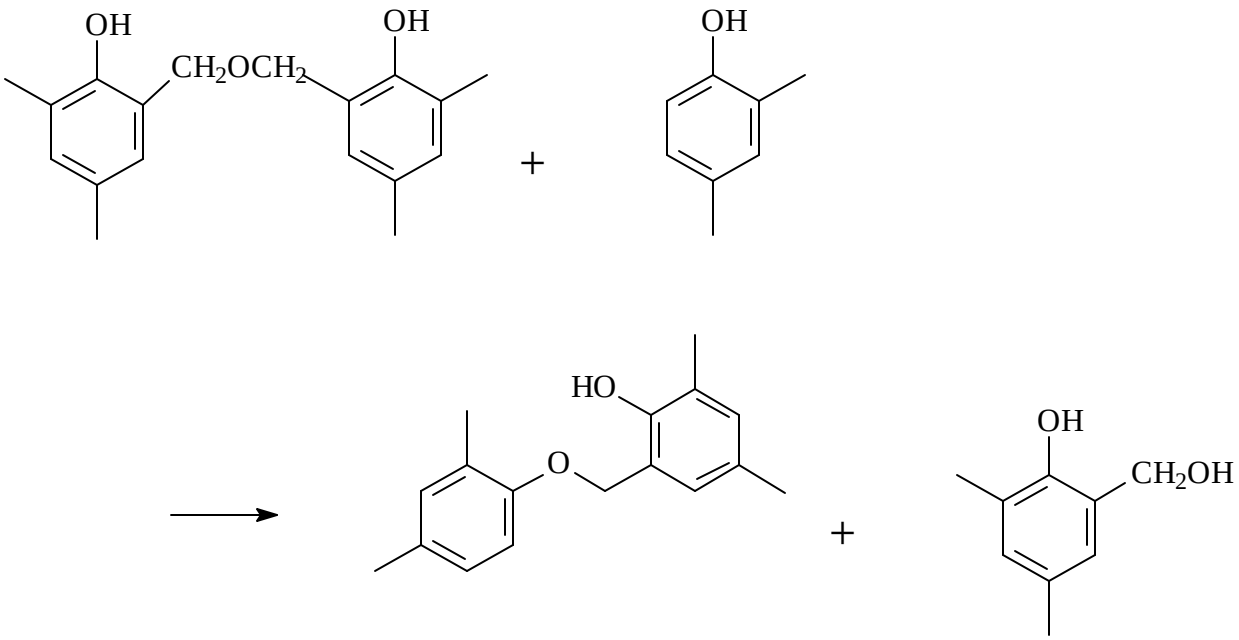

Figure I.2.10. Ether Exchange between Phenolic Hydroxyl and Ether bridge Proposed by Solomon's Group (after [33])

While these reactions remain hypothetical, it is true that the chemical crosslinks observed in PF resins suggest a very complex cure chemistry. Along with the changes in chemical structure, cure causes dramatic changes in the physical and mechanical properties of PF resins. Namely, PF cure is marked by two characteristic thermosetting events, gelation and vitrification. Gelation marks the onset of infinite molecular weight. At the gelation point, viscosity rises to infinity. As the gel is further cured, it passes through a vitrification process during which the material glass transition temperature (T_g) reaches the cure temperature. At this vitrification point the polymer behavior changes from that of a rubber to that of a glass. In other words, cooperative molecular motions are suddenly frozen and the resin solidifies. Past this thermal event, the resin is an insoluble, infusible, highly crosslinked, 3 dimensional network. For PF resins to be efficient load transferring materials in wood joints, the resin ought to be vitrified. Therefore, it is critical to understand the curing properties of PF resins from a physical or mechanical standpoint. As a consequence, extensive research has focused on developing techniques for characterizing PF thermosetting events.

I.2.3.2 Cure Characterization

Many scientists have attempted to characterize PF cure on the basis of gelation and vitrification events as first introduced by Gillham in the well known Time-Temperature-Transformation cure diagrams [37]-[42]. A TTT cure diagram provides a complete cure characterization of thermosetting systems in that it defines the time and temperature required for achieving specific viscoelastic properties (Figure I.2.11).

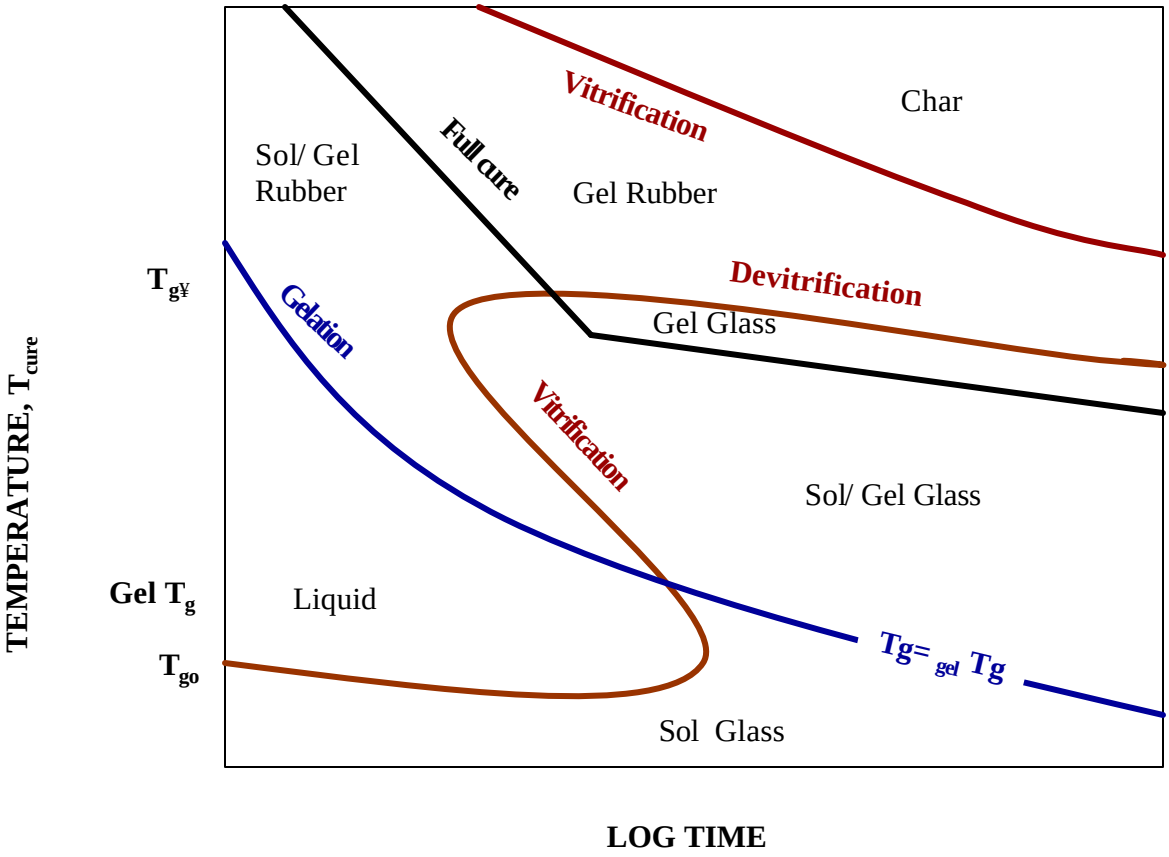

Figure I.2.11. Generalized Time-Temperature-Transformation (TTT) Cure Diagram, (after [37])

Dynamic techniques such as Dynamic Mechanical Analysis (DMA), Torsional Braid Analysis (TBA) and Micro-Dielectric Spectroscopy have shown potential for detecting PF thermosetting events [39]-[42]. For DMA and TBA, glass fiber braids are typically impregnated with liquid PF and cure events are detected from changes in

storage and loss properties. Gillham demonstrated that thermoset gelation and vitrification events are accompanied by a damping peak as well as a rapid increase in storage modulus [37]. Likewise, vitrification has been detected in several cure studies of neat PF resins [41], [40]. Interestingly however, none of these studies permit the detection of PF gelation. Furthermore, it has been repeatedly observed for PF resins that mechanical techniques detect earlier end of cure compared to calorimetric techniques [43], [44]. Such studies clearly demonstrate that the environment in which the cure characterization is performed is critical [43], [44]. For instance, in sealed DSC capsules, water vapor remains throughout the cure of the sample and yield different cure properties than in a water vapor free environment such as in a DMA furnace [44]. It is therefore crucial to adopt the technique that best mimics the curing conditions to be applied to the PF resin. More sophisticated techniques such as solid state ^{13}C CP/MAS NMR provide the capability to simultaneously probe the chemical and dynamic aspects of PF cure [45], [36]. For instance, Neiss demonstrated the impact of rigidity or mechanical state cure on the proton spin-spin relaxation time, $^{H}T_2$. The same solid state NMR acquisition enabled Neiss to probe PF chemical conversion from methylol to methylene structures as an indication of the degree of PF cure [45]. Another solid state NMR study establishes a direct correlation between the cured PF glass transition temperature and NMR and proton spin lattice relaxation times in the rotating frame, $^{H}T_{1\rho}$ [36]. Thus, NMR relaxation times are sensitive to PF network properties. A major drawback of the cure characterization techniques mentioned above is that the neat resin rather than the resin in presence of wood is probed. In reality, it has long been established that wood has a significant impact on PF cure kinetics and on PF strength development [47]. Hence, of greater interest are those cure characterization techniques that enable PF cure characterization *in-situ*, that is within a wood joint. DSC is a valuable technique for monitoring PF cure in presence of woods. It has been found in many DSC studies, that wood has a catalytic effect of PF cure, a catalytic effect that has been in turn ascribed to wood-PF covalent bonding and physisorption [46], [47]. However, DSC characterization is limited to the heat of the reaction, which is not always in accordance with the mechanical cure as mentioned above. As concerns in-situ mechanical cure of thermosetting adhesives, recent techniques developed by Pizzi's group have provided significant insight on wood

substrate influence on PF cure [48]-[52]. The authors utilized Thermal Mechanical Analysis (TMA) for detecting *in-situ* cure events, vitrification of PF adhesives in particular. With this technique, the influence of wood substrate on thermosets cure was further suggested [49]-[52]. Namely, the generalized TTT diagram cure diagram was found inadequate for describing the cure behavior of thermosets in presence of lignocellulosic substrates. Rather, a modified TTT and CHT cure diagram was proposed. The shape of the modified TTT cure diagram differs from the generalized TTT diagram for neat resin systems. This deviation was ascribed to adhesive/ substrate interactions [49], [52].

CHAPTER. I.3. VISCOELASTIC PROPERTIES OF POLYMERS

I.3.1 Introduction

When a polymer is at equilibrium, molecular motions occur randomly. Therefore under equilibrium the net mass flux averages to zero and molecular motions are not detectable. When a polymer is submitted to an external stress however, the biased molecular motions occur in an oriented fashion so as to reestablish equilibrium. In that process, a net flux of mass flow is generated and gives rise to specific viscoelastic properties [53]. The temperature dependence of such viscoelastic properties reveals the identity of molecular motions [54]. For instance, side-group motions, or secondary relaxations are characterized by an Arrhenius temperature dependence. On the other hand, the alpha-relaxation, which is attributed to the glass-rubber transition, displays a non-Arrhenius behavior [55]. Hence the interrelations between three parameters: time, temperature, and viscoelastic property provide significant insight on the underlying molecular motions. Dynamic Mechanical Analysis (DMA) is the most common technique for determining viscoelastic properties and their dependence on time and temperature. When performing dynamic mechanical experiments on amorphous polymers, the most dramatic change occurs at the glass transition, where the characteristic time for main chain motion becomes comparable with the experimental time scale. While deviation from Arrhenius behavior for the alpha relaxation has long been established, recent theoretical developments provide a greater understanding of the physical chemistry underlying this observation. In that matter, one of the most successful models has been afforded by the work from Ngai, Plazeck and Roland [73], [76]. Ngai developed a coupling model which quantifies intermolecular cooperativity associated with the glass transition [57]. Since this development, the so termed “cooperativity analysis” has proved to be a powerful tool for characterizing polymer molecular dynamics on the basis of molecular structure and molecular interactions [76]. In miscible polymer blends, intermolecular interactions have been proposed on the basis of the cooperativity analysis [84]. In that perspective, the cooperativity analysis appears as a promising tool for probing interactions at the wood/adhesive interphase. Hence, this chapter reviews the theoretical background and development of the cooperativity

analysis. The power of the cooperativity analysis will be illustrated with some of the most significant studies on synthetic polymers. In particular, the significance of the cooperativity analysis for probing intermolecular interactions in synthetic polymer blends will be emphasized. However, prior to considering these recent developments on polymer glass transition, some background on DMA is required. Finally, the actual understanding of wood viscoelasticity will be reviewed with a special emphasis on the detection of wood polymer glass transitions. This knowledge will help one appreciate the potential of the cooperativity analysis for complex polymeric systems such as wood and wood/adhesive composites.

I.3.2 Dynamic Mechanical Analysis

When a material is submitted to a sinusoidal stress (σ), it responds to the stress induced departure from equilibrium by an alternating strain (ε). Dynamic mechanical Analysis (DMA) is a common method to characterize material properties on the basis of dynamic stress-strain properties. In a DMA experiment, a stress (or strain) is applied with a small angular frequency (ω) and the strain (or stress) is simultaneously recorded:

(I.3.1) $$s(t) = \cos(wt)$$

(I.3.2) $$e(t) = \cos(wt + y)$$

For elastic solids submitted to infinitesimal strain, Hooke's law states a linear stress-strain relationship [53]. Hence, under transient loading of elastic solids, the strain is in phase with the stress. A spring, with a finite modulus E, is often used as a phenomenological model for elastic behavior, where the elastic solid stores the energy input by the external stress. Elastic solids can therefore revert to their original state upon removal of the stress (Figure I.3.1). For a viscous liquid on the other hand, Newton's law describes a linear relationship between stress and strain rate under infinitesimal strain rate [53]. This implies that viscous liquids respond to a sinusoidal stress with a sinusoidal strain, that is 90°out of phase with the stress. In other words, under transient loading

viscous liquids dissipate energy through irreversible flow. As a consequence, viscous liquids cannot revert to their original shape upon removal of the stress. Such a behavior is analogous to that of a dashpot filled with a liquid of viscosity η (Figure I.3.1). Real materials display viscoelastic behavior in that their response to an external stress is a combination of that from elastic and viscous materials. In a viscoelastic material, part of the energy is stored while the remaining is dissipated through viscous flow. Provided that the material obeys linear viscoelasticity, its viscoelastic properties may be modeled from Hookes's and Newton's laws by virtue of the Boltzman Superposition Principle [54]. Linear viscoelasticity requires that the stress strain ratio depends exclusively on time, a condition that is verified at small strains and strain rates [53]. As a consequence DMA experiments should be set up at small strains and strain rates for obeying linear viscoelasticity. Under these conditions, a viscoelastic material will exhibit a strain response that is out of phase with the input stress. Figure I.3.1 illustrates the behaviors and governing differential equations (GDE) respective of elastic solids, viscous liquids and of a viscoelastic material.

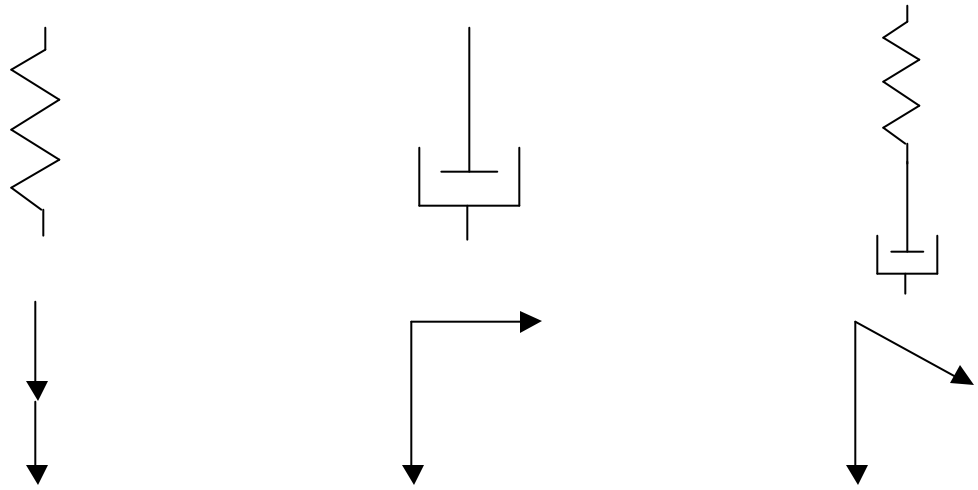

(I.3.3) $s(t) = Ee(t)$ (I.3.4) $s(t) = h\left(\frac{de(t)}{dt}\right)$ (I.3.5) $s(t) + \frac{h}{E}\frac{ds(t)}{dt} = h\left(\frac{de(t)}{dt}\right)$

Figure I.3.1. Mechanical Analogs, GDE, and Dynamic Stress-Strain Vectors for an Elastic Material, a Viscous Material and a Viscoelastic Material (Adapted from [54]).

In Figure I.3.1, a Maxwell element has been chosen for modeling viscoelastic behavior. Subsequent DMA background is illustrated on the basis of this particular model. However, other viscoelastic models may be envisioned and it must be recognized that neither a Maxwell element nor any complex combination of springs and dashpots succeeds in portraying the overall response of a viscoelastic material. For instance a Maxwell element may predict a stress relaxation experiment but fails to describe a creep experiment [53]. Such mechanical analogs are nevertheless valuable for modeling molecular relaxation in viscoelastic materials under a particular type of loading. When a Maxwell element is utilized to model a stress relaxation experiment ($e(t) = e_0$), the time dependence of the modulus is easily derived from the Maxwell element GDE (I.3.6). The relaxation time defined in equation (I.3.7) is the characteristic relaxation time, τ, for the Maxwell element to describe a molecular motion. It is therefore a material property.

(I.3.6) $$E(t) = E_0 e^{-\frac{t}{t}}$$

(I.3.7) $$t = \frac{h}{E}$$

Under transient loading of a Maxwell element, a complex notation is needed to describe the time dependency of the strain:

(I.3.8) $$e^*(t) = \bar{e}\left(\cos wt + i \sin wt\right) = \bar{e} e^{iwt}$$

The stress-strain relationship under dynamic loading is then simply obtained by substituting expressions for $\varepsilon(t)$ and $\sigma(t)$ in the GDE of the Maxwell element. Solving the GDE in the complex domain yields the complex modulus:

(I.3.9) $$E^*(iw) = \frac{s(t)}{e(t)} = \frac{w^2 t^2}{1 + w^2 t^2} + i \frac{wt}{1 + w^2 t^2}$$

The complex modulus may be differentiated into two independent viscoelastic properties. The real part (or component in phase) of the complex modulus represents the

elastic component and is therefore termed storage modulus, E'. The imaginary part represents the out of phase or viscous component and is called loss modulus, E". The ratio of loss and storage moduli is referred to as the loss tangent (tan δ) and is proportional to the phase angle between stress and strain.

(I.3.10)
$$\tan d = \frac{E''(t)}{E'(t)} = \frac{1}{v\,t}$$

The relationships between the three dynamic properties, storage modulus, loss modulus and loss tangent are easily pictured with a vectorial representation (Figure I.3.2).

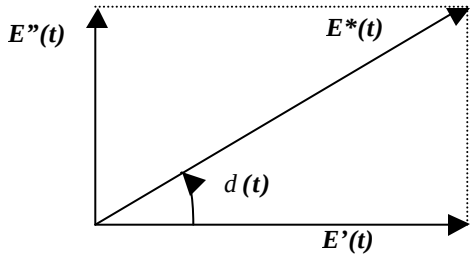

Figure I.3.2. Relationship between the Dynamic Properties in a DMA Experiment

This treatment of one Maxwell element illustrates that in a DMA experiment, two independent properties, storage and loss moduli, along with their time dependence provide a complete description of viscoelastic properties at a given temperature. Polymers fall in the category of viscoelastic materials. Polymers are therefore often modeled with a combination of springs and dashpots. A generalized Maxwell ladder may be utilized to model polymer properties (Figure I.3.3)

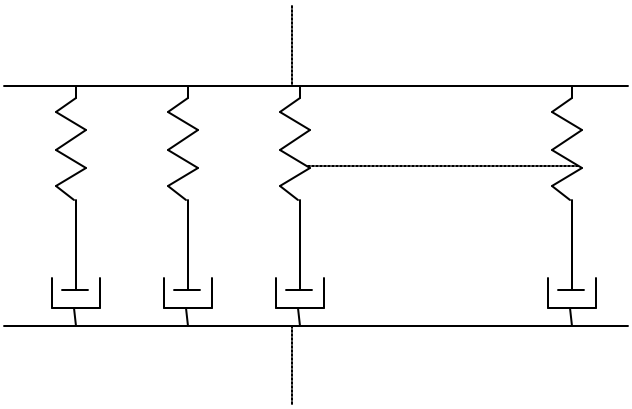

Figure I.3.3. Generalized Maxwell Model

In a Maxwell ladder, each element represents a specific mode of molecular motion with its characteristic relaxation time. In linear viscoelasticity, the Boltzman Superposition Principle states that effects are additive and allows one to perform the same mathematical derivations as for one Maxwell element [54]. The response of a Maxwell ladder to stress relaxation yields then an integral function for the time dependent modulus.

(I.3.11)
$$E(t) = \int_0^{\infty} E(t)e^{-\frac{t}{t}}dt$$

In Equation (I.3.11), the integral function encompasses the distribution of relaxation mechanisms associated with the distribution of molecular motions. The same derivations may be performed for dynamic loading of a generalized Maxwell ladder. Under dynamic loading, the dynamic properties of a viscoelastic polymer are obtained by generalizing equation (I.3.9) as:

(I.3.12)
$$H(t) = tE(t)$$
$$E^*(iw) = E_{\infty} + \int_0^{\infty} H(t)\frac{w^2t^2}{1+w^2t^2}d\ln t + i\int_0^{\infty} H(t)\frac{wt^2}{1+w^2t^2}d\ln t$$

In this equation, H(τ) represents the relaxation spectrum. The relaxation spectrum describes the distribution of relaxation times and can be viewed as the unified relaxation

response of the material [55]. In a dynamic mechanical experiment, assumptions can be made to derive the relaxation spectrum from dynamic properties as illustrated in Figure I.3.4 [53].

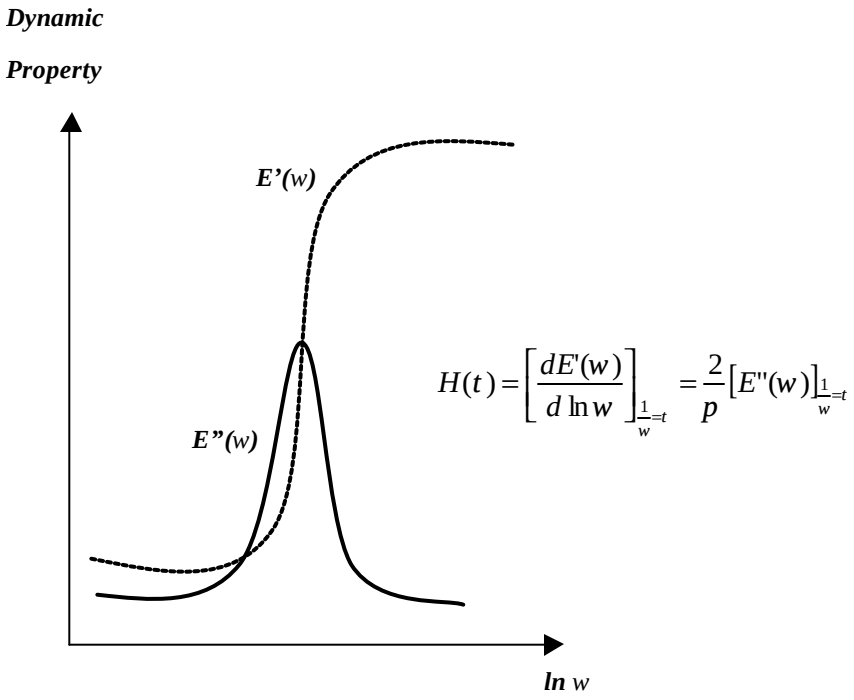

Figure I.3.4. Relaxation Spectrum and Dynamic Mechanical Properties (After [54])

Therefore probing polymer viscoelastic properties with DMA reveals the distribution of relaxation mechanisms. With DMA, molecular motions in the 10^{-3}-10^{2} Hertz frequency range are typically probed. The distribution of relaxation mechanisms reflects the variety of polymer molecular motions within the measurement frequency window. However, molecular interpretation of relaxation mechanisms is difficult on the sole basis of the time dependence of viscoelastic properties. Rather, the temperature dependence of such relaxations needs to be examined for obtaining a molecular interpretation of relaxation mechanisms.

I.3.3 Temperature Dependence of Polymer Properties

Temperature has a dramatic effect on polymer properties. This is particularly true for amorphous polymers, which undergo a dramatic change in mechanical properties at

the glass transition. For this reason, polymer science has extensively focused on understanding the process of glass formation. In that matter, empirical models have found exceptional success in portraying polymer viscoelasticity around the glass transition.

I.3.3.1 Time-Temperature Superposition Principle

It has long been established that viscoelastic properties at two different temperatures can be related by a change in the time scale of the experiment [54]. However, the principle of Time-Temperature-Superposition (TTSP) was best demonstrated by Williams, Landel and Ferry [59]. TTSP holds for amorphous polymers above their glass transition provided that the polymer is thermorheologically simple [57]. Thermorheological simplicity implies that the individual relaxation times display the same temperature dependence [54], [57]. In other words, the shape of the relaxation time distribution is the same at all temperatures. For such thermorheologically simple polymers, TTSP is used to generate master curves that describe viscoelastic properties on a large time scale. A master curve is created by shifting isotherms on a frequency scale. More specifically, a reference temperature is selected and isotherms are shifted so as to superimpose on the reference isotherm. The amount of shifting for each isotherm is referred to as the shift factor, log at , and represents the ratio of the relaxation times for a temperature, T, and the reference temperature, Tr. The validity of the TTSP principle (or of thermorrheological simplicity) may be judged by the quality of the master curve and shift factor plot [54]. Typically smooth master curves and smooth shift factor plots are the criteria for validity. In addition, all viscoelastic properties have to be superimposable with the same shift factor plot. In some cases, vertical shifting may be required and can be deduced from rubber elastic theory. Figure I.3.5 and Figure I.3.6 illustrate a master curve and a shift factor plot for the storage compliance of poly-n-octyl methacrylate, for example [54].

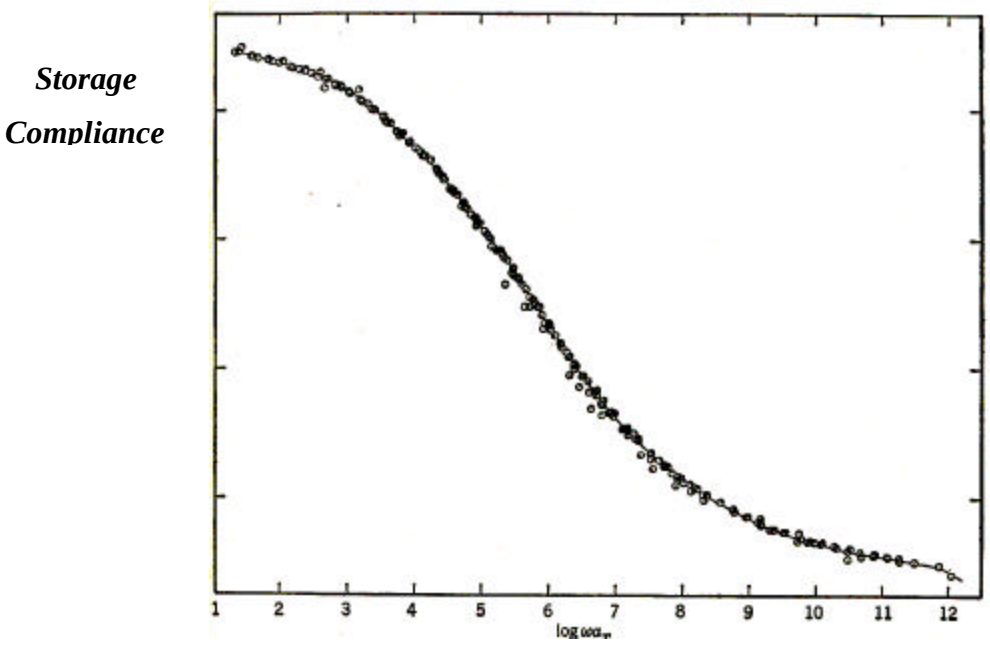

Figure I.3.5. Storage Compliance Master Curve for Poly-n-Octyl Methacrylate Demonstrating the Smooth Fit of Thermorheological Simplicity (From [54])

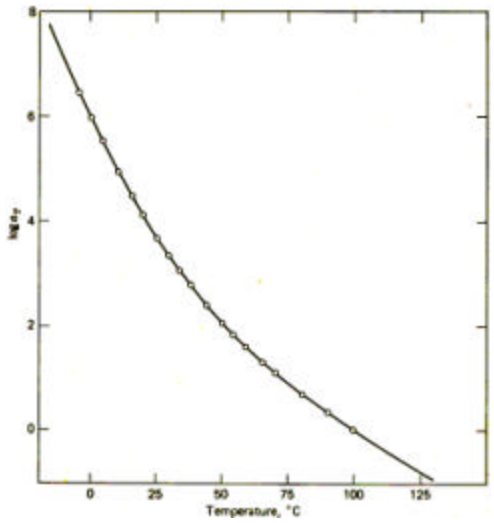

Figure I.3.6. Temperature Dependence of the Shift factor for Fig 5. (From [54])

For those materials that follow TTSP, Williams Landel and Ferry found that the temperature dependence of the shift factor may be modeled as [54]:

(I.3.13)
$$\log a_T = \log \frac{E'(T)}{E'(T_r)} = \log \frac{t(T)}{t(T_r)} = \frac{-C_1(T-T_r)}{C_2+(T-T_r)}$$

Equation (I.3.13) is referred to as the WLF equation and is typically valid in the temperature window [T_g-10°C; T_g +100°C]. The WLF constants, C_1 and C_2 can be retrieved by linearizing the WLF equation.

(I.3.14)
$$\frac{1}{\log a_T} = -\frac{C_2}{C_1}\frac{1}{(T - T_r)} - \frac{1}{C_1}$$

For amorphous polymers, WLF constants with values, C_{1g} = 16.7 and C_{2g} = 51.6K have been repeatedly measured when the master curves are referenced to the glass transition temperature [54]. While these values were first believed to be universal, it is now recognized that different polymers display different constants [53]. However, the success of the WLF equation for portraying polymer viscoelastic properties around the glass transition raises the hypothesis that a universal phenomenon may underlie the glass transition. In fact, a number of glass formation theories give significance to the apparent success of empirical models such as the WLF equation for portraying viscoelastic properties of glasses.

I.3.4 Glass Formation Theories

Among the theories developed to explain glass formation in polymers, the free volume theory is one of the most commonly accepted [54]. However, recent developments in this field have seen the emergence of another concept, that of intermolecular cooperativity, which offers another perspective on the "universal behavior" of amorphous polymers near their glass transition temperature.

I.3.4.1 Free Volume theory

The free volume (V_f) refers to the volume which is not occupied by matter within the total volume (V). The fractional free volume, f, is then simply the fraction of the free volume over the total volume (Figure I.3.7). As an amorphous polymer is heated, the free volume undergoes a sudden increase in its temperature dependence at the glass transition temperature. The glass transition temperature marks the onset of free volume expansion (Figure I.3.7).

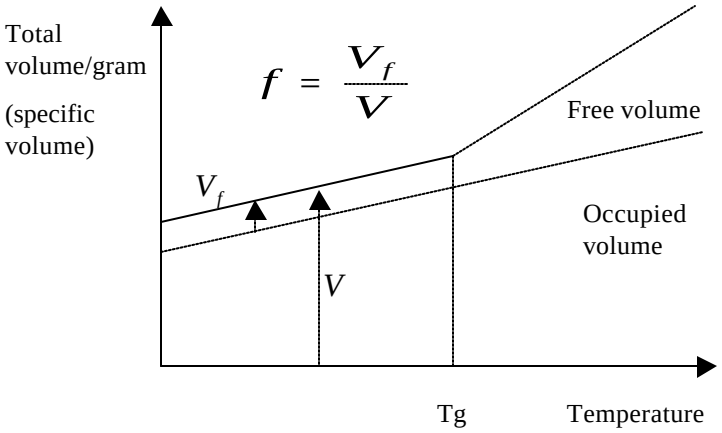

Figure I.3.7. Free Volume-Temperature Relationship forAmorphous Polymers

Assuming a constant free volume below T_g, the fractional free volume, f, may be expressed as [54]:

(I.3.15) $$f = f_g + \Delta a_f (T - T_g)$$

In Equation (I.3.15), f_g represents the fractional free volume at T_g and $\Delta\alpha_f$ is the difference in expansion coefficients between the liquid state and the glassy state. It is generally accepted that the glass transition is an iso-fractional free volume point meaning that all polymers display the same value for f_g of approximately 0.025±0.003 [54]. Doolittle experimentally demonstrated that the temperature dependence of viscosity relates to that of the free volume [60].

(I.3.16) $$h(T) = Ae^{\left(\frac{B}{V_f(T)}\right)}$$

In equation (I.3.17) A and B represent some constants. Substituting the expression for fractional free volume (I.3.15) into the Doolittle equation and recognizing that $a_T = \frac{h_T}{h_{T_g}} = \frac{t_T}{t_{T_g}}$ yields another expression for the temperature dependence of the shift factor:

(I.3.17)
$$\log a_T = -\frac{\left(B/2.303 f_g\right)\cdot\left(T - T_g\right)}{f_g/\Delta a_f + T - T_g}$$

Hence the WLF constants are easily rewritten in terms of the fractional free volume at the glass transition temperature and the thermal expansion coefficients. These material properties therefore provide a fundamental ground for the success of the WLF equation in describing relaxation mechanisms around the glass transition. Another perspective on the temperature dependence of molecular motions around the glass transitions has been afforded by the concept of molecular cooperativity.

I.3.4.2 Cooperative Motion at the Glass Transition

Adam and Gibbs first introduced the concept of molecular cooperativity with their model of glass relaxation in 1965 [61]. The Adam-Gibbs model (AG) stems from the transition state theory for molecular relaxation. The transition state theory simply pictures molecular relaxation from state A to state B as overcoming an energy barrier, where the population for each state follows a Boltzmann distribution [54]. However, rather than simply generalizing the transition state theory, Adam and Gibbs postulated that molecular relaxation occurs in a number of cooperatively rearranging molecular entities, a z* number at temperature T, z*(T) [61]. Assuming that at a fixed temperature, the cooperatively rearranging regions relax simultaneously, enabled AG to express one characteristic relaxation time:

(I.3.18)
$$t(T) = t_0(T)\exp(z*(T)\times\Delta m/kT)$$

In Equation (I.3.18), τ_0 (T) represents the relaxation time for independent relaxation at a temperature T well above T_g, k is the Boltzmann constant and $\Delta\mu$ is the transition state activation energy. Adam and Gibbs postulated that the slowing of molecular relaxation as a glass-forming liquid is cooled is associated with an increasing number of cooperatively rearranging molecular entities [61]. In addition, they associated this kinetic freezing with a decrease in configurational entropy [61], [64]:

(I.3.19)
$$z*(T) = \frac{N_A s_c^*}{S_c(T)}$$

In equation (I.3.19), s_c^* represents the entropy of the smallest number of rearranging molecular entities, N_A is Avogadro's number and S_c is the configurationel entropy of the material. Substituting Equation (I.3.19) into the expression of the characteristic relaxation time (Equation (I.3.18)) yields to the AG equilibrium equation:

(I.3.20)
$$t(T) = A\exp\left(\frac{B}{TS_c(T)}\right)$$

Where A is some constant and:

(I.3.21)
$$B = \frac{N_A s_c^* \Delta m}{kC}$$

In other words, as a glass-forming liquid is cooled, the decrease of configurational entropy is accompanied by a slowing of molecular relaxation, which occurs in larger cooperative units. This configurational entropy approach to molecular relaxation stems from previous theories on glass formation, namely the Gibbs-DiMarzio model, which attempted to resolve the "Kauzmann paradox" [62], [63]. When extrapolating the equilibrium properties of glass-forming liquids (volume, enthalpy and entropy) to low temperatures, Kauzmann identified a thermodynamic crisis [63]. Namely, the extrapolated properties become less than those of the corresponding crystal at a temperature, T_K, below the glass transition but well above absolute zero [63]. This observation violates the third law of thermodynamics. The Gibbs-DiMarzio theory solves the Kauzmann paradox by associating glass formation with a zero entropy state at a temperature T_2 [62]. The ground state temperature T_2 is then viewed as a true thermodynamic transition, which underlies the kinetic glass transition. In essence, T_2 has the same physical meaning as T_K [64]. Hence, building upon the Gibbs-DiMarzio theory, AG simply computed the temperature dependence of the configurational entropy from heat capacity changes (ΔC_p):

(I.3.22)
$$S_c(T) = \int_{T_2}^{T} \frac{\Delta C_p(T)}{T'} dT'$$

Finally assuming ΔC_p to be constant and substituting the expression for S_c into equation (I.3.20) yields the temperature dependence for structural relaxation in glasses as formulated by AG:

(I.3.23) $$t(T) = Ae^{\left(\Delta m / RT\left[1-\left(T_2/T\right)\right]\right)}$$

While the AG theory addresses for the first time glass relaxation on the basis of intermolecular cooperativity and configurational entropy, it yields an equivalent expression to the empirical Vogel-Fulcher-Tamman-Hesse equation [65], [66], [67]. It can also be demonstrated that above the glass transition, the equilibrium AG equation is comparable to the WLF equation when:

(I.3.24) $$T_2 = T_g - C_2$$

(I.3.25) $$\Delta m = 2.303RC_1C_2$$

(I.3.26) $$\ln A = \ln(t_g) - 2.303C_1$$

Therefore a configurational entropy approach seems to justify again the success of empirical viscoelastic models. At the time it was published, however, the AG theory received little attention and glass theoreticians favored the more intuitively appealing free volume theories [68]. In the past decade, the contribution of Adam and Gibbs to glass formation theories has been recognized thanks to Angell's work on inorganic glasses [69].

I.3.4.3 Angell's Concept of Fragility

Angell introduced the concept of fragility by considering a topographical representation of glass forming liquids. Namely, he pictured a glass-former hypersurface with a two-dimensional diagram of potential energy surface versus some collective coordination number, z (Figure I.3.8) [68].

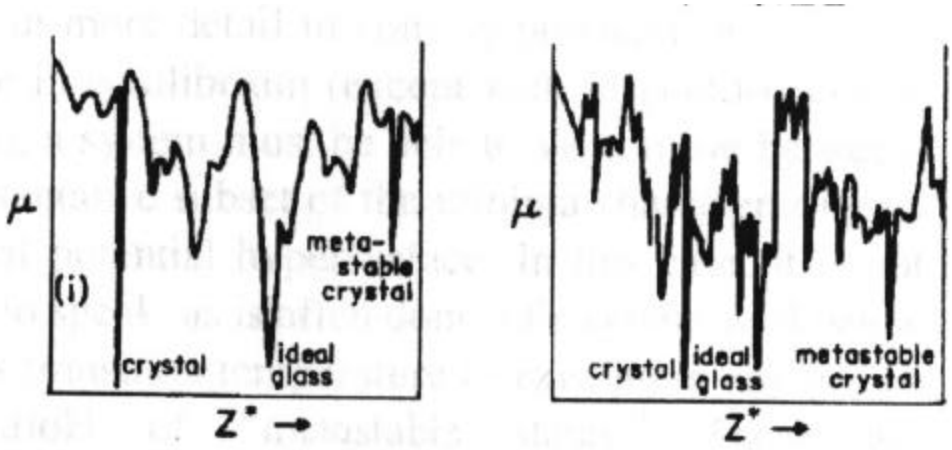

Figure I.3.8. Potential Energy Surface Proposed by Angell for "Strong"(left) and "Fragile" (right) Glass-forming Liquids (from [68])

When some thermal energy, kT, is supplied to a glass-forming liquid, it adopts those configurations of lowest energy state. This implies that, notwithstanding kinetic limitations, glass-forming liquids access all potential minima that have lower energy than kT. Angell proposes that the smaller the number of minima, the harder it is for the glass-forming liquid to find such minima [68]. This postulate is in essence equivalent to Adam and Gibbs inverse relationship between relaxation time and configurational entropy. Indeed, the smaller the number of minima, the lower the configurational entropy of the liquid and the longer the time required for relaxation to occur. On this basis, two scenarios may be envisioned as presented in Figure I.3.8. Glass-forming liquids with low density of minima exhibit a slow decrease in configurational entropy as they are cooled past the glass transition. Such glass-forming liquids are characterized by small changes in thermodynamic properties (entropy, volume and enthalpy) and small heat capacity drops at the glass transition [69]. As a consequence the structure of the glass-forming liquid is only slightly changed at the glass transition. For this reason Angell coined such materials "strong" liquids. A "fragile" liquid on the other hand, has a high density of potential minima. Upon cooling, it experiences substantial changes in the number of available potential minima and thereby substantial changes in configurational entropy,

free volume and enthalpy. For such a liquid, the heat capacity drop at the glass transition is significant and causes a loss of the liquid short-range order at the glass transition. Hence the term "fragile" introduced by Angell. Another perspective on the concept of fragility is that structural relaxation in fragile materials deviates significantly from Arrhenius behavior. Logically then, Angell found it practical to classify strong and fragile behavior from Arrhenius plots where the temperature scale is a normalized or reduced temperature, T/T_g [68]. In such "fragility plots", fragile materials display a significant curvature, while strong materials exhibit a near Arrhenius (linear) temperature dependence. Fragile and strong behaviors are illustrated in Figure I.3.9.

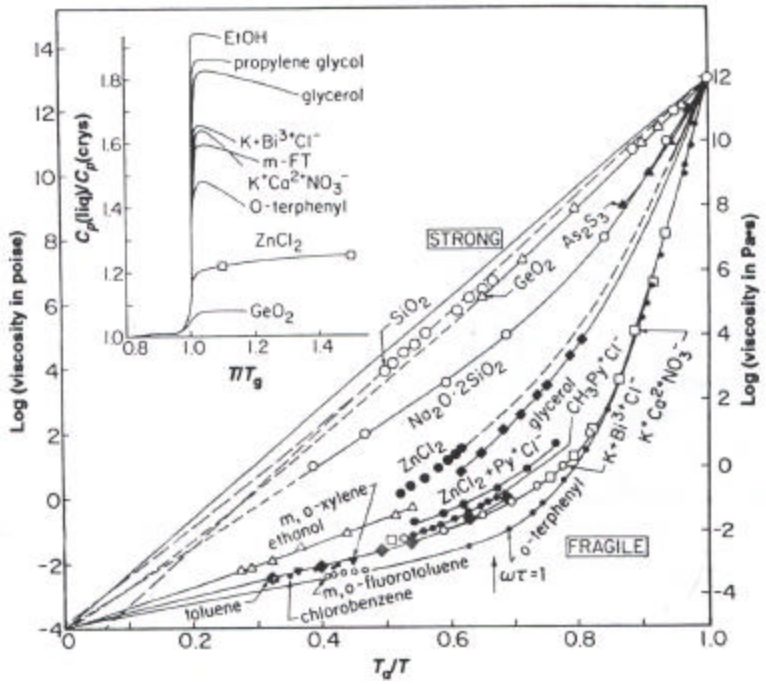

Figure I.3.9. Angell's Fragility Plot (from [69])

Qualitatively, Angell utilizes the same configurational approach as that first introduced by Adam and Gibbs. However, with Angell, the Kauzmann paradox is incorporated into the configurational entropy, by modeling ΔC_p as a hyperbolic function of temperature rather than a constant. This approach appears more appropriate than that of AG since it is in accordance with experimental observation [69]. The temperature dependence of the configurational entropy is then expressed as:

(I.3.27)
$$S_c(T) = \frac{K(T - T_k)}{TT_k}$$

Again substituting Equation (I.3.27) into the AG equilibrium equation (I.3.20) leads to:

(I.3.28)
$$t(T) = t_0(T)\exp\left[a\left(\frac{\Delta m}{K}\right)\frac{T_k}{T - T_k}\right]$$

In this expression, K represents the number of potential minima of the hypersurface and $\Delta\mu$ is the energy barrier to the potential minima. Identifying T_k as T_o, it can be shown that this expression is equivalent to the VFTH equation (I.3.29)

(I.3.29)
$$\log a_T = \frac{1}{a(T - T_0)} - b$$

Where α and β are constants. While Angell has provided one of the greatest advances in the field of glass formation, his work essentially focused on inorganic glass-formers. It did not take long however for polymer science to benefit from Angell's developments. The work from Ngai, Plazeck and Roland was decisive in this matter.

I.3.4.4 The Cooperativity Analysis for Polymeric Glasses

In an attempt to apply the concept of fragility to polymers, Ngai was able to refine the AG theory for polymeric glasses, which yielded a novel coupling model for describing relaxation in amorphous polymers [56], [57]. In the Ngai coupling model, two domains of relaxation are proposed. At a temperature far above T_g ($T > T_g + 80K$), segmental relaxation is independent of non-bonded segments and occurs via bond rotation with a characteristic relaxation time, the primitive relaxation time [70]. The primitive relaxation time (τ_0) is that of an isolated chain as in the AG model and involves conformational transition rates (Equation (I.3.18)). At temperatures below $T > T_g + 80K$, molecular motions are restricted by intermolecular coupling between non-bonded segments. Hence, relaxation times in this temperature region are longer due to

organization in cooperatively rearranging molecular entities. Matsuoka provides a descriptive picture of the concept of intermolecular cooperativity among non-bonded segments (Figure I.3.10) [58].

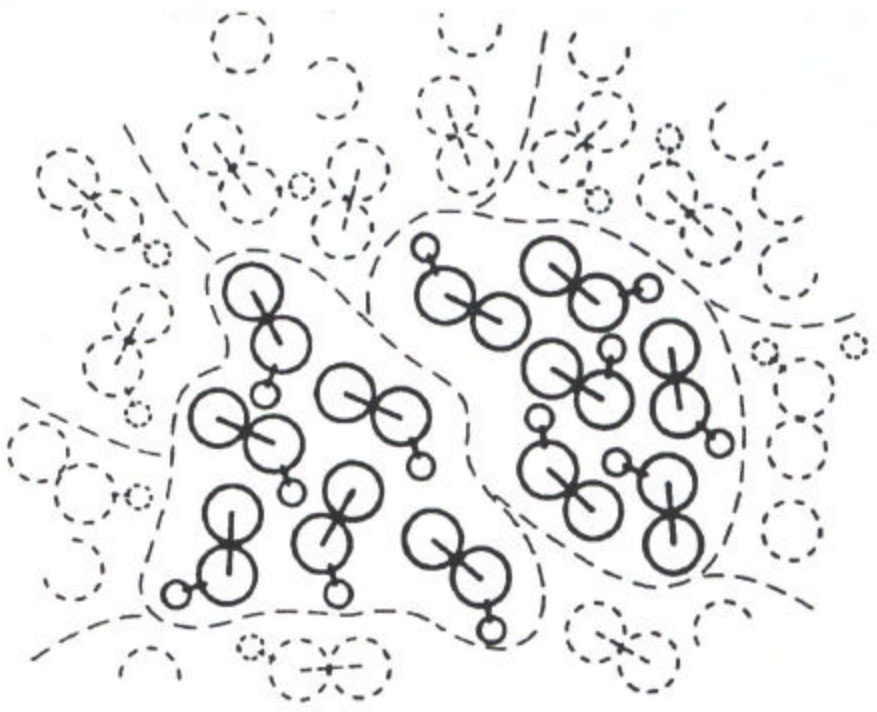

Figure I.3.10. Matsuoka Representation of Cooperative Domains with z=6 (from [58])

Again the occurrence of cooperative regions is nothing novel compared to the AG theory. In the AG theory however, it is assumed that all cooperative regions z* (T) relax simultaneously so that one single relaxation time describes the relaxation process at one temperature (Equation (I.3.18)). This allows the AG theory to model the relaxation process as a simple exponential function of time. It is empirically well established, however, that the relaxation function near the glass transition deviates from simple exponential behavior. In fact, for glass-forming polymers, the Kohlrausch-Williams-

Watts (KWW) equation describes a stretched decay function, $\phi(t)$, for portraying the distribution of characteristic relaxation times (τ^*) around the glass transition [71]:

(I.3.30) $$f(t) = \exp\left[-\left(t/t^*\right)^b\right]$$

In Equation (I.3.30), β ($0 < \beta \leq 1$) is the non-exponentiality parameter which describes the distribution breadth of relaxation times [71]. Recognizing this major pitfall of the AG theory, Ngai proposed to reconcile the AG approach with the experimental observation of non-exponential behavior of the glass transition dispersion. Specifically, Ngai argued that in condensed matter, interactions between neighboring molecules impede simultaneous and independent relaxation of cooperative regions [72]. Rather, intermolecular interactions generate dynamic heterogeneity, which is well portrayed by a distribution of relaxation times. At a temperature-insensitive cross-over time t_c, molecular relaxation changes from an independent and exponential process to an intermolecularly coupled process. At times below t_c, the relaxation function is equivalent to that obtained from the AG theory with independent and simultaneous relaxation:

(I.3.31) $$f(t) = \exp\left(-t/t(T)\right)$$

For time scales longer than t_c however, intermolecular interactions slow down the relaxation process so that the relaxation function becomes a stretched exponential function as in the KWW expression:

(I.3.32) $$f(t) = \exp\left[-\left(t/t^*(T)\right)^{1-n}\right]$$

In Equation (I.3.32), the coupling constant, n, quantifies the extent of intermolecular coupling among non-bonded segments and assumes values from 0 to 1. It is easily seen that the coupling parameter relates to the KWW exponent as $n = 1-\beta$. Continuity of the relaxation function at $t = t_c$, allowed Ngai to generalize the coupling model for any time scale as:

(I.3.33) $$t^*(T) = \left[(1-n)w_c^{\,n} t_0(T)\right]^{1/(1-n)}$$

In equation (I.3.33), ω_c is the crossover frequency between independent segmental relaxation and cooperative segmental relaxation. Hence when n equals 0 the coupling model describes a single exponential relaxation function with a characteristic time τ_0 as for a simple Maxwell element. When the coupling constant assumes a positive value, the model describes a non-exponential distribution of relaxation times. High values of the coupling parameter indicate high degrees of intermolecular coupling or cooperativity. The equivalence between the magnitude of intermolecular coupling and the breadth of the relaxation spectrum proposed by Ngai is intuitively satisfactory. Indeed, polymers are best described by statistical factors, such as average molecular weights, average topology and average stereochemistry. Statistical heterogeneity in polymers yields molecular motions that are dynamically heterogeneous hence generating a broad distribution of relaxation times. As a consequence segmental relaxation does differ throughout a bulk polymer sample. The more intermolecular coupling, the more each polymer segment has its relaxation mechanisms influenced by the neighboring segments and the broader the distribution of relaxation mechanisms. Hence the coupling model succeeds in quantifying the deviation from exponentiality observed in polymeric glass relaxation. What also clearly emerges from the coupling model is that the temperature dependence of τ_0 is amplified in the dense phase by the power 1/(1-n) as a result of intermolecular coupling. Because the coupling model captures the temperature dependence of a characteristic relaxation time, Plazeck and Ngai reformulated the model with a shift factor function [73]. Taking the ratio of relaxation times at a temperature T and at a temperature T_g, they obtained:

(I.3.34) $$(1-n)\log a_T = (1-n)\log\frac{t^*(T)}{t^*(T_g)} = \log\frac{t_0(T)}{t_0(T_g)}$$

When plotting the shift factor versus $(T-T_g)/T_g$, the fractional deviation from T_g, polymers exhibiting the steeper slope were associated with higher intermolecular cooperativity (Figure I.3.11). When further plotting the shift factor corrected by the term (1-n) for the same series of polymers versus $(T-T_g)/T_g$, Plazeck and Ngai found that all polymers fall on the same curve (Figure I.3.12) [73]. In other words, the primitive segmental motion in all polymers was found to display the same temperature dependence [73]. This suggests that the segmental motion underlying the glass relaxation is the same in all polymers. It is important to point out however that this study was based on data for polymers that were slowly cooled into the glassy state closer to thermodynamic equilibrium. Polymers that are far away from thermodynamic equilibrium may therefore diverge from this behavior.

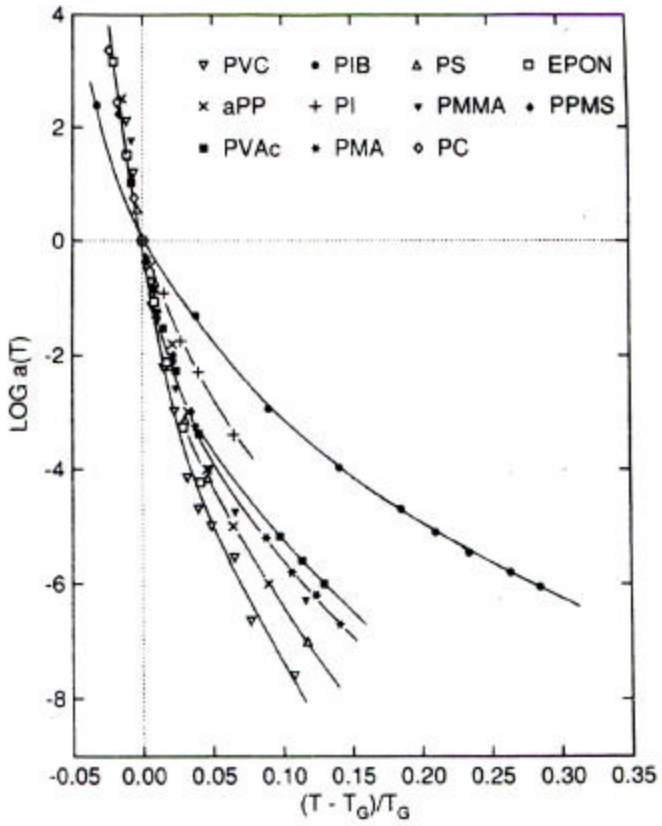

Figure I.3.11. Cooperativity Plots for a Variety of Polymers (from [73])

In this study, Plazeck and Ngai empirically found that a WLF-form equation fits the data when the constants are defined as C_1= 5.49 and C_2=0.141

(I.3.35)
$$(1-n)\log a_T = \frac{-C_1\left(\frac{T-T_g}{T_g}\right)}{C_2+\left(\frac{T-T_g}{T_g}\right)}$$

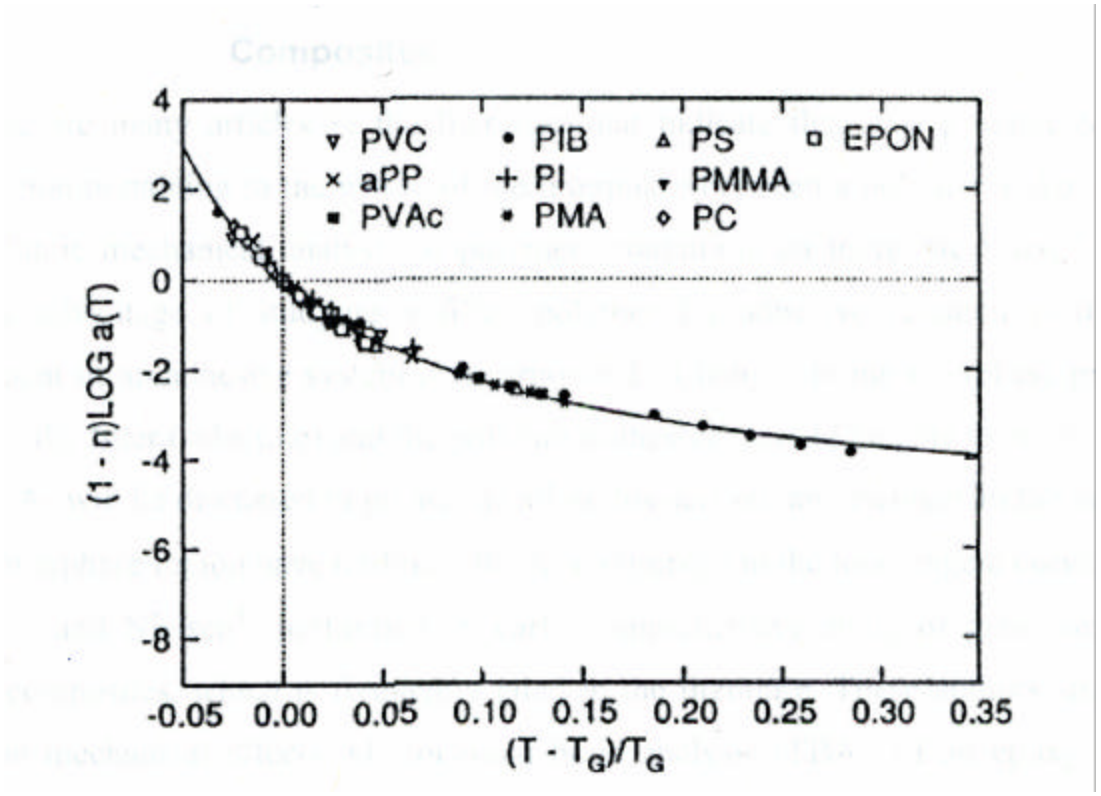

Figure I.3.12. Shift Factor Corrected by (1-n) for a Variety of Polymers (from [73])

The coupling constant can therefore be retrieved by normalizing the WLF shift factor to the fractional deviation from the T_g. This implies that in addition to portraying the distribution of relaxation mechanisms in the vicinity of the glass transition (or non-exponential behavior), the coupling model quantifies deviations from Arrhenius behavior. Typical coupling constants for polymers lie in the 0.35-0.75 range [76]. Polymers that display high intermolecular cooperativity (high n value) around the T_g are characterized

by a broad distribution of relaxation mechanisms and a significant deviation from Arrhenius behavior around the glass transition. On the other hand, polymers with little intermolecular cooperativity (low n value) around the T_g are dynamically more homogeneous and display a relatively narrow distribution of relaxation mechanisms as well as near Arrhenius behavior. In this perspective, the coupling model has emerged as a unique tool to further characterize polymer alpha transitions. The contribution of the coupling model to the fundamental understanding of polymer viscoelasticity can be appreciated by its remarkable success on a variety of polymers [74]-[78]. In fact, intermolecular cooperativity has been explained on the basis of polymer chemical structure [74]. As expected, structural features of the polymer backbone (polarity, symmetry and steric hindrance) are reflected in the coupling constant [76]. In general, polymers with smooth, flexible and symmetrical backbones display low coupling constants while polymers with less flexible backbones, sterically-hindering pendant groups and high polarity exhibit broader segmental relaxation and greater intermolecular cooperativity [74]. For instance, Robertson and coworkers showed that the α relaxation of polybutadienes broadens and intermolecular coupling increases as the vinyl content increases from 1,4 polybutadiene to 1,2 polybutadiene [78]. Similarly, epoxydization of 1,4-polyisoprene promotes segmental cooperativity at the glass transition [75]. In fact, the recent literature abounds with cooperativity studies on bulk polymers and the success of the coupling model for investigating intermolecular interactions in bulk polymers is well established.

Of greater interest for the scientist seeking to adapt such methods to wood/adhesive composites are those studies that deal with polymer blends. A few studies are available on polymer blends [79]-[84]. A review of cooperativity analysis for common miscible polymer blends such as poly(vinylethylene)/ polyisoprene, polyvinylmethylene/ polystyrene and tetramethyl polycarbonate/ polystyrene is provided by Roland and Ngai [82]. Regardless of specific interactions in polymer blends, a general trend indicates broadening and steeper temperature dependence of the alpha-relaxation upon blending [82]. This phenomenon can be ascribed to the fluctuations in local composition in the blend. In addition, Roland and Ngai often observe an asymmetrical broadening on the low frequency side of the glass transition for miscible

polymer blends [82]. Inhomogeneous broadening is in accordance with the high T_g component influencing the low frequency tail of the blend glass transition [82]. A more recent study suggests that the cooperativity analysis may be utilized for probing specific interactions in miscible polymer blends [84]. In this study, the temperature dependence of relaxation mechanisms in blends of polystyrene (PS) and poly(2,6-dimethyl-1,4-phenylene oxide) (PPO) is investigated as a measure of intermolecular cooperativity. It is reported that PS/PPO blends display greater intermolecular cooperativity than that expected on the basis of the neat polymers [84]. The authors point out that while compositional heterogeneity in blends is generally invoked for greater cooperativity in miscible polymer blends, attractive intermolecular interactions shall have a similar effect on cooperativity [84]. It seems however difficult to assess the specific contributions of concentration fluctuations and intermolecular interactions to enhanced cooperativity in polymer blends. In this study nevertheless, both specific interactions and concentration fluctuations are believed to induce the broadening and steeper temperature dependence of the alpha-relaxation in PS/PPO blends [84]. More interesting, the coupling model has been successfully applied to complex composite systems such as Epoxy/E-glass composites [85]. For Epoxy/E-glass composites, the coupling constant afforded a more sensitive probe of viscoelastic properties than the simple determination of glass transition temperatures [85].

The widespread success of the coupling model for neat polymers and more complex polymeric systems is well established. It is especially noteworthy that the coupling model successfully describes relaxation in composites. Wood itself is a complex composite structure of polymers. In spite of its complexity, one may expect that the coupling model affords a greater understanding of wood viscoelastic properties. The next section aims at reviewing the advances in the field of wood viscoelasticity. Reviewing the actual knowledge on the viscoelastic characterization of wood will help one appreciate the potential of the coupling model for wood itself but also for wood/ adhesive composites.

I.3.5 Viscoelastic Properties of Wood

Owing to its importance in forest product technologies, extensive efforts have concentrated on wood viscoelasticity. Wood polymer glass transitions are particularly critical to the manufacture of many wood products. For instance, lignin softening plays a crucial role in pulp and paper manufacture [95]. As a consequence, the past two decades have seen significant advances in the understanding and modeling of wood polymer glass transitions. Along with these advances, analysis of wood viscoelastic properties has emerged as a powerful tool to characterize the molecular scale changes induced by a variety of treatments. Of particular interest for the wood adhesives field, changes in wood viscoelastic properties may reveal wood/adhesive interactions [113]. In this section, the reader is introduced to the most important advances in characterizing and modeling wood viscoelastic properties. Analysis of wood viscoelastic properties as a tool to probe interactions with extraneous compounds will also be discussed.

I.3.5.1 Viscoelastic properties of wood

Early studies have focused on the viscoelastic properties of isolated wood polymers. While it is recognized that properties from isolated wood components may not reflect the in-situ polymers, a thorough understanding of the viscoelastic response of each wood component aids in comprehending wood viscoelastic behavior.

I.3.5.1.1 Viscoelastic Properties of Isolated Wood Polymers

Wood is a composite of 3 polymers, cellulose, hemicellulose and lignin. Each of these polymers has a specific chemical structure, topology, molecular weight distribution and morphology, and therefore they display different viscoelastic properties. Owing to the importance of the cellulose industry, cellulose viscoelastic properties have been extensively studied [86], [89]-[92]. Cellulose can be either amorphous or semi-crystalline. However, because of the strong association in the cellulose crystal lattice, thermal degradation of cellulose occurs before melting and only the glass transition can be detected. For dry cellulose, the glass transition temperature has been repeatedly measured at around 230 °C from heat capacity and mechanical measurements [87], [95]. As expected for semi-crystalline polymers, the crystallinity index has a significant impact on cellulose glass transition [93]. In fact, upon recrystallization of amorphous cellulose,

Yano et al. observed an increase of the glass transition temperature from 200°C to 236°C [86]. In addition, the abundance of water adsorption sites suggests that water shall have a major effect on the cellulose glass transition temperature. Salmén and Back performed a systematic study of the water content effect on cellulose glass transition and observed a T_g depression with increasing moisture content in accordance with the Kaelble equation [93]. Water plasticizing effect on cellulose is dramatic. For instance, at moisture contents exceeding 30% and regardless of the crystallinity index, the glass transition of cellulose is depressed from 220°C to sub-ambient temperatures [93]. At sub-ambient temperatures also, secondary relaxations have long been recognized for dry and wet amorphous cellulose [86]. More specifically, water-sensitive relaxations, termed γ and β relaxations have been repeatedly observed at around -120 °C and –50°C respectively [88]. Montes and coworkers recently proposed a molecular interpretation for these relaxations [89], [90], [91]. Based on dielectric, mechanical measurements and molecular modeling, the authors attributed the γ relaxation to the rotation of hydroxyl and hydroxymethyl groups. The entropic origin of the β relaxation on the other hand favored the hypothesis of localized motions of the main chain [89]-[91]. These molecular interpretations are at odds with more recent studies [92]. In fact, Norimoto et al. propose that the γ relaxation reflects the rotation of hydroxymethyl groups only while the β relaxation may be associated with motion of hydroxyl groups rather than localized segmental motion [92]. In spite of this controversy, it remains that cellulose viscoelasticity is well characterized by two sub-ambient secondary relaxations and an α relaxation which occurs around 200°C in the dry state and is depressed to sub-ambient temperatures in the wet state.

The molecular structure of hemicelluloses is somewhat similar to that of cellulose, although hemicelluloses are highly branched heteropolysaccharides of lower molecular weight. Hence, the secondary relaxations observed for cellulose, namely the hydroxymethyl rotation and adsorbed water relaxation are also characteristic of isolated hemicellulose [92]. However, hemicelluloses experience a glass transition at somewhat lower temperature, at 165°C-225°C for dry hemicellulose [94], [95]. The plasticizing effect of water on hemicellulose has also been evidenced and under water saturated conditions the glass transition drops to approximately 0°C. Recently, Olsson et al.

developed a viscoelastic technique specifically suited for studying the softening behavior of isolated and in-situ hemicelluloses [96]. The method consists of dynamic mechanical measurements of wood during relative humidity scans. Thanks to the sensitivity of this novel technique, it has been found that xylans soften at lower relative humidity than galactoglucomannans [96]. In other words, isolated xylans have a lower glass transition temperature than galactoglucomannans [96]. Xylans are proposed to be closely associated with lignin while galactoglucomannans may be more oriented owing to their intimate association with cellulose. There is as a consequence a good understanding of hemicellulose viscoelastic properties.

Lignin is a highly branched, high molecular weight, and more hydrophobic polymer built upon phenyl propane units. Studies on isolated lignin have helped identifying a glass transition temperature in the vicinity of 200°C for its dry state [87]. Lignin glass transition is also water sensitive, but to a lower extent than wood carbohydrates owing to its reduced hydrophilicity. For instance water saturated spruce lignin exhibits a glass transition in the vicinity of 90°C [97].

It clearly emerges from the viscoelastic properties of isolated wood polymers, that under dry conditions all three polymers display comparable glass transition temperatures while water differentiates the temperature window over which each polymer experiences the glass transition. Therefore, in wood, notwithstanding the effect of morphology on polymer relaxations, one can hope to isolate the *in-situ* glass transition of each wood polymer within a temperature window by varying wood moisture content. The next section provides an overview of wood component viscoelastic properties, as they have been observed and modeled *in-situ* within specific ranges of temperature and moisture content.

I.3.5.1.2 In-situ Viscoelastic Properties of Wood

Because plasticizers play an important role in the pulp and paper technology, early research has focused on wood viscoelastic properties under the influence of plasticizers [94], [97], [98]. Water is the most universal plasticizer in the manufacture of wood products. In 1984, Irvine utilized Differential Thermal Analysis (DTA) to characterize wood softening as a function of moisture content [94]. Under saturated

conditions, wood exhibited a main softening in the vicinity of 60-90°C, which was ascribed to the lignin glass transition. It must be remembered that under wet conditions, both isolated cellulose and hemicellulose have their glass transition temperatures depressed to or below 0°C [94], [93]. Hence, at room temperature or higher, the viscoelastic properties of saturated wood is governed by *in-situ* lignin softening. The same year, Salmén published significant results on the viscoelastic characterization and modeling of *in-situ* lignin glass transition under water saturated conditions [97]. In this paper, Salmén demonstrated the applicability of dynamic mechanical measurements for detecting the *in-situ* glass transition of lignin, and for applying TTSP above the lignin α transition [97]. A master curve was created around lignin glass transition and the WLF equation adequately portrayed wood viscoelastic properties in the temperature range [T_g; T_g+70°C]. This work was the first successful attempt to utilize simple viscoelastic models on wood. Soon after this finding, Kelley et al. utilized DMA for characterizing wood viscoelastic properties under a range of moisture contents [98]. In this study, the authors were able to detect two distinct glass transitions, one for hemicellulose and one for lignin, thereby evidencing phase separation in the amorphous wood matrix [98]. In addition, water was found to depress the *in-situ* hemicellulose and lignin glass transitions in accordance with the Kwei approach [98]. The authors were also able to perform TTSP around the *in-situ* lignin glass transition for ethyl formamide plasticized wood [98]. This study demonstrated again that simple viscoelastic models derived for polymers may be applicable to wood. While in both studies, wood was tested across the grain, it was later demonstrated that mechanical testing along the grain also reflects *in-situ* lignin softening and is also amenable to WLF analysis [99]. Typically however, dynamic mechanical testing of saturated wood in the longitudinal direction is less sensitive to lignin glass transition and yields a somewhat higher glass transition temperature [99], [101]. This anisotropic behavior is common for reinforced composites [99]. While the above mentioned studies clearly demonstrate the applicability of simple viscoelastic models to wood, one can question the sensitivity of viscoelastic measurements to the macroscopic and molecular features of wood. In that matter, a comparative study of viscoelastic properties of earlywood and latewood is worth mentioning [106]. In this study, wood was saturated with ethylene glycol and water. With both diluents, earlywood and

latewood displayed similar softening behavior [106]. In addition, plasticization with ethylene glycol was found valuable for probing the entire softening region of *in-situ* lignin [106] and yielded lower glass transition temperatures than water, specifically 84°C versus 90°C as measured by the tan delta peak at 1 Hz. However, in spite of the influence of the supramolecular organization of wood (such as its anisotropy), wood viscoelastic properties also portray the molecular features of its components. In fact a number of viscoelastic studies illustrate the sensitivity of saturated wood viscoelastic properties to lignin molecular features [102], [103], [104]. For instance, Östberg et al. observed from Torsional Braid Analysis that lignin extracted from the middle lamella of wood cells exhibits a higher glass transition temperature than that from the primary wall [102]. Structural and morphological differences were proposed to account for this phenomenon. Lignin in the middle lamella comprises a lower content of free phenolic hydroxyl groups, which according to the authors is indicative of a more cross-linked lignin structure thereby yielding higher T_g values [102]. While the term "cross-linked lignin" may be controversial, the concept of greater branching as a result of more substituted phenolic hydroxyl groups seems appropriate for rationalizing differences in softening behavior on the basis of molecular structure. In this particular study, however, minor structural differences between middle lamella lignin and primary wall lignin may not solely account for the observed difference in lignin glass transition temperatures. More likely, the intimate association of lignin with low T_g proteins would depress its glass transition temperature, as further hypothesized by the authors [102]. In any case, this study suggests that wood viscoelastic properties afford significant sensitivity to the molecular scale morphology and structure of wood components.

Additional comparative studies on various wood species clearly demonstrate the sensitivity and power of viscoelastic measurements for probing the *in-situ* molecular features of wood polymers. For instance, it is now established that hardwood lignins generally display lower softening temperatures than softwood lignins [103], [104], [105]. Some exceptions are reported in the literature and are probably consistent with a large interspecies variability for wood [98]. For instance, in a study comprising 10 hardwood species and 5 softwood species, softwood lignins had a glass transition in the 88-92°C temperature range while hardwood lignins appeared to soften in the 73-88°C temperature

range when saturated wood was tested at 1 Hz [104]. In fact, an inverse correlation between lignin softening temperature and methoxyl group content suggests that the presence of side groups, such as methoxyl groups and free phenolic hydroxyl groups on lignin depresses lignin glass transition [104]. In line with these results, compression wood, which is characterized with a low methoxyl content, exhibits a higher glass transition temperature than normal wood [107]. Such studies illustrate the sensitivity of viscoelastic measurements for probing *in-situ* wood polymer molecular features. More important, the work from Kelley et al. and Östberg et al. illustrate that dynamic measurements can shed light on wood morphology [98], [102]. In that matter, a viscoelastic study utilizing relative humidity scans has largely contributed to a novel comprehension of wood morphology [108]. In this study, comparisons of hemicellulose softening points in native wood, delignified wood and xylan extracted wood suggest a preferred association of xylan with lignin on the one hand and of glucomannans with cellulose on the other hand [96], [108]. This work demonstrates again that dynamic testing under specific conditions can focus on the viscoelastic properties of one particular wood polymer, hemicellulose glass transition in this study. Under humidity and temperature environments that pertain to the hotpressing of wood-based composites, hemicellulose glass transition is also believed to exert a major effect on wood viscoelasticity [109]. For *in-situ* hemicellulose glass transition, several studies suggest that simple viscoelastic models such as the WLF equation also portray adequately wood viscoelastic properties [100], [109]. For instance, Wolcott et al. validated the principle of time-temperature-moisture superposition from stress relaxation experiments of wood at moisture contents pertaining to manufacture of wood-based composites [100]. In a dielectric thermal analysis (DETA) of moist wood, Lenth et al. evidenced a moisture dependent relaxation in line with the in-situ glass transition of amorphous holocellulose [109]. In this study, TTSP was effectively performed around the glass transition for moist wood specimens with up to 20% MC. The same study evidenced differences in the softening behavior of juvenile and mature wood, further illustrating the sensitivity of viscoelastic measurements to wood structural features [109]. The sensitivity of wood viscoelastic properties to structural changes suggests that such properties shall also be

sensitive and informative of the molecular scale impact of physical and chemical treatments of wood. The next section examines this potential.

I.3.5.2 Wood Viscoelasticity as a Tool to Probe Chemical Treatments of Wood

For decades, researchers have utilized viscoelasticity in order to comprehend the molecular scale changes induced by physico-chemical treatments of wood [110], [111], [112]. Of particular interest are the studies that investigate the effect of such treatments on wood component glass transitions. Nakano and coworkers demonstrated that the *in-situ* glass transition temperature of wood components is lowered upon esterification [110]. This effect is all the more marked that the introduced acyl groups have high molar volume, in accordance with the concept that introducing bulky side groups on polymers lower the glass transition [111]. Other researchers have confirmed similar effects for wood acetylation and impregnation with propylene oxide, low molecular weight polyethylene glycol and methyl methacrylate [112]. On the other hand, an opposite trend is expected when the chemical treatment induces crosslinking reactions among wood components. This is for instance the case of formalization, which introduces oxymethylene bridges among wood polymers and which has indeed been observed to restrict the main chain motion of wood polymers [112].

One of the most relevant viscoelastic studies for assessing wood/adhesive interactions has been recently reported by Marcinko et al. [113]. In this study, Marcinko et al. compared the effect of urea-formaldehyde adhesives and isocyanate (pMDI) adhesives on wood softening, which although it is not explicitly attributed to any wood polymers, can be ascribed to *in-situ* lignin. In this study, pMDI induced a severe depression of the glass transition temperature, ΔT_g= 25 °C approximately. The DMA traces published in this study suggest a similar trend for UF treated wood albeit T_g is depressed to a minor extent (approximately 5°C) [113]. The most striking difference between pMDI treated wood and UF treated wood remains that only pMDI induces a significant broadening of the glass transition [113]. In contrast, UF adhesives do not broaden the alpha relaxation of wood. Broadening of the glass transition generally reflects a wider distribution of relaxation mechanisms at the glass transition. pMDI is a very low molecular weight adhesive, which is known to mix intimately with wood

components. Polymeric adhesives such as UF on the other hand are sterically hindered from penetrating deeply into the wood structure. This difference in pMDI and UF adhesives characteristics may well, as proposed by Marcinko et al., generate a wood/adhesive interphase with very different morphologies [113]. This latter study provides a solid ground to believe that viscoelastic measurements are sensitive to the scale of wood/adhesive interactions.

I.3.6 Conclusions

Wood viscoelasticity is successfully modeled with universal and simple viscoelastic models for synthetic polymers. For in-situ lignin and in-situ amorphous holocellulose, the WLF equation adequately portrays the temperature dependence of relaxation mechanisms around the glass transition. In addition, viscoelastic measurements display a significant sensitivity to the molecular features of wood polymers and to the morphology of wood. Because of this sensitivity, viscoelastic measurements on wood and modified wood have encountered great success in detecting the molecular and morphological impact of chemical treatments. Hence, there seems to be a great potential for assessing wood/adhesive interactions on the basis of viscoelastic properties and more specifically viscoelastic properties around the glass transition. Recent theories on glass relaxations have afforded a wealth of information on polymer structure and polymer blend interactions. Logically the next step in characterizing wood viscoelastic properties and wood interactions with extraneous compounds such as adhesives involves the assessment of such theories on wood.

CHAPTER. I.4. CP/MAS NMR OF POLYMERS

I.4.1 Introduction

The development of Cross-Polarization and Magic Angle Spinning Nuclear Magnetic Resonance, CP/MAS NMR, has permitted high-resolution NMR in condensed matter [134]. With this resolution, CP/MAS NMR affords a probe of molecular dynamics in solid polymers [114]. In addition, because NMR measurements reveal chemical structures, molecular dynamics can be probed locally. This is especially true in that isotopic labeling may be used to enhance site specificity. Overall, there exists three CP/MAS NMR methods for probing local molecular dynamics in polymers, namely relaxation time measurements, lineshape measurements and field gradient methods [115]. Relaxation times designate characteristic time scales for the build up or decay of various states of nuclear spin order [115]. Because relaxation times are affected by molecular motions, they constitute an ideal tool for examining molecular scale interactions in polymer blends [114], [115]. That is, when polymers interact on a molecular scale their bulk dynamics and consequently relaxation times are altered. Other CP/MAS NMR experiments take advantage of relaxation behavior to investigate polymer blend morphology. For example, deuterium NMR permits assessing intermolecular CP between blend components [137]-[141]. In blends, intermolecular CP is indicative of angstrom stale miscibility [137]-[141]. Recently, advances in multidimensional NMR have permitted the estimation of domain sizes in miscible polymer blends on the nanoscale [120]. Hence there exists a variety of NMR experiments, relaxation measurements in particular, that are useful for probing polymer blend interactions. Such experiments are promising methods for probing wood/adhesive interactions. In fact, researchers in the field of wood science have long taken advantage of solid state NMR, clearly establishing its potential [128]. For instance, solid state NMR has been decisive for better understanding wood morphology but also for assessing the effect of various treatments on wood polymer dynamics [128]. More recently, the benefit of solid state NMR for probing wood/adhesive bondlines has been clearly demonstrated [142]. The following discussion aims at reviewing the use of CP/MAS NMR and in particular the use of relaxation time measurements for revealing molecular scale morphology. Further

discussion addresses CP/MAS NMR application to wood and especially wood adhesive bondlines. In that objective, it is necessary to lay the foundations of NMR concepts and solid state techniques in the first place.

I.4.2 Nuclear Magnetic Resonance Spectroscopy-Basic Concepts

Nuclei carry charges that in presence of a magnetic field can be described as spinning around the nuclear axis at a specific frequency, the Larmor frequency (ν). As a result, a magnetic dipole is created along the nuclear axis. The magnetic nuclear moment, μ, characterizes the magnitude of the induced dipole. It can be described in terms of quantum mechanics with the spin numbers of 0,1/2, 1 etc. In the presence of an external magnetic field, nuclei with a spin number ($I \neq 0$) assume 2I+1 numbers of orientations or energy states. For instance when a spin- ½, such as ^{13}C or ^{1}H, is placed in a external magnetic field, B_0, its magnetic moment aligns with B_0 in two orientations, α and β respectively associated with the energy levels E_α and E_β (Figure I.4.1).

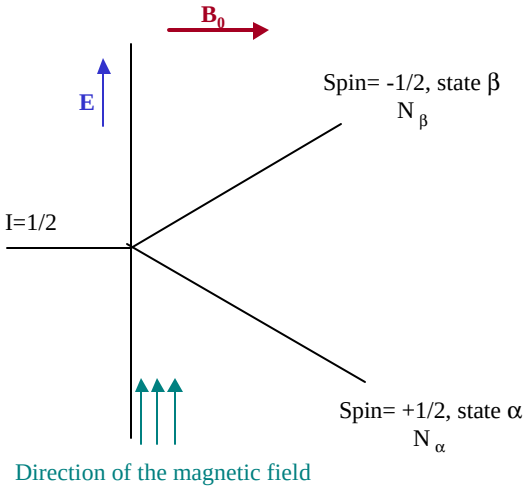

Figure I.4.1. Energy levels for a Spin-½ Nucleus Placed in a Magnetic field B_0 (Adapted from [116])

In accordance with the Boltzmann distribution of spin states, the lowest energy state, E_α, has an excess population ($N_\alpha > N_\beta$) and the difference in energy state is given by:

(I.4.1) $$\Delta E = \frac{hg}{2p} B_0$$

where h is the Planck's constant and γ is the magnetogyric ratio. The magnetogyric ratio is a fundamental nuclear property. Now, when an oscillating magnetic field B_1 is applied perpendicular to B_0, the excess population (N_α - N_β) experiences an energy state transition provided that B_1 oscillates at a frequency ν_1, which satisfies $\Delta E = hn$. In other words, the applied radiofrequency (rf) ν_1 shall satisfy:

(I.4.2) $$n_1 = \frac{g}{2p} B_0$$

This energy state transition induces a magnetic resonance, recorded as the NMR signal. Its intensity scales with the displaced spin population (N_α - N_β). Equation (I.4.2) suggests that all nuclei with the same magnetogyric ratio, γ, enter in resonance at the same applied frequency. In reality, chemically distinct nuclei resonate at distinct frequencies. Indeed, nuclei are shielded from the external magnetic field as a result of their specific electronic environments. Consequently, the effective resonance frequency (or Larmor frequency) depends on the electronic environment as modeled in equation (I.4.3), where σ is a characteristic shielding constant.

(I.4.3) $$n_{eff} = \frac{g}{2p} B_0 (1 - s)$$

It results that chemically different nuclei can be distinguished by NMR. Simply then, an NMR experiment consists of scanning the applied frequency so that Larmor frequencies are successively detected for chemically distinct nuclei. In reality frequency scans have been in use in the early developments of NMR only. Nowadays, pulse techniques permit simultaneous resonance for all nuclei (and therefore shorter acquisition times) and the detected resonance waves or Free Induction Decay (FID) are deconvoluted by Fourrier transform [116]. The detected magnetic resonance is typically represented on a chemical shift scale or "normalized Larmor frequency" scale. A chemical shift (parts per million) is simply defined as the ratio of Larmor frequency (referenced to that of a

reference compound) and the stationary magnetic field. While this description of NMR entails to quantum physics, a mechanical approach is well suited for "physically" depicting NMR spectroscopy. In that approach, the nuclear magnetic dipole precesses at the Larmor frequency about a z-axis, aligned with the external stationary magnetic field B_0. It follows that an assemblage of chemically equivalent nuclei has a net magnetization, M_0, along the z-axis only (Figure I.4.2). When an oscillating field, B_1 is applied perpendicular to B_0 at the Larmor frequency, M_0 is tipped towards the x-y axis where a receiving coil detects the magnetic resonance (Figure I.4.2)

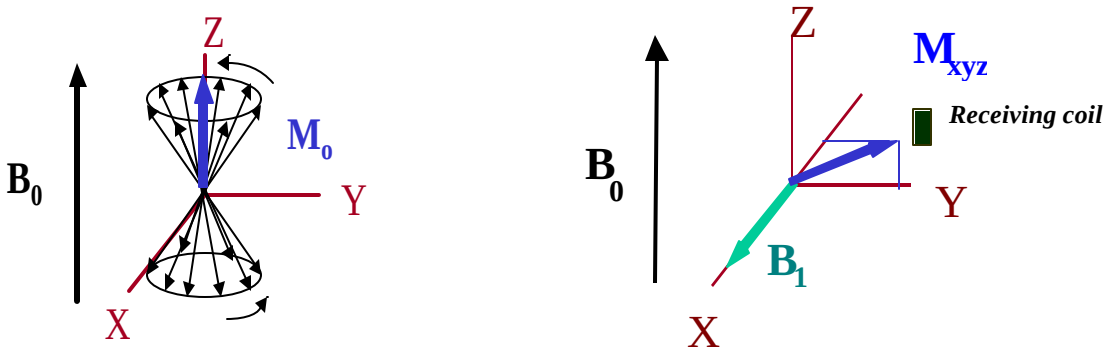

Figure I.4.2. Precession and Magnetic Resonance of a Spin-1/2 in B_o (Adapted from [117])

Following resonance, the M_{xyz} magnetization relaxes progressively towards the equilibrium M_0. The disappearance of the magnetization in the x-y plane takes place at a characteristic time termed the spin-spin relaxation time, T_2. The spin-spin relaxation is reflected in the chemical shift linewidth. The magnetization reappearance along the z-axis results from equilibration with neighboring nuclei and is therefore named the spin-lattice relaxation time, T_1. Spin-lattice relaxation can also be characterized with reference to a frame rotating at the Larmor frequency, in which case it proceeds at a characteristic time $T_{1\rho}$. In essence, molecular motions govern T_1, $T_{1\rho}$ and T_2, although on different time scales. Relaxation time measurements are therefore relevant for probing molecular dynamics and are most widely utilized in solid state NMR. However, solid state NMR requires more sophisticated techniques than solution NMR. In solution NMR, chemical

shift resolution is possible because molecular tumbling averages all anisotropic interactions between the magnetic field and nuclei. For solids on the other hand, anisotropic interactions, mainly dipolar interactions and chemical shift anisotropy dramatically broaden the NMR signal [134]. Dipolar interactions result from interactions between magnetic moments of any non-zero spin nuclei. Chemical shift anisotropy arises from anisotropic shielding with respect to the main magnetic field. In 1976, Schaefer and Stejskal combined two methods, Cross-Polarization (CP) and Magic Angle Spinning (MAS) which first afforded high-resolution NMR spectra of solids [118]. By combining CP and MAS, Schaefer and Stejskal opened novel research avenues towards the chemical, dynamic and morphological characterization of solid polymers [118].

I.4.3 Solid State NMR Techniques

As mentioned above, the dipolar interaction and the chemical shift anisotropy are major causes of line broadening and low resolution for NMR in the solid state. Furthermore, for ^{13}C nuclei, the extended longitudinal relaxation impedes ^{13}C detection in the solid state. Magic angle spinning and high power dipolar decoupling are essential line-narrowing techniques that annihilate anisotropic interactions. Cross-polarization on the other hand enhances signal detection for low natural abundance nuclei such as ^{13}C.

I.4.3.1 Magic Angle Spinning (MAS)

The dipolar interaction between non zero nuclear spins, H_d, can be expressed as a function of the internuclear distance, r_0, the angle between internuclear vector and applied magnetic field, θ, and a constant, c, as [134]:

(I.4.4) $$H_d = c(1-3\cos^2 q)/r_0^3$$

From Equation (I.4.4), one easily deduces that dipolar interactions vanish for θ = 54.7°, angle referred to as the Magic Angle. Therefore, when nuclei are spun at the magic angle with respect to the main magnetic field, dipolar interactions are eliminated thereby permitting significant line narrowing of NMR signals. In addition, spinning at a fast rate neutralizes the chemical shift anisotropy so that only the isotropic chemical shift is retained. Rather, the anisotropic spin interactions become time-dependent allowing for

isotropic chemical shifts but also generating spinning sidebands (SS). When spinning rates significantly exceed the anisotropic spin interactions, SS can be reduced and can be well separated from the chemical shift spectral region [134]. In combination with MAS, solid state NMR techniques often utilize high power decoupling.

I.4.3.2 High Power Dipolar Decoupling

Dipolar decoupling is commonly used in order to eliminate heteronuclear dipolar broadening. In ^{13}C NMR for instance, proton-carbon dipolar interactions can be removed by decoupling the proton channel. In that purpose, the proton channel is irradiated with a strong rf energy. As a result, proton spins flip rapidly and the z-magnetization vanishes thereby preventing proton-carbon coupling during ^{13}C observation. While the combination of MAS with high power decoupling affords high resolution, detection of rare nuclei remains a problem in the solid state. This is especially true for ^{13}C nuclei, which are found in low natural abundance (1.1%) and have a small magnetogyric ratio (hence low detection per ^{13}C nucleus). To further complicate ^{13}C detection in solids, long $^{13C}T_1$s demand excessive recycle delays between pulses. On the other hand, cross-polarization (CP) is a static transfer of spin polarization from abundant to rare nuclei that enhances rare nuclei detection and shortens acquisition times.

I.4.3.2.1 Cross-Polarization

CP techniques are best described with a thermal analogy of spin dynamics [134]. Recall that for spin-1/2 nuclei, the population of high and low energy levels is distributed according to Boltzmann's equation, where C is a constant:

(I.4.5)
$$\frac{N_a}{N_b} = C \exp^{-((E_a - E_b)/RT)}$$

It follows that a spin temperature conceptually portrays spin state distributions. The cooler the temperature, the more unequal the spin state distribution and the more polarized the spin reservoir. Because in NMR, signal intensity directly relates to spin polarization, cooler spin temperatures lead to enhanced sensitivity. In a CP experiment then, rare nuclei are cooled by thermal contact with abundant spins that have been

significantly cooled beforehand. This concept is illustrated in Figure I.4.3, where the abundant and rare spin reservoirs are respectively labeled I and S.

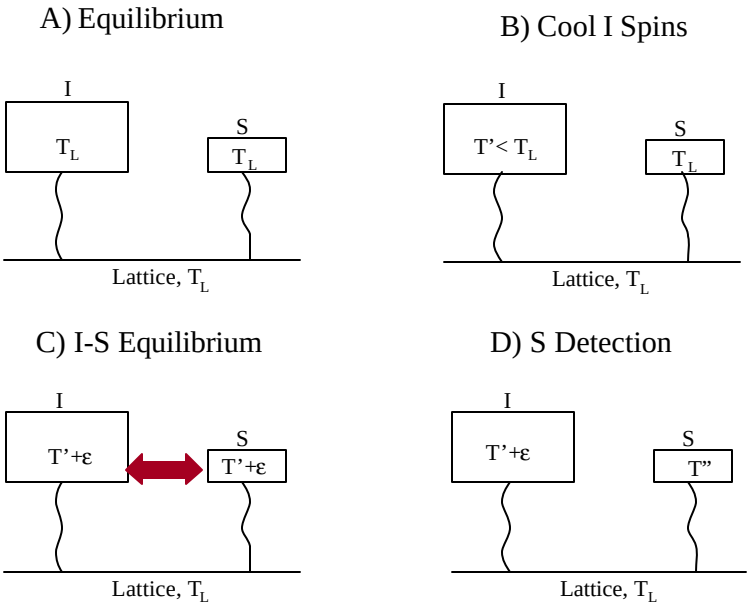

Figure I.4.3. CP Experiment from the Standpoint of Spin Temperatures (after [119])

At equilibrium, both reservoirs have a temperature T_L in accordance with the lattice (Figure I.4.3, A). Reservoir I is then rapidly cooled to a temperature T' so that its polarization is magnified (Figure I.4.3, B). Subsequently, thermal contact is established between the I-spins and the S-spins reservoirs. As a result, the S reservoir is significantly cooled to an intermediate temperature T'+ε (Figure I.4.3, C). In essence this is the CP process during which polarization is statically transferred from abundant to rare nuclei. After a contact time, t_c, thermal contact is released and the highly polarized S-spins are detected (Figure I.4.3, D). During acquisition, the I-spin reservoir is decoupled. From a mechanical standpoint again, proton magnetization is achieved by irradiating the I-spins reservoir with a rf pulse so that the proton magnetization is tipped 90° along the x-axis. Thermal contact is then established by further irradiating both spin reservoirs with appropriate rf pulses. In doing so, both proton and carbon channels are tipped along the

y-axis. This process requires that the proton and carbon rf pulses are matched. In other words the Hartmann-Hahn condition ($w_I = w_s$) must be achieved:

(I.4.6) $$g_I B_I = g_s B_s$$

In equation (I.4.6), B_I and B_S represent the field strength of rf pulses for I and S spin reservoirs, respectively. The CP process with Hartmann-Hann match is depicted for ^{13}C and ^{1}H spin reservoirs in Figure I.4.4.

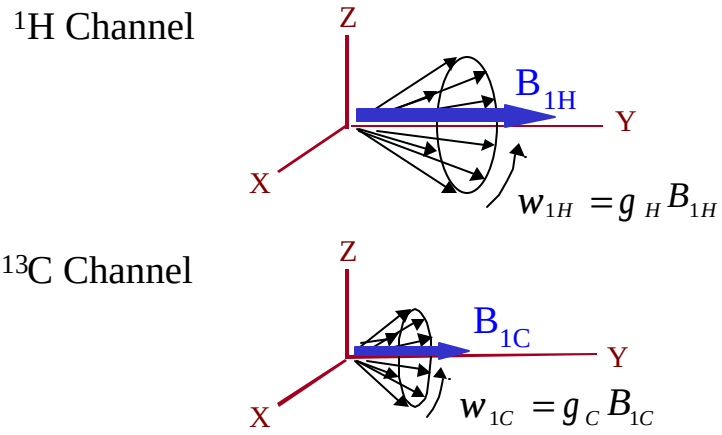

Figure I.4.4. Hartmann-Hahn Match Between ^{13}C and ^{1}H Spins (adapted from [117])

A typical pulse program associated with proton-carbon CP is presented in Figure I.4.5.

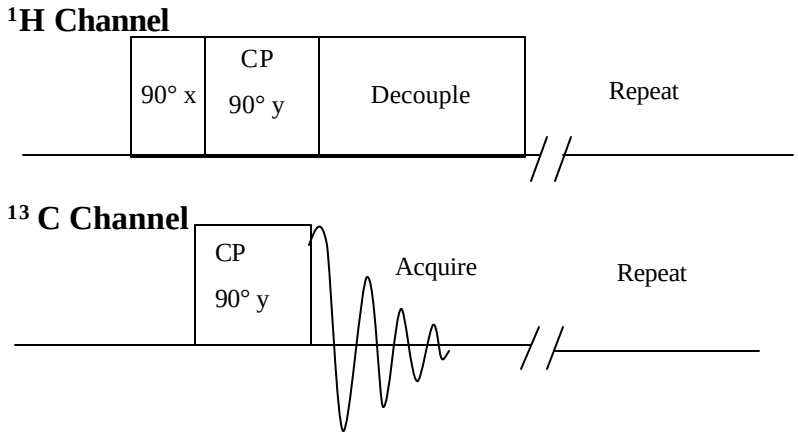

Figure I.4.5. CP Pulse Program (adapted from [134])

The Hartmann-Hahn condition therefore allows magnetization transfer between I and S spin reservoirs. For such a magnetization transfer to be efficient however, the interacting nuclei need to be in close spatial proximity, namely within 10 to 20 angstroms [134]. In addition, the interacting nuclei need to be stationary with respect to the main magnetic field [134]. Consequently both angstrom scale proximity and molecular rigidity play an important role for CP. One easily foresees with these requirements that CP constitutes an ideal tool for probing angstrom scale proximity and molecular scale dynamics in solids. Consequently, probing intermolecular CP between two distinct polymers is one of the most powerful relaxation experiments for assessing angstrom scale miscibility as in polymer blends for instance. There exist a variety of well-established relaxation measurements for probing polymer dynamics with CP/MAS NMR. The next section examines the most common relaxation measurements that probe a specific range of molecular motions or domain sizes. In that matter, particular attention shall be placed on those relaxation experiments that reveal molecular scale morphology in polymer blends since similar experiments may be envisioned for wood/adhesive systems.

I.4.4 CP/MAS NMR, a Probe of Polymer blend Morphology

The insight provided by CP/MAS NMR on polymer blend morphology stems from relaxation rate/ dynamic domain size correspondence [114]. Understanding such

equivalence warrants adequate design of CP/MAS NMR measurements for assessing blend morphology on the desirable domain size.

I.4.4.1 Spin Dynamics and Polymer Blend Morphology

I.4.4.1.1 Fundamentals of Solid State Spin Relaxation

When an assembly of nuclear spins is in resonance, its population is biased from Boltzmann's distribution. Logically then, relaxation towards equilibrium ensues. Relaxation may occur via spin-spin interactions at a characteristic time T_2 (transverse relaxation) or via spin-lattice interactions at a characteristic time T_1 or $T_{1\rho}$ (longitudinal relaxation) depending upon the reference frame considered (laboratory or rotating frame respectively). Such relaxation mechanisms portray molecular scale dynamics. For instance, megahertz frequency motions influence T_1 while $T_{1\rho}$ is affected by mid-kilohertz frequency motions [134]. Furthermore, owing to the abundance and spatial proximity of protons in organic solids, additional relaxation mechanisms are effective. CP is one example of such a mechanism and has already been discussed in detail. Let us just recap that CP rates, T_{CH}, are affected by spatial proximity (10 to 20 angstroms) and molecular rigidity as embodied by near static molecular motions [134]. Spin diffusion is another common relaxation mechanism for organic solids. Spin diffusion refers to a static magnetization transfer between abundant and adjacent protons. It is a non-motional mechanism. Nevertheless, spin diffusion contributes to spin-lattice relaxations, T_1 and $T_{1\rho}$. In other words, on top of the motional contribution to T_1 and $T_{1\rho}$, spin diffusion can average molecular motions of the so-called coupled-spins [134]. It follows that distinct nuclei (with distinct molecular motions) may have their T_1 and $T_{1\rho}$ converge to a common value by virtue of spin diffusion. In the same way that CP hinges upon spatial proximity however, spatial proximity is required for effective spin diffusion. Namely, spin diffusion occurs over nanometer scale domains. Conversely, spin diffusion is ineffective across phase boundaries [134]. As a result, polymer blends that are homogeneous on a nanoscale have their nuclei spin-coupled as reflected by a common $T_{1\rho}$. Phase separated polymer blends however, may exhibit distinct $T_{1\rho}$ for nuclei in separate domains. Of course, the same reasoning applies to T_1 rates since these are also

affected by spin diffusion. However, T_1 and $T_{1\rho}$ refer to different time scales and therefore distinct domain sizes. Namely, T_1 rates typically lie in the 100-500 ms range, while $T_{1\rho}$ rates are on the order of 5-15 ms. Because spin diffusion occurs at approximately 0.5-1 nm^2/ ms in polymers, $T_{1\rho}$ may be associated with 2-30 nanometer domains while T_1 is relevant of 30 nanometer or greater domain sizes. Consequently, morphological information can be obtained on specific domain sizes from T_1 and $T_{1\rho}$. Let us now consider how practically, one may probe morphology in polymer blends with relaxation mechanisms.

I.4.4.1.2 Relaxation Rate Measurements and Polymer Blend Morphology

Consider a polymer blend that comprises two spin reservoirs, a ^{13}C and ^{1}H spins reservoir. All possible magnetization transfers and relaxation mechanisms are illustrated in Figure I.4.6 for this polymer blend.

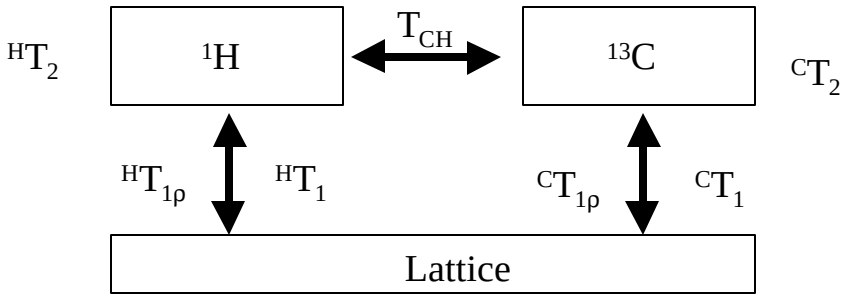

Figure I.4.6. Spin Relaxation in a CP/MAS NMR Experiment (adapted from [134])

The initial stage of a CP experiment is dominated by CP rate, T_{CH} (typically in the order of 0.1-1 ms). This results in ^{13}C-detection enhancement as long as contact times remain short enough i.e. in the order of T_{CH}. With longer contact times (typically 5-15 ms), owing to rotating frame spin lattice relaxation, the ^{1}H reservoir experiences a decrease in magnetization. This results in a decay of ^{13}C magnetization at the rate $^{H}T_{1\rho}$. Hence the magnetization curve of ^{13}C nuclei with respect to contact time bears the competing effects of T_{CH} and $^{H}T_{1\rho}$. In fact, both T_{CH} and $^{H}T_{1\rho}$ can be retrieved from the magnetization equation in a variable contact time experiment (I.4.7) [134].

(I.4.7)
$$I(t) = I^{*}\left(\frac{{}^{H}T_{1r}}{{}^{H}T_{1r} - T_{CH}}\right)\left(\exp^{-t/{}^{H}T_{1r}} - \exp^{-t/T_{CH}}\right)$$

In Equation (I.4.7), I(t) is the signal intensity at a contact time (t) and I* is the corrected signal intensity for infinitely fast cross-polarization and infinitely slow proton spin-lattice relaxation in the rotating frame. In Figure I.4.6, no discrimination between the blend components has been considered. Oftentimes however, individual polymers can be monitored from distinct ^{13}C chemical shifts. As a result, variable contact time CP experiments allow simultaneous monitoring of T_{CH} and $^{H}T_{1\rho}$ for each polymer. Simply then, blend morphology can be determined from changes in the bulk polymer relaxation rates. If polymers interact on the time scale (and domain size) characteristic of a relaxation rate then this relaxation rate shall be altered as a result of blending. Changes in T_{CH} upon blending are thus indicative of angstrom scale interactions while changes in $^{H}T_{1\rho}$ reflect nanometer scale interactions between polymers. This approach constitutes the simplest experiment one can envision for assessing polymer blend morphology. Another approach hinges upon the spatial requirements in static magnetization transfers, CP and spin diffusion. In that matter, deuterium NMR experiments have been devised to assess intermolecular CP in polymer blends [137]-[141]. Such experiments assess intermolecular CP in blends where one polymer is fully deuterated. Recall that deuterium is magnetically inactive and that ^{1}H-^{13}C CP occurs on 10 to 20 angstroms domains. In a miscible blend of two dissimilar polymers, where one of the polymers is deuterated, i.e. devoid of any protons, carbons in the deuterated polymer may be detected only through CP from the protonated polymer. In an immiscible blend, the deuterated polymer remains undetected because its ^{13}C nuclei are too far removed from a proton source. Hence, detection of a deuterated polymer in so designed polymer blends is evidence of angstrom scale miscibility. Such experiments have been extensively utilized in the early 1980's and remain one of the most powerful probes of angstrom scale morphology [137]-[141]. In the same way, the spatial requirement inherent to spin diffusion has been widely utilized to probe nanoscale morphology in polymer blends. The detection of a unique $^{H}T_{1\rho}$, regardless of the ^{13}C monitored, indicates nanoscale homogeneity. Distinct

$^{H}T_{1\rho}$'s for ^{13}C nuclei pertaining to distinct polymers on the other hand reveals nanoscale phase separation. This approach is certainly attractive in that it does not require deuterium labeling and can be carried out from simple variable contact time CP [135], [136]. While these 3 approaches, molecular dynamics, intermolecular CP and spin diffusion are the most common experiments for polymer blends, alternative experiments can be envisioned. For instance, T_1 measurements can be utilized to probe polymer blend morphology on 30 nanometers and greater domain sizes [135]. Recently, the development of two-dimensional pulses has granted novel probes of polymer blend morphology [120]. Generally, 2D experiments examine the time dependence of ^{1}H spin diffusion between distinct regions of a polymer blend (mobile versus rigid for instance). ^{1}H-Wideline separation or the WISE experiment is one example of a 2D experiment that permits measuring the scale of heterogeneity in polymer blends [120]. Certainly also, one foresees in the near future that an increasing number of pulse sequences will be available for probing polymer blend morphology. In spite of CP/MAS NMR capabilities, wood scientists have utilized such techniques with reserve. In recent years however, a growing number of papers have been published, which demonstrate CP/MAS NMR value for *in-situ* investigations of wood [128]. In the following section, significant CP/MAS NMR studies on wood are reviewed. Special emphasis is placed on relaxation measurements that give insight on wood morphology. The next section also examines the capability of CP/MAS NMR to reveal molecular aspects of various treatments of wood and adhesive treatment in particular. However, the reader is directed towards Gil et al. for a more detailed survey of CP/MAS NMR application to wood and other lignocellulosic materials [128].

I.4.4.2 Application of CP/MAS NMR to Wood

Nowadays, assignments of wood ^{13}C chemical shifts are well established and are exemplified with yellow-poplar CP/MAS NMR spectrum in Figure I.4.7 [121].

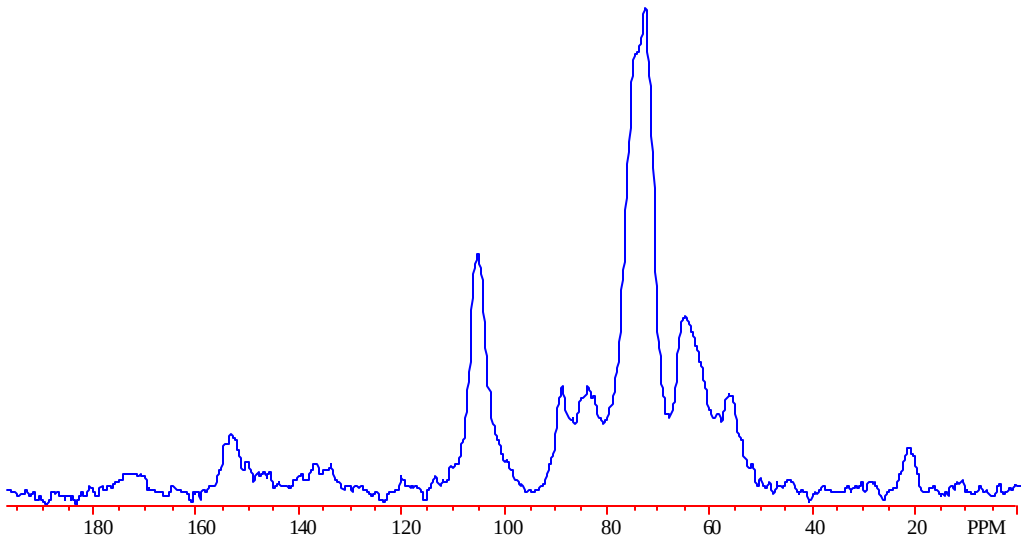

Figure I.4.7. ^{13}C *CP/MAS NMR Spectrum of Yellow-poplar (Liriodendron tulipifera)*

The spectrum is dominated by carbohydrate resonances at 63-66, 72-74, 83-89, and 105 ppm. In particular, carbohydrate C_4 and C_6 appear in the 85-90 ppm and 63-66 ppm regions respectively. Carbohydrates C_2, C_3 and C_5 on the other hand dominate the 72-74 ppm region. It can be noticed that C_4 and C_6 chemical shifts both comprise a sharp resonance and a broader upfield resonance or shoulder in the case of the C_6. The sharp resonance stems from crystalline regions of cellulose (and that fraction of hemicellulose that may be crystalline such as xylans) and the upfield resonance arises from more disordered amorphous regions [128]. Finally, a distinct resonance at 105 ppm is characteristic of cellulose C_1 and overlaps with that of hemicellulose C_1 at 103 ppm. Hemicellulose is largely manifest in the broad background between 50 and 90 ppm. Hemicellulose acetyl groups can also be seen at 22 ppm (methyl carbon) and 175 ppm (carbonyl carbon). Lignin contributes to the wood spectrum at 56 ppm and in the 130-150 ppm region. The peak at 56 ppm corresponds to methoxyl groups and resonances at 122, 135, 153 ppm arise from unsubstituted, alkylated and oxygen-substituted aromatic carbons respectively. Clearly evident with these assignments is CP/MAS NMR capability to distinctively monitor *in-situ* wood polymers. As a result, fine structural information can be obtained from CP/MAS NMR analysis of wood. For instance,

quantitative CP/MAS NMR permits *in-situ* assessment of Syringyl/ Guaiacyl ratios for lignin but also cellulose crystallinity [122], [123]. With this resolution of *in-situ* wood polymers, CP/MAS NMR has emerged as an ideal probe of wood morphology and wood polymer dynamics.

I.4.4.2.1 Use of Relaxation Measurements for Wood based Systems

Nuclear spin relaxation experiments have been widely utilized to characterize wood morphology [124]. Newman for instance performed delayed-contact pulse experiments and acquired distinct subspectra of wood for long and short $T^H_{1\rho}$'s [124]. In this study, the short $T^H_{1\rho}$ (mobile fraction) subspectrum comprises lignin and hemicellulose, while cellulose appears in the long $T^H_{1\rho}$ (rigid fraction) subspectrum [125]. The occurrence of distinct $T^H_{1\rho}$ for mobile and rigid wood components suggests nanoscale phase separation between wood amorphous matrix and crystalline cellulose phases. Tekely et al. on the other hand, reported identical $T^H_{1\rho}$ values for wood polymers thereby hinting towards phase homogeneity on a nanoscale [129]. Surprisingly, the same authors measured distinct T^H_1 for all wood polymers, indicating phase heterogeneity on a scale greater than 30 nanometers [130]. This controversy on wood morphology was reconciled thanks to additional CP/MAS NMR analyses by Newman [126]. Newman established that moisture plays a critical role on wood relaxation. Specifically, moisture helps discriminate between cellulose and lignin $T^H_{1\rho}$'s [126]. Upon moisture uptake, lignin $T^H_{1\rho}$ decreases while that of cellulose increases [126]. Divergent $T^H_{1\rho}$'s with increasing moisture content was ascribed to two mechanisms. On the one hand, moisture alters cellulose microstructure from an amorphous to a more ordered state induced by hydrogen bonding [127]. For lignin on the other hand, moisture enhances spin diffusion, thereby decreasing its $T^H_{1\rho}$. Spin diffusion contribution to lignin $T^H_{1\rho}$ is clearly evidenced by differences in $T^H_{1\rho}$'s between H_2O and D_2O moistened wood [126]. The same comparison indicates no notable moisture induced spin diffusion for cellulose [126]. With this thorough investigation of moisture effect on wood relaxation, Newman has put an end to this controversy on wood morphology as detected by CP/MAS NMR. Namely, under moist conditions, phase separation is indicated by distinct $T^H_{1\rho}$ values for crystalline and amorphous phases while under dry conditions homogeneous morphology

is suggested from efficient spin diffusion. Other CP/MAS NMR investigations have tackled the effect of various treatments on wood molecular packing. For instance, early CP/MAS NMR studies have concentrated on the molecular impact of steam explosion (SE) on wood morphology [129]. Steam explosion consists of contacting wood chips with superheated steam under high pressure for a brief period of time. Upon abrupt decompression, the chips are exploded. Steam explosion not only leads to condensation of degradation products but also reduces wood polymer molecular mixing as evidenced by distinct $T^{H}_{1\rho}$ for steam exploded components [129]. Other treatments pertaining to the manufacture of pulp and paper such as sulfonation and methylation have also been studied by CP/MAS NMR [131], [132]. In that matter, Argyropoulos and coworkers measured T^{H}_{1} of sulphonated and methylated spruce pulps [131]. Interestingly, changes in lignin T^{H}_{1} upon sulfonation and methylation were found to parallel those in carbohydrates. More specifically, both sulfonation and methylation appeared to decrease wood polymers T^{H}_{1} thereby indicating enhanced molecular mobility on the megahertz frequency range [132]. Similarly, parallel trends for lignin and cellulose T^{H}_{1}'s with changes in pH were observed for megahertz frequency motions [132]. As wood is treated under alkaline conditions, wood functional groups are ionized and the resulting repulsive forces enhance wood polymer mobility thereby allowing for shorter T^{H}_{1}. This effect is prominent for pH values exceeding 10 [132]. Above pH 10, wood carboxyl, phenolic and enolic hydroxyl groups are predominantly ionized while weakly acidic primary and secondary hydroxyl groups remain minimally ionized. Hence the significant enhancement in molecular mobility detected above pH 10 results from ionization of specific functional groups [132]. Both studies are further interesting in that the parallel trend for lignin and carbohydrates T^{H}_{1} suggests molecular connectivities between wood components [131], [132]. Thermal treatment is certainly the most common treatment performed on wood. Thermal treatment is thought to cause several chemical changes. On the one hand, organic acids released from hemicellulose are likely to cleave ligno-polysaccharide complexes. On the other hand, condensation reactions may generate secondary lignin-carbohydrates bonds. Kosikova et al. utilized T^{H}_{1} measurements for better understanding the influence of heat treatment on wood [133]. Alkaline pretreatment was also investigated in this study. When thermal treatment followed a

sodium hydroxide conditioning, cellulose crystallinity index was found to increase while lignin degraded mainly through β aryl-linkage cleavage [133]. In addition, evidence for lignin hydrogenation was found. The authors also proposed heat induced carbohydrate-lignin linkages as a result of unique $T^{H}_{1\rho}$ for lignin and amorphous cellulose in a model lignin-carbohydrate compound [133]. While this study demonstrates the power of CP/MAS NMR to elucidate chemical and morphological changes upon wood treatment, it certainly emphasizes the complexity of chemical and morphological changes induced by any treatment of wood. Hence, complementary information such as that obtained from cross-polarization rates is useful for probing molecular order and packing in wood [146]. Let us recall that T_{CH}, is a distance dependent phenomenon and is sensitive to near static motions. It therefore reflects local packing arrangements as well as near-static motions. Again, the influence of moisture content on wood polymer T_{CH} has been the subject of early CP/MAS analysis on wood treatment. Marcinko and coworkers reported faster cross polarization rates for Aspen and Southern Pine polymers upon hydration [148]. Faster T_{CH} rates were ascribed to increases in cellulose ordering and hydrogen bonding of lignin [148]. This data is consistent with Newman's interpretation of moisture effect on wood polymers $T^{H}_{1\rho}$. More interesting, wood T_{CH} has been shown to correlate with wood dynamic modulus, thereby establishing a bridge between molecular arrangement and macroscopic performance [146]. Such studies clearly indicate that T_{CH} measurements are well suited to probe the intimate environment and near static molecular motions of wood polymers and their changes upon treatments. Along with T^{H}_{1} and $T^{H}_{1\rho}$ measurements, T_{CH} measurements shall therefore be ideally suited for probing the morphology of wood/ adhesive interphases. In fact, the use of CP/MAS NMR relaxation time measurements for probing wood bondlines is now well established.

I.4.4.2.2 Application of CP/MAS NMR Techniques for Wood/Adhesive Bondlines

In-situ wood adhesion mechanisms can be explored by directly investigating the wood adhesive bondline. Because adhesives can be enriched in magnetically active nuclei, fine structural and morphological information can be obtained from CP/MAS NMR analysis of wood adhesive bonds [142]. The method has proved successful for *in-situ* investigations of wood-isocyanate cure chemistry [143], [144]. In fact, semi-

quantitative structural information can be obtained from CP/MAS NMR analysis of wood-adhesive bondlines. As mentioned in chapter II-1, PF resin cure may be monitored *in-situ* thanks to CP/MAS NMR [145]. The cure of PF resins proceeds via condensation of hydroxymethyl groups to methylene bridges. In a CP/MAS NMR spectrum of a wood-PF resin bondline, these functionalities can be resolved provided the resin is enriched in ^{13}C [145]. Hence, the proportion of methylene and methylol carbons can be measured by integration of their respective signal [145]. Quantitative analysis additionally requires the knowledge of T_{CH} and $T^{H}_{1\rho}$ relaxation times since both relaxation rates control carbon magnetization in a CP experiment. More interesting on a morphological standpoint, relaxation rates for adhesives and wood can be monitored from CP/MAS NMR. For instance, it has been demonstrated that wood induces nanometer scale heterogeneity in a PF resin network [145]. That is, while the neat PF resin exhibits a similar $T^{H}_{1\rho}$ value whether it is measured through the methylene or methylol carbon, the $T^{H}_{1\rho}$ from these two carbons diverges in wood-PF systems [145]. Similar phenomena have been observed with isocyanates. With long curing time, nanometer scale heterogeneity develops in an isocyanate bondline as evidenced by different $T^{H}_{1\rho}$ for distinct pMDI functionalities [150], [143]. While these studies essentially examine the bondline from the standpoint of the adhesive, the reverse approach shall be similarly fruitful. In other words, morphological information shall stem from changes in wood polymer relaxation upon adhesive application. Such an approach has been taken by So et al. to elucidate the effect of resole on wood microstructure [149]. Resole effect on cellulose crystallinity appears to depend on the length of resin application on the substrate. At short curing time, resole disrupts cellulose crystallinity while at longer curing times recrystallization (presumably alkali induced transformation from cellulose I to cellulose II) increases cellulose crystallinity [149]. Following this study, a number of researchers have attempted to further elucidate adhesive impact on wood molecular motions. Marcinko et al. reported for instance that liquid isocyanate binders decrease wood components $T^{H}_{1\rho}$ in Aspen wood thereby indicating intimate changes in the nanometer scale environment of wood polymers [151]. Such an effect was ascribed to pMDI ability to achieve intimate contact with wood polymers through plasticization. On the other hand for yellow-poplar, liquid pMDI did not affect wood polymers $T^{H}_{1\rho}$ [147].

This discrepancy may arise from species dependence of pMDI penetration in wood. In the same study the cured pMDI was reported to have no effect on wood polymers $T^{H}_{1\rho}$. This again is at odds with Marcinko and coworkers results, which found that cured pMDI also dramatically changes wood polymers $T^{H}_{1\rho}$ [150]. In spite of some diverging results, these morphological studies clearly establish the validity of NMR relaxation times for assessing intimate mixing between wood polymers and adhesives. Overall, $T^{H}_{1\rho}$ and T_{CH} measurements nicely complement each other to yield a molecular scale understanding of adhesive penetration into wood.

I.5 REFERENCES

[1] White M.S., Influence of Resin Penetration on the Fracture Toughness of Bonded Wood, Doctoral Dissertation, Virginia Polytechnic Institute and State University, 1975.

[2] Siau J.F., Transport Processes in Wood, Springer-Verlag, New York, 1984.

[3] Nearn W.T., Application of the Ultrastructure Concept in Industrial Wood Products Research, Wood Science, 6 (3) 285, 1974.

[4] Nearn W.T., Wood-Adhesive Interface Relations, Conference on the Wood-Paint Interface, Berkeley, October 1964.

[5] Jonson S.E. and F.A. Kamke, Quantitative Analysis of Gross Adhesive Penetration in Wood Using Fluorescence Microscopy, J. Adhesion, 40, 47, 1992.

[6] Sernek M., J. Resnik and F.A. Kamke, Penetration of Liquid Urea-Formaldehyde Adhesive into Beech Wood, Wood Fiber Sci., 31 (1)41, 1999.

[7] Gray V.R., The Wetting, Adhesion and Penetration of Surface Coatings on Wood, Oil and Colour Chemists Association, 44, 756, 1961.

[8] White M.S., G. Ifju and J.A. Johnson, Method for Measuring Resin Penetration into Wood, For. Prod. J., 27, (7) 52, 1977.

[9] Saiki H., Electron Microscopy of Wood Cell Wall Impregnated with Aqueous Solution of Silver Nitrate, 19 (8) 367, 1973.

[10] Smith L.A., Resin Penetration of Wood Cell Walls, Implications for Adhesion of Polymers to Wood, Doctoral Dissertation, State University College of Forestry at Syracuse University, 1971.

[11] Robison R.G., Wood-Coating Interactions, Doctoral Dissertation, State University College of Forestry at Syracuse University, May 1972.

[12] Tarkow H., W.C. Feist and C.F. Southerland, Interaction of Wood With Polymeric Materials, Penetration Versus Molecular Size, For. Prod. J., 16 (10) 61, 1966.

[13] Siau J.F., The Swelling of Basswood by Vynil Monomers, Wood Sci. 1 (4) 250, 1969.

[14] Frazier C.E., Personal Communication.

[15] Mantanis G.I., R.A. Young and R.M. Rowell, Swelling of Wood. Part II. Swelling in Organic Liquids, Holzforschung, 48 (6) 480, 1994.

[16] Pizzi A., Advanced Wood Adhesives Technology, Marcel Dekker, Inc., New York, p89-151, 1994.

[17] Sellers T., Plywood and Adhesive Technology, Marcel Dekker Inc., New York, 1985.

[18] Astarloa-Aierbe G., J.M. Echeverria, M.D. Martin and I. Mondragon, Kinetics of Phenolic Resol Resin Formation by HPLC. 2. Barium Hydroxide, Polymer, 39 (15) 3467, 1998.

[19] Astarloa-Aierbe G., J.M. Echeverria, A Vazquez and I. Mondragon, Influence of the Amount of Catalyst and Initial pH on the phenolic Resol Resin Formation, Polymer, 41, 3311, 2000.

[20] Kaledkowski B. and J. Hetper, Synthesis of Phenol-Formaldehyde Resole Resins in the Presence of Tetraalkylammonium Hydroxides as Catalysts, Polymer, 41 (5) 1679, 2000.

[21] Freeman J.H. and C.W. Lewis, Alkaline-Catalyzed Reaction of Formaldehyde and the Methylols of Phenol, J. Am. Chem. Soc., 76, 2080, 1954.

[22] Caesar P.D. and A.N. Sachanen, Thiophene-formaldehyde Condensation, Ind. Eng. Chem., 40, 922, 1948.

[23] Grenier-Loustalot M.F., S Larroque and P. Grenier, Phenolic Resins: 1. Mechanisms and Kinetics of Phenol and of the First Polycondensates Towards Formaldehyde in Solution, Polymer, 35 (14) 3047, 1994

[24] Grenier-Loustalot M.F., S Larroque and P. Grenier, Phenolic Resins, 3. Study of the Reactivity of the Initial monomers Towards Formaldehyde at Constant pH, Temperature and Catalysts Type, Polymer, 37 (6) 939, 1996.

[25] Werstler D.D., Quantitative 13C NMR Characterization of Aqueous Formaldehyde Resins: 1:Phenol-formaldehyde Resins, Polymer 27 (5) 750, 1986.

[26] Knop A. and L.A. Pilato, Phenolic Resins, Chemistry Applications and Performance, Springer-Verlag, New York, 1985.

[27] Pizzi A., Handbook of Adhesive Technology, Marcel Dekker Ed., New York, 1994.

[28] Miller H.A., Particle Board Manufacture, Noyes Data Corporation, New Jersey, 1977.

[29] Pizzi A., Wood Adhesives, Chemistry and Technology, Vol. 1 and 2, Marcel Dekker Inc., New York, 1983.

[30] Jones T.T., Preliminary Investigations of the Phenol-Formaldehyde Reaction, J. Soc. Chem. Ind., 65, 264, 1946.

[31] Maciel G.E., I. S. A. Chuang and L. Gollob, a Solid-State Carbon-13 NMR Study of Resol-Type Phenol-Formaldehyde Resins, Macromolecules, 17 (5) 1081, 1984.

[32] Zinke A, The Chemistry of Phenolic Resins and the Process Leading to their Formation, J. Applied Chem. (London), 1, 257, 1951.

[33] Lenghaus K., Qiao G.G. and D.H. Solomon, Model Studies of the Curing of Resole Phenol-Formaldehdye Resins Part 1. The Behaviour of Quinone Methide In a Curing Resin, Polymer 41 (6) 1973, 2000.

[34] Holopainen T., L. Alvila, J. Rainio and T.T. Pakkanen, Phenol-Formaldehyde Resol Resins Studies by 13C NMR Spectroscopy, Gel Permetation Chromatography, and Differential Scanning Calorimetry, J. Appl. Polym. Sci, 66 (6) 1183, 1997.

[35] So S. and A. Rudin, Analysis of the Formation and Curing Reactions of Resole Phenolics, J. Appl. Polym. Sci, 41 (1-2) 205, 1990.

[36] Schmidt R.G. and C.E. Frazier, Network Characterization of Phenol-Formaldehyde Thermosetting Wood Adhesive. Int. J. Adhes. Adhes. 18 (2) 139, 1998.

[37] Palmese G.R. and J.K. Gilham, Time-Temperature-Transformation (TTT) Cure Diagrams Relationship between Tg and the Temperature and Time of Cure for a Polyamic Acid/ Polyimide System, J. Appl. Polym. Sci., 34 (5) 1925, 1987.

[38] Young R.H., P.W. kopf and O. Salgado, Curing Mechanisms of Phenolic Resins, Tappi J., 64 (4) 127, 1981.

[39] Steiner P.R. and S.R. Warren, Rheology of Wood-Adhesive Cure by Torsional Braid Analysis, Holzforschung, 35 (6) 273, 1981.

[40] Kim M.G., W. L-S Nieh and R.M. Meacham, Study of Phenol-Formaldehyde Resol Resins by Dynamic Mechanical Analysis, Ind. Eng. Chem. Res. 30, 798, 1991.

[41] Kim M.G. and W. L.-S. Nieh and R.M. Meacham, Study on the Curing of Phenol-Formaldehyde Resol Resins by dynamic Mechanical Analysis, Ind. Eng. Chem. Res. 30, 4, 1991.

[42] Rials T.G. Cure Analysis of Phenol-Formaldehyde Resins by Microdielectric Spectroscopy, American Chemical Society Symposium Series 489, ACS, Washington D.C. 1989.

[43] Wang X.-M, B. Riedl, R.L. Geimer and A.W. Christiansen, Phenol-Formaldehyde Resin Curing and Bonding under Dynamic Conditions, Wood Sci. Technol., 30 (6) 423, 1996.

[44] Myers G.E., A.W. Christiansen, R.L. Geimer, R.A. Follensbee and J.A. Koutsky, Phenol-Formaldehyde Resin Curing and Bonding in Steam-Injection Pressing. I. Resin Synthesis, Characterization, and Cure behavior, J. Appl. Polym. Sci., 43, 237, 1991.

[45] Neiss T.G., Solution and Solid-State NMR Analysis of Phenolic Resin Cure Kinetics, Macromol. Symp. , 86, 117, 1994.

[46] Mizumachi H. and H. Morita, Activation Energy of the Curing Reaction of Phenolic Resin in the Presence of Woods, Wood Sci., 7, 3, 256, 1975.

[47] Pizzi A., B. Mtsweni and W. Parsons, Wood-Induced Catalytic Activation of PF Adhesives Autopolymerization vs. PF/ Wood Covalent Bonding, J. Appl. Polym. Sci., 52, 1847, 1994.

[48] Lu X. and A. Pizzi, Curing Conditions Effects on the Characteristics of Thermosetting Adhesives-Bonded Wood Joints, Holz-als Roh-Werkstoff, 56, 393, 1998.

[49] Lu X. and A. Pizzi, Curing Conditions Effects on the Characteristics of Thermosetting Adhesives-Bonded Wood Joints, Part 1: Substrate influence on TTT and CHT Curing Diagrams of Wood Adhesives, 56, 339, 1998.

[50] Garcia R and A. Pizzi, Crosslinked and Entanglement Networks in Thermomechanical Analysis of Polycondensation Resins, J. Appl. Polym. Sci., 70, 1111, 1998.

[51] Onic L., Bucur V., Ansell M.P., Pizzi A., Deglise X. and A. Merlin, Dynamic Thermomechanical Analysis as a Control Technique for Thermoset Bonding of Wood Joints, Int. J. Adhes. Adhes., 18, 89, 1998.

[52] Pizzi A., Lu X. and R. Garcia, Lignocellulosic Substrates Influence on TTT and CHT Curing Diagrams of Polycondensation Resins J. Appl. Polym. Sci, 71, 915, 1999.

[53] Ward I.M., Mechanical Properties of Solid Polymers, Second Ed., John Wiley & Sons Inc., New York, 1979.

[54] Ferry J.D., Viscoelastic Properties of Polymers, Second Ed. John Wiley & Sons, Inc., New York, 1970.

[55] Greener J., Relaxation Phenomena in Polymers: A Snapshot, PMSE News, incomplete reference, 1993.

[56] Ngai K.L. and R.W. Rendell, From Conformational Transitions in a Polymer Chain to Segmental Relaxation in a Bulk polymer, J. Non-Cryst. Solids 131-133, 942, 1991.

[57] Ngai K.L. and D.J. Plazeck, Identification of Different Modes of Molecular Motion In Polymers That Cause Thermorheological Complexity, Rubber Chemistry and Technology, 68, 376, 1995.

[58] Matsuoka S., Relaxation Phenomena in Polymers, Ed. Hanser, Vienna, 1992.

[59] Williams M.L., R.F. Landel and J.D. Ferry, The Temperature Dependence of Relaxation Mechanisms in Amorphous Polymers and Other Glass-forming Liquids, J. Am. Chem.Soc., 77, 3701, 1955.

[60] Doolittle A.K., Newtonian Flow. II. The Dependence of the Viscosity of Liquids on Free Space., J. Applied Phys., 22, 1471, 1951.

[61] Adam G. and J.H. Gibbs The Temperature Dependence of Cooperative Relaxation Properties in Glass-forming Liquids, J. Chem. Phys., 43 (1) 139, 1965.

[62] Mc Kenna, in Comprehensive Polymer Science, Vol. 2, Polymer Properties (ed. C. Booth and C. Price), Pergamon, Oxford, pp311-362 (Chapter 10), 1989.

[63] Kauzmann W., The Nature of the Glassy State and the Behavior of Liquids at Low Temperatures, Chemical Revs, 43, 219, 1948.

[64] Hodge I.A., Journal of Research of the National Institute of Standards and Technology, Adam-Gibbs Formulation of Enthalpy Relaxation near the Glass transition, 102 (2), 195, 1997.

[65] Vogel H., The Law of the Relation between the Viscosity of Liquids and the Temperature, Phys. Z., 22, 645, 1921.

[66] Fulcher G.S., Analysis of Recent Measurements of the Viscosity of Glasses. J. Am. Ceram. Soc., 8, 339, 1925.

[67] Tamman G. and W. Hesse, The dependence of Viscosity upon the Temperature of Supercooled Liquids. Z. Anorg. Allgem. Chemie,, 156, 245, 1926.

[68] Angell C.A., Journal of Research of the National Institute of Standards and Technology, 102 (2), 171, 2001.

[69] Angell C.A., Formation of Glasses from Liquids and Biopolymers, Science, 267, 1925, 1995.

[70] Hall C. K., and E. Hellfand, Conformational State Relaxation in Polymers: Time Correlation Functions, J. Chem. Phys., 77 (6) 3275, 1982.

[71] Williams, G.; Watts, D. C., Non-symmetrical Dielectric Relaxation Behavior arising from a Simple Empirical Decay Function, Trans Faraday Soc, 66 (1) 80, 1970.

[72] Ngai K. L., Modification of the Adam-Gibbs Model of the Glass Transition for Consistency with Experimental Data, J Phys. Chem B, 103, 5895, 1999.

[73] Plazeck D. J. and K. L. Ngai, Correlation of Polymer Segmental Chain Dynamics with Temperature-Dependent Time-Scale Shifts, Macromolecules, 24, 1222, 1991.

[74] Roland C.M. and K.L. Ngai, Segmental Relaxation and Molecular Structure in Polybutadienes and Polyisoprene, Macromolecules, 24, 5315, 1991.

[75] Roland C.M., Terminal and Segmental Relaxations in Epoxidized Polyisoprene, Macromolecules (25), 7031, 1992.

[76] Ngai K. L., and C. M. Roland, Chemical Structure and Intermolecular Cooperativity: Dielectric Relaxation Results, Macromolecules, 26, 6824,1993.

[77] Connolly M and F. Karasz, Viscoelastic and Dielectric Relaxation Behavior of Substituted poly(p-Phenylenes), Macromolecules, 28, 1872, 1995.

[78] Robertson C.G. and C.M. Roland, Breadth of the a Relaxation Function in 1,4-Polybutadiene, Macromolecules, 33, 1262, 2000.

[79] Roland C.M. and Ngai K.L., Segmental Relaxation in Miscible Polymer Blends, J. Rheol, 36 (8), 1992.

[80] Roland C.M. and K.L. Ngai, Dynamical Heterogeneity in a Miscible Polymer Blend, Macromolecules, 24, 226, 1991.

[81] Ngai K.L, C.M. Roland, J.M. O'Reilly and J.S. Sedita, Trends in the Temperature Dependency of Segmental Relaxation in TMPC/PS Blends, Macromolecules, 25, 3906, 1992.

[82] Roland C.M. and K.L. Ngai, Segmental Relaxation in Miscible Polymer Blends, J. Rheol. 36 (8) 1691, 1992.

[83] Vernel J, R.W. Rychwalski, V. pelisek, P. Saha, M. Schmidt and F. Maurer, Physical Aging in Poly(ethylene Oxide)/atactic-poly(methyl methacrylate) Blends, Thermochimica Acta, 342, 115, 1999.

[84] Robertson C.G and G. L. Wilkes, Glass-Formation Kinetics of Miscible Blends of Atactic Polystyrene and Poly (2, 6-dimethyl-1,4-phenylene oxide), Journal of Polymer Science: Part B: Polymer Physics, 39, 2118, 2001.

[85] Jensen R. E, C. E. Johnson and T. C. Ward, Investigation of a Waterborne Epoxy for E-Glass Composites, J. Polym. Sci., Part B: Polym. Phys., 38 (18), 2351, 2000.

[86] Yano S., H. Hatakeyama and T. Hatakeyama, Effect of hydrogen Bond Formation of Dynamic Mechanical Properties of Amorphous Cellulose, J. Appl. Polym. Sci., 20, 3221, 1996.

[87] Goring D.A.L., Thermal Softening of Lignin, Hemicellulose and Cellulose, Pulp Paper Mag. Can. 64 (12) T-51, 1986.

[88] Bradley S.A., and S.H.Carr, Effect of Fungal Degradation on Mechanical Properties of Cellophan, J. Polym. Sci., Polym. Phys. Ed., 14 (1), 125, 1976.

[89] Montes H., K. Mazeau and J.Y. Cavaille, Secondary Mechanical Relaxations in Amorphous Cellulose, Macromolecules 30, 6977, 1997.

[90] Montes H., K. Mazeau and J.Y. Cavaille, The Mechanical b Relaxation in Amorphous Cellulose, Journal of non-Crystalline Solids, 235-237, 416, 1998.

[91] Montes H. and J.Y. Cavaille, Secondary Dielectric Relaxations in Dried Amorphous Cellulose and Dextran, Polymer 40, 2649, 1999.

[92] Obataya E., M. Norimoto and B. Tomita, Mechanical Relaxation Processes in Wood in the Low-Temperature Range, J. Appl. Polym. Sci., 81 3338, 2001.

[93] Salmén N.L. and E.L. Back, The Influence of Water on The Glass Transition Temperature of Cellulose, Tappi, 60 (12) 137, 1977.

[94] Irvine G.M., The Glass Transitions of Lignin and Hemicellulose and Their Measurement by Differential Thermal Analysis, Tappi Journal 67 (5) 118, 1984.

[95] Salmén N.L., Thermal Softening of Paper: its Effect on Mechanical Properties, Pulp Paper Can. Trans Techn. Sec. 5 (3): TR 45, 1979.

[96] Olsson A.M. and L. Salmén , Humidity and Temperature Affecting Hemicellulose Softening in Wood, Proc. Int. Conf. of COST Action E8, June 16-17, Copenhagen, p.269, 1997.

[97] Salmén L., Viscoelastic Properties of In-situ Lignin Under Water Saturated Conditions, J. Mater. Sci., 19, (9), 3090,1984.

[98] Kelley S.S., T.G.Rials and W.G. Glasser, Relaxation Behaviour of the Amorphous Components of Wood, J. Mater. Sci., 22, 617, 1987.

[99] Salmén L., Directional Viscoelastic Properties of Wood, Progress and Trends in Rheology II, Proceedings of the Second Conference of European Rheologists, Prague June 17-20, p. 234, 1986.

[100] Wolcott M.P., F.A. Kamke and D.A. Dillard, Fundamental Aspects of Wood Deformation Pertaining to Manufacture of Wood-Based Composites, Wood Fiber Sci. 26 (4), 496, 1994.

[101] Furuta Y., M. Makinaga, H. Yano and H. Kajita, Thermal Softening Properties of Water Swollen Wood II. Anisotropic Characteristics of Thermal-softening Properties, Mokuzai Gakkaishi, 43 (1) 16, 1997.

[102] Östberg G. and L. Salmén , Characterization of Softening of Wood Fiber Wall Layers, Cellulose Chemistry and Technology, 21, 241, 1987.

[103] Olsson A.M. and L. Salmén , Viscoelasticity of In-situ Lignin as Affected by Structure, In: Viscoelasticity of Biomaterials, Eds. W.G. Glasser and H. Hatakeyama, American Chemical Society Symposium Series No 489, 133, 1992.

[104] Olsson A.M. and L. Salmén , The Effect of Lignin Composition on the Viscoelastic Properties of Wood, Nordic Pulp and Paper Research Journal, 3 (12), 140, 1997.

[105] Hamdan S., W. Dwianto, T. Morooka and M. Norimoto, Softening Characteristics of Wet Wood under Quasi Static Loading, Holzforschung, 54 (5) 557, 2000.

[106] Wennerblom M., A.M. Olsson and L. Salmén , Softening Properties of Earlywood and Latewood of Spruce, Nordic Pulp and Paper Research Journal, 4 (11) 279, 1996.

[107] Olsson A.M. and L. Salmén , Mechanical Spectroscopy- A Tool for Lignin Structure Studies, personal communication 2000.

[108] Salmén L. and A.M. Olsson, Interaction between Hemicelluloses, Lignin and Cellulose: Structure-Property Relationships, J.Pulp Paper Sci. 24 (99) 103, 1998.

[109] Lenth C.A. and F.A. Kamke, Moisture Dependent Softening Behavior of Wood, Wood and Fiber Science, 33 (3) 492, 2001.

[110] Nakano T. and Nakamura H., Viscoelasticity of Esterified Wood Specimens IV. The effect of Introduced Acyl Groups on Dynamic Mechanical Properties, Mokuzai Gakkaishi 21 (10) 820, 1987.

[111] Nakano T., Viscoelasticity of Esterified Wood Specimens IV. The effect of Molar Volume of Introduced Acyl Groups, Mokuzai Gakkaishi 33 (6) 472, 1988.

[112] Sugiyama m. and M. Norimoto, Temperature Dependence of Dynamic Viscoelasticities of Chemically Treated Woods, Mokuzai Gakkaishi 42 (11) 1049, 1996.

[113] Marcinko J.J., S. Devathala, P.L. Rinaldi, S. Bao, Investigating the Molecular and Bulk Dynamics of PMDI/Wood and UF/Wood Composites, Forest Products Journal, 48 (6) 81, 1998.

[114] Tycko R., Nuclear Magnetic Resonance Probes of Molecular Dynamics, Understanding Chemical Reactivity Vol. 8, Kluwer Academic Publishers, London, 1994.

[115] Havens J.R. and J.L. Koenig, Applications of High-Resolution Carbon-13 Nuclear Magnetic Resonance Spectroscopy to Solid Polymers, Applied Spectroscopy, 37, 3, 226, 1983.

[116] Silverstein R. M. and F. X. Webster, Spectrometric Identification of Organic Compounds, Sixth Ed. John Wiley& Sons, Inc, New York, 1998.

[117] Bruch M. D., NMR Spectroscopy Techniques, Practical Spectroscopy Series, Vol. 21, 2nd Ed., Ed. Marcel Dekker, Inc., New York, 1996.

[118] Schaefer J. and E. O. Stejskal, Carbon-13 Nuclear Magnetic Resonance of Polymers Spinning at the Magic Angle, J. Am. Chem. Soc., 98 (4) 1031, 1976.

[119] Kohler S. J., Introduction to NMR Spectroscopy of Solids, NMR Spectroscopy Application Note, IBM Instruments Inc. Incomplete Reference.

[120] Schmidt-Rohr K. and H. W. Spiess in "Multidimensional Solid-State NMR and Polymers", Academic Press, New York, 1994.

[121] Kolodziejski V., J. S. Frye and G. E. Maciel, Carbon-13 Nuclear Magnetic Resonance Spectrometry with with Cross Polarization and Magic-Angle Spinning for Analysis of Lodgepole Pine Wood, Anal. Chem, 54, 1419, 1982.

[122] Newman R.H. and J.A. Hemmingson, Determination of the Degree of Cellulose Crystallinity in Wood by Carbon-13 Nuclear Magnetic Resonance Spectroscopy, Holzforschung, 44, 5, 1990.

[123] Manders W.F., Solid State ^{13}C NMR Determination of the Syringyl/ Guaiacyl Ratio in Hardwoods, Holzforschung 41, 1, 1987.

[124] Newman R.H., Carbon-13 Nuclear Magnetic Resonance Studies of Molecular Motion in Wood and Paper, unknown Source.

[125] Newman R. H., Solid-State ^{13}C NMR Spectroscopy of Multiphase Biomaterials, American Chemical Society, Viscoelasticity of Biomaterials, Ed. W. Glasser, 311, 1992.

[126] Newman R.H., Nuclear Magnetic Resonance Study of Spatial Relationships Between Chemical Components in Wood Cell Walls, Holzforschung, 46 (3) 205, 1996.

[127] Willis J.M. and F. G. Herring, Effect of Water in the ^{13}C CP/MAS NMR Spectrum of White Spruce Wood, Macromolecules, 20, 1554, 1987.

[128] Gil A. M. and C. Pascoal Neto, Solid State NMR Studies of Wood and Other Lignocellulosic Materials, Annual Reports on NMR Spectroscopy, 37, 76, 1999.

[129] Tekely P. and M.R. Vignon, Cross-polarization/ Magic Angle Spinning ^{13}C- NMR Characterization of Steam Exploded Poplar Wood, Journal of Chemistry and Technology, 7 (2) 215, 1987.

[130] Tekely P. and Vignon M.R. Proton T_1 and T_2 Relaxation Times of Wood Components Using ^{13}C CP/MAS NMR, Journal of Polymer Science: Part C: Polymer Letters, 25, 257, 1987.

[131] Argyropoulos D.S. and F. G Morin, Probing the Macromolecular Structure of Wood and Pulps With Proton Spin-Lattice Relaxation Time Measurements in the Solid State, Wood Sci. Technol., 29, 19, 1995.

[132] Ahvazi B. and D. S Argyropoulos, Proton Spin-Lattice Relacation Time Measurements of Solid Wood and its Constituents as a Function of pH: Part I, Wood Sci. and Technol., 34, 45, 2000.*

[133] Kosikova B., M. Hricovini and C. Cosentino, Interaction of Lignin and Polysaccharides in Beech Wood (Fagus Salvatyca) during Drying Processes, Wood Sci. and Technol., 33, 373, 1999.

[134] Mehring M., Principles of High Resolution NMR in Solids, 2nd ed., Springer-Verlag, Berlin, 1983.

[135] Chu P.P and H.D. Wu, Solid State NMR Studies of Hydrogen Bonding Network Formation of Novolac Type Phenolic Resin and Poly(ethylene Oxide) Blend. Polymer 41, 101, 2000.

[136] Lee H.Y. and S.Y. Kwak, Dynamical heterogeneity and Molecular Mobility of hyper branched Poly(ether ketone)with Respect to the Homologous Linear, Polymer 42, 1375, 2001.

[137] Zhang X., A. Natansohn and A. Eisenberg, Intermolecular Cross-polarization Studies of the Miscibility Enhancement of PS/PMMA Blends through Ionic Interactions. Macromolecules 23 (2) 412, 1990.

[138] Schaefer J., M.Sefcik, Stejskal E. and R. McKay, Magic-angle Carbon-13 Nuclear Magnetic Resonance Analysis of the Interface between Phases in a Blend of Polystyrene with a Polystyrene-Polybutadiene Block Copolymer, Macromolecules 14 (1) 188, 1981.

[139] Parmer J., L. Dickinson, J. Chien and R. Porter, Macromolecules 20, 2308, 1987.

[140] Guo M. and H.G. Zachmann G. Intermolecular Cross-polarization Nuclear Magnetic Resonance Studies of the Miscibility of Poly(ethylene naphthalenedicarboxylate / poly(ethylene terephthalate) Blends, Polymer, 34 (12) 2504, 1993.

[141] Walton J., M. Lizak, M. Conradi, T. Gullion and J. Schaefer, Hydrostatic Pressure Dependence of Molecular Motions in Polycarbonates, Macromolecules 23 (2) 416, 1990.

[142] Frazier C. E., J. Ni and R. G. Schmidt, Applications of NMR Spectroscopy to the Analysis of Wood/Adhesive Bondlines, Adv. Lignocellulosic Charact., Ed. D. Argyropoulos, 145, 1999.

[143] Wendler S. L., and C. E. Frazier, The ^{15}N CP/MAS NMR Characterization of the Isocyanate Adhesive Bondline for Cellulosic Substrates, J Adhes., 50 (2-3) 153, 1995.

[144] Wendler S. L., and C. E. Frazier, Effect of Moisture Content on the Isocyanate/Wood Adhesive Bondline by ^{15}N CP/MAS NMR , J. Appl. Polym Sci., 61 (5) 775, 1996.

[145] Schmidt R. G. and C.E. Frazier, ^{13}C CP/MAS NMR as a Direct Probe of the Wood-Phenol Formaldehyde Adhesive Bondline, Wood And Fiber Science, 30 (3), 250, 1998.

[146] Ni J. and C. E. Frazier, Molecular Correlations to Macroscopic Wood Performance Using CP/ MAS NMR, Holzforschung, 50 (4) 327, 1996.

[147] Frazier C.E. and J.Ni, On the Occurrence of Network Interpenetration in the Wood-Isocyanate Adhesive Interphase, Int. J. of Adhes. Adhes. 18, 81, 1998.

[148] Marcinko J. J., Measuring the Molecular Order and Dynamics of Hydrated Wood, Incomplete Reference, 1996.

[149] So S., J.W. The, A. Rudin, W.J. Tchir and C.A. Fyfe, Effect of Resole Adhesives on the Crystallinity of Cellulose, J. Appl. Polym. Sci., 39, 531, 1990.

[150] Marcinko J. J., P. L. Rinaldi and S. Bao, Exploring the Physicochemical Nature of PMDI/Wood Structural Composite Adhesion, For. Prod. J., 49 (5) 75, 1999.

[151] Marcinko J.J., W. H. Newman and C. Phanopoulos, Second Pacific Rim Bio-Based Composites Symposium, Vancouver, Canada, p. 286-293, 1994.

II DYNAMIC METHODS

CHAPTER. II.1. INTERMOLECULAR CP AT THE WOOD/PF INTERPHASE

II.1.1 Introduction

Solid-state ^{13}C NMR spectroscopy has been widely utilized for assessing miscibility in polymer blends. In particular, the detection of intermolecular CP is evidence for angstrom scale miscibility [1]-[5]. Intermolecular CP may be detected in polymer blends that have been designed with specific deuterium labeling. In such deuterium CP experiments, one polymer is hampered from intramolecular CP through proton depletion while intermolecular CP remains possible between protonated and perdeurated components provided that angstrom scale miscibility occurs [1]-[5]. The objective of this study is to assess the feasibility of deuterium CP experiments for detecting angstrom scale miscibility at the wood/PF interphase. Indeed, one can envision a wood/PF composite, which is isotopically designed for detecting intermolecular CP between wood and the PF resin. More precisely, in a wood/PF composite where the PF resin is fully deuterated, detection of the PF resin would indicate intermolecular CP from wood protons i.e. angstrom scale miscibility. For this experiment, complete deuteration of the PF resin is required. In addition, ^{13}C enrichment of the PF resin is necessary for allowing resin detection within the composite [6]. Hence, for deuterium CP experiments to be applicable to industrial composites, ^{13}C and deuterium enriched PF resins need to be synthesized. Owing to the distinct chemical shifts for PF hydroxymethyl and methylene carbons in the CP/MAS NMR spectrum of wood/PF composites, formaldehyde is ideally suited for bearing the ^{13}C label. Unfortunately, doubly labeled formaldehyde (deuterated and ^{13}C enriched) is not commercially available and needs to be synthesized in the laboratory. Hence the feasibility of intermolecular CP experiments in wood/PF composites hinges in a first place upon the capability to synthesize formaldehyde-^{13}C-d_2. Besides, a ^{13}C and deuterium labeled PF resin cannot be synthesized with 100% deuterium. Phenol for instance can be purchased with 98% deuterium labeling [7]. The remaining 2% protons will generate intramolecular CP that is readily detected due to ^{13}C enrichment. Intramolecular CP may also arise from proton transfer at PF acidic sites (Figure II.1.1) [8].

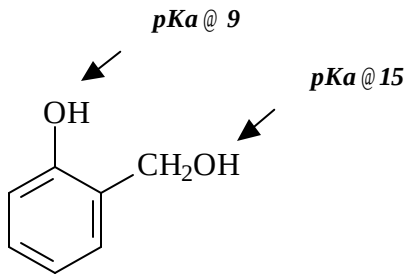

Figure II.1.1. Exchangeable Protons in Hydroxymethyl Phenol

Recall that PF resoles are synthesized under basic conditions (pH typically greater than 9). Under such conditions, phenolic hydroxyl groups are primarily in their ionic form. Wood on the other hand is acidic. When a basic PF is put in contact with wood, resin ionic sites may become predominantly protonated. In a deuterated PF resin then, proton exchange with wood could generate some degree of intramolecular CP (Figure II.1.2).

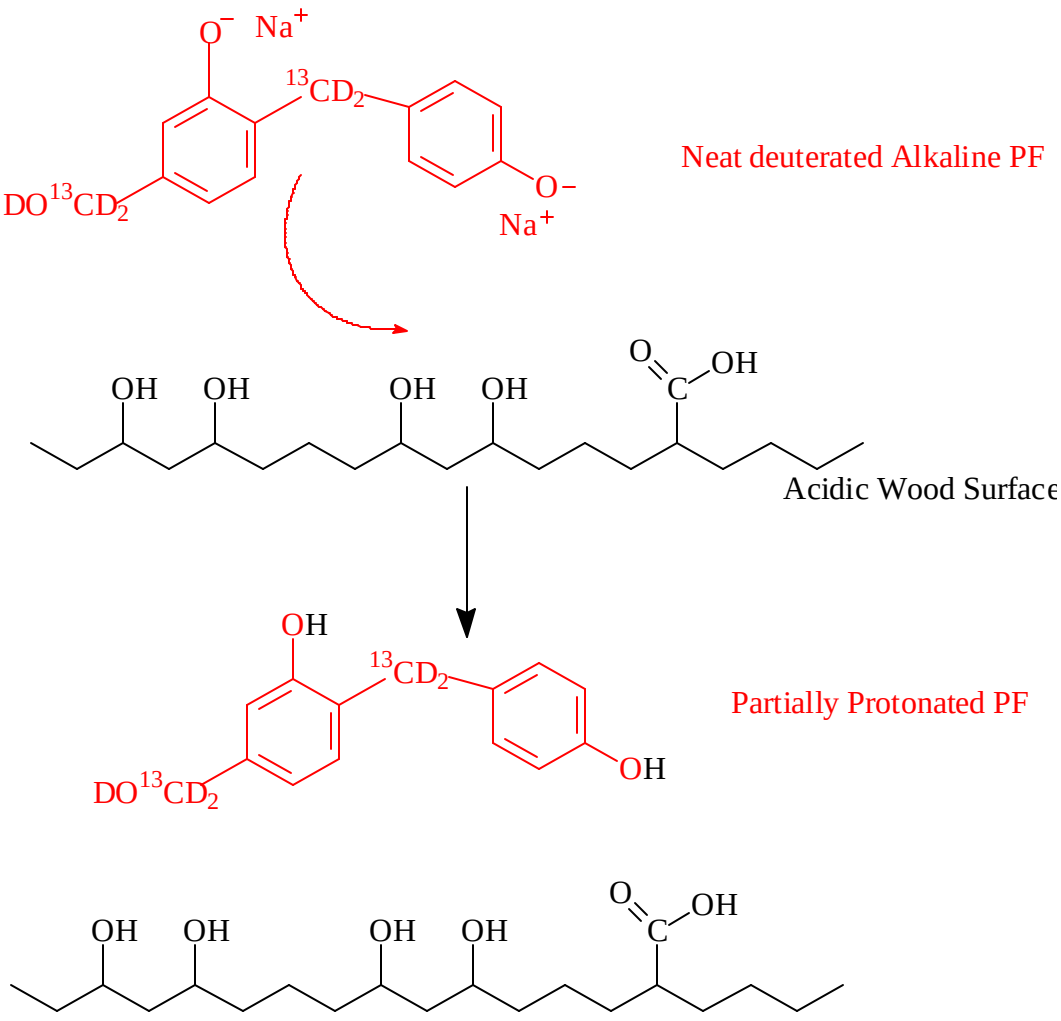

Figure II.1.2. Possible Proton Exchange between a Deuterated PF Resole and Wood

Therefore, in order to detect intermolecular CP between wood and a ^{13}C and deuterium enriched PF resin, reference to intramolecular CP must be made by evaluating CP in a control PF-^{13}C-d, which has been protonated at its acidic sites. With this control PF resin, ^{13}C-PF-$_{D/H}$, the maximum intramolecular CP that could take place in a wood/ ^{13}C-PF-$_{D/H}$ composite as a result of proton transfer can be quantified. It follows that intermolecular CP may be detected by comparing CP in the neat control ^{13}C-PF-$_{D/H}$ resin to that in the wood/^{13}C-PF-$_{D/H}$ composite. If cross-polarization in the ^{13}C-PF-$_{D/H}$ is enhanced by the presence of wood, then intermolecular CP from wood protons to the

resin is taking place thus indicating angstrom scale proximity at the wood/PF interphase. To date, no technique has been successfully applied to demonstrate wood/adhesive interactions on the angstrom scale. Decisive steps towards the molecular engineering of the wood/adhesive interphase could be taken with such a tool. It is therefore the objective of this study to assess the feasibility of deuterium CP experiments for wood/PF composites. In that purpose, the following tasks are addressed:

- Synthesis of ^{13}C-d_2 labeled paraformaldehyde
- Preparation of a control ^{13}C $PF_{D/H}$ resin that permits reference for intramolecular CP
- Comparison of CP rates in the neat ^{13}C $PF_{D/H}$ and in the wood/ ^{13}C $PF_{D/H}$ composite.

II.1.2 Lab-Scale Synthesis of Paraformaldehyde

Schmidt determined the most viable route for the lab scale synthesis of doubly labeled formaldehyde [15]. It consists of a gas phase oxidation of methanol over a molybdenum-iron oxide catalyst. The reaction proceeds via a two-step mechanism (Figure II.1.3).

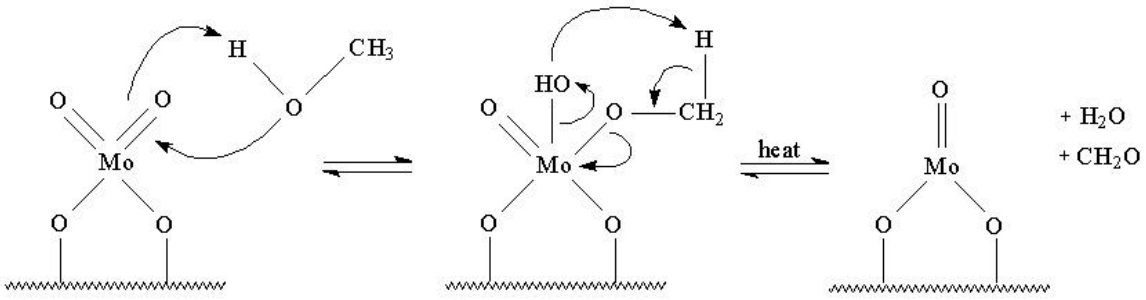

Figure II.1.3. Reaction Mechanism for Methanol Oxidation into Aqueous Formaldehyde with a Molybdenum-iron Oxide Catalyst ([15])

Initially, methanol is adsorbed onto the oxidized catalyst. The catalyst is subsequently reduced and methoxy decomposition into formaldehyde and water follows. The reaction is heat activated. An aqueous formaldehyde and paraformaldehyde slurry is obtained. Figure II.1.4 depicts the experimental set up Schmidt utilized for this reaction.

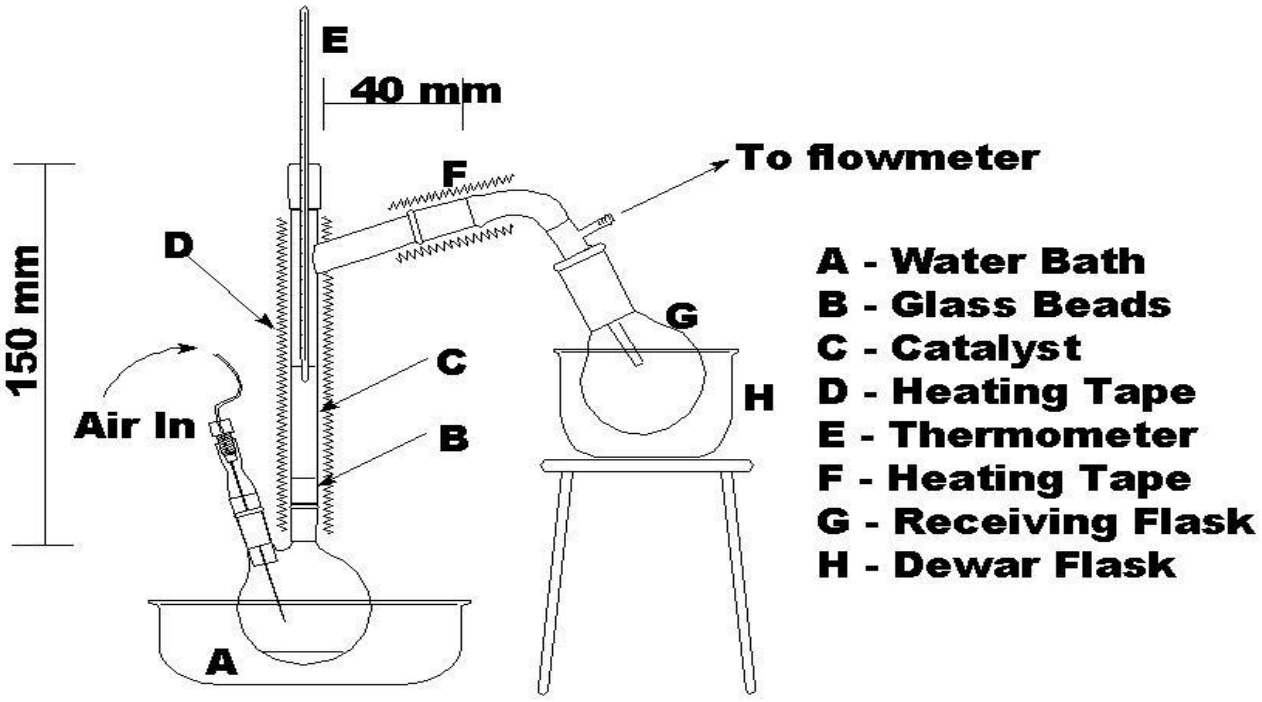

Figure II.1.4. Schmidt's Experimental Set up for Formaldehyde Synthesis, Except F, Which was Added in this Work ([12])

Liquid methanol is placed in a double neck flask immersed in a water bath (A). Dry air is blown on methanol at a controlled rate and the methanol/air vapors are mixed in a column through glass beads (B). The molybdenum iron oxide catalyst (C) is heated through a heating tape (D) to a controlled temperature (E). When the methanol/air mixture passes through the catalyst, methanol oxidation takes place thereby generating vapors of water and formaldehyde. The reaction products pass through the reaction vessel (F) and are finally condensed in the receiving flask (G), which is immersed in liquid nitrogen (H).

In this work, Schmidt 's experimental set up was utilized, however a number of modifications were applied. For instance, Schmidt first stabilized the catalyst temperature to 340°C under constant air flow and then replaced the empty flask with one containing approximately 1 ml of methanol [15]. Because the reaction is highly exothermic, a

substantial increase in catalyst temperature (30°C) occurs during the course of the synthesis. In the present work, it was deemed important to more thoroughly control the catalyst temperature by incrementally adding small amounts of methanol. More precisely, 0.25 ml aliquots of methanol were injected stepwise in the flask throughout the course of the reaction. Between each methanol injection, the catalyst temperature was allowed to stabilize back to the initial temperature. In addition, a heating tape was wrapped on the vessel walls (F) in Figure II.1.4 past the catalyst so as to prevent formaldehyde vapors from condensing on the glass wall ahead of the receiving flask. This second heating tape was stabilized at 120°C.

Schmidt also proposed a drying procedure for obtaining paraformaldehyde from the aqueous formaldehyde slurry. The drying procedure consisted of blowing dry air on the formaldehyde solution overnight and subsequently vacuum drying for 4 hours [15]. With this procedure, Schmidt was able to achieve 49% yield of paraformaldehyde-^{13}C-d_2 from methanol-^{13}C-d_4 [15]. However, methanol-^{13}C-d_4 cost motivates efforts towards improving the reaction yield. Hence, the first objective of this study has been to optimize the synthesis of paraformaldehyde-^{13}C-d_2. Logically, optimization focused on methanol conversion into formaldehyde and then on the drying procedure towards paraformaldehyde.

II.1.2.1 Optimization of Methanol Conversion to Aqueous Formaldehyde

Experimental plans were designed with a view to optimizing the synthesis parameters. The experimental set up was as in Figure II.1.4 and Schmidt ‘s procedure was utilized except for the modifications mentioned above. Experimental details can be found in reference [12]. Methanol purchased from Aldrich was used as received. The Molybdenum-iron Oxide catalyst obtained from Neste Resins Corp, was manufactured by Perstop Polyols. The catalyst was ground with mortar and pestle and particles with mesh size greater than 18 only were utilized. Experimental plans were based on Taguchi methods [22]. Taguchi methods help define the critical parameters and their optimum level toward a desirable response [22].

II.1.2.1.1 Principle of Taguchi Methods

Taguchi experimental plans are valuable tools for optimizing a procedure with a minimum number of experiments [22]. External and internal factors are defined [22]. External factors are those experimental variables that may be adjusted, while internal factors are inherent to the process and remain fixed. Distinct levels are assigned to the external factors and a Taguchi experimental table is designed in accordance with the number of factors and levels [22]. For instance, assessing two factors (A and B) at two levels (1 and 2) along with their interaction requires a $L2^2$ experimental table, which simply amounts to four experiments (Table II.1.1).

Table II.1.1. $L2^2$ Taguchi Experimental Table

Experiment	***Factors Levels***			***Response***
#1	A_1	B_1	A_1B_1	R_1
#2	A_1	B_2	A_1B_2	R_2
#3	A_2	B_1	A_2B_1	R_3
#4	A_2	B_2	A_2B_2	R_4

The influence of each factor at each level (and interaction) is computed from the experimental response. For example, contribution of factor A at level 1, A_1, is obtained from the average response to experiments 1 and 2 (II.1.1). Similarly, the contribution of A at level 2, A_2, can be compiled from experimental responses(II.1.2).

(II.1.1)
$$A_1 = \frac{R_1 + R_2}{2}$$

(II.1.2)
$$A_2 = \frac{R_3 + R_4}{2}$$

Comparing contributions from distinct levels helps indicate the favorable level for each factor. This is best visualized in a response plot such as in Figure II.1.5. In this

particular response plot, A_2 is clearly favorable towards maximal response while B bears little influence on the response.

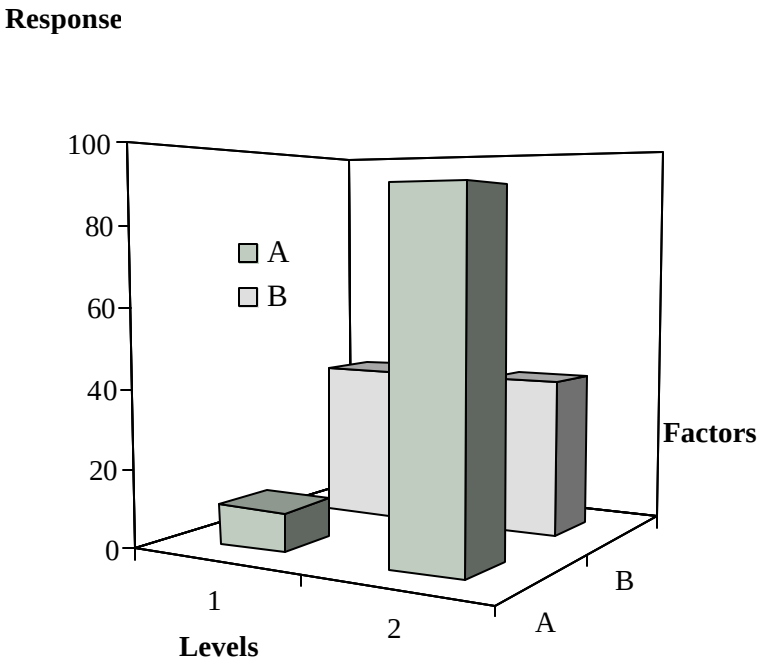

Figure II.1.5. Influence of Factors A and B on Response

A logical follow up for this response plot would consist of testing factor A in the vicinity of level 2 while the B factor would be discarded.

II.1.2.1.2 Application of Taguchi Methods for Optimizing Formaldehyde Yield

Because oxygen/methanol ratio and catalyst are reported to be critical in methanol oxidation towards formaldehyde, three parameters were defined as external factors [21]:

1) Catalyst temperature
2) Catalyst amount
3) Airflow rate

Successive Taguchi plans were performed, each of these assessing simultaneously two factors at two levels with $L2^2$ experimental tables. For each experiment, the response, formaldehyde yield, was measured by sodium sulfite titration [21]. The sodium

sulfite method consists of converting formaldehyde into base by reaction with 1M sodium sulfite (Figure II.1.6).

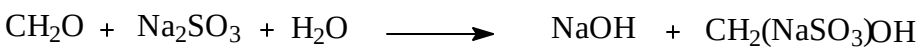

Figure II.1.6. Formaldehyde Reaction with Sodium Sulfite (from [21])

The base is then titrated with an acid using a color indicator. In the present study, 0.1 N hydrochloric acid and thymophtalein were utilized. Each mole of formaldehyde yielding one mole of sodium hydroxide, formaldehyde mass is defined as:

(II.1.3) $$formaldehyde(mg) = V \times N \times M$$

In Equation (II.1.3), V is the volume of the HCl solution in milliliters, N its normality and M the molar mass equal to 30.03 g/mol. Formaldehyde yield was measured on a percent mole basis. Three successive Taguchi plans were undertaken.

- *Experimental Plan #1*

In the first experimental plan, catalyst amount, airflow rate and interaction between these factors were considered. These factors were set at extreme levels in comparison with Schmidt's procedure (Table II.1.2) [15]. Catalyst temperature remained fixed throughout experimental plans 1 and 2, at 340°C.

Table II.1.2. Table of Factors for Taguchi Plan #1

	Catalyst amount (g)	***Airflow rate (ml/min)***
Level 1	***5***	***70***
Level 2	***20***	***210***

The response of the $L2^2$ experimental table is presented in Table II.1.3.

Table II.1.3. Experimental Table and Responses for Taguchi Plan #1

Experiment	*Catalyst amount (g)*	*Airflow rate (ml/min)*	*Interaction level*	*formaldehyde yield (mole %)*
#1	*5*	*70*	*1*	*29.9*
#2	*5*	*210*	*2*	*44.4*
#3	*20*	*70*	*2*	*19.1*
#4	*20*	*210*	*1*	*13.8*

It was found by plotting the table of response (Figure II.1.7), that both factors as well as the interaction were critical to the reaction yield.

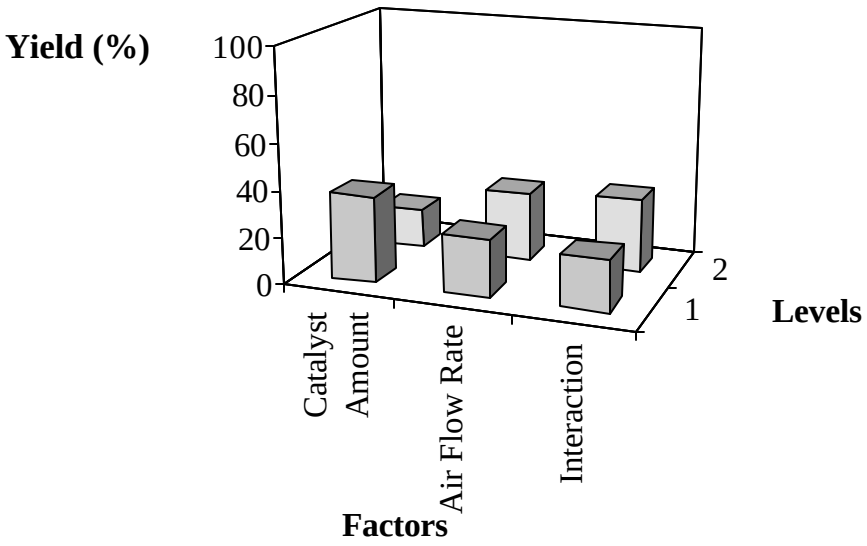

Figure II.1.7. Effect of Airflow rate, Catalyst Amount and their Interaction on Formaldehyde Yield (Taguchi plan #1)

Catalyst amount appeared as the most critical factor with a 20% gain in formaldehyde yield between level 2 (20g) and level 1 (5g). The interaction between airflow rate and catalyst amount was the second most significant factor with level 2 being the most favorable (i.e. high flow rate combined with low catalyst amount). Airflow rate

also displayed a minor effect on formaldehyde yield with high flow rates being preferable. In accordance with these results, a second Taguchi plan was undertaken.

- *Experimental Plan #2*

Table II.1.4 presents the levels that were selected for catalyst amount and airflow rate in the second Taguchi plan.

Table II.1.4: Table of Factors for Taguchi Plan #2

	Catalyst amount (g)	***Airflow rate (ml/min)***
Level 1	***4***	***130***
Level 2	***3***	***170***

Figure II.1.8 reveals that the catalyst amount remained the most critical factor in this second plan, with level 1 (3g) yielding a higher response than level 2. The flow rate exhibited the same trend as that observed in plan #1, namely high flow rates (level 2 i.e.170 ml/min) were more favorable to formaldehyde yield than low flow rates.

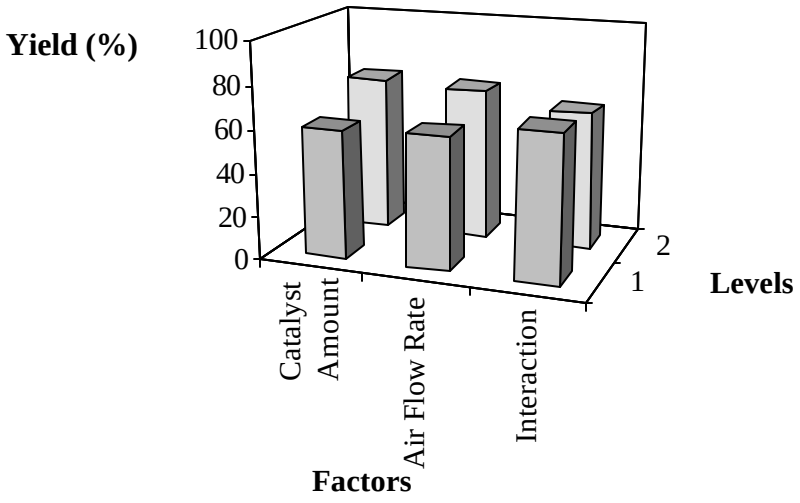

Figure II.1.8. Effect of Airflow rate, Catalyst Amount and their Interaction on Formaldehyde Yield (Taguchi plan #2)

At these levels however, the interaction was no longer critical to formaldehyde yield. One can also recognize that overall, the experimental conditions utilized in this second Taguchi plan gave higher yields (60-80%) than those from Taguchi plan #1 (20-40%). Clearly confirmed with this observation is the adequacy of the directions followed as a result of Taguchi plan #1. These directions were pursued in a third Taguchi plan.

II.1.2.1.3 Experimental Plan #3

In Taguchi plan #3, catalyst amount was retained as a factor while assigned with lower levels. The Airflow rate was no longer considered and remained at its optimum level (170 ml/min) for all experiments. Rather, catalyst temperature was introduced as an external factor (Table II.1.5).

Table II.1.5. Table of Factors for Taguchi Plan #3

	Catalyst amount (g)	***Temperature (°C)***
Level 1	***2.5***	***340***
Level 2	***1.5***	***280***

Results from this third experimental plan are illustrated in Figure II.1.9.

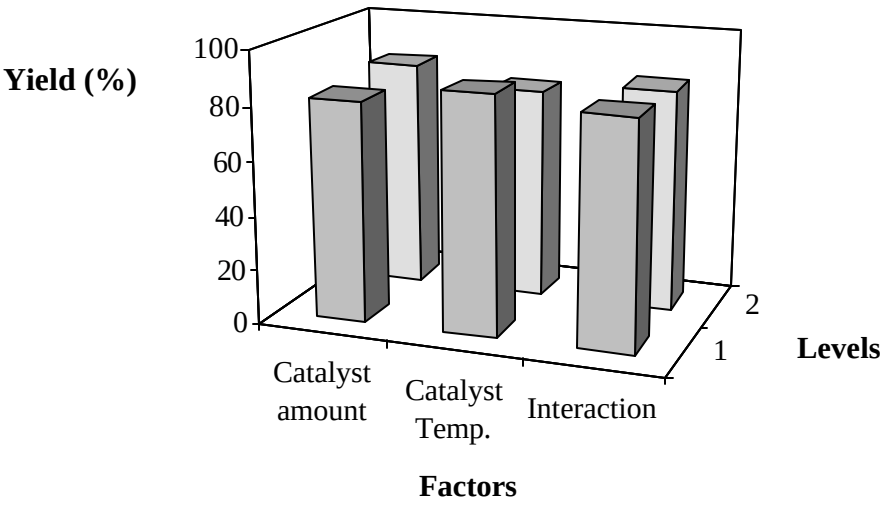

Figure II.1.9. Effect of Catalyst Amount, Catalyst Temperature and their Interaction on Formaldehyde Yield (Taguchi Plan #3)

At these levels, the factors assessed displayed a minor effect on formaldehyde yield. However, low catalyst amounts (1.5g) appeared again slightly favorable to formaldehyde yield. Catalyst temperature also had a minor effect on the reaction yield with level 1 (340°C) being more favorable than level 2 (280°C). No statistical interaction was found between catalyst amount and temperature at these levels. In any cases, all experiments performed in this third plan gave yields above 80%. Additional experiments were performed to further optimize catalyst temperature and amount but did not result in any yield enhancement. Thus optimal conditions for converting 1 ml of methanol into

aqueous formaldehyde under the particular experimental set up utilized in this study were finally defined as:

- Catalyst amount: 1.5g
- Catalyst temperature: 340°C
- Airflow rate: 170 ml/min

Using these conditions, 88% methanol conversion into aqueous formaldehyde was achieved. Murray et al., whom Schmidt adapted its synthesis procedure, reports 79% aqueous formaldehyde yield with this route [10]. Optimization efforts subsequently focused on minimizing formaldehyde loss during the drying step towards paraformaldehyde formation.

II.1.2.2 Optimization of the Drying Protocol towards Paraformaldehyde

Monomeric formaldehyde converts to paraformaldehyde through removal of water (Figure II.1.10) [21]. The equilibrium depends on formaldehyde concentration [21]. Specifically, the greater the formaldehyde concentration, the more the equilibrium shifts toward paraformaldehyde [21].

$$n\ (HO\text{-}CH_2\text{-}OH) \rightleftharpoons HO\text{-}(CH_2O)_n\text{-}H + (n\text{-}1)\ H_2O$$

Figure II.1.10. Formaldehyde and Paraformaldehyde Equilibrium

Unfortunately, formaldehyde has a low boiling point (-19°C) and significant formaldehyde loss occurs upon water evaporation [21]. In order to minimize formaldehyde loss, various drying techniques were evaluated:

1. The reaction product was dried under vacuum for 4 hours (room temperature and 0.1 mm Hg).
2. A steady air stream was blown on the reaction product overnight (at room temperature) and procedure 1) followed.
3. Paraformaldehyde was added to the reaction product and procedure 2) followed. Paraformaldehyde addition was intended to shift the equilibrium (Figure II.1.6) towards paraformaldehyde formation.
4. The reaction product was freeze dried.

These drying procedures were implemented on commercial formalin (37 weight percent formaldehyde). Paraformaldehyde yield was measured on a weight percent basis. Procedure 3) gave the highest yield of approximately 84%. Overall, methanol to paraformaldehyde yields were approximately 64%. The second step of the study was then undertaken, namely the preparation of a control PF destined to quantifying intramolecular CP.

II.1.3 Preparation of a Control ^{13}C $PF_{D/H}$ Resin

Thermodynamic considerations suggest that, in a wood/PF composite, angstrom scale interactions are favored with a low molecular weight PF resin, which has significant amount of monomers and dimers. It is therefore appropriate to utilize a low molecular weight PF resin for assessing the feasibility of deuterium CP experiments at the wood/PF interphase. In addition, the neat resin must provide a reference for quantifying intramolecular CP that may arise from proton transfer with wood. Therefore a procedure was developed for synthesizing a low molecular weight PF resin and protonating this resin at its exchangeable sites. The procedures were developed using unlabeled reagents and the resulting PF resin was characterized with common analytical techniques.

II.1.3.1 PF Resin Synthesis

Phenol crystals, 37% formaldehyde solution and 30% sodium hydroxide solution were purchased from Aldrich and used as received. Phenol, formaldehyde and sodium hydroxide were mixed in a triple neck flask in P: F: NaOH molar ratios of 1: 2: 0.2. Distilled water was added so as to obtain a theoretical solid content of 55%. The reaction flask, connected to a condenser, was immersed in a silicone oil bath at 80°C. Polymerization was allowed to proceed under stirring for one hour under a steady flow of N_2 gas. The resulting PF resin had a number average molecular weight of 190g / mole and a solid content of 44%. The resin had a pH of 9.5. The ^{13}C NMR spectrum confirms the low degree of condensation of the resin (Figure II.1.11). Namely, a minute signal is apparent for the methylene carbon bridging two phenol rings (35 to 45 ppm). In addition, significant signals for free formaldehyde (84 ppm) and hemiformal moieties (60-72 ppm and around 90 ppm) substantiate the low advancement of the polymerization. The carbons in the 120-160 ppm range are aromatic carbons. The signals above 150 ppm

arise from the carbon bearing the hydroxyl group i.e. the phenolic carbon. Overall, the PF-Low mixture comprises essentially monomers and dimers of mono-, di- and tri-substituted hydroxymethyl phenols.

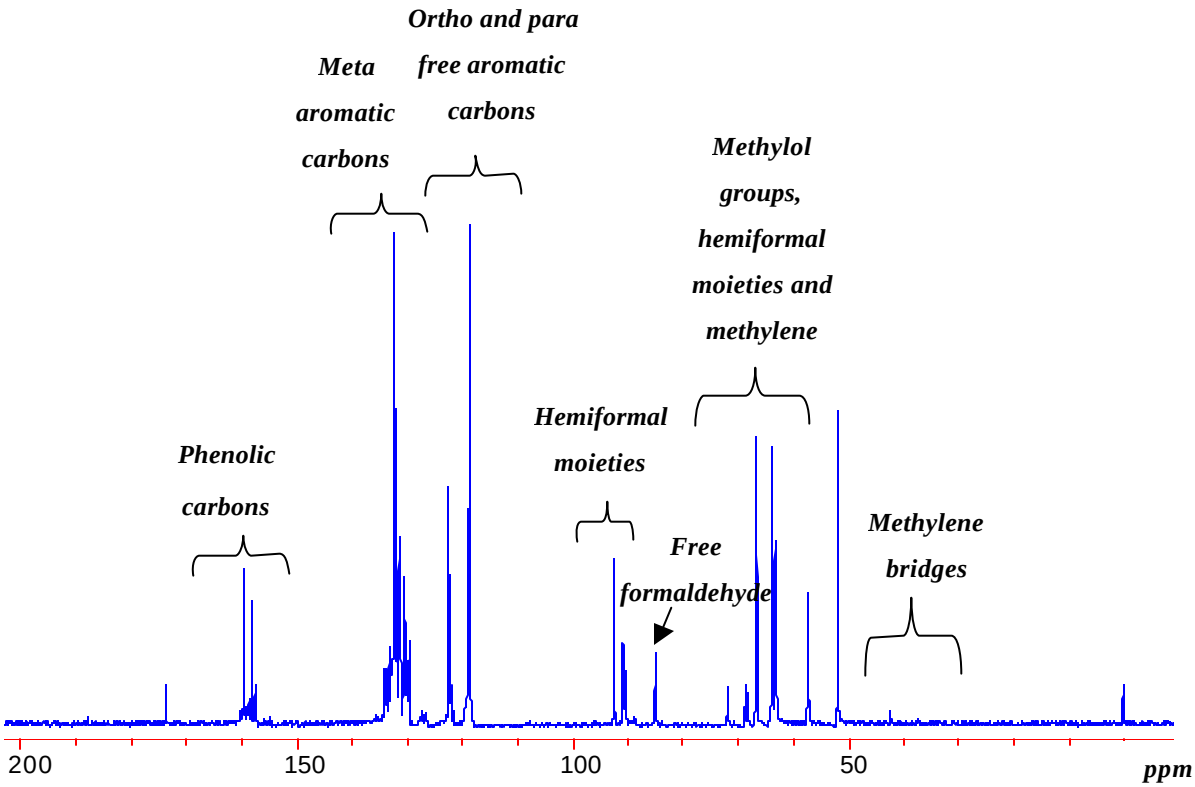

Figure II.1.11. ^{13}C *NMR Spectrum of Low Molecular Weight PF Resole in* D_2O*, Internally Referenced to DSS (Sodium 2,2-dimethyl-2-silapentane-5-sulfonate).*

An acidification procedure was then developed for mimicking the proton transfer that could take place during application and cure of a deuterated resin on wood.

II.1.3.2 Acidification Procedure

The acidification procedure aimed at decreasing the resin pH to at least 4. In that purpose, a 37 weight percent hydrochloric (HCl) solution was added dropwise in 1 g of PF resin by means of disposable micro-capillaries. The pH was continuously monitored during acidification. Typically, upon adding 20±10 µl of HCl solution, the PF resin turned transparent and exhibited an abrupt drop to the pH range 1-3. In many trials, pH

control proved tedious and the acidified resin would gel or phase separate during acidification. This is expected when one considers the pH dependence of PF polymerization rate and the influence of alkali on PF solubility in water [11]. At such acidic pH's, the rate of PF polymerization is generally enhanced [11]. With care, the acidification procedure was successfully achieved. The ^{13}C NMR spectrum of the freshly acidified PF resin indicates no significant advancement in the degree of condensation (Figure II.1.12). In fact, this spectrum is the same as that for the PF resole except for the upfield shift of the phenolic carbons by approximately 2 ppm. The chemical shifts for phenol and resorcinol have been established to be pH dependent [13], [14]. This is especially the case for carbons bearing the hydroxyl group, which exhibit lower chemical shifts with reduced alkalinity [14]. The upfield shift observed for the phenolic carbons in the acidified PF is therefore consistent with greater shielding as a result of protonation.

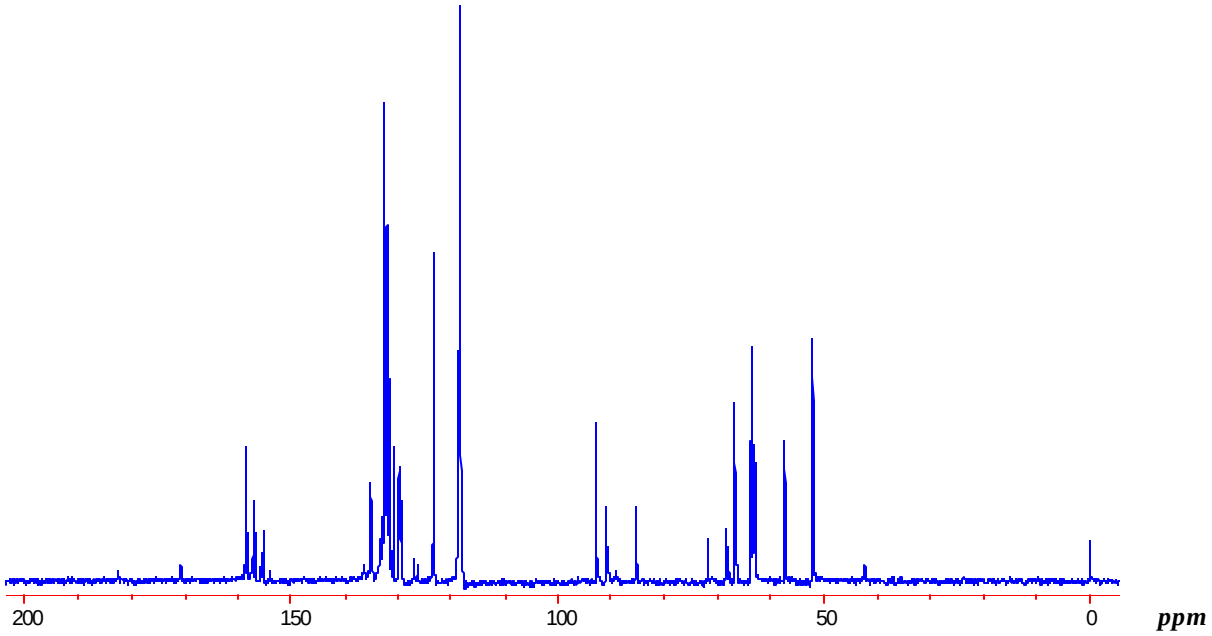

Figure II.1.12. ^{13}C NMR Spectrum of Acidified PF Resole in D_2O, Internally Referenced to DSS.

Synthesis and acidification procedures were implemented on labeled reagents for performing the deuterium CP experiment at the wood/^{13}C-PF-$_{D/H}$ interphase.

II.1.4 Intermolecular CP Experiments at the Wood/PF Interphase

With the capability to synthesize and protonate a ^{13}C and deuterium enriched low molecular weight PF resin, intermolecular CP experiments at the wood/PF interphase were assessed.

II.1.4.1 Materials and Methods

II.1.4.1.1 Synthesis of Paraformaldehyde-^{13}C-d_2

Methanol-^{13}C-d_4 (99% ^{13}C and 99% d_4) was purchased from Cambridge isotopes and used as received. From 5 ml labeled methanol, 3.7grams paraformaldehyde-^{13}C-d_2 were synthesized according to the procedure described in reference [12]. Figure II.1.13 represents the ^{13}C NMR spectrum of the doubly labeled paraformaldehyde after dissolution for 4 hours in D_2O in a heated sealed tube. Two signals are evident at 80.8 and 84.6 ppm. The 80.8 ppm signal arises from deuterated ^{13}C methylene glycol. It consists of a pentet signal with an intensity pattern of 1: 2: 3: 2: 1. Deuterium is a spin 1 nucleus. The (2n+1) rule predicts that 2 deuterons create five distinct local fields for the ^{13}C nucleus of methylene glycol. The observed splitting pattern therefore establishes deuterium attachment on the methylene glycol carbon.

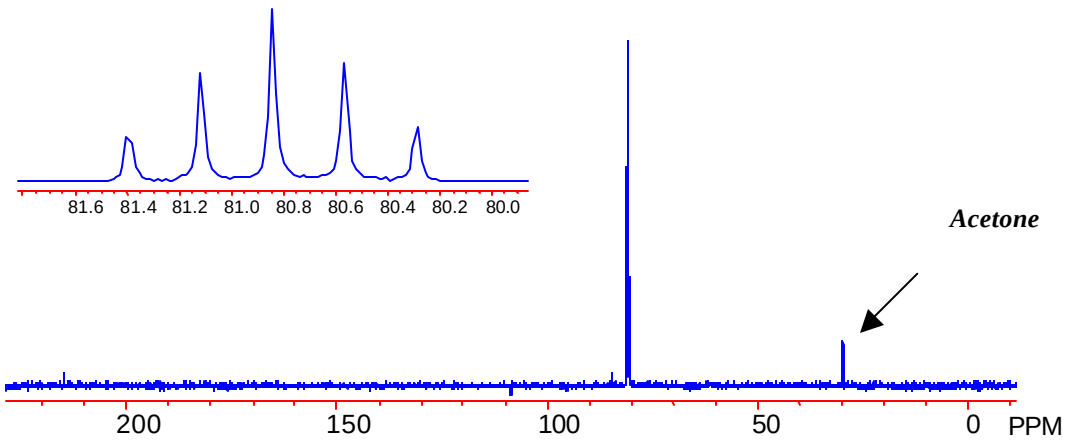

Figure II.1.13. ^{13}C NMR Spectrum of ^{13}C-d_2 Paraformaldehyde in D_2O , Internally Referenced to Acetone

The downfield pentet centered at 84.6 ppm arises from the dimer of methylene glycol. The doubly labeled paraformaldehyde was utilized to synthesize the low molecular weight ^{13}C-PF-$_{D/H}$ resin.

II.1.4.1.2 Synthesis of ^{13}C PF $_{D/H}$ Resin

98% deuterated Phenol-d_6, 30% sodium deuteroxide (99.5% d) and D_2O (99% d) were purchased from Cambridge isotopes inc. Reagents were used as received. 0.5287 grams of lab-scale synthesized ^{13}C-d_2 paraformaldehyde were mixed with 1.142 grams D_2O in a sealed tube filled with N_2 and submersed in an oil bath at 170°C. After 10 minutes of stirring the solution turned clear, indicating hydration of formaldehyde in D_2O. The formaldehyde-^{13}C-d_2 solution was utilized to synthesize a ^{13}C-PF-$_{D/H}$ resin according to the procedure described above. For the labeled resin, the synthesis was performed under N_2 gas. Immediately after the polymerization, 1gram of ^{13}C-deuterated PF resole was acidified with 20±10 µl of 37% HCl solution. Neat cured ^{13}C-PF-$_{D/H}$ samples and yellow-poplar/^{13}C-PF-$_{D/H}$ composites were subsequently manufactured.

II.1.4.1.3 Preparation of ^{13}C PF $_{D/H}$ Neat Samples and Yellow-poplar/^{13}C PF $_{D/H}$ Composites

Extracted yellow-poplar (*Liriodendron tulipifera*) powder was utilized for the manufacture of wood/^{13}C-PF-$_{D/H}$ composites. Extraction was deemed necessary for eliminating any intermolecular CP detection between wood extractives and the resin. Hence, yellow-poplar chips were ground to mesh 40 and submitted to soxhlet extraction in a series of solvents. Specifically, extraction in 50% aqueous acetone was repeated three times, each time for a period of 24 hours. Extractions in 50% aqueous methanol and 50 % aqueous tetrahydrofuran were subsequently performed over 12 hour periods. The amount of extractives was not measured. The extracted yellow-poplar powder was then dried in a desiccator over drierite for 48 hours. The final moisture content was 1.5% approximately. Composites were manufactured by mixing 0.410 grams extracted yellow-poplar powder with 0.604 grams ^{13}C-PF-$_{D/H}$ in a vial thereby yielding 65% theoretical resin solids on wood. In order to enhance resin diffusion and penetration into wood, the mixture was allowed to stand at room temperature for 30 minutes prior to cure. Cure was then performed by submersing the mixture in a vial in a silicone oil bath at 150°C for 15 minutes. Similarly, neat ^{13}C-PF-$_{D/H}$ samples were prepared by curing the PF resin in a

vial immersed in oil bath at 150°C for 15 minutes. The cured resin was then ground with a pestle and mortar. Both composite and neat resin samples were vacuum dried (room temperature and 0.1 mm Hg) overnight and kept in a dessicator with drierite until CP/MAS NMR analysis.

II.1.4.1.4 ^{13}C CP/MAS NMR Measurements

Cross-polarization experiments were performed on a Bruker MSL-300 MHz spectrometer using a 7 mm probenkopf MAS.07.D8 probe. The spectrometer frequency was set at 75.47 MHz for ^{13}C Nuclei and the spin locking frequency for the proton channel was approximately 56 kHz. Adamantane was utilized for establishing the Hartmann-Hahn match. Neat resin and composite powdered samples were packed in a zirconium oxide rotor, sealed with a Kel-f cap. The samples were spun at 5 kHz ± 20 Hz. A standard CP pulse with variable contact time wase performed. As many as 12 contact times were utilized within the 0.1-12 ms range. For each contact time, 600 scans were accumulated. The recycle delay was 3.75 s and the acquisition time was 50 ms. Three neat ^{13}C-PF-$_{D/H}$ resin samples and two wood/^{13}C-PF-$_{D/H}$ composites were analyzed.

II.1.4.2 Results and Discussion

^{13}C CP/MAS NMR spectra for the neat ^{13}C-PF-$_{D/H}$ resin and the wood/ ^{13}C-PF-$_{D/H}$ composite are presented in Figure II.1.14. In both spectra, PF methylene carbons are clearly detected in the 30-40 ppm region. This region comprises two overlapping resonances, one around 31 ppm, which corresponds to ortho-ortho methylene bridges and the other centered at 40 ppm, which is characteristic of para-para methylene bridges [19]. A resonance at 63 ppm arises from PF hydroxymethyl carbons. Additional peaks are detected around 71 and 90 ppm. Signal intensities suggest that these peaks stem from other formaldehyde-based chemical structures in the PF network. In fact, signals that generally arise from the aromatic PF carbons (here without ^{13}C label) and from the wood polymers remain undetected in this spectrum, at least compared to the 100% ^{13}C enriched PF carbons. Similarly, spinning side bands that are typically generated from the aromatic PF carbons are not apparent in the spectra. In a CP/MAS NMR study of PF resins, Maciel ascribes resonances around 71 ppm to methylene carbons of ether structures [18]. Dibenzyl ether linkages are believed to form under acid condensation of PF resins [20].

Hemiformal species may also contribute to the 71 ppm resonance. In fact, the small peak centered at 90 ppm confirms the presence of hemiformal species. It is established from solution ^{13}C NMR that hemiformal moieties attached to phenolic rings appear in the vicinity of 90 ppm [19].

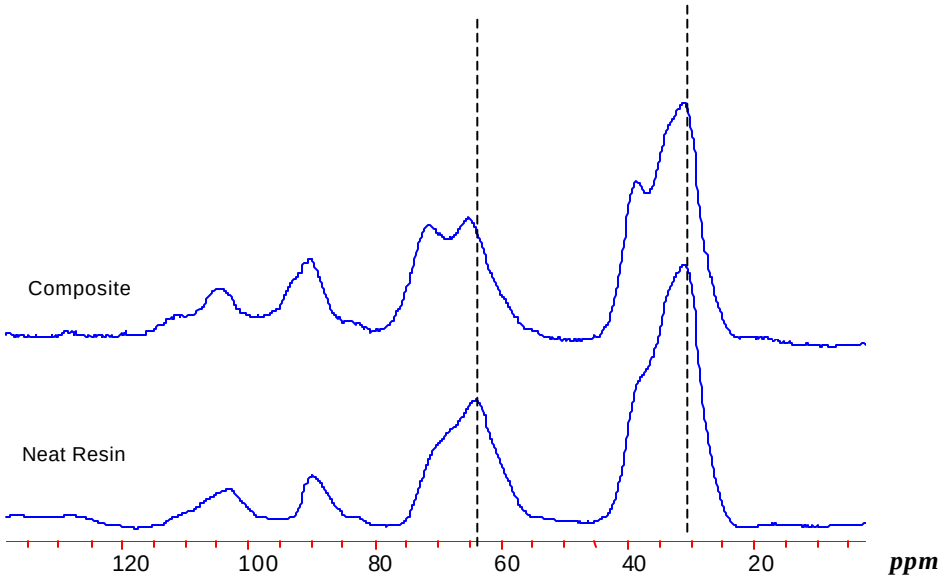

Figure II.1.14. ^{13}C CP/MAS NMR Spectrum of Neat ^{13}C PF $_{D/H}$ (top) and ^{13}C PF $_{D/H}$ / Yellow-poplar Composite

Clearly from Figure II.1.14, ^{13}C enrichment allows monitoring PF nuclei both in the neat ^{13}C-PF-$_{D/H}$ sample and in the wood/ ^{13}C-PF-$_{D/H}$ composite. Detection of the resin indicates that PF ^{13}C nuclei are cross-polarized from a proton source in neat and composite samples. A more informative characterization of CP behavior in both systems is obtained by assessing magnetization of PF methylene carbons. In Figure II.1.15 the logarithm of the normalized intensity of PF methylene carbon is plotted as a function of contact time for neat resin and composite samples. The data are averages of 3 samples for the neat ^{13}C-PF-$_{D/H}$ and 2 samples for the wood/ ^{13}C-PF-$_{D/H}$ composite. One sees on Figure II.1.15 that at short contact times, the signal intensity rises rapidly to its maximum value. The build up of the signal stems from cross-polarization between proton and ^{13}C nuclei. Therefore faster CP is evidenced when shorter contact times are required to

achieve maximum signal intensity. In that perspective, Figure II.1.15 indicates faster CP of methylene carbons within neat ^{13}C-PF-$_{D/H}$ resins than within yellow-poplar/ ^{13}C-PF-$_{D/H}$ composites. Cross-polarization between the resin and wood is therefore not evidenced. Also apparent in this figure, is the effect of deuterium enrichment. Namely, at long contact times (5-15 ms), ^{13}C magnetization typically decreases as a result of proton spin lattice relaxation in the rotating frame, $^{H}T_{1\rho}$.

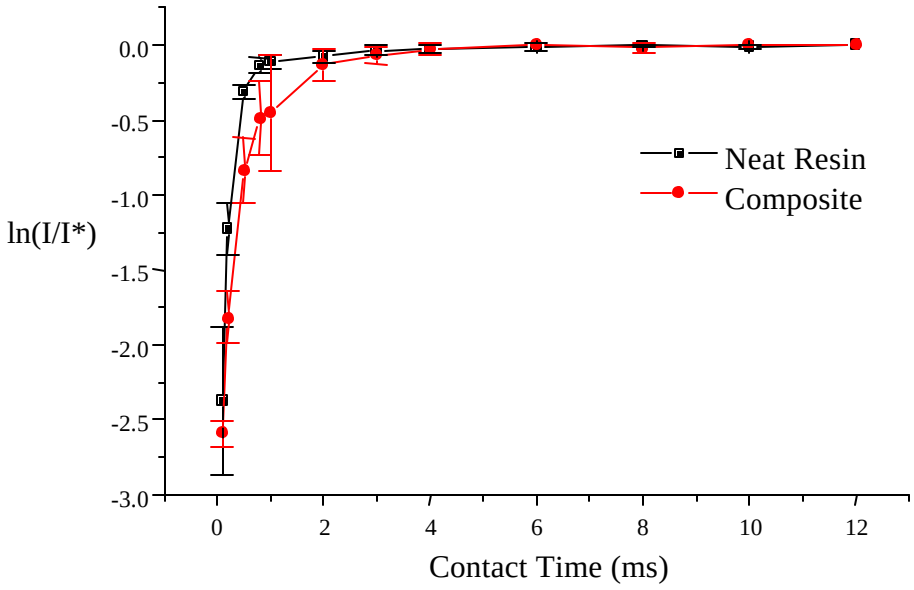

Figure II.1.15. Magnetization Curve for Methylene Carbon (35 ppm) in Neat ^{13}C-PF-$_{D/H}$ Resin and in Yellow-poplar/^{13}C-PF-$_{D/H}$ Composite

Spin diffusion is known to contribute significantly to $^{H}T_{1\rho}$ relaxation. In particular, the contribution of spin diffusion to $^{H}T_{1\rho}$ in PF networks has been demonstrated [16]. In Figure II.1.15, no loss of magnetization is evident at long contact times. Deuterium enrichment acts to physically separate protons thereby hindering spin diffusion. It is therefore not unexpected that ineffective spin diffusion hampers $^{H}T_{1\rho}$ relaxation in these systems.

Slower CP in composites than in neat resin samples suggests that intermolecular cross-polarization between wood protons and PF resin does not occur in this particular wood/ PF composite. Experimental conditions have been selected so as to favor

molecular scale interactions in the interphase (low molecular weight PF resin, significant diffusion time of the PF resin in wood). Slower CP in the composite sample therefore suggests that no miscibility on the 10-20 angstrom level is detected. However, an additional parameter must be taken into account. Namely, CP efficiency not only depends on proton spatial proximity but also on the molecular rigidity of the interacting nuclei pair [9].

Cross-polarization is especially affected by near static molecular motions [9]. In other words, the more rigid materials on the near static frequency scale cross-polarize faster than mobile materials on this frequency scale. Therefore, changes in CP may also stem from differences in near static molecular motions. When comparing a highly crosslinked thermosetting resin in the neat state to that cured in the presence of wood, differences in the network rigidity may occur. In fact, Schmidt demonstrated that wood has a substantial influence on PF network molecular structure and dynamics [15]. When comparing $^{H}T_{1\rho}$ values for methylene carbons in neat cured resin and in wood/PF composites, Schmidt evidenced a dramatic decrease of PF $^{H}T_{1\rho}$ in the presence of wood. For PF methylene carbons, decrease in $^{H}T_{1\rho}$ is associated with lower network crosslink density and lower glass transition temperature [16]. These observations indicate that PF network mobility is enhanced when curing the PF resin in the presence of wood. Although molecular motions probed by $^{H}T_{1\rho}$ differ from those affecting CP, it can be speculated that curing a PF resin in the presence of wood hinders its CP as a result of lower molecular rigidity. Consequently, the present observation that wood delays cross-polarization in the PF resin does not necessarily invalidate the hypothesis of angstrom scale miscibility at the wood/PF interphase. Rather, it indicates that in wood/adhesive systems, morphological information may be obscured by substantial differences in molecular rigidities between neat resin and composite samples. Consequently, two scenarios can equally be envisioned: 1) intermolecular CP between wood and the PF resin is not detected because angstrom miscibility is not occurring in wood/PF systems. 2) intermolecular CP is inhibited in the composite sample because of increased network motion caused by wood.

It is further interesting to recall a morphological difference between neat PF networks and PF networks cured in the presence of wood. Namely, Schmidt et al.

showed that wood induces phase heterogeneity in a PF network as revealed by distinct $^{H}T_{1\rho}$ values for the methylene and hydroxymethyl carbons [17]. This dynamic heterogeneity in composites contrasts with homogeneity that is observed in neat PF networks [16]. The study suggested that hydroxymethyl carbons are more intimately associated with wood polymers. Closer proximity is in favor of intermolecular CP detection. On the other hand, closer association with wood polymers may alter the nuclei dynamics more significantly. In such a case, morphological information would be obscured to a greater extent than for the methylene carbon. In order to test this hypothesis, intermolecular CP was assessed through PF hydroxymethyl carbon. Average magnetization curves for hydroxymethyl carbons in neat ^{13}C-PF-$_{D/H}$ resin and in the yellow-poplar/ ^{13}C-PF-$_{D/H}$ composite are compared in Figure II.1.16.

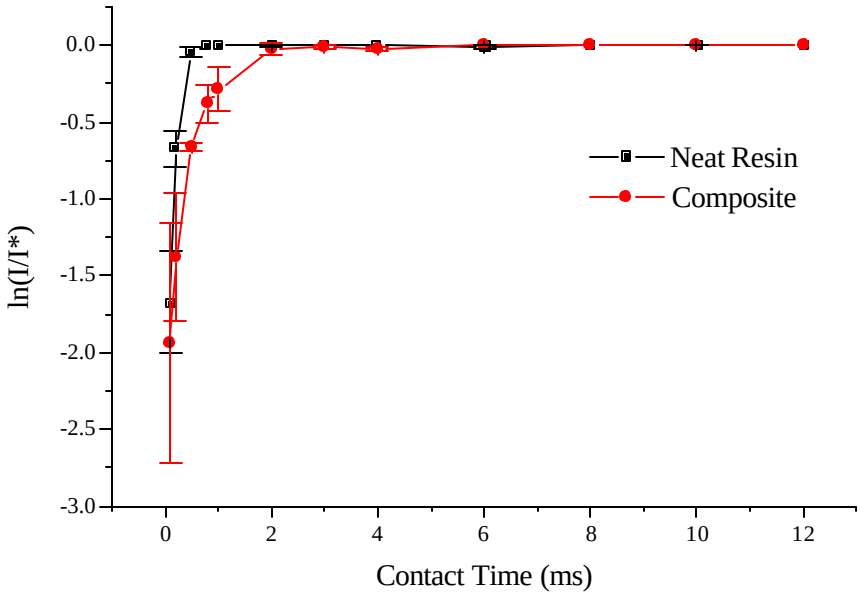

Figure II.1.16. Magnetization Curves for the Hydroxymethyl Carbons (65 ppm) in Neat ^{13}C-PF-$_{D/H}$ Resin and Yellow-poplar/^{13}C-PF-$_{D/H}$ Composite

In Figure II.1.16, one sees again that CP occurs faster in the neat ^{13}C PF $_{D/H}$ resin than in the composite thereby denying the occurrence of intermolecular CP detection.

This observation supports the hypothesis that significant dynamic changes between neat PF resin and wood/PF composites obscure the morphological information typically obtainable from deuterium CP experiments. It seems that deuterium CP experiments are not suited for detecting angstrom scale morphological features of wood adhesive composites.

II.1.5 Conclusion

In this study, the steps necessary for adapting deuterium CP experiments to wood/PF composites have been completed. Namely, the in-lab synthesis of doubly labeled formaldehyde has been revisited and optimized [12]. A PF resin with specific isotopic design has been prepared in order to account for the complications of proton transfer in deuterated resins. Comparing CP in neat control deuterated PF resins and wood/PF composites did not indicate any intermolecular CP, whether the PF methylene or hydroxymethyl carbon was probed. While detection of intermolecular CP would reveal angstrom scale interactions, the opposite observation does not rule out angstrom scale miscibility at the wood/PF interphase. Rather, the study suggests that intramolecular CP in the neat resin and dynamic changes between neat resin and composite obscure morphological information. In wood/adhesive systems, owing to the substantial difference in component rigidity, CP efficiency is likely to be reduced by molecular mobility. As a consequence, deuterium CP experiments used to detect molecular miscibility in synthetic polymer blends cannot yield angstrom scale morphology into wood-PF composites.

II.1.6 References

[1] Zhang X., A. Natansohn and A. Eisenberg, Intermolecular Cross-polarization Studies of the Miscibility Enhancement of PS/PMMA Blends through Ionic Interactions. Macromolecules 23 (2) 412, 1990.

[2] Schaefer J., M.Sefcik, Stejskal E. and R. McKay, Magic-angle Carbon-13 Nuclear Magnetic Resonance Analysis of the Interface between Phases in a Blend of Polystyrene with a Polystyrene-Polybutadiene Block Copolymer, Macromolecules 14 (1) 188, 1981.

[3] Parmer J., L. Dickinson, J. Chien and R. Porter, Macromolecules 20, 2308, 1987.

[4] Guo M. and H.G. Zachmann G. Intermolecular Cross-polarization Nuclear Magnetic Resonance Studies of the Miscibility of Poly(ethylene naphthalenedicarboxylate)/poly(ethylene terephthalate) Blends, Polymer, 34 (12) 2504, 1993.

[5] Walton J., M. Lizak, M. Conradi, T. Gullion and J. Schaefer, Hydrostatic Pressure Dependence of Molecular Motions in Polycarbonates, Macromolecules 23 (2) 416, 1990.

[6] Frazier C.E., J. Ni and R.G. Schmidt, Applications of NMR Spectroscopy to the Analysis of Wood/Adhesives Bondlines, Advances in Lignocellulosic Characterization, Chapter 6, p145-156, Ed. D. S. Argyropoulos, Tappi press, Atlanta, 1999.

[7] Cambridge Isotopes Inc. Catalog, 1998-1999.

[8] Kresge A.J. and Y. Chiang, Journal of American Chemical Society, 89, 17, 4411-4417, 1967.

[9] Mehring M., Principle of High Resolution NMR in Solids, Second Ed., Springer-Verlag, New York, 1983.

[10] Murray A. and D. L. Williams, Organic Synthesis With Isotopes, Chapter 6, Part I. Compounds of Isotopic Carbon, p. 607, Interscience Publishers, New York, 1958.

[11] Pizzi A. and K.L. Mittal, Handbook of Adhesive Technology, Marcel Dekker, Inc., New York, p. 336, 1994.

[12] Schmidt R.G, M.P. Laborie and C.E. Frazier, Lab Scale Synthesis of Doubly Labeled Formaldehyde for Formaldehyde Based Wood Adhesives, Holzforschung, 54, 1999.

[13] Nakashima T. T. and Maciel G.E., Effects of pH on the Carbon-13 Magnetic Resonance Spectrum of Phenol, Applied Spectroscopy, 26 (2) 220, 1972.

[14] Christiansen A.W., Resorcinol-Formaldehyde Reactions in Dilute Solution Observed by Carbon-13 NMR Spectroscopy., Journal of Applied Polymer Science, 75, 1760, 2000.

[15] Schmidt R.G., Aspects of Wood Adhesion: applications of ^{13}C CP/MAS NMR and Fracture Testing, Doctoral Dissertation, Virginia Polytechnic Institute and State University, Doctoral Dissertation, p.92-106, January 30 1998.

[16] Schmidt R.G. and C.E. Frazier, Network Characterization of Phenol-Formaldehyde Thermosetting Wood Adhesive. Int. J. Adhes. Adhes. 18 (2) 139, 1998.

[17] Schmidt R.G. and C.E. Frazier, ^{13}C CP/MAS NMR as a Direct Probe of the Wood PF Adhesive Bondline, Wood and Fiber Science, 30 (3), 250, 1998.

[18] Chuang I. S. and G.E. Maciel, ^{13}C NMR Investigation of the Stability of Resol-Type Phenol-Formaldehyde Resin Toward Formalin, Toward Base, and toward Nonoxidizing or Oxidizing Acid, Macromolecules, 24, 1025, 1991.

[19] Werstler D.D., Quantitative ^{13}C NMR Characterization of Aqueous Formaldehyde Resins: 1. Phenol –Formaldehyde Resins, Polymer, 27, 750, 1986.

[20] Grenier-Loustalot M-F. , S. Larroque and P. Grenier, Phenolic Resins: 1. Mechanisms and Kinetics of Phenol and of the First Polycondensates Towards Formaldehyde in Solution, Polymer, 35 (14) 3047, 1994.

[21] Walker, J. F. Formaldehyde. 3rd ed., R. E. Krieger Publishers. Huntington, New York. 1975.

[22] Peace, G. S., Taguchi Methods: a Hands-on Approach, Addison-Wesley, Reading Massachusetts, 1993.

CHAPTER. II.2. COOPERATIVITY ANALYSIS FOR LIGNIN GLASS TRANSITION

II.2.1 Introduction

One objective of this research is to develop methodologies that probe the scale of wood/adhesive interactions through molecular dynamics. Among polymer relaxation mechanisms, the alpha relaxation, or glass transition, typically involves nanometer to micron scale domains. In wood science, lignin glass transition constitutes the most studied relaxation mechanism. Interest in the lignin glass transition arises from its impact on the processing of several wood-based products (pulp and paper, wood-based composites). Several studies indicate that the glass transition of lignin can be detected *in-situ* [1], [14], [2]. It is important to emphasize however that the *in-situ* lignin glass transition is largely influenced by the interactions and the associations with the other wood components. In fact, the softening behavior of isolated lignin is dramatically different from that of *in-situ* lignin, clearly indicating the contribution of all wood components to lignin *in-situ* softening [20]. In the present study, the term *in-situ* lignin glass transition therefore refers to the lignin segmental motion as influenced by the plasticizing effect of wood carbohydrates for instance and other effects from interactions with wood components.

In dry wood, lignin glass transition occurs in the vicinity of 200°C. Its *in-situ* detection is therefore difficult without damaging the wood structure. However, lignin glass transition temperature is dramatically reduced in plasticized wood. Depending upon the wood species and the nature of the diluent, the lignin glass transition can be decreased to the 60-90°C range [1], [14], [2]. Salmén was the first to apply the time-temperature superposition principle (TTSP) for water-saturated wood around the lignin glass transition [1]. Kelley et al. further determined the influence of moisture content on wood softening and observed phase separation in the amorphous matrix of wood by detecting distinct glass transitions for hemicellulose and lignin [2]. In addition, Kelley et al. demonstrated that TTSP applies to the *in-situ* lignin transition for wood plasticized by ethyl formamide [2]. Both studies indicated that the Williams-Landel-Ferry (WLF) equation [3] provides a good treatment of wood viscoelastic properties above the lignin

glass transition [1]-[2]. The applicability of the WLF equation for plasticized wood suggests that the empirical coupling model developed by Plazeck and Ngai may also be suitable for describing wood viscoelastic behavior [5]. The reader is directed to Chapter I-3 for a detailed review of the Ngai coupling model along with the concept of intermolecular cooperativity. Briefly, deviations from Arrhenius behavior around the glass transition can be related to intermolecular coupling between non-bonded neighboring segments. At a temperature far above T_g (T_g + 80K), segmental relaxation is independent of non-bonded segments and occurs via bond rotation with a characteristic relaxation time, the primitive relaxation time [6]. The primitive relaxation time (τ_0) is therefore characteristic of conformational transition rates of an isolated chain. At much lower temperatures, molecular motions are restricted by intermolecular cooperativity between non-bonded segments. Hence, characteristic relaxation times in this temperature region are retarded due to intermolecular coupling. The Ngai coupling model quantifies the restriction in molecular motions induced by intermolecular coupling [5]:

$$t^*(T) = \left[(1-n)w_c^{\,n} t_0(T)\right]^{1/(1-n)} \qquad \textit{(II.2.1)}$$

In equation (II.2.1), τ^* represents the characteristic relaxation time under the influence of molecular coupling at a given temperature T, τ_0 is the primitive relaxation time, n is the coupling constant and ω_c represents the crossover frequency between time domains for independent segmental relaxation on the one hand and cooperative segmental relaxation on the other hand. The coupling constant, n, quantifies the extent of intermolecular cooperativity among non-bonded segments and ranges from 0 to 1 with high values representing a high degree of intermolecular cooperativity. Empirically, Plazeck and Ngai determined that polymers cooled closer to thermodynamic equilibrium obey the WLF form of the coupling model [5]:

$$(1-n)\log a_T = \frac{-C_1\left(\dfrac{T-T_g}{T_g}\right)}{C_2 + \left(\dfrac{T-T_g}{T_g}\right)} \qquad \textit{(II.2.2)}$$

In equation (II.2.2), the authors postulated empirical universal values of C_1= 5.49 and C_2=0.141, [5]. The coupling constant can therefore be retrieved by normalizing the WLF shift factor to the fractional deviation from the T_g. In addition to quantifying deviations from Arrhenius behavior, the coupling constant reflects the distribution of relaxation mechanisms in the vicinity of the glass transition. In fact, for neat polymers, the coupling constant correlates to the Kohlrausch-Williams-Watt (KWW) exponent, β, which describes the non-exponentiality of the alpha dispersion [7]:

(II.2.3) $$n = 1 - b$$

Therefore, the coupling constant not only reflects the severity of the deviation from an Arrhenius behavior, but also the distribution breadth of relaxation mechanisms involved in the alpha relaxation. Polymers that display high intermolecular cooperativity (high n value) around the T_g are characterized by a broad distribution of relaxation mechanisms. On the other hand, polymers with little intermolecular cooperativity (low n value) around the T_g are more dynamically homogeneous and display a more narrow distribution of relaxation mechanisms. Typically, polymers have coupling constants in the 0.35-0.75 range [4]. The widespread success of the coupling model for neat polymers and more complex polymeric systems is well established and the reader is again referred to chapter-I-2-A on that matter. Wood itself is a complex composite structure of polymers. In spite of this complexity, universal viscoelastic models such as the TTSP are suitable to describe the viscoelastic properties of wood and of lignin softening in particular [1]. This fact suggests that the cooperativity analysis may also be applicable to the *in-situ* lignin glass transition. Note however, that an *in-situ* analysis would reflect lignin characteristics but also its association with other wood components. With the feasibility of such an analysis, a novel tool would be available to investigate molecular aspects of the amorphous wood matrix. Of particular interest for the present research, the cooperativity analysis may provide an additional probe for interactions between wood polymers and adhesives. The objective of the present study is to investigate the feasibility of the cooperativity analysis on wood. Specifically the validity of the Ngai coupling model for the *in-situ* lignin glass transition is investigated. In addition,

preliminary data are sought so as to establish whether such analyses could be applied to wood/adhesive composites.

II.2.2 Materials and Methods

II.2.2.1 Materials

Two wood species were selected for analysis, these were yellow-poplar (*Liriodendron tulipifera*), a hardwood, and Norwegian Spruce (*Picea abies*), a softwood. Flakes with dimensions 3.5 mm in the radial direction, 0.85 mm in the tangential direction and 10 mm in the longitudinal direction were manufactured from soaked wood blocks using a disk flaker. These were manufactured from sapwood exclusively. For yellow-poplar, the samples consisted of earlywood only, while in Spruce a small amount of latewood was also sampled owing to the smaller annual rings (approximately 3 mm/ annual ring). The specimens were allowed to air dry to approximately 6-8% moisture content. They were subsequently saturated in ethylene glycol. Ethylene glycol was chosen as the diluent because of its high boiling point (approximately 150°C) thus enabling subsequent viscoelastic measurements on a large temperature window. Sample saturation in ethylene glycol consisted of immersing the sample in an ethylene glycol bath that had been set up in open air and adjusted to a temperature of 120±3 °C. The mass of ethylene glycol absorbed by wood was not measured. After conditioning the sample for one hour in the ethylene glycol bath, the sample was submitted to viscoelastic measurements. A minimum of five samples was prepared for each species.

II.2.2.2 Dynamic Mechanical Analysis (DMA)

Viscoelastic measurements consisted of DMA measurements with a Perkin Elmer DMA 7e. The sample was tested in a dual cantilever beam mode along the grain. Throughout DMA measurements the specimen remained immersed in ethylene glycol. Viscoelastic measurements on immersed samples were afforded by using a Teflon cup that was manufactured to fit in the instrument furnace. The Teflon cup was filled with approximately 40 cm^3 of ethylene glycol thus allowing submersion measurements with regular dual cantilever beam clamps. During the measurements, evaporation of ethylene glycol and vapor contamination of the DMA driveshaft was minimized by covering the

Teflon cup with aluminum foil. In addition, helium (flow rate of 70 ml/min) was utilized as the purge gas. For each sample, DMA conditions were determined from consecutive dynamic stress scans at 20°C and also at 120 °C. From these dynamic stress scans, a strain level was selected for remaining in the linear viscoelastic domain at both temperatures. Some samples did not afford a common strain level for linear viscoelasticity at the two temperatures and were discarded. For the satisfactory samples, the selected strain level did not exceed 0.1%. It was deemed important to perform the high temperature dynamic stress scan (lignin in the rubbery state) just before the actual viscoelastic measurements as a means to erase the sample thermal history. Hence, following the dynamic stress scan at 120°C, the sample was cooled to 20°C at a controlled rate (1.5°C/ min) while remaining in the ethylene glycol bath. Thereafter, temperature scans were performed at the predetermined strain level with a static load of 120% of the dynamic load. Temperature scans were performed at a fixed frequency from 20°C to 120 °C using a heating rate of 2°C/min. Five measurement frequencies were successively applied, namely 0.2, 0.6, 1, 2 and 6 Hertz. Between each temperature scan, the sample was allowed to cool to 20° C at 1.5°C/min in the ethylene glycol bath. Hence each of the successive temperature scans was preceded by the same thermal treatment (same cooling rate after reaching the rubbery state of lignin).

II.2.2.3 Data Analysis

Fifth order polynomials were fitted to the log (E')-temperature curves at the five frequencies according to the procedure utilized by Olsson et al. (Figure II.2.1) [14].

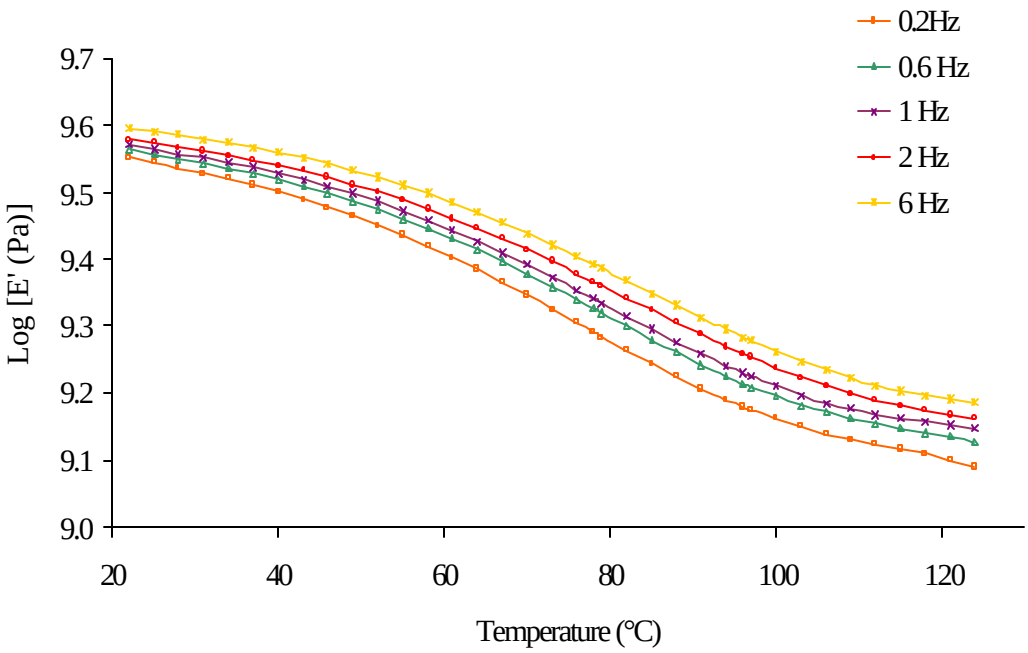

Figure II.2.1. Polynomial fit for Storage Modulus versus Temperature at 5 Frequencies.

The polynomial fits were utilized to generate isotherms every 3°C (Figure II.2.2).

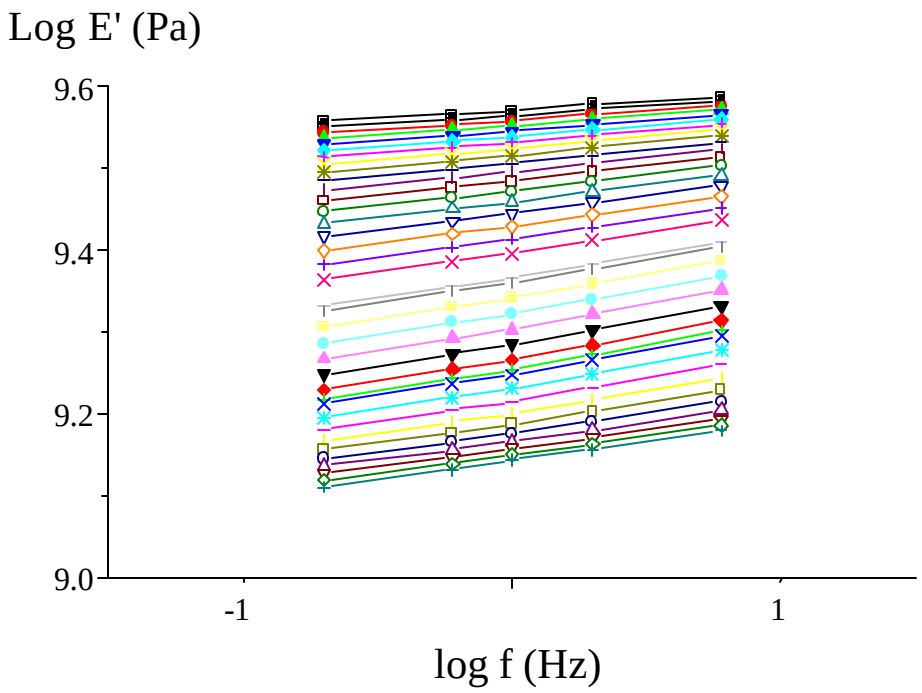

Figure II.2.2. Isotherms (3°C Increments) from 20 to 120°C Generated from Polynomial Fit in Figure II.2.1

Isotherms were shifted horizontally on a frequency scale to a reference isotherm and master curves of log (E') were created. The reference temperature utilized for the TTSP corresponded to the measured T_g at 2 Hertz and was selected as the inflection point in the storage modulus-temperature curve. The inflection point was determined from taking the minimum in the storage modulus derivative with respect to temperature. Shift factor plots were created and the WLF constants were determined by taking the linear part of the graph obtained from plotting $(T-T_{ref})/\log a_T$ versus $(T-T_{ref})$ (Equation (II.2.4), Figure II.2.3)

(II.2.4) $$(T - T_{ref})/\log a_T = (-1/C_1)(T - T_{ref}) - C_2/C_1$$

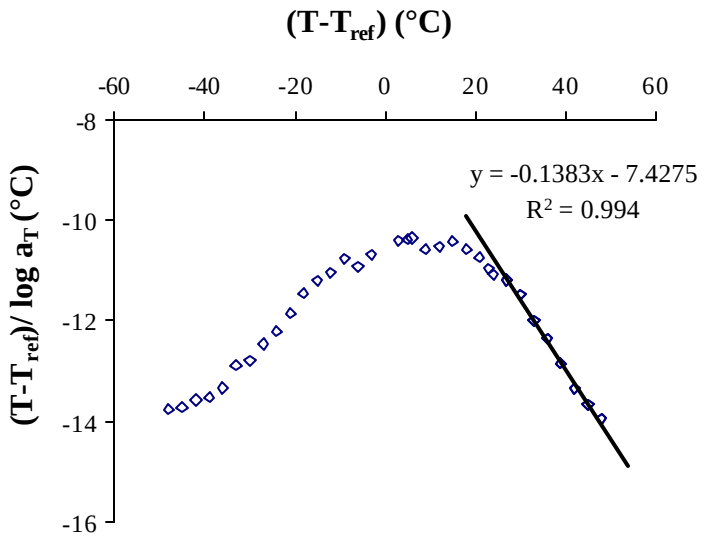

Figure II.2.3. Linearized WLF Form and Determination of C_1 and C_2 WLF Constants

Figure II.2.4 compares the experimental shift factor plot to the WLF equation. Good agreement is found at temperatures above T_g.

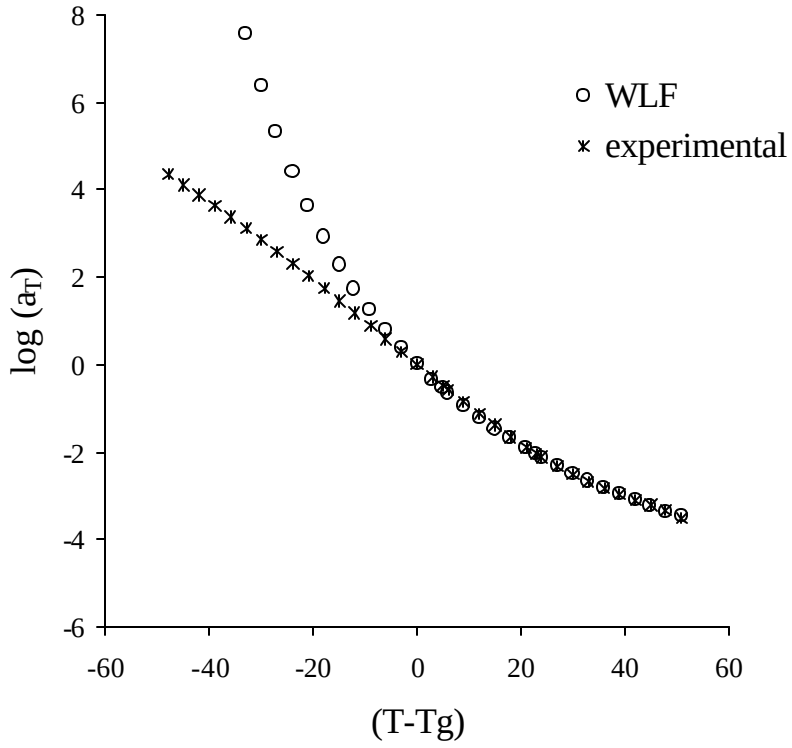

Figure II.2.4. Typical Experimental Shift factor versus WLF fit for EG Plasticized Wood

The shift factor was normalized to the fractional deviation from the T_g yielding cooperativity plots. The data analysis was performed for the individual samples but also average cooperativity plots were constructed. Average cooperativity plots were constructed after the method by Jensen [17]. Namely, the average T_g was utilized and for each sample the shift factor data were recalculated at each value of $(T-T_g)/T_g$. Cooperativity plots were then compared to the Ngai coupling model by determining the best fit to Equation (II.2.2).

II.2.3 Results and Discussion

DMA of ethylene glycol plasticized Spruce and Yellow-poplar woods was amenable for detecting the *in-situ* lignin glass transition. A tan delta peak appeared in the range of 85-95° and was accompanied by a drop in the storage modulus (Figure II.2.5).

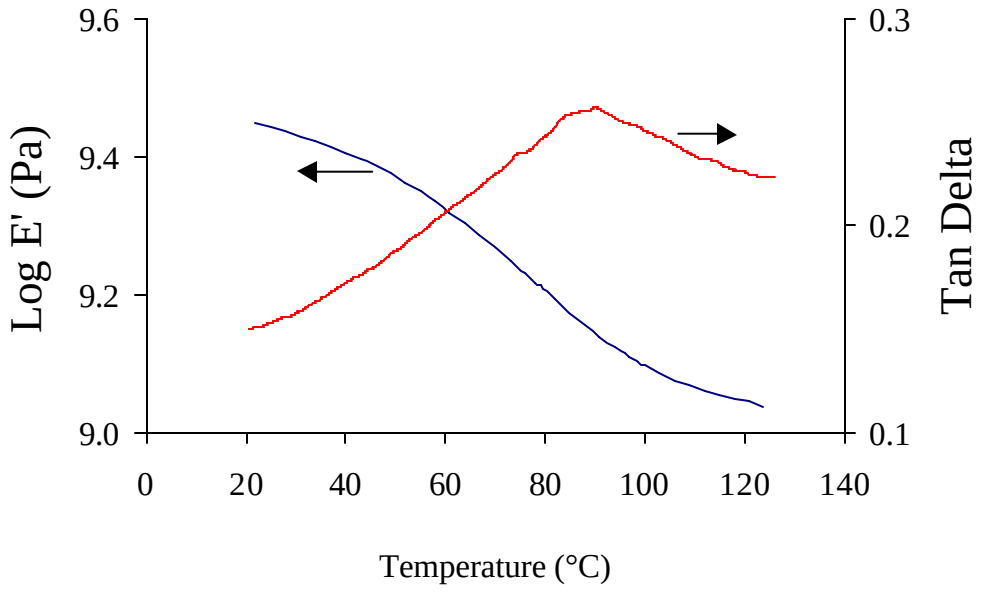

Figure II.2.5. DMA Temperature Scan at 1Hertz for EG Plasticized Wood

For Spruce wood saturated in ethylene glycol and tested along the grain, a tan delta peak characteristic of lignin softening has been reported at 84°C at 1 Hertz [12]. In addition, it has been repeatedly observed that dynamic mechanical measurements of wood along the grain yield higher T_g values than measurements across the grain [9], [13]. According to Furuta et al., the tan delta peak is shifted up by 10°C when wood is tested along the grain versus test across the grain [11]. Salmén also reported a small difference between the tan delta peak measured along and across the grain [9]. This anisotropic behavior has been ascribed to artifacts on the measurements of dynamic moduli as a result of fiber reinforcement[9]. Hence, the tan delta peak observed in this study in the 85-95°C for ethylene glycol swollen wood tested along the grain can be ascribed to the *in-situ* lignin glass transition. It is known however that lignin in different locations of the wood cell displays diverse softening behavior so that the softening observed in this study reflects the average softening of lignin for bulk wood. While saturation in ethylene glycol was efficient for detecting the *in-situ* lignin transition, the pretreatment in ethylene glycol prior to DMA measurements (1 hour conditioning at 120°C) clearly affected the

wood. One indication of the severity of the pretreatment was the brown discoloration of the ethylene glycol bath utilized for sample conditioning. Organosolvolysis of wood by ethylene glycol has long been recognized and is thought to involve the rupture of glycosidic linkages in the holocellulose fraction as well as some dissolution of the lignin fraction [19]. Therefore, the viscoelastic measurements performed in this study apply to wood that has been partially degraded as a result of organosolvolysis by ethylene glycol. With that treatment however, TTSP of ethylene glycol swollen wood was possible within the frequency and temperature windows utilized in this study. As previously reported for ethyl formamide and water plasticized wood, vertical shifting was not necessary to yield smooth master curves [1], [2]. While a wide frequency window is desirable to perform TTSP, experimental limitations hampered measurements on a greater frequency range. More specifically, at frequencies higher than 6 Hertz, the system resonance frequency approached that of the test frequency. It is generally recommended to perform measurements at a frequency 10 times less than the system resonance frequency [10]. In this study, the resonance frequency typically decreased from 120 Hertz to 80 Hertz as the sample was heated from 20°C to 120°C. For some samples then, superposition at the highest temperatures proved difficult, presumably owing to the system resonance frequency approaching the testing frequency. In this respect, thicker samples would likely permit a wider frequency range. However, because this study intended to be applicable to wood/adhesive interphases, thin specimens were preferred. Thin wood specimens should be more amenable to a uniform distribution of the adhesive throughout the thickness of the flakes. In any case, for most samples the construction of smooth master curves over the entire temperature window and the frequency window utilized in this study was possible (Figure II.2.6).

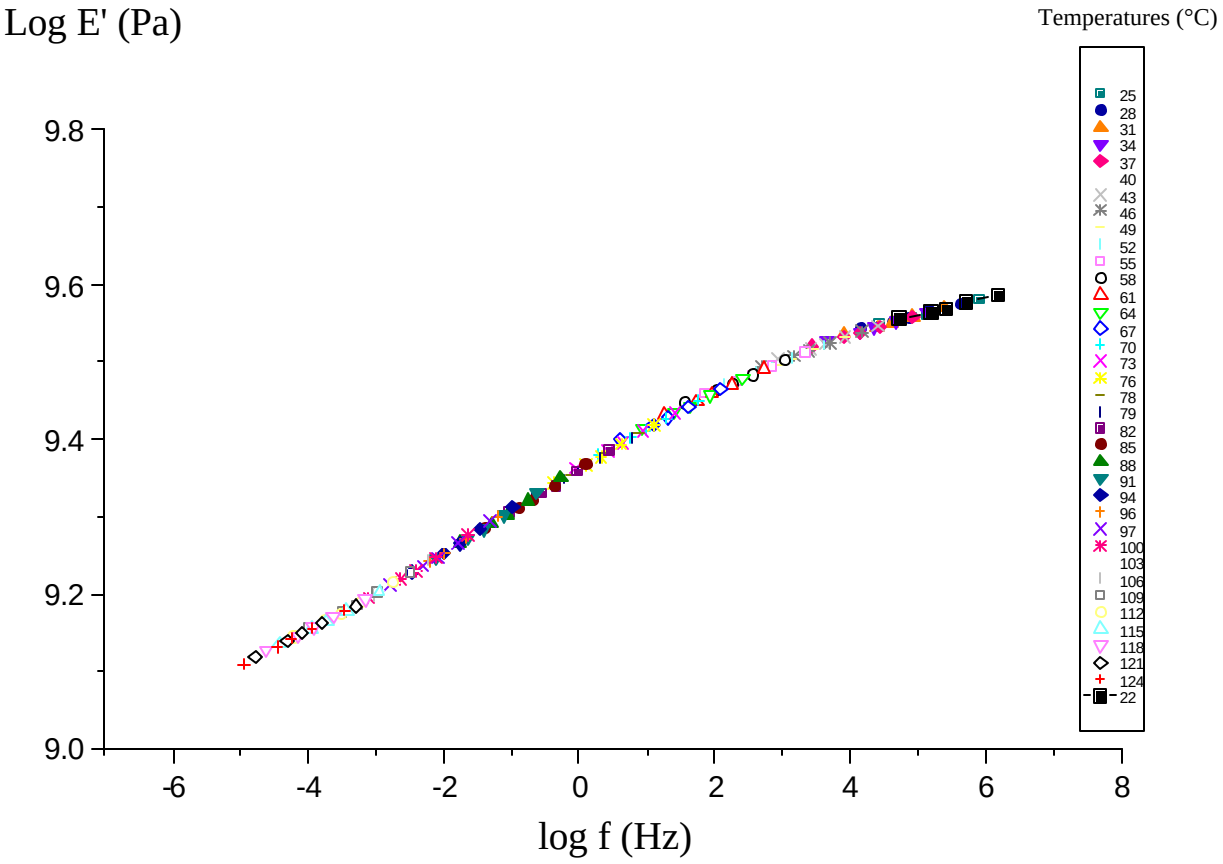

Figure II.2.6. A Typical Master Curve for Ethylene Glycol Plasticized Wood

The ability to create smooth master curves associated with a "smooth" shift factor (i.e. no abrupt change in curvature) indicates that only one mechanism of motion is probed, lignin glass transition in this particular case. The reproducibility of the master curves can be appreciated by creating average master curves for the yellow-poplar and spruce wood specimens. For that purpose, the individual master curves were vertically shifted to the same average modulus value at the reference temperature. Figure II.2.7 and Figure II.2.8 represent the superposition of all individual master curves for spruce and yellow-poplar woods respectively.

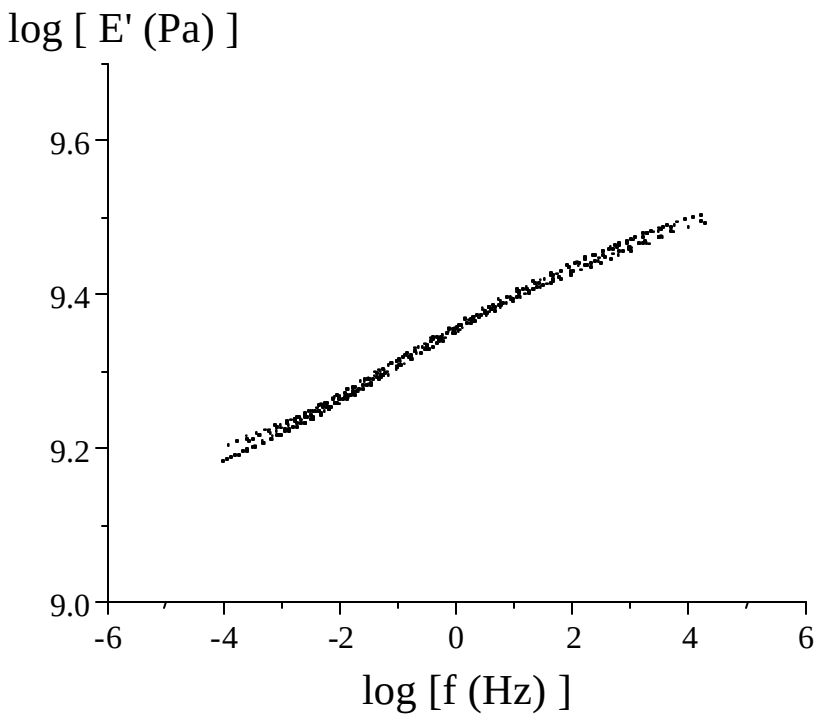

Figure II.2.7. Average Master Curve for Five Different Samples of EG Plasticized Spruce

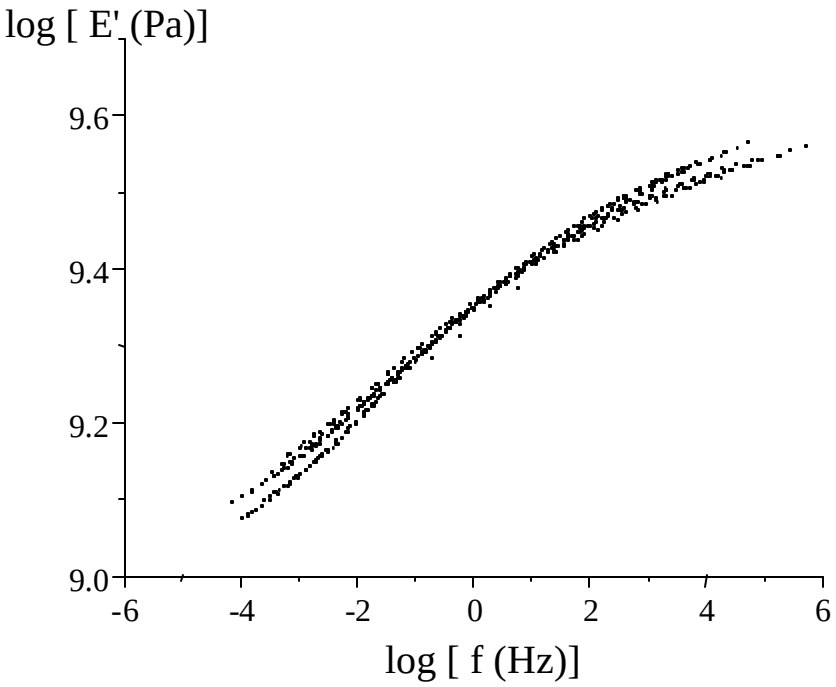

Figure II.2.8. Average Master Curve for Six Different Samples of EG Plasticized Yellow-poplar

Considering the natural variability of wood, a good reproducibility is observed especially in the case of Spruce Wood. Average T_g and WLF constants are presented in Table II.2.1. In addition, the apparent activation energies at the T_g have been calculated from the WLF constant as:

(II.2.5)
$$E_a(T_g) = R\frac{d(\ln a_T)}{d(1/T)} = 2.303RC_1T_g^2/C_2$$

Where R is the universal gas constant.

Table II.2.1. Viscoelastic Properties of EG Plasticized Spruce and Yellow-Poplar Woods Derived from DMA Raw Data and WLF analysis (Standard Deviations in Parenthesis)

	Spruce	Yellow-poplar
Number of Samples	5	6
T_g @ 0.2 Hz (°C)	65 (7)	64 (4)
T_g @ 0.6 Hz(°C)	68 (5)	67 (4)
T_g @ 2 Hz (°C)	74 (3)	71 (4)
T_g @ 6 Hz (°C)	77 (4)	75 (4)
C_1	-9.4 (1.3)	-9.4 (2.2)
C_2	87 (15)	78 (21)
Ea (@T_g) (kJ/mol)	252 (21)	274 (12)

Note that the reported T_g values in Table II.2.1 arise from the storage modulus inflection point rather than the tan delta peak. The storage modulus inflection point yields T_g that are typically 10°C lower than that obtained from the tan delta peak. Table II.2.1 indicates similar T_g values for spruce and yellow-poplar woods albeit a trend for higher T_g values in spruce may be found for the highest frequencies. Alpha relaxations have activation energies typically greater than 100 kJ/mol. The activation energies measured in this study for Spruce and Yellow-poplar woods are in the vicinity of 250 kJ/mol thus confirming the signature of an alpha relaxation. For ethylene glycol plasticized spruce wood, the apparent activation energy of the glass transition has been estimated to 190 kJ/mol using an Arrhenius equation [12]. It has also been reported for several wood species that activation energies derived from the Arrhenius equation are 10 to 40 kJ/mol lower than those calculated from the WLF equation [14]. The activation energies measured in this study are therefore consistent with those reported in the literature. A one tail t-test was performed in order to determine whether the T_g measured at 2 Hertz (reference temperature for the WLF analysis) for Spruce was greater than that for yellow-poplar. The p-value of 0.11 indicated that the glass transition temperature of

Spruce wood might be slightly higher than that of yellow-poplar; but the difference was not highly significant. Typically, softwood species exhibit higher lignin T_g than hardwood species [14], [16]. Higher softening temperatures for lignin softwoods have been ascribed to structural differences between softwood and hardwood lignins. Softwood lignins are built upon guaiacyl units, which are more prone to yield a highly condensed lignin structure. Hardwood lignins on the other hand comprise an equal mixture of syringyl and guaiacyl units (and p. hydroxyphenyl units to a lower extent) whose pendant methoxyl groups may hinder a highly condensed state of lignin [14].

Cooperativity plots were constructed by normalizing the shift factor to the fractional deviation from the T_g. In a first attempt to evaluate the Ngai coupling model on wood, cooperativity plots were constructed over the entire temperature range utilized in this study. Figure II.2.9 compares the measured shift factor over the entire temperature range to the best fit provided by the coupling model.

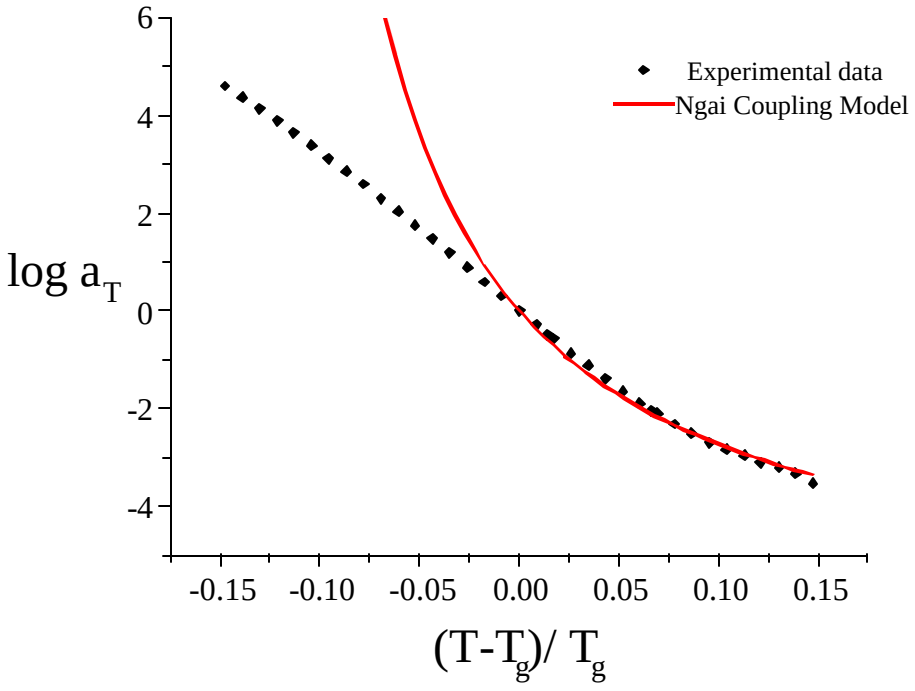

Figure II.2.9. Evaluation of the Ngai Coupling Model (Equation (II.2.2)) for EG Plasticized Wood from 20 to 120°C

The coupling model fails to describe the cooperativity plot over the entire temperature window. However, it must be kept in mind that the coupling model in its "universal" form (Equation (II.2.2)) has been empirically developed for polymers, which were slowly cooled into the glassy state closer to equilibrium [5]. Low free volume in the glassy state is known to delay structural relaxation, which is necessary for approaching equilibrium as required for the Ngai coupling model. Structural relaxation may be all the more delayed if the polymer under probe is highly condensed or crosslinked. Such a phenomenon has been observed in epoxy resins [17]. For epoxy resins, the coupling model was found applicable only to experimental data above the T_g, that is when fast structural relaxation towards equilibrium is possible [17]. In this study, wood samples were allowed to cool at a controlled rate of approximately 1.5°C/min. It may be that in the glassy state, lignin is restricted from approaching equilibrium. Hence, evaluating the Ngai coupling model at temperatures above T_g appeared more appropriate in the case of lignin. In that temperature range, the Ngai coupling model provides a good fit to the cooperativity plot, Figure II.2.10.

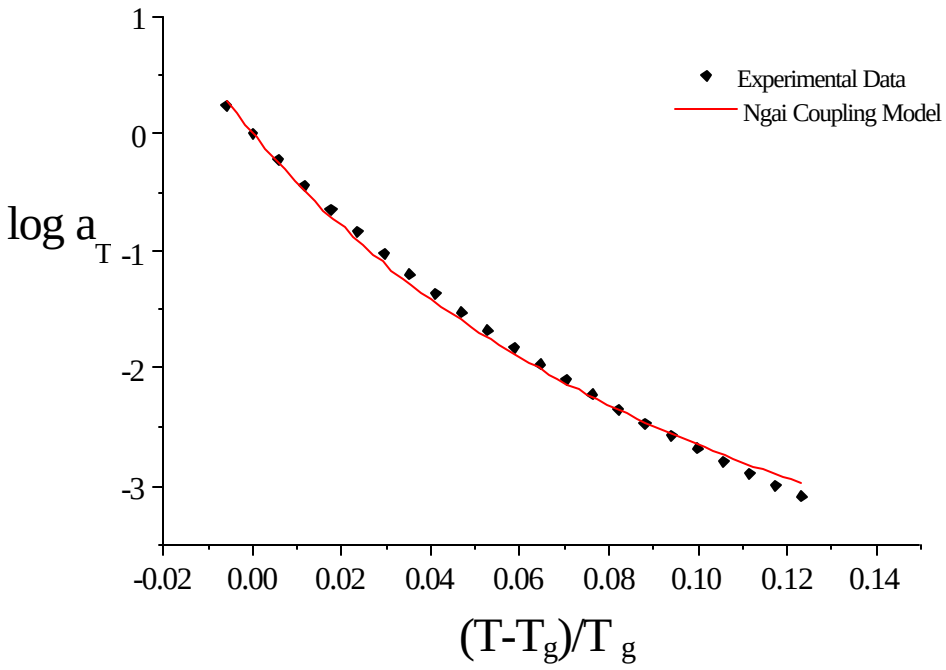

Figure II.2.10. Evaluation of the Ngai Coupling Model for EG Plasticized Wood above Lignin T_g

The fit in the high temperature range is all the more remarkable considering the complexity of the wood structure. For each sample the coupling constant was retrieved from the best fit to equation (II.2.2). The average T_g utilized for the cooperativity analysis and the average coupling constants for yellow-poplar and spruce wood are summarized in Table II.2.2. Table II.2.2 also presents a χ^2 value for the goodness of the fit to Ngai coupling model obtained from the average cooperativity plots (Figure II.2.11). The χ^2 value represents the sum of the squared differences between theoretical and experimental data. Small χ^2 values are therefore indicative of a good fit.

Table II.2.2. Cooperativity Constants and Reference T_g for EG Plasticized Spruce and Yellow-poplar Woods (standard error in parenthesis)

	Spruce	***Yellow-poplar***
Reference Tg (°C)	***74.4 (2.9)***	***71.3 (4.3)***
N	***0.13 (0.05)***	***0.19 (0.04)***
c^2	***0.006***	***0.005***

In-situ lignin softening in ethylene glycol swollen yellow-poplar exhibits a coupling constant of 0.19 ±0.04 while for spruce wood the coupling constant averages 0.13±0.05. Such measured n values for *in-situ* lignin appear small compared to those typically encountered in synthetic polymers. For example, poly(vinyl-methyl-ether) has a coupling constant of 0.5 and the more polar poly (vinyl-chloride) has a coupling constant of 0.77. Two experimental conditions are believed to contribute to low measures of the coupling constants in this study. First of all, saturation of wood in ethylene glycol certainly creates free volume, which in turn decreases intermolecular cooperativity. Recall that conditioning in EG depresses lignin glass transition from 200°C to approximately 75°C. Lignin is therefore dramatically plasticized in this study. Second, the selection of T_g influences to some extent the absolute cooperativity plots and the determination of the coupling constant. The glass transition temperature is typically determined as the onset of ΔC_p increase in DSC temperature scans at 10K/min. While *in-situ* lignin glass transition has been reported to be detectable by DSC, it is notoriously difficult [2], [18]. Another convention consists of determining T_g from DMA temperature scans at a frequency corresponding to $\tau^* = 100s$, i.e. a much lower frequency than that utilized in the present study. Unfortunately, instrumental limitations hampered measurements at such a low frequency. Therefore, in this study, DMA scans at 2 Hertz were utilized for selecting the reference glass transition temperature needed for the cooperativity analysis.

Because the same conventions were applied to construct cooperativity plots for yellow-poplar and for spruce, the comparative value of the analysis is preserved. Figure II.2.11 presents the average cooperativity plots obtained for spruce and yellow-poplar. A steeper temperature dependence of relaxation is suggested for yellow-poplar than for spruce, albeit standard deviations are large. In fact, a t-test revealed no significant difference between the coupling constant obtained for spruce wood and for Yellow-poplar ($p = 0.26$).

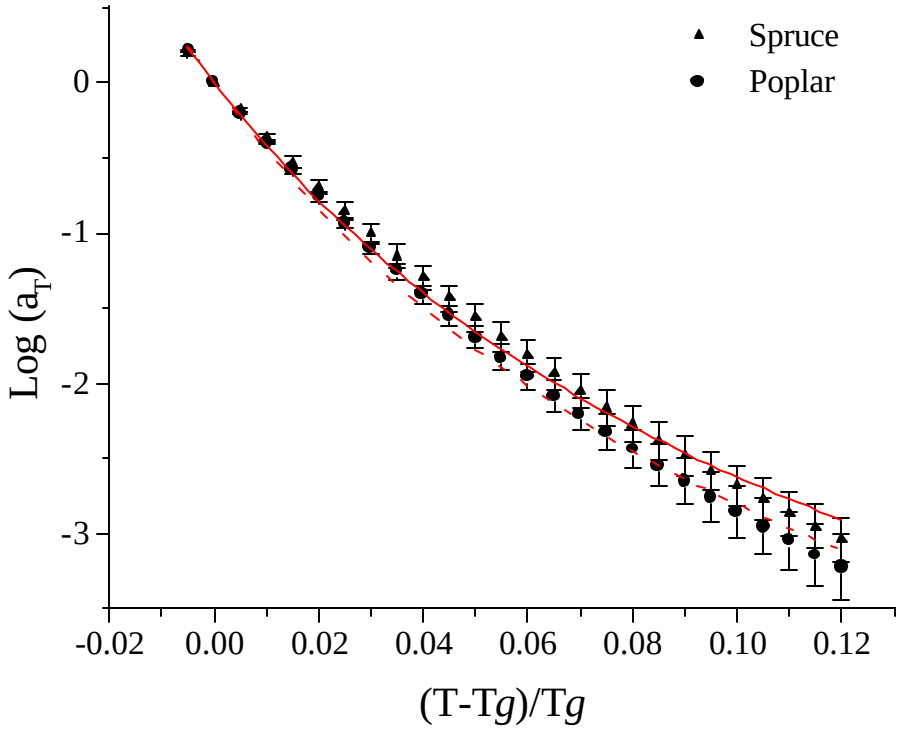

Figure II.2.11. Comparison of Average Cooperativity Plots for Spruce (5 Different Samples) and Yellow-poplar (6 Different Samples)

While there is for these two species no significant difference for lignin in-situ cooperativity, the applicability of the cooperativity analysis suggests that it would be a suitable tool for investigating in-situ molecular features. In fact a systematic study of the influence of lignin composition on intermolecular cooperativity would be of great value to further understand the molecular aspects of *in-situ* lignin relaxation. Such a

systematic study has evidenced a correlation between lignin glass transition temperature and methoxyl content and similar approaches can be envisioned with the cooperativity analysis [14], [15]. Besides, wood is a composite structure in which the lignin-hemicellulose amorphous matrix is constrained within rigid cellulose fibers. Therefore, it is likely that intermolecular cooperativity measured within bulk lignin phases is largely influenced by lignin interactions with the surrounding polymers. For instance, lignin is covalently linked with hemicellulose. Hemicelluloses are to a large extent responsible for the depression of lignin glass transition when comparing *in-situ* lignins and isolated lignins [20]. No doubt then that hemicelluloses also affect the intermolecular cooperativity measured around the *in-situ* lignin glass transition. Furthermore hemicelluloses are intimately connected to cellulose through hydrogen bonding. Such interactions are dynamic. Again the cooperativity analysis, albeit applied around lignin *in-situ* softening is likely sensitive to these dynamic interactions. One could envision for instance that the constraint imposed by cellulose fibers on the lignin- hemicellulose matrix enhances intermolecular cooperativity within lignin phases. In that matter, intermolecular cooperativity appears as a potential tool to provide further insight on the *in-situ* molecular arrangement of wood polymers. More specifically, the impact of the surrounding environment on lignin morphology could be assessed by evaluating the effects of wood anisotropy on intermolecular cooperativity. If wood anisotropy were found to influence intermolecular cooperativity, indication for some molecular orientation in the amorphous matrix of wood would be provided. There is therefore great potential and certainly great information yet to be learned from the cooperativity analysis of wood from various species and in various environments. However, another objective of this study was to determine if viscoelastic measurements may also be suitable for characterizing the *in-situ* lignin glass transition in wood-PF composites. In that purpose, preliminary data were obtained on wood–PF composites. The reader is directed to chapter III-1 for a detailed description of the composite manufacture. Temperature scans were thus performed under similar experimental conditions as those described for the neat wood samples.

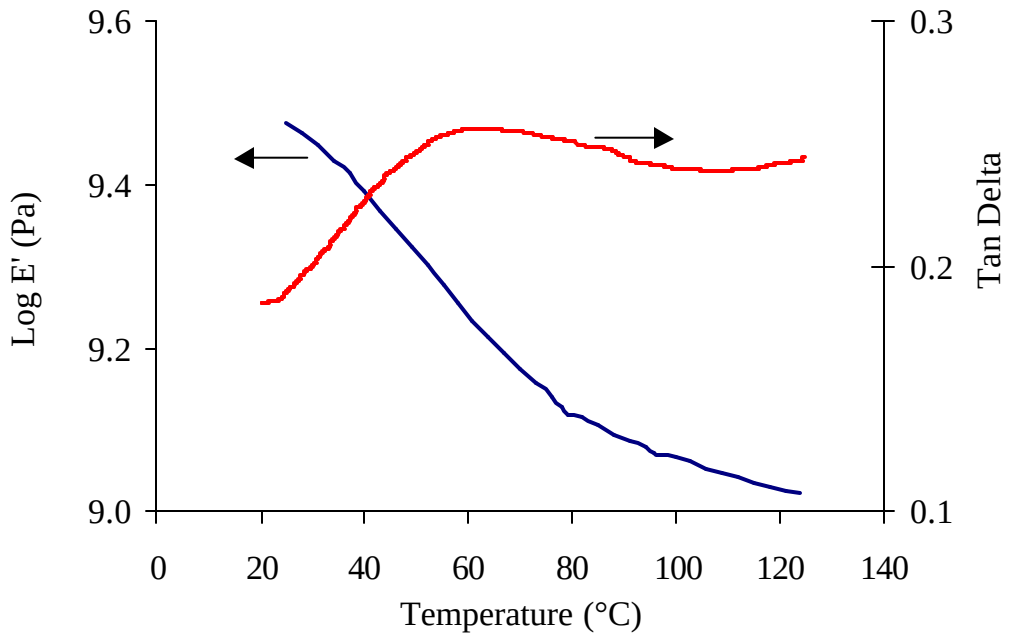

Figure II.2.12. DMA Temperature Scan of a Wood-PF composite (@ 0.2 Hertz)

Figure II.2.12 illustrates the Tan Delta and Storage Modulus data for a PF composite plasticized in Ethylene glycol. The composite comprises 40% resin solids on wood. A clear drop in modulus is evident in Figure II.2.12 and is associated with a tan delta peak. The damping peak may be ascribed to *in-situ* lignin softening albeit again caution is required in any strict assignment. Again, while wood main softening is generally ascribed to lignin (for the particular conditions utilized in this study), it is well established that lignin association with carbohydrates has a substantial effect on its softening temperature [20]. Considering the high resin solids on wood, it is also possible that some fraction of the PF resin participates in the softening. This is especially true that PF resins are very similar in structure to lignin. In fact just as for bulk wood, the softening observed in the PF composite arises mainly from *in-situ* lignin and is largely influenced by its association with carbohydrates and with the PF resin interactions with lignin.

The detection of a softening in the PF composites suggests that the cooperativity analysis may also be applicable in wood/PF composites. If not however, it remains that glass transition temperatures of *in-situ* lignin shall be easily monitored in PF composites.

II.2.4 Conclusion

This viscoelastic study on ethylene glycol plasticized wood has provided an additional tool for characterizing *in-situ* lignin glass transition. More precisely the *in-situ* glass transition of lignin can be probed with the cooperativity analysis as described by Ngai and coworkers. Two wood species, one pertaining to hardwood and the other pertaining to softwood have been examined on the basis of this analysis. While no significant differences were found between yellow-poplar and spruce in this study, the applicability of the cooperativity analysis for wood holds great promise for a better understanding of the *in-situ* molecular features of lignin but also for better characterizing wood morphology. In addition, preliminary data on wood/PF composites indicate that lignin glass transition can also be monitored within the composites. The ability to probe lignin glass transition in neat wood and in composites may help understand the viscoelastic influence of PF resins on wood.

II.2.5 References

[1] Salmén L., Viscoelastic Properties of In-situ Lignin Under Water Saturated Conditions, J. Mater. Sci., 19, (9), 3090,1984.

[2] Kelley S.S., T.G.Rials and W.G. Glasser, Relaxation Behaviour of the Amorphous Components of Wood, J. Mater. Sci., 22, 617, 1987.

[3] Williams M.L., R.F. Landel and J.D. Ferry, The Temperature Dependence of Relaxation Mechanisms in Amorphous Polymers and Other Glass-forming Liquids, J. Am. Chem.Soc., 77, 3701, 1955.

[4] Ngai K. L., and C. M. Roland, Chemical Structure and Intermolecular Cooperativity: Dielectric Relaxation Results, Macromolecules, 26, 6824, 1993.

[5] Plazeck D. J. and K. L. Ngai, Correlation of Polymer Segmental Chain dynamics with Temperature-Dependent Time-Scale Shifts, Macromolecules, 24, 1222, 1991.

[6] Hall C. K., and E. Hellfand, Conformational State Relaxation in Polymers: Time Correlation Functions, J. Chem. Phys., 77 (6) 3275, 1982.

[7] Williams, G.; Watts, D. C., Non-symmetrical Dielectric Relaxation Behavior arising from a Simple Empirical Decay Function, Trans Faraday Soc, 66 (1) 80, 1970.

[8] Ngai K.L. and D.J. Plazeck, Identification of Different Modes of Molecular Motion in Polymers that Cause Thermorheological Complexity, Rubber Chemistry and Technology, 68, 376, 1995.

[9] Salmén L., Directional Viscoelastic Properties of Wood, Progress and Trends in Rheology II, Proceedings of the Second Conference of European Rheologists, 234, 1986.

[10] Salmén L., Personnal Communication, 2001.

[11] Furuta Y. , M. Makinaga, H. Yano and H. Kajita, Thermal Softening Properties of Water-Swollen Wood II. Anisotropic Characteristics of Thermal Softening Properties, Mokuzzai Gakkaishi, 43 (1) 16, 1997.

[12] Wennerblom M., A. M. Olsson and L. Salmén, Softening Properties of Earlywood and Latewood of Spruce, Nordic Pulp and Paper Research Journal, 11, 279, 1996.

[13] Furuta Y. and H. Yano, Thermal-Softening Properties of Water-Swollen Wood III. Ethylene Glycol-swollen wood, Mokuzzai Gakkaishi, 43 (8) 642, 1997.

[14] Olsson A. M and L. Salmén, Viscoelasticity of In-situ Lignin as Affected by Structure, Softwood vs. Hardwood, ACS Symp.Ser., Viscoelasticity of Biomaterials, Ed. W.G. Glasser and H. Hatakeyama, No. 489, 133, 1992.

[15] Olsson A.M. and L. Salmén, The Effect of Lignin Composition on the Viscoelastic Properties of Wood, Nordic Pulp and Paper Research Journal, 3 (12) 140, 1997.

[16] Hamdan S., W. Dwianto, T. Morooka and M. Norimoto, Softening Characteristics of Wet Wood under Quasi Static Loading, Holzforschung, 54, 557, 2000.

[17] Jensen R.E., Investigation of Waterborne Epoxies for E-Glass Composites, Doctoral Dissertation, Virginia Polytechnic Institute and State University, June 1999.

[18] Östberg G. L., Salmén and J. Terlecki, Softening Temperature of Moist Wood Measured by Differential Scanning Calorimetry, Holzforschung, 44 (3) 223, 1990.

[19] Bouchard J., Lacelle S., E. Chornet, PF Vidal and R.P. Overend, Mechanism of Depolymerization of Cellulose by Ethylene-Glycol Solvolysis, Holzforschung, 47 (4) 291, 1993.

[20] Glasser W. G., Classification of Lignin According to Chemical and Molecular Structure, ACS Symp.Ser., Viscoelasticity of Biomaterials, Ed. W.G. Glasser and H. Hatakeyama, No. 489, 216, 1992.

CHAPTER. II.3. TECHNIQUE FOR IN-SITU CURE CHARACTERIZATION

II.3.1 Introduction

The remaining work presented in this dissertation involves the analysis of wood/PF composite samples. As previously mentioned, the purpose is to assess how wood resin interactions influence wood molecular motions as an indication of interphase morphology. However, molecular motions in the composite samples will also be influenced by the degree of cure of the PF resin. It is therefore important to have a technique for characterizing and controlling the cure of PF resins. The cure characterization technique will then be useful for preparing adequate composite samples.

In trying to select a cure characterization technique for our purpose, it is worth recalling that PF cure kinetics are influenced by the presence of wood [1]-[4]. More specifically, it has been established that wood lowers the activation energy of cure [1], [4]. In another study, Thermal Mechanical Analysis (TMA) of bonded wood joints resulted in the construction of modified Time-Temperature-Transformation cure diagrams [6]. The shape of the modified TTT cure diagram differs significantly from the classic TTT cure diagram proposed by Gillham on neat systems. It is therefore important to characterize PF cure *in-situ.* Finally, it has been observed that dynamic mechanical characterization of PF cure yields earlier detection of PF end of cure compared to calorimetric characterization [3], [8]. This observation emphasizes that a cure characterization technique should be selected to best mimic the actual curing conditions pertaining to the manufacture of the wood/adhesive composite.

In this study, a Dynamic Mechanical Thermal Analysis (DMTA) method is proposed that permits *in-situ* cure characterization of PF resins. The DMTA method is compared to DSC analysis for the neat PF resin.

II.3.2 Materials and Methods

II.3.2.1 PF Resin Synthesis

A PF resin synthesized in the laboratory was utilized in order to establish the cure characterization protocol. The PF resin was manufactured by reacting phenol crystals,

37% formaldehyde solution and 30% sodium hydroxide in P: F: NaOH molar ratios of 1: 2: 0.2. Distilled water was added so as to obtain a theoretical solid content of 55%. The condensation proceeded for 2 hours in a triple neck flask, which was connected to a condenser and immersed in a silicone oil bath at 80°C. After two hours of polymerization, the PF resin was quenched by immersion in an ice bath. The PF resin was kept frozen in small batches until use for cure characterization.

II.3.2.2 Dynamic Mechanical Analysis

A Polymer Laboratories DMTA equipped with a universal temperature programmer and interfaced to a computer was utilized. Because *in-situ* cure characterization is desirable in this study, dry wood flakes were utilized for supporting the PF resin. Yellow-poplar flakes were manufactured from water saturated yellow-poplar blocks with a disk flaker. In order to minimize wood response on the overall dynamic behavior of the composite, thin wood flakes were utilized and high resin loading on wood was necessary. More precisely, a thin yellow-poplar flake (30*8*0.3 mm) was immersed in PF resin for approximately 2 minutes. Excess resin was wiped of the flake and aluminum foil was placed on the end and center of the sample to protect the DMTA clamps. After clamping the specimen, additional PF resin was coated on the flake using a pipette. The resulting resin solid was approximately 100 to 120 % on dry wood mass. The impregnated sample was tested in dual cantilever beam mode at a frequency of 1Hz. The DMTA furnace was purged with nitrogen during the measurements. Cure was performed in the DMTA under isothermal conditions. In that purpose, the optimum temperature ramping procedure was determined so that target cure temperature was obtained within 2 minutes with a precision of 5°C.

II.3.2.3 Differential Scanning Calorimetry

A Perkin-Elmer DSC-7 controlled by a system-4 microprocessor was utilized to characterize the cure of the neat resin. A major concern in studying PF cure with DSC is that volatiles obscure the curing reactions. This issue is easily overcome by using high-pressure capsules and rescanning the cured sample under identical conditions. Under such conditions, overlapping events, mainly water and formaldehyde evaporation, are corrected by using the second scan as the baseline. This procedure was utilized on

samples consisting of approximately 10 mg liquid PF resin placed in 200 µl high-pressure stainless steel capsules and cured under isothermal conditions.

II.3.3 Results and Discussions

Typical tan delta and storage modulus curves obtained during an isothermal DMTA scan are presented in Figure II.3.1. Two damping peaks are clearly apparent and are associated with a steep increase in storage modulus (Figure II.3.1). These events are ascribed to PF resin *in-situ* gelation and vitrification. An artifact is observed during the first two minutes of the DMTA thermogram. During this period, the furnace temperature is raised to reach the target isothermal cure temperature. Water evaporation likely contributes to the observed artifact. Hence the procedure was efficient in detecting main PF curing events. With this procedure, cure characterization was performed at different cure temperatures.

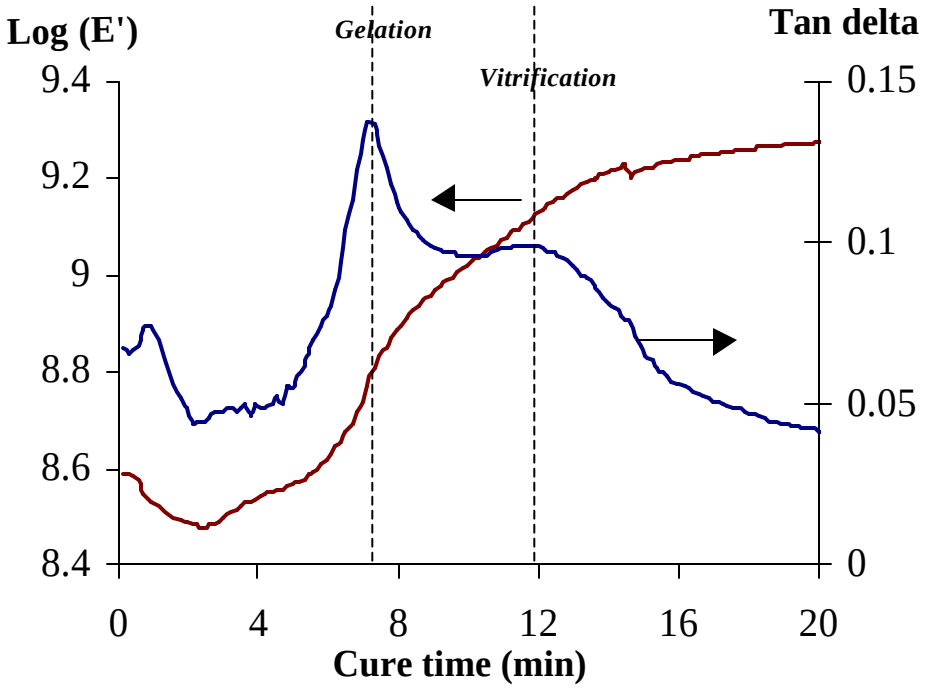

Figure II.3.1. A Typical DMA Trace During In-situ Isothermal Cure of a PF resin

Figure II.3.2 illustrates the tan delta traces obtained from DMTA isothermal cure at temperatures varying from 110°C to 190°C in 10°C increments. In this figure, Tan delta traces have been shifted vertically with increasing cure temperature. Clearly demonstrated with this figure is the ability to detect gelation and vitrification events at various cure temperatures with the *in-situ* DMTA cure method established for PF resins.

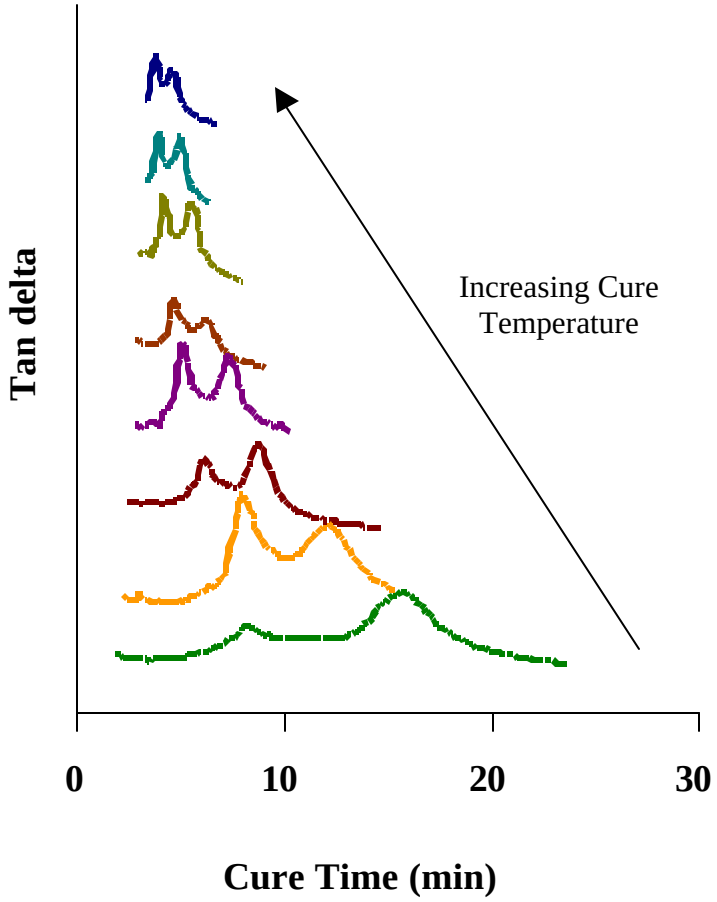

Figure II.3.2. Tan Delta Traces during In-situ PF cure at Various Temperatures

A typical DSC thermogram for the neat PF resin is illustrated in Figure II.3.3. In Figure II.3.3, the corrected thermogram is obtained by subtracting the second scan (baseline) to the first scan, during which cure occurs. The thermogram consists of two overlapping exotherms. The low temperature exotherm is generally ascribed to formaldehyde addition to the phenolic ring while the high temperature exotherm corresponds to the condensation reactions of hydroxymethyl phenol species [3].

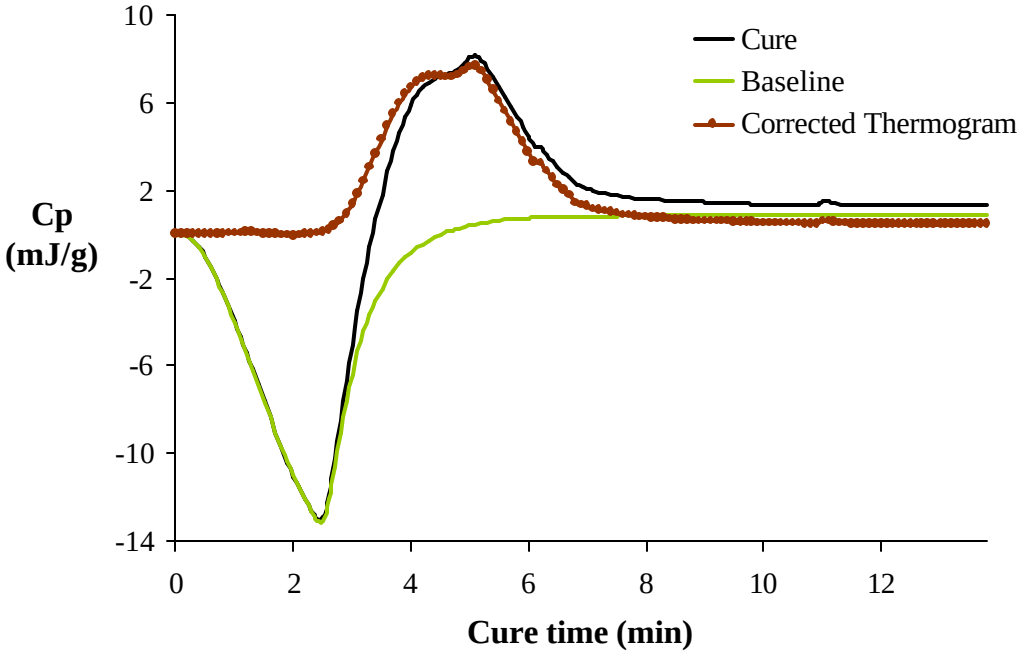

Figure II.3.3. A Typical DSC Thermogram during Isothermal Cure of a Neat PF Resin

The time to reach end of conversion at a given cure temperature was determined from the corrected thermogram at that temperature. Again, this analysis was performed at several curing temperatures. For the particular resin utilized in this study, the thermogram revealed cure information at high cure temperatures (120°C to 150°C) while at lower temperatures it was difficult to locate ends of conversion due to a weaker signal. Combining DMTA and DSC data, a partial TTT cure diagram could be created for this particular PF resin (Figure II.3.4). The approach is similar to that initiated by Hoffman on lignin-based epoxy resins [7]. On this diagram, one sees that the end of conversion obtained from DSC measurements appears later than the resin vitrification detected by DMTA. A possible explanation is that past resin vitrification, additional crosslinking may proceed albeit at a much slower rate. The differences may also reflect the differences in cure conditions. Cure conditions in sealed capsules certainly differ from those in a DMTA furnace at atmospheric pressure. It may also be, as suggested by previous authors [6], that the difference arises from wood influence of PF cure kinetics,

although this effect should not be so prominent in the present *in-situ* cure characterization method considering the high resin loading on wood.

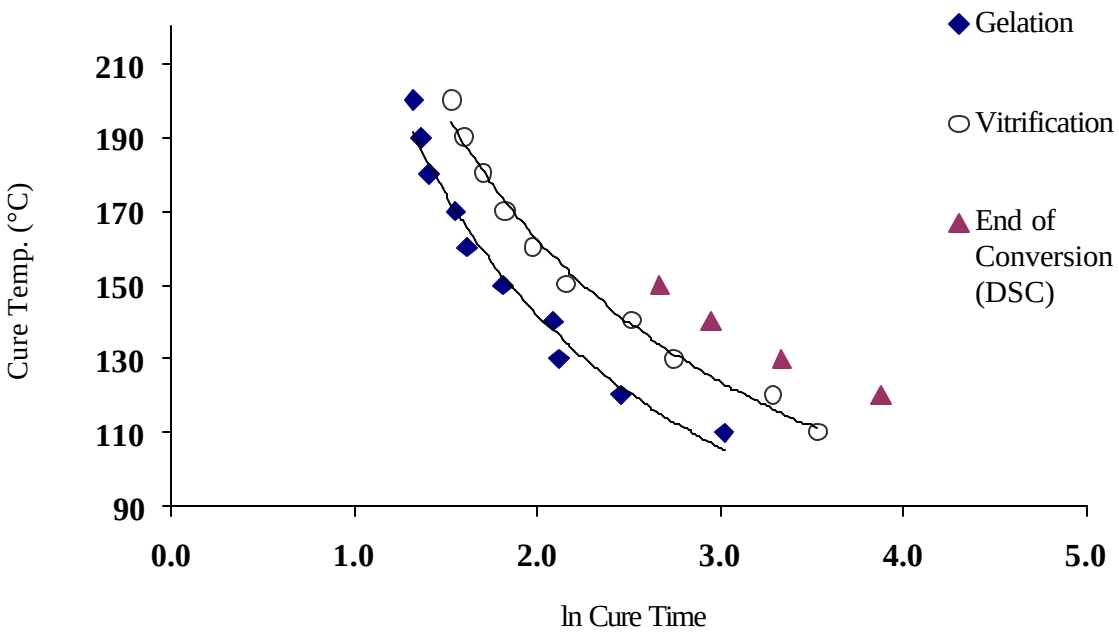

Figure II.3.4. Partial in-situ Cure Diagram for a PF Resin

II.3.4 Conclusion

A method has been applied that allows *in-situ* cure monitoring of wood thermosetting adhesives. For PF resins, DSC and DMTA procedures yield slightly different cure characterizations most likely as a result of differences in cure conditions [3], [8]. The observation that DMTA yields earlier cure events than the DSC is consistent with previous reports for PF resins [8]. Because the wood/PF composites destined for morphological investigation will be cured in a oven, DMTA is the most adequate technique for characterizing PF-resin *in-situ* cure in this research.

II.3.5 References

[1] Chow S.Z., A Kinetic Study of the Polymerization of Phenol-Formaldehyde Resin in the Presence of Cellulosic Materials, Wood Sci. 1, 4, 215, 1969.

[2] Mizumachi H. and H. Morita, Activation Energy of the Curing Reaction of Phenolic Resin in the Presence of Woods, Wood Sci., 7, 3, 256, 1975.

[3] Wang X. M, B. Riedl, A.W. Christiansen and R. L. Geimer, The Effect of Temperature and Humidity on Phenol-formaldehyde Resin Bonding, Wood Sci. Technol., 29, 253, 1995.

[4] Pizzi A., B. Mtsweni and W. Parsons, Wood-Induced Catalytic Activation of PF Adhesives Autopolymerization vs. PF/ Wood Covalent Bonding, J. Appl. Polym. Sci., 52, 1847, 1994.

[5] Schmidt R.G. and C.E. Frazier, Network Characterization of Phenol-Formaldehyde Thermosetting Wood Adhesive. Int. J. Adhes. Adhes. 18 (2) 139, 1998.

[6] Pizzi A., Lu X. and R. Garcia, Lignocellulosic Substrates Influence on TTT and CHT Curing Diagrams of Polycondensation Resins, J. Appl. Polym. Sci, 71, 915, 1999.

[7] Hofmann K. and W.G. Glasser, Engineering Plastics from Lignin, Network Formation of Lignin-based Epoxy Resins, Macromol. Chem.. Phys., 195, 65, 1994.

[8] Myers G.E., A.W. Christiansen, R.L. Geimer, R.A. Follensbee and J.A. Koutsky, Phenol-Formaldehyde Resin Curing and Bonding in Steam-Injection Pressing. I. Resin Synthesis, Characterization, and Cure behavior, J. Appl. Polym. Sci, 43, 237, 1991.

III. MOLECULAR WEIGHT DEPENDENCE OF THE WOOD/PF INTERPHASE MORPHOLOGY

CHAPTER. III.1. MATERIALS

III.1.1 Introduction

Monitoring the influence of PF resins on wood molecular motions is expected to shed some light on the wood/PF interphase. A main research objective is to investigate the molecular weight dependence of the wood/PF interphase morphology. In wood-based composites, PF resins for Oriented Strandboard (OSB) have a low molecular weight distribution. On the other hand, PF resins destined for plywood are highly condensed and have a broad distribution of molecular weight [1]. In this research, two PF resins, one crudely modeling OSB PF resins and the other mimicking plywood PF resins were synthesized. The two PF resins therefore differ by their degree of polymerization. Wood/PF composites were subsequently manufactured by impregnating wood flakes with these two PF resins. A major concern for manufacturing these composites was to obtain homogeneous materials on a macroscopic scale. In addition, similar resin solids on wood dry mass were targeted for both PF composites. Special attention was also paid to tailor the *in-situ* cure of each resin so as to yield comparable rigidity for both series of composites. Finally, control specimens were prepared so as to provide a reference for the influence of alkali and heat treatment involved in the preparation of the composites.

III.1.2 PF Resin Synthesis and Characterization

III.1.2.1 Resin Synthesis

The synthesis apparatus consisted of a two liter reaction kettle equipped with mechanical stirring and a condenser. The reaction kettle was placed in a heating mantle regulated by a power regulator. A thermocouple, connected to the temperature programmer, was utilized to monitor the reaction temperature. The temperature was initially set at 80°C. The PF resins were synthesized in P: F: NaOH molar ratios of 1: 2: 0.2. Distilled water was added so as to attain 50% and 40% theoretical solid contents for the low molecular weight and the high molecular weight PF resin, respectively. A lower solid content for the high molecular weight PF was utilized in order to promote higher molecular weights while preventing resin gelation in the reactor. The synthesis

procedure for the two PF resins differed essentially by the length of the cook as well as the schedule of reagent addition in the reaction kettle. Phenol crystals, formalin solution (37% aqueous formaldehyde) and 30% weight concentration of sodium hydroxide were obtained from Aldrich and used as received. For the low molecular weight resin, 282.33 g (3 moles) phenol and 486.98 g (6 moles) formaldehyde were simultaneously fed in the reactor and allowed to stabilize at 80°C. At this point, 80.02 g (0.6 moles) sodium hydroxide and 124.45g (7 moles) distilled water were added in the reaction kettle. After 20 minutes of reflux at 80°C±2, the reaction was quenched by immersing the reaction kettle into an ice bath. For the high molecular weight resin, a split-cook schedule was utilized [1]. That is, only half of the sodium hydroxide/distilled water load was charged in the reaction kettle initially. The polymerization was allowed to proceed at 80°C for 1 hour. After one hour, the remaining sodium hydroxide/water load was charged. The polymerization was quenched after another two and a half-hours polymerization at 70°C. The PF resins were kept frozen in 200ml batches until use.

III.1.2.2 Resin Characterization

Routine physical and chemical characteristics for the PF resins are summarized in Table III.1.1. The two resins are labeled PF-Low and PF-High in reference to their molecular weights. The resin viscosity's are substantially different. Discrepancy between target and measured solid content (for PF-Low in particular) is in line with the presence of free formaldehyde and free phenol in the resin.

Table III.1.1. Characteristics of PF-Low and PF-High

Sample	*pH*	*Target Solid Content (%)*	*Measured Solid Content (%)*	*Viscosity at 20°C (mPa.s)*
PF-Low	***9.7±0.1***	***50%***	***41.8%±2.2***	***20±5***
PF-High	***9.8±0.2***	***40%***	***37.3 %±1.7***	***8 400±2000***

A triple detector Size Exclusion Chromatography technique, developed by Dynea, Inc. was utilized for molecular weight analysis of the resins (Table III.1.2) [2]. As expected, PF-Low and PF-High resins significantly differ in their molecular weights and molecular weight distribution. Mathematical calculations of the average molecular weights was performed but the numbers need to be considered with caution especially for the PF-High resin, which did not display a normal distribution of molecular weights (Figure III.1.1).

Table III.1.2. Molecular Weight Distribution of PF-Low and PF-High Resins (obtained from Dynea, Inc.)

	Mz (g/mol)	*Mw (g/mol)*	*Mn (g/mol)*	*Mw/Mn*	*Rg (nm)*
PF-Low	***390***	***330***	***270***	***1.22***	***0.65***
PF-High	***30 400***	***14 200***	***2 840***	***5.00***	***2.48***

In fact, the UV chromatograms reveal that PF-Low essentially comprises low condensation products. The PF-High embodies a highly condensed fraction of PF species as well as a low molecular tail, similar to PF-Low (Figure III.1.1). The broad distribution of PF-High is expected from the split-cook procedure and is further evidenced by the greater polydispersity for PF-High than for PF-Low (Table III.1.2).

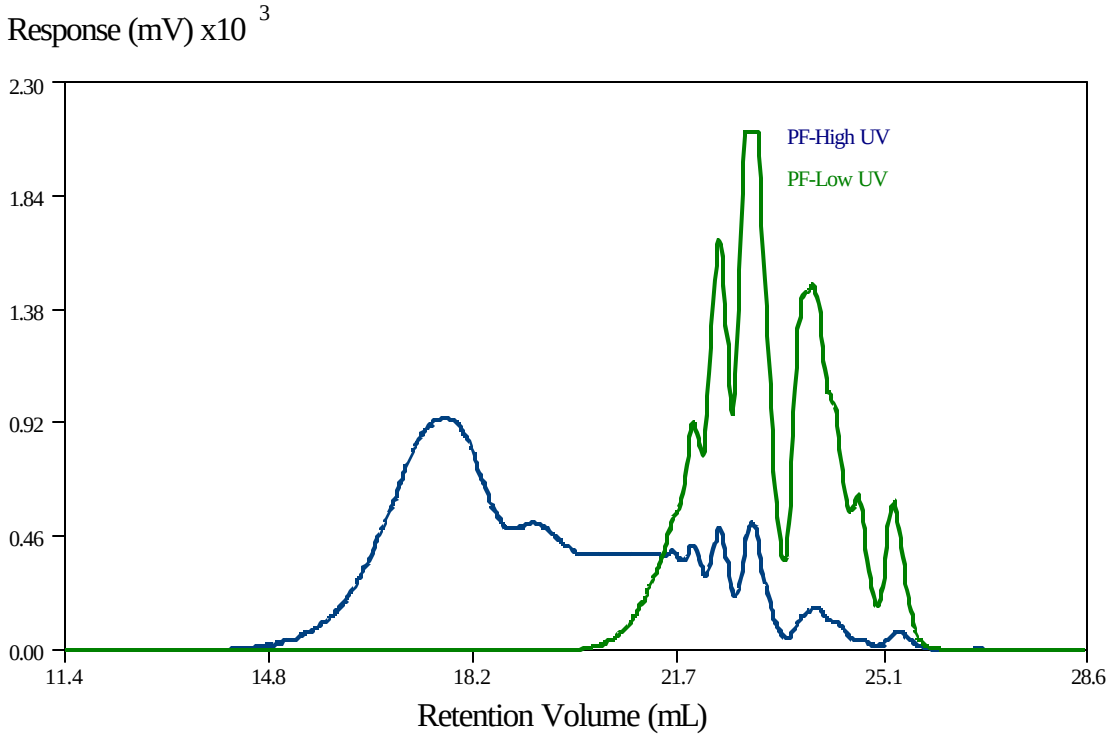

Figure III.1.1. UV Chromatogram of PF-Low and PF-High Resins Demonstrating the Differences in Molecular Weights and in Molecular Weight Distribution

III.1.3 Preparation of Wood /PF Composites

A major concern for manufacturing wood/PF composites from PF-Low and PF-High resins was to impregnate the wood samples as uniformly as possible and to monitor the cure in both series of composites. This concern was addressed by monitoring adhesive impregnation and *in-situ* cure for both resins.

III.1.3.1 Impregnation Protocol

Adhesive gross penetration in wood is in part governed by resin flow properties. It was thus desirable to obtain similar flow properties for both PF resins. In that purpose, PF-High was diluted while monitoring its viscosity with a Brookfield viscometer. By mixing approximately 1 part of PF-High with one part of distilled water, similar flow

properties were attained for PF-Low and PF-High. PF-High solid content after dilution was measured as 21.9%. In addition, rheological properties were also compared using an Advanced Rheometer AR 1000 manufactured by TA. Viscosity measurements were performed between 25 mm aluminum plates on the diluted resins. Under such conditions both PF resins display Newtonian behavior and viscosity in the vicinity of 50 m.Pa.s (Figure III.1.2).

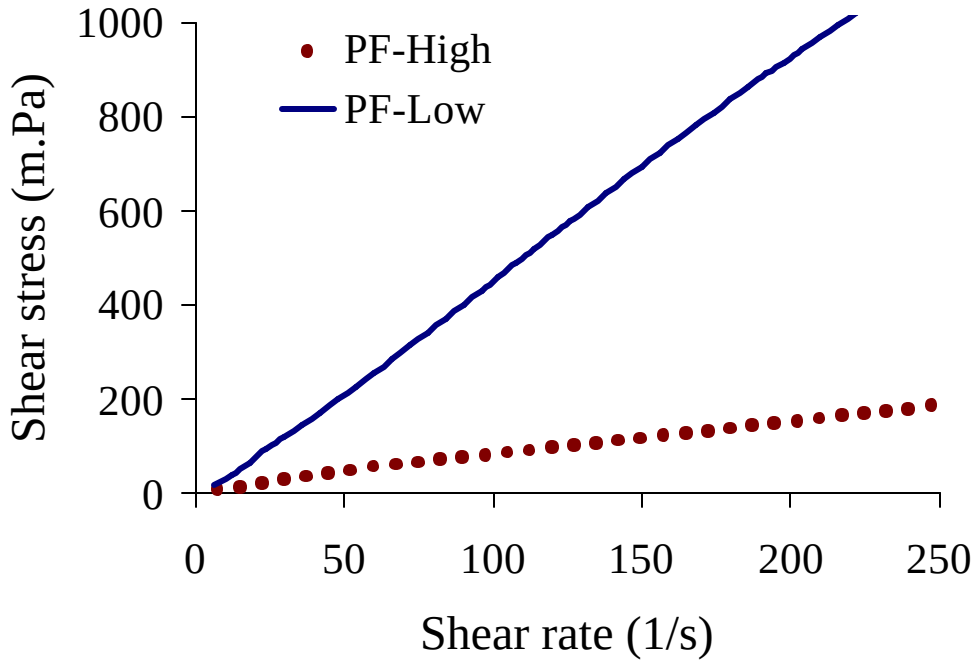

Figure III.1.2. Rheological Characterization of PF-Low and PF-High after Dilution

Wood impregnation with PF-Low and PF-High resins was subsequently monitored. In that purpose, yellow-poplar (*Liriodendron tulipifera*) flakes with dimensions 3.5 mm in the radial direction, 0.85 mm in the tangential direction and 50 mm in the longitudinal direction were manufactured from water saturated yellow-poplar blocks using a disk flaker. The samples were allowed to air dry (approximately 6-8% moisture content) prior to impregnation. Specific impregnation procedures were devised for manufacturing the PF-Low and PF-High composites.

III.1.3.2 Impregnation with PF-Low

The effect of impregnation time on PF-low macroscopic penetration in wood was investigated. A 200 ml beaker was filled with PF-Low and placed in a dessicator. The wood flakes were immersed in the beaker containing the PF and 92 kPa vacuum was pulled on the dessicator. After a specific time of vacuum impregnation, the flakes were retrieved and excess liquid resin was wiped off the flake surface using kim-wipes. The samples were oven cured at 110°C for 30 minutes. Resin solid content was calculated as the percent resin mass on the dry mass of wood. Resin solids as a function of vacuum impregnation time are presented in Figure III.1.3. Each data point is the average of three measurements.

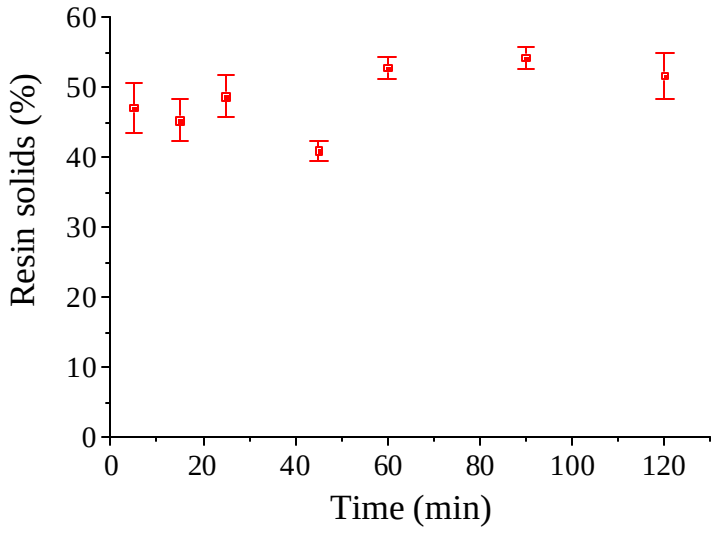

Figure III.1.3. Resin Solids of Yellow-poplar Impregnated with PF-Low in as a function of Impregnation Time

A rapid uptake of PF-Low by the wood substrate is evidenced. Past 40 minutes of impregnation, the uptake of PF-Low is at its maximum. Figure III.1.4 represents the 10X microscopic slide of cross-section of a composite impregnated for 40 minutes. The cross section has been taken from the center of the specimen as indicated by the scheme in

Figure III.1.4. On the microscopic slide, the brown, reddish areas reveal the presence of PF-Low. The samples were not stained and the brown coloration was not found on neat wood. The figure shows that PF-Low penetrates some wood vessel lumens in the center of the wood flake (arrows). PF-Low has thus been able to penetrate throughout the thickness of the flake. However, most cell lumens are not filled with resin, presumably owing to the low viscosity of PF-Low.

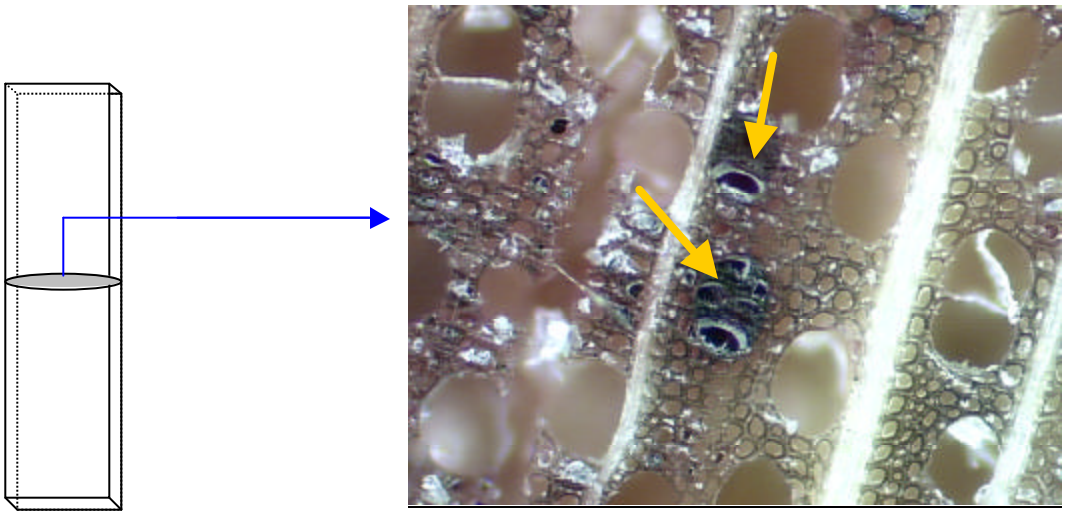

Figure III.1.4. 10X magnified View (Specimen Cross-section) of Wood/PF-Low Composites

In addition, the brown coloration in the cell wall illustrated in Figure III.1.5. could suggest some degree of cell wall penetration. While cell wall penetration of phenol-formaldehyde resins has never been detected with optical microscopy of bondlines, the present study differs from other PF penetration studies in that the resin is present in large amounts (50% resin solids on dry wood). These composites are therefore very different from actual bondlines in which cell wall penetration may only involve a very small amount of resin. The brown coloration may also indicate that the resin is forming a thin coating on the lumen walls. In any case, this brown coloration was not evidenced in the neat wood specimens.

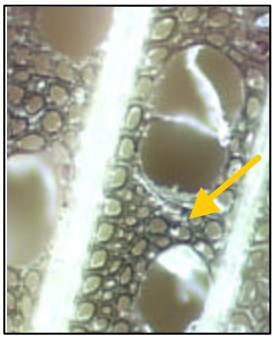

Figure III.1.5. 15X magnified View of Wood/PF-Low Composites Suggesting some Degree of Cell Wall Penetration

Under such conditions, resin solids on wood are approximately 52%.

III.1.3.3 Impregnation with PF-High

The same impregnation procedure as for PF-Low was attempted for the PF-High resin. However, when monitoring the resin solids on wood as a function of impregnation time under 92 kPA vacuum, substantially lower resin solids on wood were attained, namely in the vicinity of 25% (Figure III.1.6).

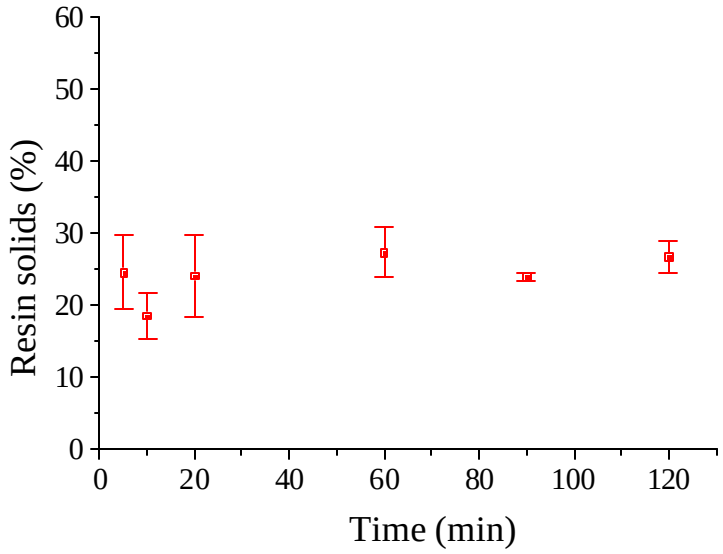

Figure III.1.6. Resin Solids of PF-High impregnated in Yellow-poplar as a function of Impregnation Time

A microscopic view of the cross-sectional area retrieved in the center of PF-High composites after 2 hours of impregnation is shown in Figure III.1.7. The absence of brown, reddish coloration in the cell lumens indicates no gross penetration in the center of the specimen. However, some degree of cell wall penetration may again be suggested by the brown coloration within the circled area in Figure III.1.7. This could indicate that the low molecular weight fraction of PF-High is able to penetrate into wood cell wall.

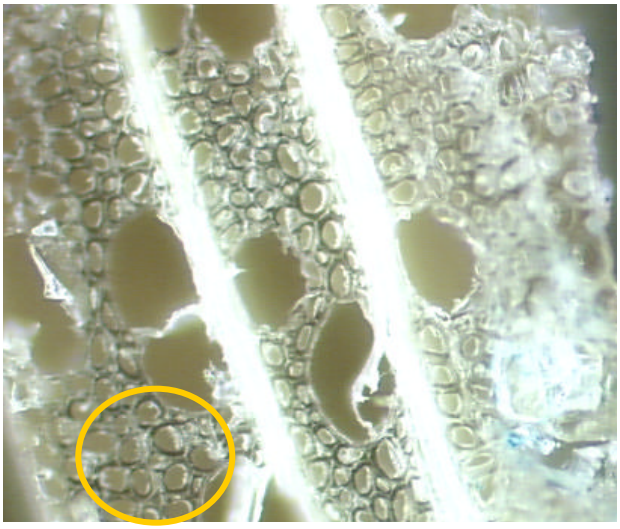

Figure III.1.7. 10X magnified View (Specimen Cross-Section) of Wood/PF-High composites after 120 min. Vacuum Impregnation

In order to augment the gross penetration of PF-High into wood, alternative impregnation procedures were attempted. A 3-step impregnation procedure proved most useful for augmenting resin solids on wood and for enhancing gross adhesive penetration throughout the thickness of the sample. This impregnation procedure consisted of a 30 minute period under 92 kPa vacuum followed by a 30 minute period under atmospheric pressure and a final 30 minute period of vacuum impregnation. Under such conditions, 38% ± 2.4 % resin solids on wood were attained. Microscopic observation of the so obtained PF-High composites demonstrated gross adhesive penetration throughout the thickness of the flake (Figure III.1.8). Namely, in the middle of the cross-sectional area, some vessel cell lumens were filled with the brown, reddish adhesive (indicated with arrows in Figure III.1.8). In addition, some degree of cell wall penetration may again be suggested on this slide (circled area).

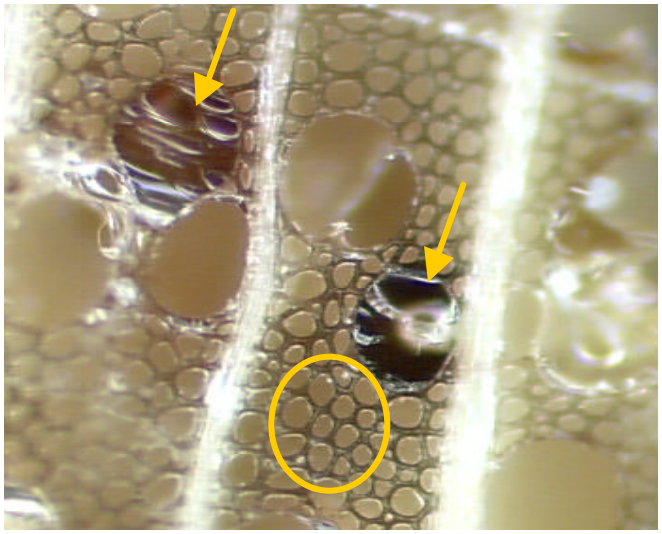

*Figure III.1.8. 10X magnified View (Specimen Cross-Section) of PF-High/Wood composite after Vacuum cycle Impregnation for 3*30 min.*

Therefore, the 3-step impregnation cycle was selected for manufacturing the PF-High composites although the PF-High resin solid was still substantially lower than with PF-Low (38 % on the dry wood mass versus 52%). It must be pointed out in that respect that resin uptake may depend on the average scale of adhesive penetration. That is, if on average, a larger penetration scale occurs for PF-High than for PF-Low, then PF-Low uptake by wood should be higher than that of PF-High. The next step in the manufacture of wood/PF composites involved the selection of cure conditions for PF-Low and PF-High composites.

III.1.3.4 Wood/PF Composite Cure

For comparing wood molecular motions within the composites with NMR and DMA, PF-low and PF-High composites need to have similar degrees of cure. When curing a thermosetting adhesive under isothermal conditions, the glass transition temperature typically reaches the cure temperature [3]. With post cure, the glass transition is further brought to that of the post cure temperature. This behavior has been clearly evidenced for neat PF resins [4]. Therefore, isothermal cure and post cure were selected for yielding similar resin cure states in the two composite series. For the

isothermal cure, it was deemed necessary to ensure resin vitrification. In that objective, the DMTA *in-situ* cure characterization previously developed for wood thermosetting adhesives was utilized. PF-Low and PF-High were thus impregnated in yellow-poplar flakes according to the procedure described in chapter II-3. *In-situ* cure thermograms were obtained for both PF-resins under isothermal cure conditions, at 110°C specifically. Two replicate measurements were performed. The cure thermograms for PF-Low and PF-High are presented in Figure III.1.9 and Figure III.1.10 respectively. The general shape of the DMTA traces differs slightly from those presented in chapter I-4. The high dilution of the resins and therefore the low resin solids on wood is likely responsible for this difference.

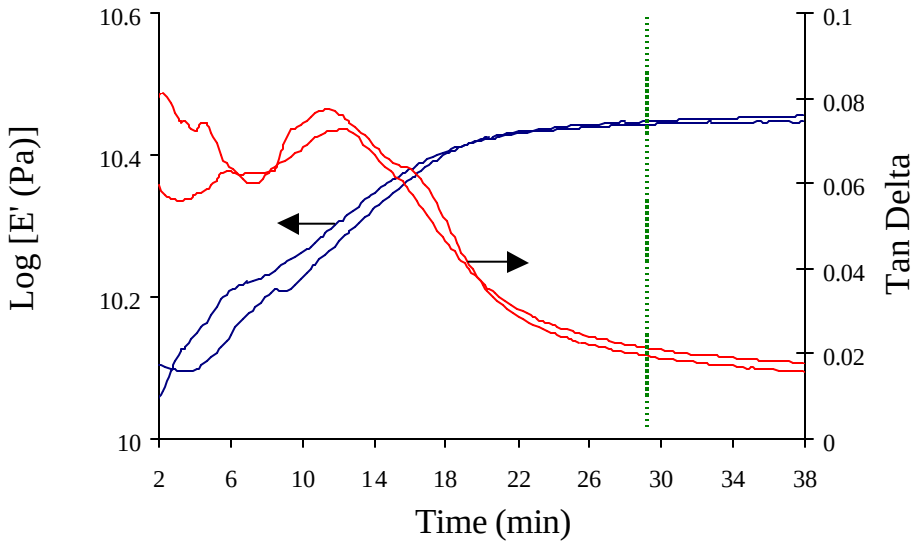

Figure III.1.9. Isothermal DMA Thermogram of In-situ Cure of PF-Low at 110°C.

For the PF-Low resin, 30 minutes of oven cure at 110°C are required in order to vitrify the resin. For the more advanced PF-High resin, 15 minutes only of oven cure at 110°C are sufficient for vitrifying the resins within the composite (Figure III.1.10).

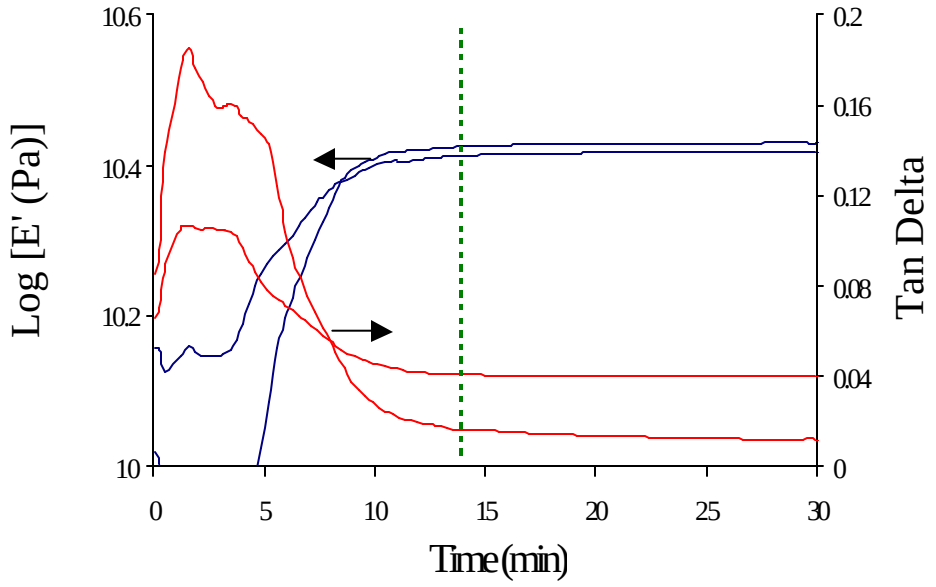

Figure III.1.10. Isothermal DMA Thermogram of In-situ Cure of PF-High at 110°C.

Therefore, Wood/PF low composites were cured at 110°C for 30 minutes while wood/PF –High composites were cured for 15 minutes at that same temperature. The cure was performed in an oven at 110° ±3°C. Post cure at 150°C for 20 minutes was then performed for PF-Low and PF-High composites. Once impregnation and cure protocols had been established for both series of composites, control samples were prepared.

III.1.4 Control Samples

Control samples were deemed necessary to decipher the effect of alkali present in each resin as well as the effect of heat treatment required for the cure of each resin on further dynamic investigations. Because, impregnation procedure and heat treatment for the resin cure differed for PF-Low and PF-High composites, two control groups were required. Namely, a control-Low group was needed to mimic alkali and heat effect involved in the preparation of wood/PF-Low composites. Similarly, a control-High group was needed to mimic alkali and heat treatments involved in the manufacture of wood/PF-High. In that purpose, an aqueous sodium hydroxide solution with similar pH

as those of the resins i.e. 9.1 ±0.2 was prepared. The control-Low series were obtained by impregnating yellow-poplar flakes under 92 kPa vacuum for 30 minutes in the control sodium hydroxide solution. Flakes were subsequently submitted to heat treatment in oven at 110°C for 30 minutes and at 150°C for 20 minutes. The control-High series was manufactured by impregnating wood flakes in the control sodium hydroxide solution in accordance with the 3 steps cycle utilized for the manufacture of PF-High composites. The PF-High curing conditions were then applied to the control-High group. The four series of samples, PF-Low, PF-High, Control-Low and Control-High were stored in refrigerator until use.

III.1.5 Conclusions

Impregnation and cure procedures have been devised for manufacturing adequate wood/PF composites with two PF resins, a very low molecular weight PF resin, PF-Low, typical of OSB resins and a high molecular weight PF resin, PF-High representative of plywood resins. Control treatments (alkali and heat treatment) have also been prepared. Therefore 4 series of samples, PF-Low composite, PF-High composite and their respective control treatments, Control-Low and Control-High were made available for further DMA and CP/MAS NMR analysis. It must be pointed out that the control groups are only models for the effect of the alkali present in the resin on wood. Namely, in PF resins the alkali is bound to PF species, while the control treatments consist of free alkali. This sample preparation appeared however as the most representative effect of bound akali and heat treatment involved in the manufacture of the composites.

III.1.6 References

[1] Sellers T., Plywood and Adhesive Technology, Marcel Dekker Inc., New York, 1985.

[2] Mbachu R.A. D., R.G. Schmidt and B.M. Broline, The Use of Triple Detector Size Exclusion Chromatography Technique and C-13 NMR in the Development of Phenolic Resins for Wood Bonding, Proceedings of the 23rd Annual Meeting of the Adhesion Society, Myrtle Beach, South Caroline, Feb 20-23, 2000.

[3] Turi E.A., Thermal Characterization of Polymeric Materials, Academic Press, New York, 1981.

[4] Schmidt R. G., Aspects of Wood Adhesion: Applications of ^{13}C CP/MAS NMR and Fracture Tests, Ph.D. Dissertation, Virginia Polytechnic Institute and State University, January 1998.

CHAPTER. III.2. PF INFLUENCE ON THE VISCOELASTIC PROPERTIES OF WOOD

III.2.1 Introduction

An experimental protocol with DMA has been developed to quantify the amount of intermolecular cooperativity for the *in-situ* lignin glass transition in wood. Using this DMA protocol, the Ngai coupling model has been demonstrated to adequately portray the temperature dependence of relaxation above the lignin glass transition temperature. The present study aims at assessing the influence of PF resin on the viscoelastic properties of wood. More specifically, the study intends to monitor the influence of PF resin on the *in-situ* glass transition temperature of lignin. In addition, the applicability of TTSP and of the Ngai coupling model for characterizing the *in-situ* lignin glass transition in wood/PF composites is assessed. The influence of PF resin on the viscoelastic properties of wood shall give some insight on the micron scale and nanometer scale morphology of the wood/PF interphase. This study is undertaken on two PF resins with distinct molecular weights and molecular weight distributions (see chapter III-1). PF-Low is a low condensation resin, representative of an OSB resin. PF-High is a more advanced resin, which crudely models a plywood resin. Control specimens (see chapter III-1) are also inspected in order to decipher the influence of alkali and heat treatments, which are imposed on wood during the impregnation and cure of the PF resins.

A word of caution is necessary before entering the study. Wood is a complex material in which three polymers (lignin, hemicellulose and cellulose) are intimately associated. In this study, the main softening observed under the experimental conditions is assigned to the *in-situ* properties of lignin. Recall however, that the *in-situ* properties of lignin refer in fact to the complex response or lignin along with its interactions with other wood components. The contribution of other wood components to lignin softening is well exemplified by the dramatic difference in softening temperature between isolated and *in-situ* lignin [3]. One may find more appropriate to label the *in-situ* glass transition of lignin as wood main softening. In the present study, the term *in-situ* lignin glass transition is utilized and encompasses the complex influence of wood components on lignin glass transition.

In addition, caution must be exerted when assessing the influence of PF resins on the *in-situ* softening of lignin. This because PF influence of the *in-situ* softening of lignin can be envisioned to be direct or indirect. A direct effect would for instance refer to specific interactions between the PF resin and lignin. An indirect effect also needs to be considered because as pointed out in Chapter II-2, it may be that changes in lignin *in-situ* viscoelastic behavior are induced by a change in its association with other wood polymers. Again, lignin is believed to be covalently linked with hemicellulose, which in turn is in close association with cellulose by virtue of their hydrogen bonding capabilities. A PF resin could induce changes in these associations, which in turn would be reflected in the *in-situ* lignin glass transition temperature and intermolecular coupling. The complexity of wood structure and the lack of comparison from studies with such complex systems therefore invite caution for interpreting the results. Finally, caution in interpretation is also required by the experimental conditions of the analysis. Namely, a major drawback of this analysis is that it requires the specimens to be plasticized in ethylene glycol. It is however unknown to what extent the individual components of the composites are plasticized. It is for instance not unlikely that lignin in neat and composite samples is plasticized to a different extent. It is further possible that plasticization of the resin and lignin in the two composites is different, especially that plasticization may relate to the morphology.

Bearing these limitations in mind, one can propose a valid insight on the wood/PF interphase morphology from the present viscoelastic analysis.

III.2.2 Materials and Methods

III.2.2.1 Materials

The reader is directed to chapter III-1 for a detailed description of the materials utilized in this study. Briefly, two PF resins, PF-Low and PF-High, were synthesized so as to yield different molecular weight distributions. PF-Low had a number average molecular weight of 270 g/mol and a polydispersity of 1.22. PF-High had a number average molecular weight of 2840 g/mol and a polydispersity of 5. A low molecular weight tail was clearly present in PF-High. The two PF resins were utilized to manufacture composites. The composites consisted of yellow-poplar (*Liriodendron*

tulipifera) flakes (3.5 R * 0.85 T*10 L mm^3) that were impregnated with PF-Low and PF-High. For each resin, the impregnation procedure was adjusted so as to yield similar resin solids on dry wood and similar microscopic penetration throughout the sample. Resin solids on wood dry mass were approximately 52% and 38% for PF-Low and PF-High composites. The PF-Low and PF-High composites were oven cured at 110°C until vitrification. Post-cure at 150°C for 20 minutes followed.

Control-Low and control-High samples were manufactured to provide a control of the impregnation and heat treatments applied on wood during the manufacture of the PF-Low and PF-High composites, respectively. Namely, yellow-poplar flakes were impregnated with a control sodium hydroxide solution and heat treated in accordance with the impregnation and cure procedures utilized for the PF resins.

III.2.2.2 Methods

The reader is directed to chapter II-2 for a detailed description of the viscoelastic measurements and analyses. Briefly, the specimens were saturated in an ethylene glycol prior to viscoelastic analysis. Viscoelastic measurements consisted of DMA measurements with a Perkin Elmer DMA 7e. The specimens were tested in dual cantilever beam mode along the grain. Throughout DMA measurements the specimens remained immersed in ethylene glycol. For each sample, DMA conditions were determined from consecutive dynamic stress scans at 20°C and also at 120 °C. From these dynamic stress scans, a strain level was selected for remaining in the linear viscoelastic domain at both temperatures. Thereafter, temperature scans were performed at the predetermined strain level with a static load of 120% of the dynamic load. Temperature scans were performed at a fixed frequency from 20°C to 125°C using a heating rate of 2°C/min. Five measurement frequencies were successively applied, namely 0.2, 0.6, 1, 2 and 6 Hertz.

Fifth order polynomials were fitted to the log (E')-temperature curves at the five frequencies. The polynomial fits were utilized to generate isotherms every 3°C. Isotherms were shifted horizontally on a frequency scale to a reference isotherm and master curves of log (E') were created. The reference temperature utilized for the TTSP corresponded to the measured T_g at 2 Hertz and was selected as the inflection point in the

storage modulus-temperature curve. Shift factor plots were created and the WLF constants were determined by taking the linear part of the graph obtained from plotting $(T-T_{ref})/ \log a_T$ versus $(T-T_{ref})$. Apparent activation energies at the T_g were calculated from the WLF constants. The shift factor was then normalized to the fractional deviation from the T_g for constructing cooperativity plots. The cooperativity plots were compared to the Ngai coupling model by determining the best fit to Equation (III.2.1). This allowed the determination of the coupling constant n:

(III.2.1)

$$(1-n)\log a_T = \frac{-C_1\left(\frac{T-T_g}{T_g}\right)}{C_2+\left(\frac{T-T_g}{T_g}\right)}$$

Where C_1 =5.49 and C_2 =0.141

III.2.3 Results

III.2.3.1 Raw Data

The impact of the control treatments on wood dynamic properties is illustrated in Figure III.2.1 and in Figure III.2.2. Figure III.2.1 represents typical tan delta traces for untreated yellow-poplar and for the control-low and control-high samples. The three samples display similar glass transition temperatures as illustrated from the damping peak.

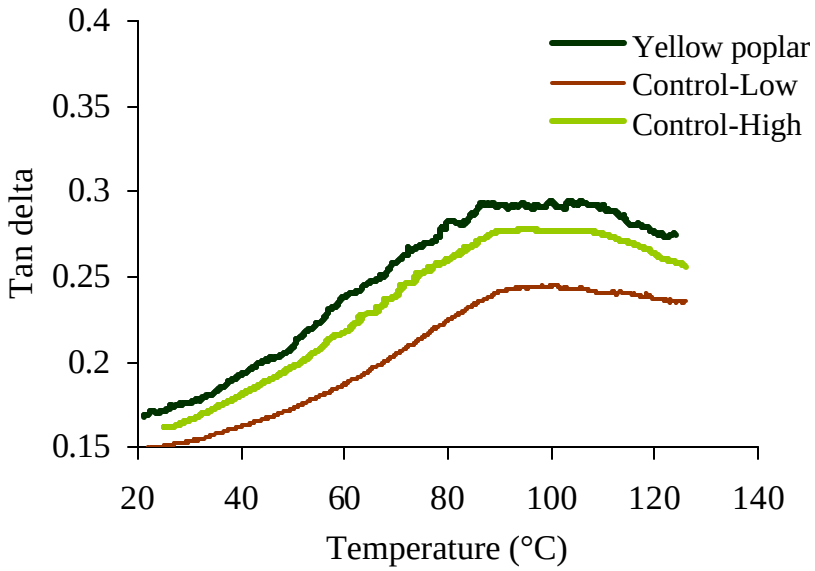

Figure III.2.1. Typical Tan delta Traces for Untreated Yellow-poplar, Control-Low and Control-High (not shifted)

In Figure III.2.2, typical storage modulus traces for the control samples and the untreated-yellow poplar are compared. The three samples display similar storage moduli over the entire temperature range. The difference between the traces for the three groups in Figure III.2.1 and in Figure III.2.2 simply reflects the natural variability of wood.

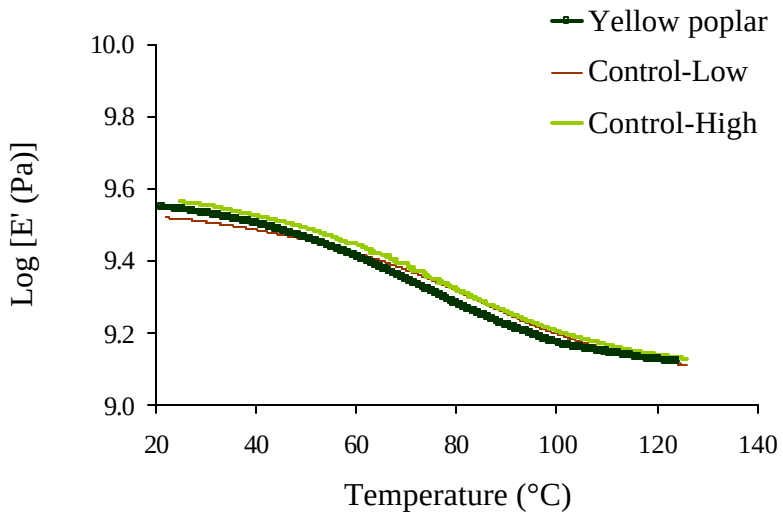

Figure III.2.2. Typical Storage Modulus Traces for Untreated Yellow-poplar,Control-Low and Control-High Specimens

For both wood/PF composites, detection of a glass transition was possible as illustrated by typical tan delta traces in Figure III.2.3. Again, it is legitimate to question whether this glass transition arises from *in-situ* lignin only, especially considering the high PF resin solid on wood and the similarity in structure of PF resins and lignin. In fact, the softening observed in the composites likely bears contribution from *in-situ* lignin as influenced by any intimate interaction with other wood components but also by any intimate interactions with the PF resin. Figure III.2.3 includes the tan delta trace for untreated yellow-poplar. The PF-Low treatment does not alter the *in-situ* lignin glass transition temperature. On the contrary, treatment with PF-High substantially shifts the glass transition to lower temperatures (Figure III.2.3). Note that in the PF-High composite substantial damping remains past the glass transition temperature.

Similar trends are apparent from the storage modulus-temperature curves (Figure III.2.4). While both the PF-Low and PF-High composites have higher modulus than yellow-poplar, the storage modulus in the PF-High composite drops more abruptly and sooner than that of yellow-poplar and of the PF-Low composite. The increase in modulus induced by the PF resins was very reproducible and was not due to wood variability.

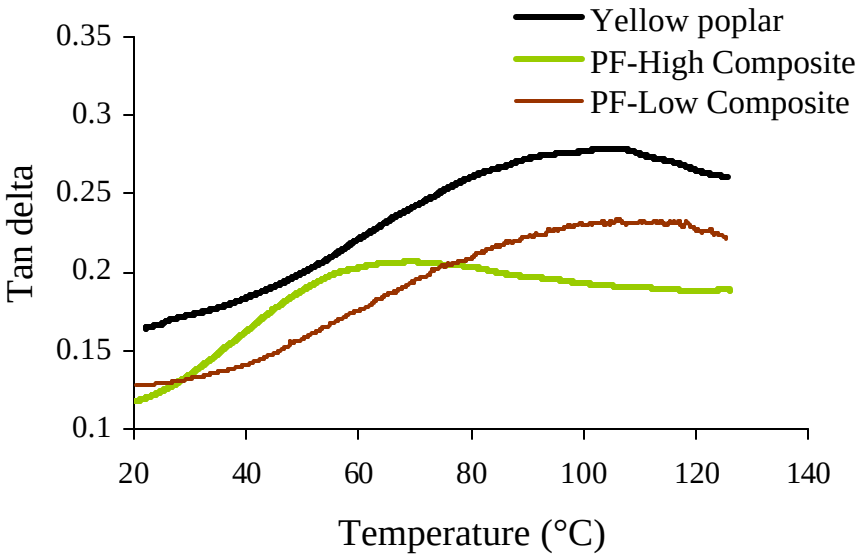

Figure III.2.3. Typical Tan Delta for Untreated Yellow-poplar, PF-Low and PF-High Composites

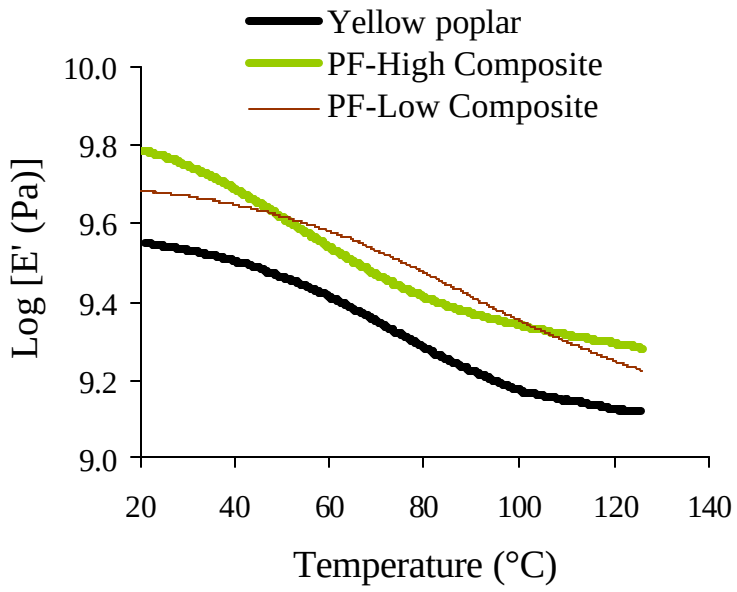

Figure III.2.4. Typical Log E' for Untreated Yellow-poplar, PF-Low and PF-High Composites

III.2.3.2 TTSP and Master Curves

TTSP was performed by shifting horizontally log E' isotherms to a reference isotherm. The reference isotherm corresponded to the T_g measured from the inflection point in the storage modulus at 2 Hz. A typical master curve for the control treatments is presented in Figure III.2.5. The master curve is smooth indicating the feasibility of TTSP on the temperature and frequency windows utilized in this study.

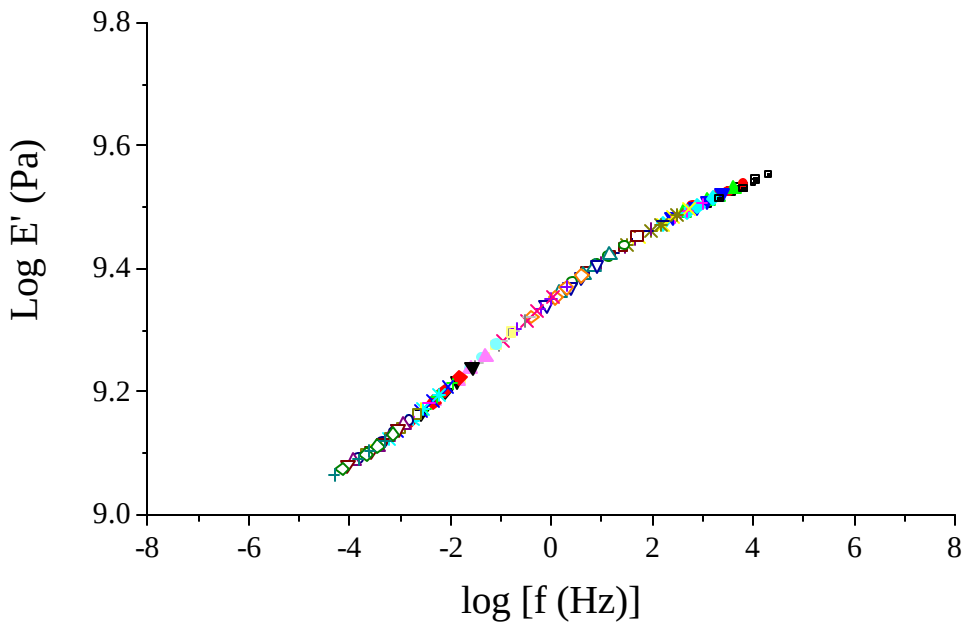

Figure III.2.5. A Typical Master Curve for Ethylene Glycol Plasticized Control-Low

A typical master curve for PF-Low composites is presented in Figure III.2.6. Again, it is evident from this figure that smooth master curves can be achieved for the PF-Low composite and that TTSP is feasible on the temperature and frequency windows utilized in this study.

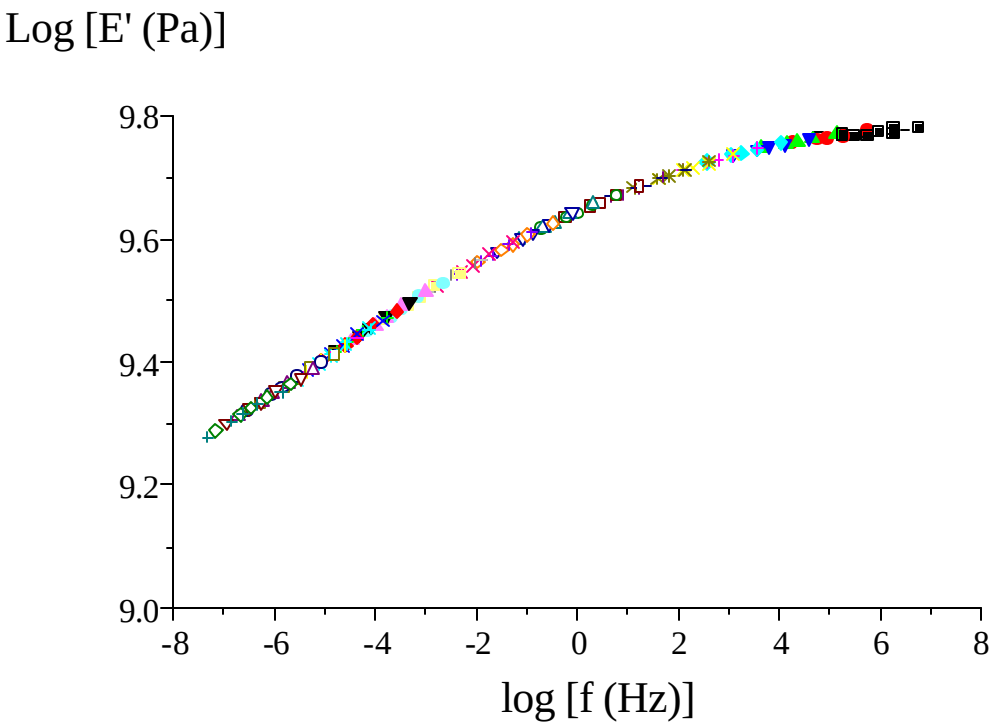

Figure III.2.6. Typical Master Curve for Ethylene Glycol Plasticized Wood/PF-Low Composite

On the other hand, difficulties were encountered when attempting to generate master curves for the PF-high composites. In fact, for most PF-High specimens, the master curves appeared noisier as illustrated in Figure III.2.7.

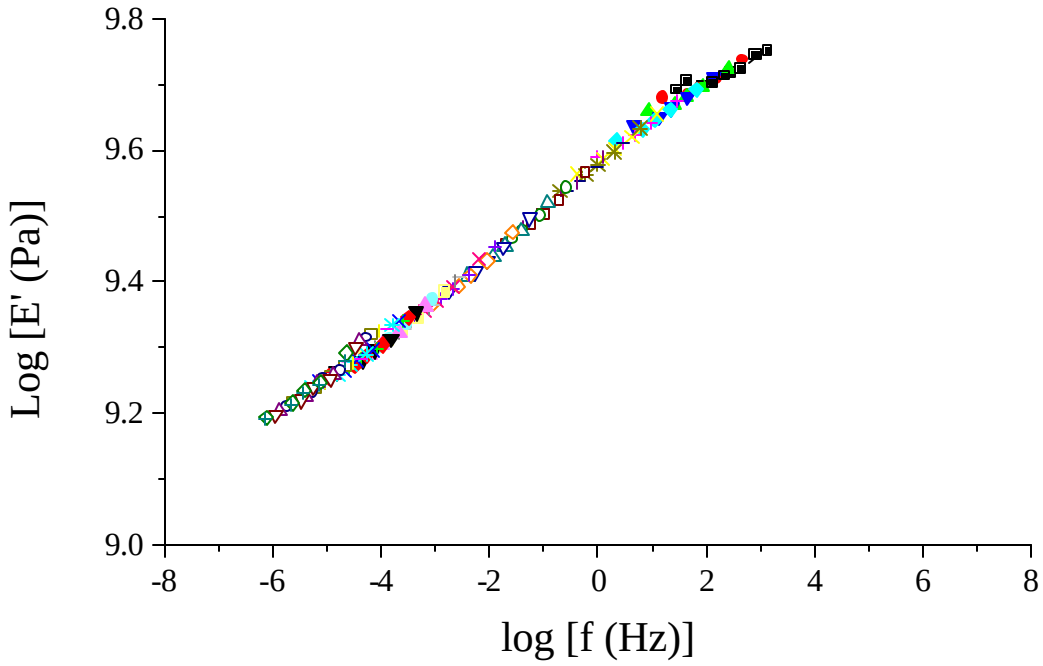

Figure III.2.7. Typical Master Curve for Ethylene Glycol Plasticized Wood/PF-High Composite

The reason behind the lower quality of the master curves for PF-High composites is unknown. It may be that the macroscopic and microscopic uniformity within the PF-High composites is lower than that in the PF-Low composites.

The average master curves for the control-low and control-high specimens are presented in Figure III.2.8 and in Figure III.2.9. The reproducibility of the master curves for the control treatments is good. In fact it is comparable to that of untreated yellow-poplar (see chapter II-2).

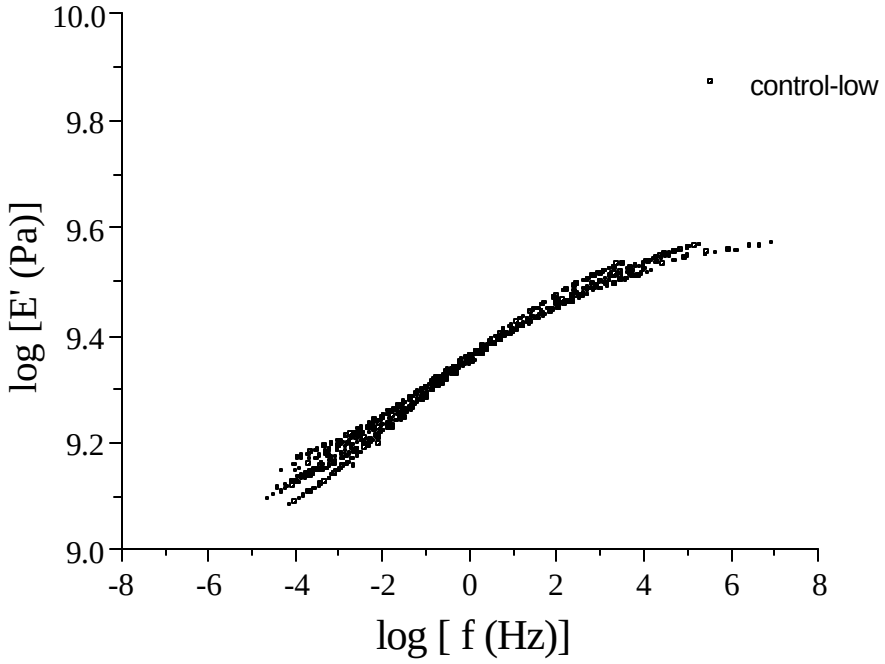

Figure III.2.8. Average Master Curve for 6 Specimens of Ethylene Glycol Plasticized Control-Low

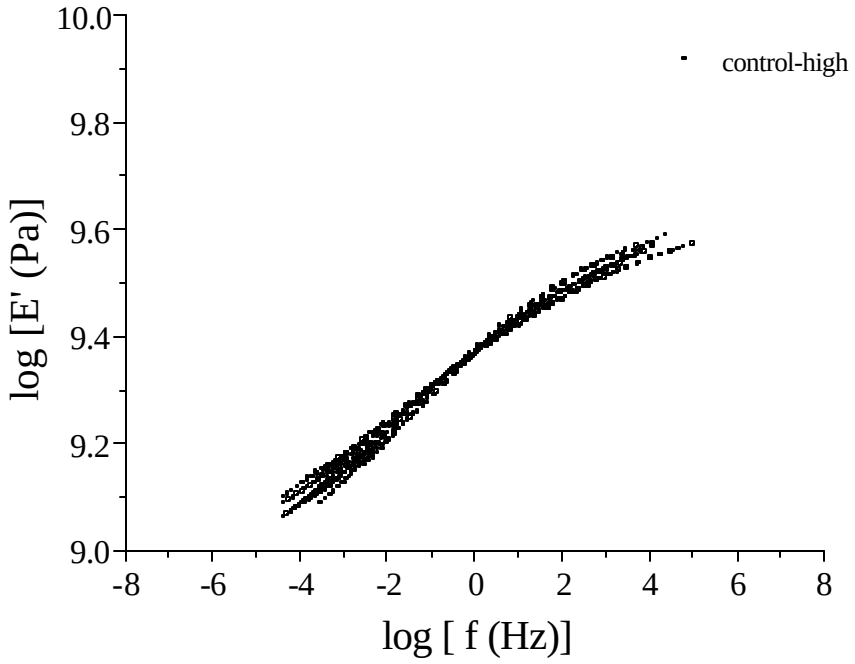

Figure III.2.9. Average Master Curve for 5 Specimens of Ethylene Glycol Plasticized Control-High

For the PF-Low composites, the reproducibility of the master curves was reasonable, albeit not as good as that of the control samples (Figure III.2.10).

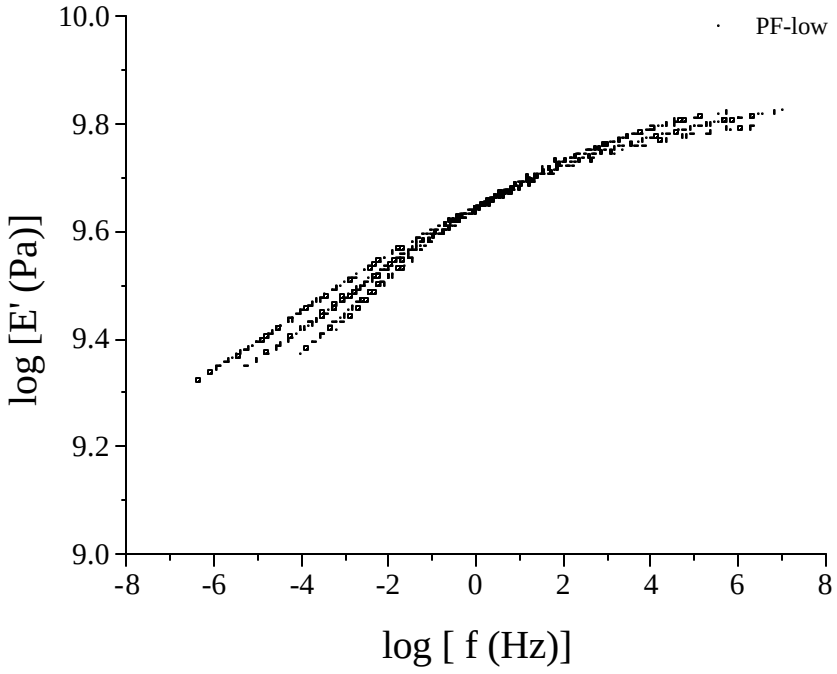

Figure III.2.10. Average Master curve for 7 specimens of Ethylene Glycol Plasticized PF-Low Composites

The PF-High composites exhibited the lowest reproducibility among all treatments as illustrated in Figure III.2.11. Lower reproducibility may again relate to greater specimen variability as a result of a less uniform inpregnation of the PF-High resin in wood.

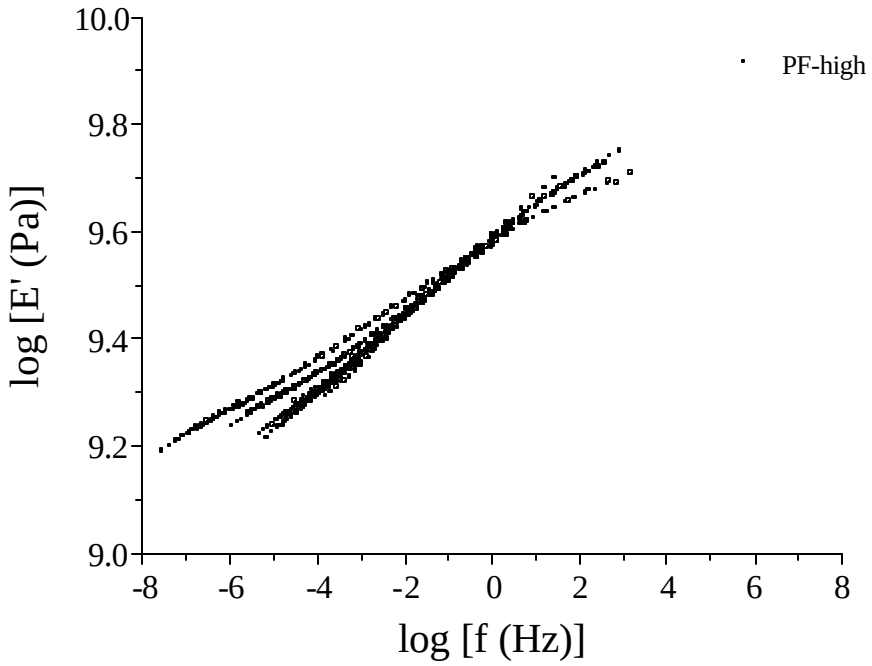

Figure III.2.11. Average Master Curve for 6 specimens of Ethylene Glycol Plasticized PF-High Composites

Overall, the reproducibility of the master curves for the PF composites was impaired compared to that of untreated Yellow-poplar and that of the control treatments. This is not unexpected since the manufacture of the composite generates variability on top of that of wood.

When one compares all master curves for the different groups, one striking feature emerges. For the PF–Low composite, the frequency range over which softening occurs is substantially wider than that for the control samples or untreated poplar. While the control specimens exhibit softening over approximately 10 decades, the PF-Low composite displays a transition region over approximately 12 decades. In fact for PF-Low, the glass rubber transition extends to lower frequencies i.e. longer times, indicating a slowing down in the relaxation mechanisms.

III.2.3.3 Cooperativity Analysis

The cooperativity analysis was undertaken on all four groups of treatment. Caution must be exerted however when considering this analysis for the PF-High

composites since the lower quality and reproducibility of the master curves may compromise the validity of TTSP for constructing cooperativity plots. Average cooperativity plots were constructed for all series of treatment by normalizing the individual shift factor to the fractional deviation from the average T_g. Figure III.2.12 compares the average cooperativity plots obtained for the control treatments and for yellow-poplar. Solid Lines correspond to the best fit from the Ngai coupling model. Anova analysis on the coupling constants allowed comparing all the data sets. It was followed by a Tukey-Kramer test in order to detect the significant differences among the different data sets. A convention was selected in order to characterize the significance of the difference from the p-values.

- p-values greater than 0.2 indicated no significant difference
- p-values greater than 0.1 and lower than 0.2 indicated little or no significant difference
- p-values lower than 0.05 indicated a highly significant difference

As for untreated yellow-poplar, the Ngai coupling model provides a good fit to the cooperativity data of the control treatments, allowing for the determination of the coupling constant, n. Figure III.2.12 reveals little difference, between the cooperativity of untreated yellow-poplar and the control treatments. Anova analysis also indicated no difference in the coupling constants obtained for the yellow-poplar, the control-low and the control-high treatments ($p= 0.23$).

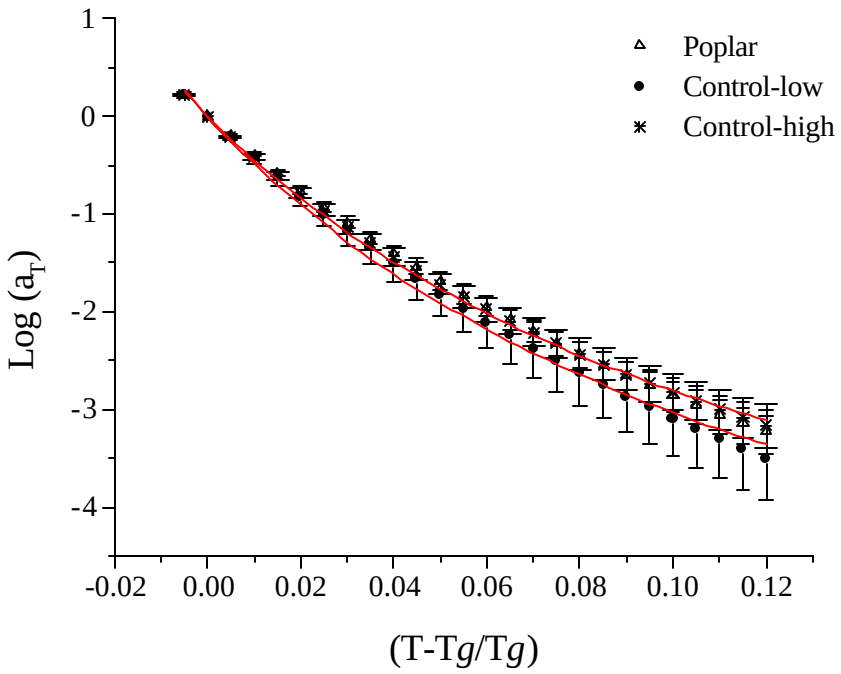

Figure III.2.12. Average Cooperativity Plots for Control-Low, Control-High and untreated Yellow-poplar

On the other hand, comparison of the average cooperativity plots for the PF-Low composites and Yellow-poplar suggests a significantly steeper temperature dependence of relaxation above lignin glass transition for the PF-Low composites (Figure III.2.13).

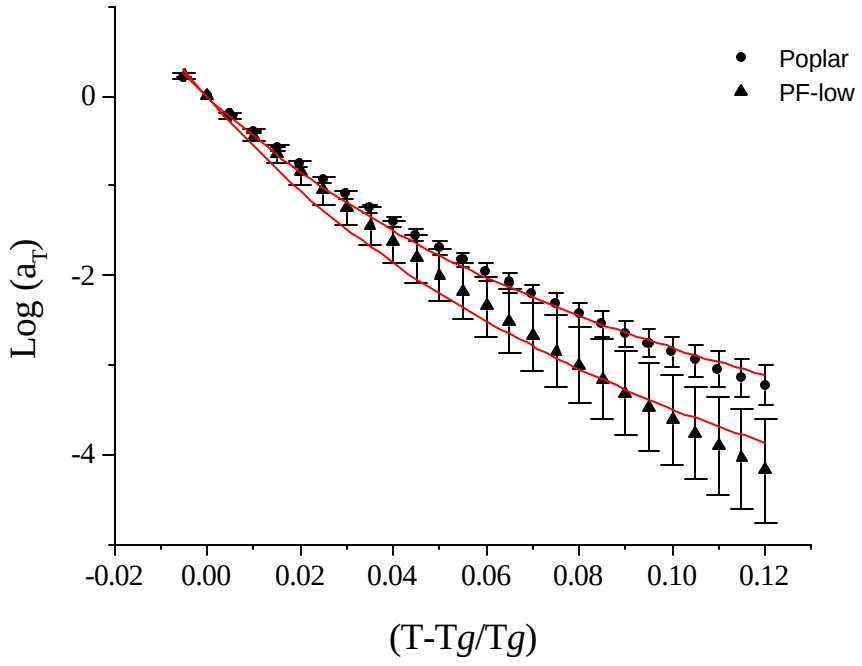

Figure III.2.13. Average Cooperativity Plots for PF-Low and Untreated Yellow-poplar

A highly significant difference was found with ANOVA analysis between the coupling constants pertaining to PF-Low and Yellow-poplar specimens (p=0.02) but also between the PF-Low and the control-Low treatment (p= 0.05).

While the cooperativity analysis may be compromised for the PF-High composites owing to the lower quality of TTSP, similar data treatment was attempted on the PF-High series as well. Average cooperativity plots comparing PF-High composites and untreated yellow-poplar are presented in Figure III.2.14.

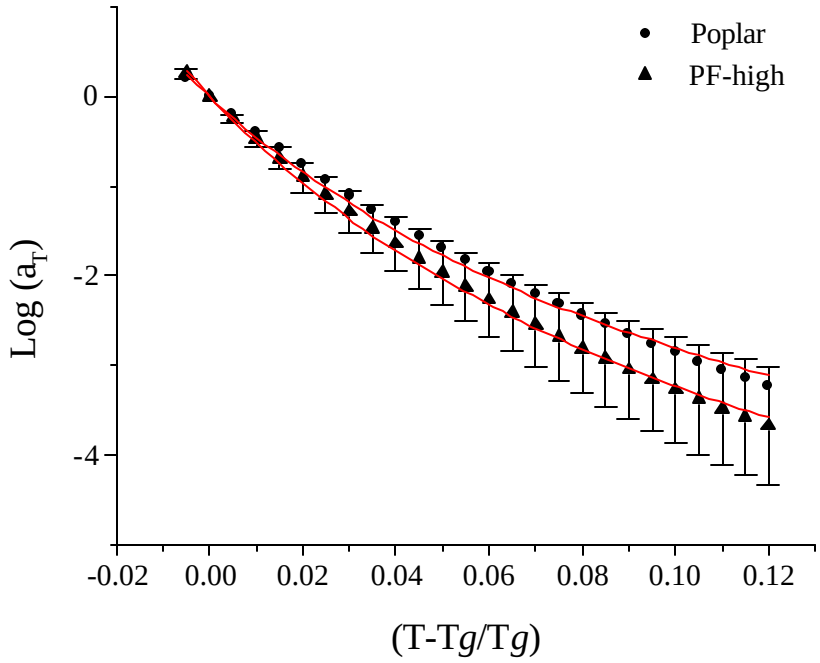

Figure III.2.14. Average Cooperativity Plots for PF-High and Untreated Yellow-poplar

Again, steeper temperature dependence is suggested in the PF-High composite than in yellow-poplar. However, little or no significant difference was found between yellow-poplar and the PF-High composite (p=0.11). Similarly, little or no significant difference was found between PF-High and Control-High (p=0.13).

Table III.2.1 summarizes the viscoelastic properties pertaining to the 5 series of specimens. Again, T_g values reported in this table correspond to the inflection point in the storage modulus at 2 Hertz. TTSP, WLF constants and coupling constants are derived by reference to this T_g value. Activation energies were calculated as for the untreated wood samples from the WLF constants (see chapter II-2). The table also presents a qualitative scaling of the quality and reproducibility of the master curve upon which hinges the validity of the WLF and cooperativity data. In addition a χ^2 parameter, representative of the goodness of Ngai coupling model fit to the cooperativity data is provided. The χ^2 value represents the sum of the squared differences between theoretical and experimental data. Small χ^2 values are therefore indicative of a good fit.

Table III.2.1. Viscoelastic Behavior of Yellow-poplar, Control Treatments and PF Treatments (standard deviation in parenthesis).

	Poplar	***Control Low***	***Control High***	***PF-Low***	***PF-High***
Number of Specimens	***6***	***6***	***5***	***7***	***6***
Master Curve* (Quality)	++++	++++	++++	++++	+
Master Curve* (Reproducibility)	+++	+++	+++	++	+
T_g (°C)	***71 (4)***	***73 (7)***	***67 (6)***	***71 (8)***	***45 (2)***
C_1	***-9.4 (2.2)***	***-10.4 (1.6)***	***-7.6 (1)***	***-19.5 (2.5)***	***-9.7 (2.3)***
C_2	***78 (21)***	***81 (14)***	***58 (8)***	***152 (22)***	***63 (10)***
E_a (T_g) (kJ/mol)	***274 (12)***	***296 (45)***	***291 (28)***	***294 (44)***	***303 (57)***
n	***0.19 (.04)***	***0.25 (.09)***	***0.18 (0.07)***	***0.37 (0.11)***	***0.28 (0.13)***
c^2 (Ngai fit)	***0.0045***	***0.0256***	***0.0099***	***0.0302***	***0.0033***

** (+: poor; ++++: excellent)*

Table III.2.1 does reflect the observations deduced from the master curves and the cooperativity plots. Control-Low and control-High have similar viscoelastic properties than untreated yellow-poplar. For these groups, the glass transition temperature, the WLF constants as well as the activation energies derived from the WLF constants at the glass transition temperature are similar. By contrast, the PF-High composite displays a lower glass transition temperature by approximately 25°C. Also apparent in this table, the fact that PF-Low substantially modifies the time-temperature equivalence in wood softening region. While the main softening temperature is similar in the PF-Low composite and in untreated or control-treated yellow-poplar groups, the WLF constants are substantially altered in the PF-Low composite.

III.2.4 Discussion

The base hypothesis of this research is that the morphology of the wood adhesive interphase depends on resin molecular weight. On thermodynamic grounds, a low

molecular weight PF resin is expected to permit a smaller scale of penetration than a high molecular weight resin. Viscoelastic studies utilizing DMA generally characterize the nanometer scale morphology of polymer blends. It is worthy before entering the discussion of PF-Low and PF-High nanoscale interphase morphologies to remind one of the molecular weight characteristics of the two starting PF resins. PF-Low had an average radius of gyration of 0.65 nanometers. The highly condensed PF-High had an average radius of gyration of 2.48 nanometers. A low molecular weight tail fraction similar to PF-Low was also present in the PF-High resin (see chapter III-1).

Obviously, the molecular weight of the resin has a significant impact on the viscoelastic properties of the composites, suggesting differences in the nanoscale interphase morphology between the PF-Low and the PF-High composites. For the PF-High composite a dramatic reduction of the composite main softening temperature is observed. While the cooperativity analysis needs to be considered with caution in the PF-High composites, little or no difference in coupling ($p=0.11$) is detected between the PF-High composite (0.28 ± 0.13) and yellow-poplar (0.19 ± 0.04). On the other hand, a highly significant ($p=0.02$) increase in cooperativity is found between the PF-Low composite (0.37 ± 0.11) and Yellow-poplar (0.19 ± 0.04). In the PF-Low composite, the sample glass transition temperature remains unchanged. These significant differences in viscoelastic behavior are not caused by the alkali nor the heat treatment imposed during the preparation of the composites, since control-Low and control-High treatments do not induce significant viscoelastic changes. There are therefore dramatic differences between the two composite systems that stem from the PF molecular weights and molecular weight distributions.

Let us first consider in greater depth the morphology of the PF-Low composite. In phase separated systems, two glass transitions are generally observed for the distinct phases. When *in-situ* lignin is plasticized with ethylene glycol (EG) its glass transition is reduced from 200°C to approximately 70 °C. In the dry state also, the glass transition of the PF-Low is expected to be close to the isothermal cure temperature, 150°C. Ethylene glycol is an efficient swelling agent of PF resins [2]. For neat cured PF resins, Schmidt reported 26% mass increase upon swelling PF resins in ethylene glycol. Table III.2.2 confirms that EG should be equally efficient in swelling PF and lignin. Saturation of the

PF-Low composite in EG is therefore expected to decrease the glass transition of the PF resin. It is however difficult to evaluate the *in-situ* glass transition of plasticized PF because the network structure and the propensity for swelling *in-situ* differ from a neat PF resin. More specifically, wood is known to increase PF network mobility, suggesting lower crosslink density and possibly greater swelling potential. One reasonable assumption on these grounds is that the *in-situ* glass transition of the EG plasticized PF must be significantly lower than 150°C.

Table III.2.2. Solubility Parameters Pertaining to Wood/PF composites Saturated in Ethylene Glycol (from [11] and [2])

	d ***(Mpa $^{1/2}$)***
Lignin	***31.05***
Ethylene Glycol	***29.7***
PF structures	***28 -33.2***

DMA temperature scans on the temperature range of 20 to 120 °C for the PF-Low composite permit the detection of *in-situ* lignin. Only one transition is detected within the temperature range of the study. The observation of one glass transition in PF-Low composites as well as increased intermolecular cooperativity suggests that *in-situ* lignin and PF-Low resin may be a miscible blend, at least on a nanometer scale. Recall that intermolecular cooperativity portrays the non-exponentiality of the alpha relaxation i.e. the breadth of the distribution of relaxation mechanisms. If on a nanometer scale the PF-Low resin mixes with lignin, then the local environment of lignin will become more heterogeneous, thus broadening its distribution of relaxation mechanisms. In fact, increase in cooperativity is typically observed in miscible polymer blends and is ascribed to local concentration fluctuation [8]. In other words, the local environment of one polymer becomes more heterogeneous when blended with a miscible polymer. Following these considerations, it seems useful to conceptualize the mechanism of interphase formation that may take place in accordance with the viscoelatic behavior of the PF-Low composite. The scenario is presented in Figure III.2.15. When the liquid

adhesive is applied to wood, the low molecular weight species (red) penetrate on a nanometer scale into the lignin domain. Upon cure of the resin, an *in-situ* network is generated. One envisions easily in the resulting interphase that segmental motions are constrained. In such an interphase also, the sample glass transition would result from main chain motion of the PF network and the *in-situ* lignin network, which cannot be discriminated from one another by DMA.

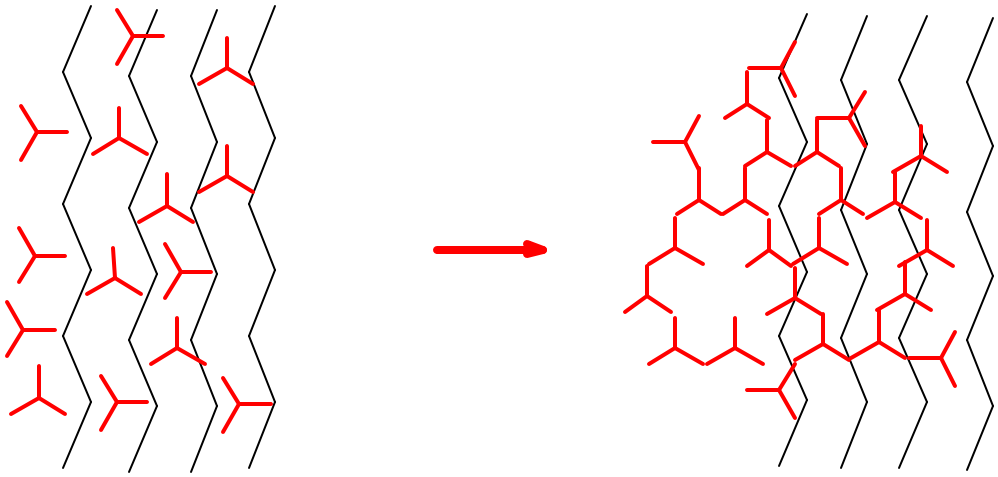

Figure III.2.15. Nanometer scale Miscibility Upon Cure of a PF-Low in Wood

Let us now consider the case of the PF-High composite. The most unexpected behavior is that in the PF-High composite, the softening temperature of the sample is depressed by 25 °C compared to that in untreated yellow-poplar. This observation suggests that the PF-High resin plasticizes the *in-situ* components responsible for the sample softening or that degradation of lignin occurs. This second hypothesis is unlikely since substantial scission would be needed in order to observe such a lowering of the *in-situ* glass transition temperature of lignin. The alternative hypothesis implies that under the influence of the PF-High resin, *in-situ* lignin is plasticized either by direct interaction with the PF-High resin or by indirect effect such as enhanced interactions with wood carbohydrates for instance. In other words, the plasticization observed in the PF-High composite could stem from a greater contribution of low T_g components (carbohydrates, ethylene glycol, PF monomers) to the sample main softening.

Figure III.2.16 helps remind one of the molecular weights and molecular weight distributions of the PF-High and PF-Low resins. In the PF-High resin, the low molecular weight tail represents at best a fifth of the total distribution of molecular weights.

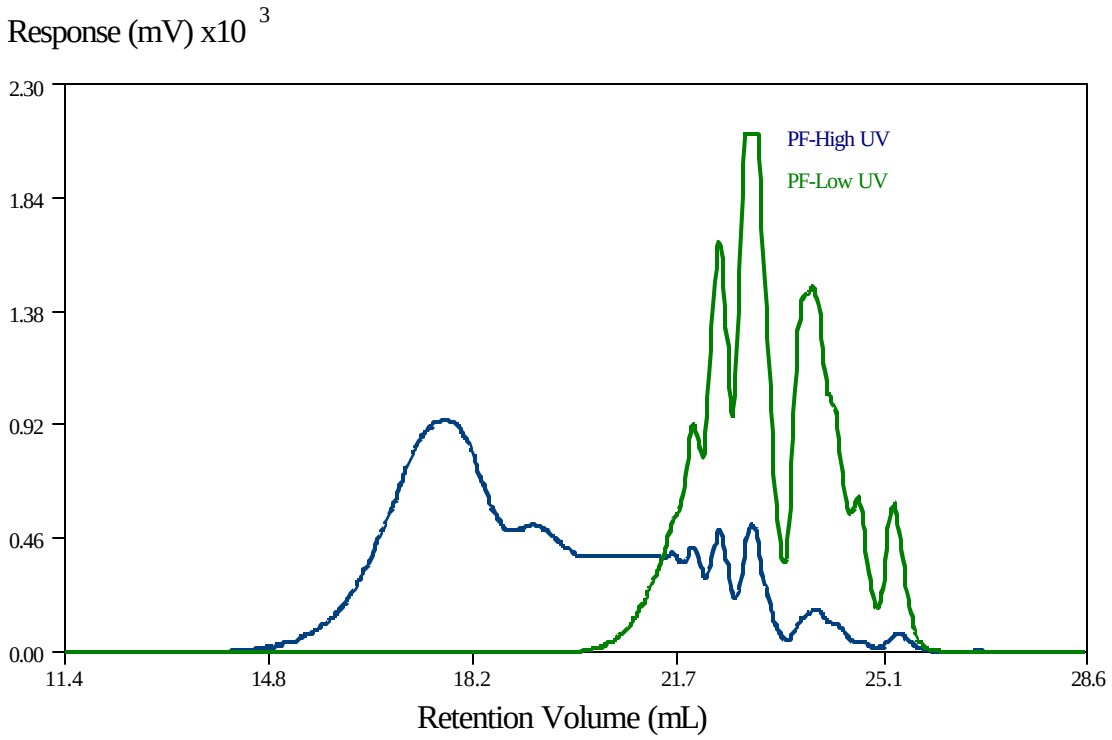

Figure III.2.16. Molecular Weight Distributions of PF-Low and PF-High

Because it is believed that PF-Low can penetrate on a nanometer scale in the lignin phase, the low molecular weight tail of PF-high should have the same ability. This can be envisioned because PF-High low molecular weight tail is very similar to the PF-Low resin (Figure III.2.16). Since the PF-High resin has only a small fraction of these low molecular weight species, the density of PF species within the lignin phase is lower than that of the PF-Low. Recall in addition, that the resin solid in PF-High composites is 15% lower than in PF-Low composites. This difference in the PF uptake by wood has previously been proposed to reflect the average penetration scale of the respective resins into wood. Now, let us consider again the mechanism for the formation of the wood/PF-

High interphase, keeping in mind that a small fraction of the resin may be penetrated on a nanoscale, while the predominant high molecular weight fraction remains outside of the lignin phase. The scenario for the formation of such an interphase is presented in Figure III.2.17.

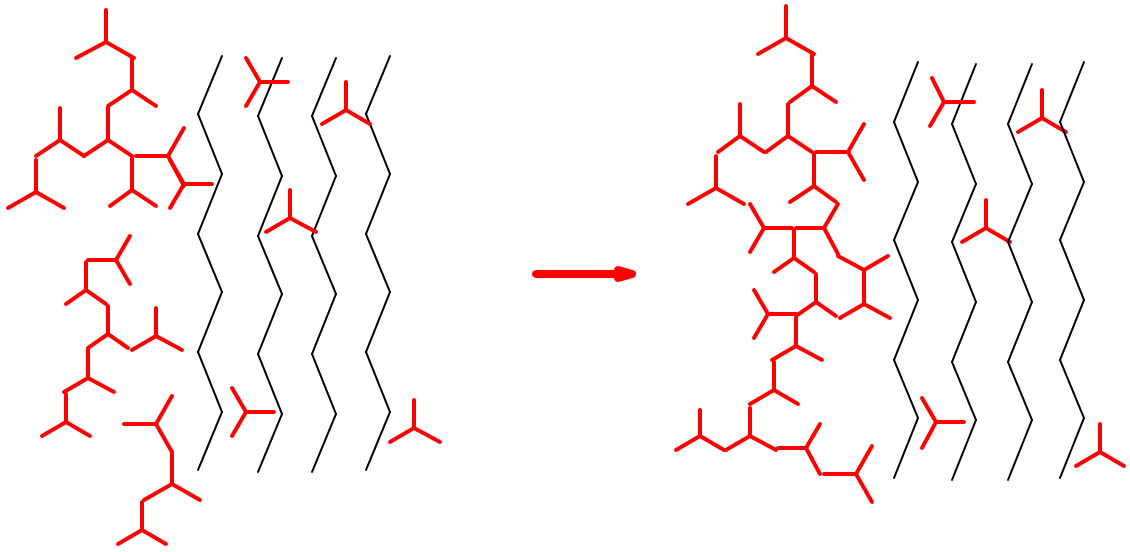

Figure III.2.17. Nanometer Scale Separation Upon Cure of a PF-High with Some Degree of Nanometer Scale Penetration

Upon cure of the composite the high molecular weight species, apart from the lignin, forms a crosslinked three dimensional network. The nanophase cured PF network, because it is less impacted by wood polymer proximity, is likely to have the characteristics of a bulk cured PF. On the other hand, the rare species dispersed within lignin have little opportunity for connecting to the crosslinked PF network. In fact one conceptually envisions that the entrapped monomers may remain uncured within wood polymers. This hypothesis is consistent with the red coloration of the ethylene glycol bath during sample conditioning. Uncured PF species entrapped within wood polymers would likely reduce the softening temperature in the composite sample. It may also be that during the conditioning step in ethylene glycol, the uncured PF species react with ethylene glycol yielding a very low T_g polymer, which again would act as an efficient

plasticizer, if intimately mixed with wood polymers. In addition, owing to lignin reactivity for hydroxymethyl phenols, it can be equally envisioned that dispersed PF monomers (or PF-ethylene glycol condensates) react with lignin aromatic sites. The attachment of pendant hydroxymethyl phenols on the lignin network is likely to inhibit the packing of lignin chains and increase the free volume thereby yielding a depression in the composite main softening temperature. Such a behavior is generally referred to as internal plasticization and has been previously observed for a series of substituted poly(p-phenylene) by Karazs's group [10]. Namely, the authors observed that upon attachment of a 4-phenoxybenzoyl side group to poly(p-phenylene), the polymer glass transition is substantially depressed (approximately 20°C) while the fractional free volume is increased. A similar effect can therefore be envisioned if monomers or dimers of hydroxymethyl phenols react with lignin.

Similarly, the possibility for resin to remain uncured within the woody material after penetration has been proposed earlier for alkyd resins [12]. In 1972, in a study of alkyd resin penetration into wood cell wall, Robison proposed that the fraction of the resin penetrated into the cell wall remains uncured. After his observation, little research has focused on considering such an hypothesis. Probably, the appreciation of adequate methods has impeded further research on this issue. Molecular motions, and thus viscoelastic properties should be however sensitive to the state of the resin in proximity with wood polymers. In fact, Marcinko observed from simple DMA temperature scans that in a wood/ pMDI composite, the glass transition temperature of wood is depressed by approximately 25°C compared to that of untreated wood [4]. pMDI is a low molecular weight aromatic adhesive that penetrates deeply wood polymers. While the authors did not attempt to interpret this effect of pMDI on wood softening behavior, their observation is similar to that presently observed with the PF-High resin. Similar scenarios can be envisioned in Marcinko's studies, especially that only 5% pMDI solids on wood was utilized in the composite manufacture. Namely, scarce pMDI species may either internally plasticize wood polymers by free volume effects or by remaining uncured within wood polymers. In Marcinko's work also, a significant broadening of the damping peak was observed in the wood/isocyanate composite [4]. This behavior was not seen in the present study with the PF-High composite. Recall however from Figure

III.2.3, that past the glass transition temperature, damping remains high in the PF-High composite. The origin for this high damping is unknown. One possibility is that the system resonance frequency approaching that of the measuring frequency at high temperatures, it may inflate the damping in this region. It may also be that a second transition, possibly the glass transition of bulk PF-High phases is to occur at higher temperatures. This would be consistent with phase-separated systems in which a cured bulk PF phase would have its own glass transition. However, it cannot be detected because of limited temperature window that can be utilized. In addition, recall that the PF-High composites were found to be less amenable to TTSP. In fact, the microscopic uniformity of the samples has been proposed as one explanation of the lower amenability of PF-High composites to TTSP. The lower reproducibility of the master curves further suggests great inter-specimen variability. In addition, multiphase polymer blends are generally associated with a break down of the TTSP [5]. Although the frequency window is small in this study and therefore does not really allow inferences on thermorheological complexity, it is surprising to see with the PF-High composite a different response to TTSP than that of all other treatments. Let us finally point out what the cooperativity analysis indicated, keeping in mind that it may be compromised by the lower quality of TTSP. The cooperativity analysis indicated little or no difference ($p=0.13$) in intermolecular cooperativity between PF-High with 0.28 ± 0.13 and Control-High (0.18 ± 0.07). With a small fraction of nanoscale penetration in the PF- high composite there may be some greater degree of concentration fluctuations. Of course this is if one accords the credibility to the cooperativity analysis in the PF-High composite in spite of the compromised TTSP.

While different morphologies have been proposed that can rationalize the viscoelastic properties of PF-Low and PF-High composites, recall that caution is necessary in the interpretation of the data. The proposed morphologies based upon the viscoelastic observations have only hypothesized a direct effect of the PF resins on lignin. However, an indirect effect is also possible, such as a change in interactions between lignin and hemicellulose. It is on the sole basis of these data impossible to determine whether the viscoelastic changes detected for lignin is directly or indirectly related to lignin/PF interactions. Certainly however, the complexity of wood structure and the lack

of comparison from studies with such complex systems make the interpretation difficult. The hypothesis proposed here remains therefore mere speculation, which is consistent with the experimental observation.

III.2.5 Conclusions

In this study, combining simple DMA measurements with TTSP and the cooperativity analysis has provided some insight on the viscoelastic properties of wood/PF resin composites and on the sample softening behavior. No change in the sample glass transition temperature is detected from simple DMA scans upon treating yellow-poplar with a low molecular weight PF resin, PF-Low. Fortunately, TTSP and the cooperativity analysis are found applicable for the low molecular weight PF composites. The analysis indicates that treatment with the PF-Low resin enhances the intermolecular coupling involved in the sample alpha relaxation thus yielding a steeper temperature dependence of relaxation and a wider distribution of relaxation mechanisms. If the PF-Low is mixed on a nanoscale with wood polymers and with the *in-situ* lignin in particular, then enhancement in cooperativity is expected. To the author knowledge, this is the first attempt of performing such an analysis on wood-based composites. On the other hand simple DMA measurements indicate that a PF resin with a broad distribution of molecular weights, PF-High, substantially lowers the sample glass transition temperature compared to untreated wood. Besides, the PF-High composites are less amenable to TTSP. It is hypothesized that greater microscopic heterogeneity in PF-High composites may be the cause for failure of TTSP. It may also be that the wood /PF-High interphase forms a phase separated morphology. However, because PF-High is observed to lower the softening temperature of the sample, some fraction of the PF-High resin is hypothesized to interact intimately with wood polymers and with the *in-situ* lignin in particular. It is proposed that the low molecular weight tail of the PF-High resin penetrates wood polymers on a nanometer scale. However, because their too great dispersion within wood polymers, the PF species are believed to remain uncured or to become substituted on wood polymers thus acting as external or internal plasticizers. While this is the first time that such a morphological interpretation of viscoelastic data is

given for wood/adhesive composites, similar results have been observed with pMDI composites of low resin content.

It clearly emerges from this study, that the molecular weights and molecular weight distribution of the adhesive is critical to the wood/adhesive interphase morphology. Viscoelastic measurements offer a powerful probe of morphology. The difference in viscoelastic behavior affords a great sensitivity to the state of the resin within the composite. This sensitivity is all the more remarkable that microscopic observation of the two PF composites had suggested for both systems some degree of cell wall penetration (Chapter III-1).

III.2.6 References

[1] Plazeck D. J. and K. L. Ngai, Correlation of Polymer Segmental Chain dynamics with Temperature-Dependent Time-Scale Shifts, Macromolecules , 24, 1222, 1991.

[2] Schmidt R.G., Aspects of Wood Adhesion: Applications of ^{13}C CP/ MAS NMR and Fracture Tests, Ph. D Dissertation, Virginia Polytechnic Institute and State University, January 1998.

[3] Glasser W. G., Classification of Lignin According to Chemical and Molecular Structure, ACS Symp.Ser., Viscoelasticity of Biomaterials, Ed. W.G. Glasser and H. Hatakeyama, No. 489, 216, 1992

[4] Marcinko J.J., S. Devathala, P.L. Rinaldi, S. Bao, Investigating the Molecular and Bulk Dynamics of PMDI/Wood and UF/Wood Composites, Forest Products Journal, 48 (6) 81, 1998.

[5] Ferry J.D , Viscoelastic Properties of Polymers; 3rd Ed, Wiley, New York, 1980.

[6] Colby R.H., Breakdown of Time-Temperature Superposition Principle in Miscible Polymer Blends, Polymer, 30, 1275, 1989 .

[7] Ngai K.L. and D.J. Plazeck, Identification of Different Modes of Molecular Motion in Polymers that Cause thermorheological Complexity, Rubber Chemistry and Technology, 68, 376, 1995.

[8] Roland C.M. and K.L. Ngai, Segmental Relaxation in Miscible Polymer Blends, J. Rheol. 36 (8), 1992.

[9] Jensen R.E., Investigation of Waterborne Epoxies for E-Glass Composites, Doctoral Dissertation, Virginia Polytechnic Institute and State University, June 1999.

[10] Connolly M., F. Karasz and M. Trimmer, Viscoelastic and Dielectric Behavior of Substituted Poly(p-phenylene), Macromolecules, 28 (6), 1872, 1995.

[11] Hansen C. M., Hansen Solubility Parameters, A User's Handbook, CRC Press, New York, 2000.

[12] Robison R.G., Wood-Coating Interactions, Doctoral Dissertation, State University College of Forestry at Syracuse University, May 1972.

CHAPTER. III.3. PF INFLUENCE ON CP/MAS NMR RELAXATIONS OF WOOD POLYMERS

III.3.1 Introduction

In a CP/MAS NMR spectrum, the carbon signal intensity is governed by molecular motions. The cross-polarization time, T_{CH}, gives rise to the carbon signal build-up at short contact times and is dictated by near static molecular motions. Proton $T_{1\rho}$ is responsible for the decay of the carbon signal at long contact times. Proton $T_{1\rho}$ reflects mid-kilohertz motions and involves domain sizes in the range 2 to 30 nanometers [3]. In homogeneous materials, spin diffusion averages the apparent molecular motions of all protons, thereby yielding a common $T_{1\rho}$ regardless of the carbon which is probed. Within phase separated materials on the other hand, spin diffusion is inefficient thus possibly generating different $^{H}T_{1\rho}$ relaxations for the distinct phases. In this study, the impact of PF resin on wood molecular dynamics is assessed by monitoring T_{CH} and $^{H}T_{1\rho}$ for wood polymers before and after impregnation with PF resins. Two PF resins are utilized. One PF resin, PF-Low, is a relatively monodisperse low molecular weight resin. The other PF resin, PF-High, has a broad distribution of molecular weights and a high degree of polymerization. Using these two resins, the nanometer scale morphology of the PF composites is also evaluated by comparing the $^{H}T_{1\rho}$ relaxation in wood polymers and in the PF resins.

III.3.2 Materials and Methods

III.3.2.1 Materials

The reader is directed to chapter III-1 for a detailed description of the materials utilized for this study. Briefly, two PF resins, PF-Low and PF-High, were synthesized so as to yield different molecular weight distributions. PF-Low had a number average molecular weight of 270 g/mol and a polydispersity of 1.22. PF-High had a number average molecular weight of 2840 g/mol and a polydispersity of 5. A low molecular weight tail was clearly present in the PF-High. The two PF resins were utilized to manufacture wood/PF composites. The composites consisted of yellow-poplar

(*Liriodendron tulipifera*) flakes (3.5 R * 0.85 T*50 L mm^3) that were impregnated with PF-Low and PF-High. For each resin, the impregnation procedure was adjusted so as to yield similar resin solids on dry wood and similar microscopic penetration throughout the sample. Resin solids on wood dry mass were respectively 52% and 38% for PF-Low and PF-High composites. The PF-Low and PF-High composites were oven cured at 110°C until vitrification; Post-cure at 150°C for 20 minutes followed.

Control-Low and control-High samples were manufactured to provide a control of the impregnation and heat treatments applied on wood during the manufacture of the PF-Low and PF-High composites, respectively. Namely, yellow-poplar flakes were impregnated with a control sodium hydroxide solution and heat treated in accordance with the impregnation and cure procedures utilized for the PF resins.

Small disks were retrieved from the samples by using a paper hole puncher. The samples were vacuum dried overnight (room temperature and approximately 0.1 mm Hg) and kept in a desiccator with drierite until analysis. The moisture content before CP/MAS NMR analysis did not exceed 0.5 %.

III.3.2.2 Methods

Cross-polarization experiments were performed on a Bruker MSL-300 MHz spectrometer using a 7 mm probenkopf MAS.07.D8 probe. The spectrometer frequency was set at 75.47 MHz for ^{13}C Nuclei and the spin locking frequency for the proton channel was approximately 56 kHz. Adamantane was utilized for establishing the Hartmann-Hahn match. The specimen disks were loaded in a zirconium oxide rotor, sealed with a Kel-f cap. The samples were spun at 5 kHz ± 20 Hz. A standard CP pulse with variable contact time was performed. As many as 12 contact times were utilized within the 0.1-15 ms range. For each contact time, 1000 scans were accumulated. The recycle delay was 3.75 s and the acquisition time was 50 ms. Three samples were analyzed for each series of treatment. Carbon T_{CH} and proton $T_{1\rho}$ relaxation were determined by fitting the carbon intensity- contact time curve to Equation (III.3.1) [1].

(III.3.1)
$$I(T) = I^{*}\left(\frac{{}^{H}T_{1r}}{{}^{H}T_{1r} - T_{CH}}\right)\left(\exp^{-t/{}^{H}T_{1r}} - \exp^{-t/T_{CH}}\right)$$

Where I(t) represents the signal intensity at a contact time t and I* is the corrected signal intensity. Anova analysis with tukey–kramer analysis was performed in order to determine the significant differences between the relaxation times. A convention was selected in order to characterize the significance of the difference from the p-values.

- p-values greater than 0.2 indicated no significant difference
- p-values greater than 0.1 and lower than 0.2 indicated little or no significant difference
- p-values lower than 0.05 indicated a highly significant difference

III.3.3 Results

Figure III.3.1 presents the superposed CP/MAS NMR spectra of neat yellow poplar, of a control specimen and of a PF composite. The lignin methoxyl carbon appears at 56 ppm in the yellow-poplar and control spectra. It remains as a shoulder in the spectrum of the composite. The cellulose C_4 appears at 85 and 90 ppm, for the amorphous and crystalline regions respectively. The signals are well resolved in the three spectra. The carbohydrate C_1 has a distinct resonance at 105 ppm, which is also clearly detected in all three spectra. The hemicellulose acetyl carbon at 22 ppm is apparent in the neat and control yellow-poplar spectra but becomes a broad peak in the composite spectrum. In the composite, the PF methylene signal at 35 ppm may be overlapping with hemicellulose acetyl group. Other hemicellulose carbons cannot be well resolved in the composite spectra either. A strong resonance appears at 130 ppm in the composite spectrum. This chemical shift is characteristic of the PF resin aromatic carbons. This signal generates spinning sidebands of low intensity at 173 and 88 ppm (labeled *SS* on the spectrum). The SS intensity is low enough, so that their contribution to the wood signals is negligible.

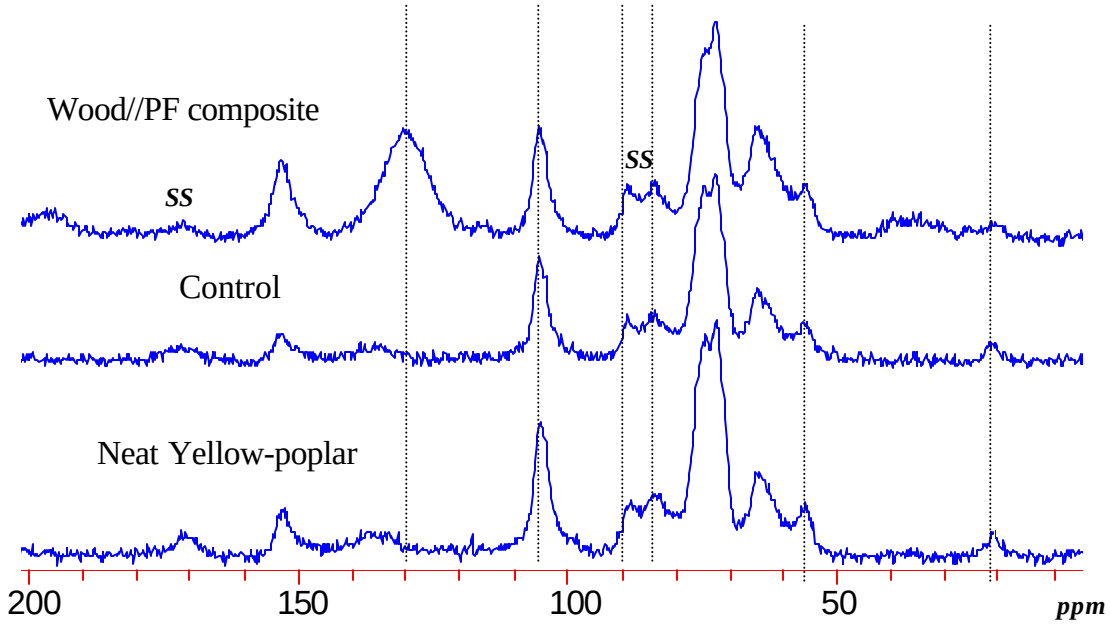

Figure III.3.1. ^{13}C CP/MAS NMR Spectrum of Dry Yellow-poplar (bottom), Control treated Yellow-poplar (middle) and Yellow-poplar /PF Composite (top)

III.3.3.1 Hemicellulose Acetyl group (22 ppm)

A typical signal versus contact time curve for the hemicellulose acetyl carbon is presented in Figure III.3.2. On the y axis the signal intensity (I) is normalized to the maximum signal intensity (I*). The solid line represents the best fit to Equation (III.3.1). The poor fit observed in Figure III.3.2 likely results from the difficulties in monitoring the weak hemicellulose signal in all spectra. This is especially the case for the hemicellulose signal in the PF composites (Figure III.3.1). Consequently, carbon T_{CH} and proton $T_{1\rho}$ could not be determined with confidence for the hemicellulose acetyl group.

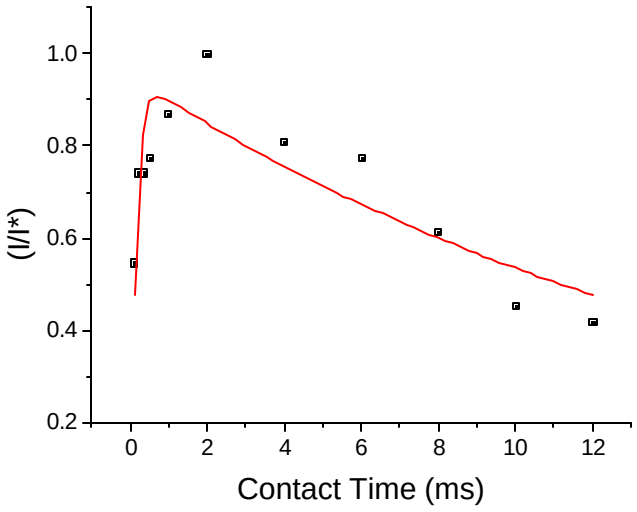

Figure III.3.2. A Typical Signal vs. Contact Time Curve for Hemicellulose Acetyl Carbon (Symbols are Data Points and the Solid Line is the Best Fit to Equation (III.3.1))

III.3.3.2 Lignin Methoxyl Group (56 ppm)

A typical signal vs contact time curve for the lignin methoxyl carbon is presented in Figure III.3.3. The fit to equation (III.3.1) was good. Some deviation from the fit was ascribed to difficulties in monitoring the shoulder signal. This was especially the case in the PF composite spectra. Figure III.3.4 presents the T_{CH} and $^{H}T_{1\rho}$ relaxation times of lignin methoxyl carbon within all datasets. For the T_{CH}, no significant difference was detected among the data sets (p=0.3). For the $^{H}T_{1\rho}$ data, the control treatments tend to decrease the relaxation time; however with a p-value of 0.17 we must conclude that little or no difference was detected. A highly significant difference (p= 0.03) between the control-low and the PF-Low composite was detected. $^{H}T_{1\rho}$ increased. In fact, the control treatment had the opposite effect from the PF-Low resin. Finally, no significant difference was detected between the PF-High and the Control-High. Note on Figure III.3.4 that the effect of PF-High on lignin $^{H}T_{1\rho}$ is opposite to that of PF-Low and essentially identical to that of the control treatments.

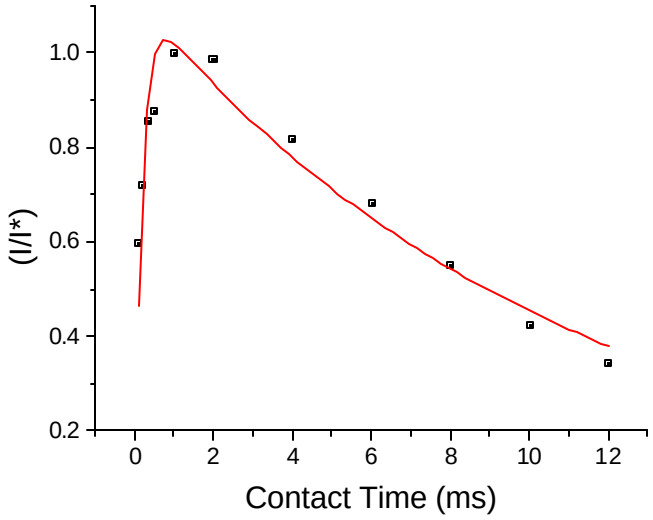

Figure III.3.3. A Typical Signal vs. Contact Time Curve for Lignin Methoxyl Carbon (Symbols are Data Points and the Solid Line is the Best Fit to Equation (III.3.1))

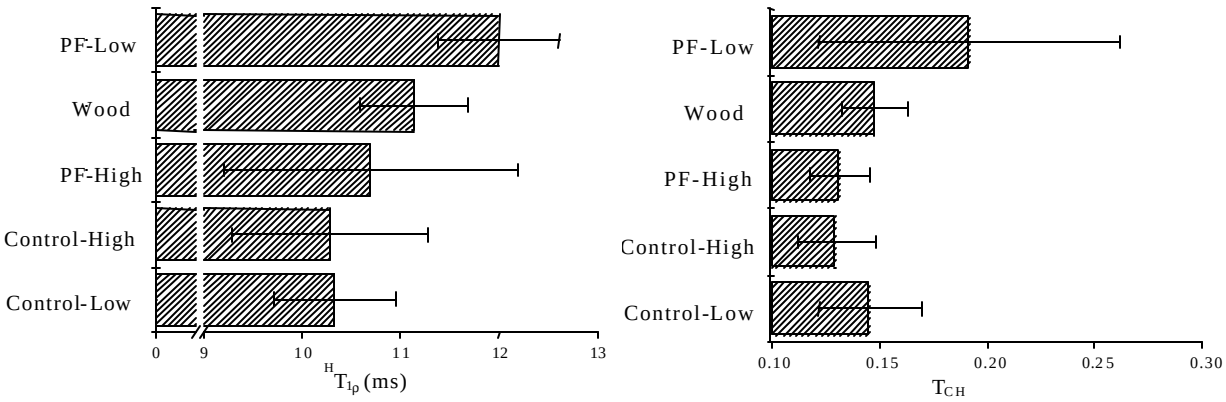

Figure III.3.4. Influence of Treatments on the T_{CH} and $^{H}T_{1r}$ Relaxation Times of Lignin Methoxyl Carbon (56 ppm)

III.3.3.3 Amorphous Cellulose C_4

The relaxation times of the amorphous cellulose C_4 was monitored with confidence as indicated by the good data fit shown in Figure III.3.5.

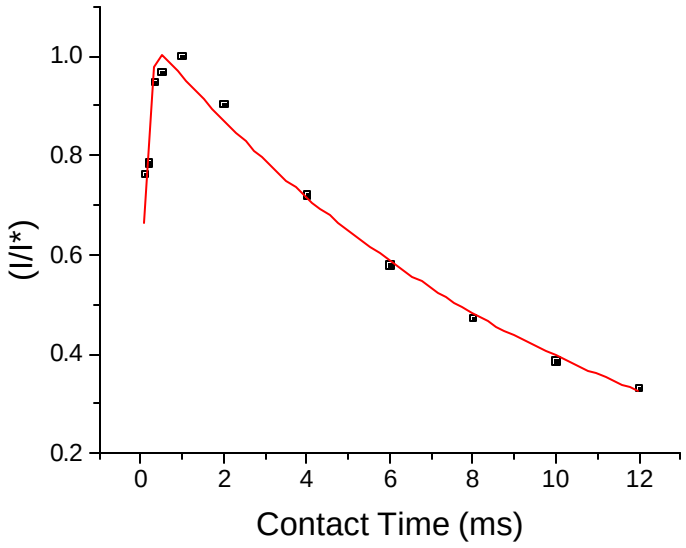

Figure III.3.5. A Typical Signal Vs Contact Time Curve for Amorphous Cellulose C_4 (Symbols are Data Points and the Solid Line is the Best Fit to Equation (III.3.1))

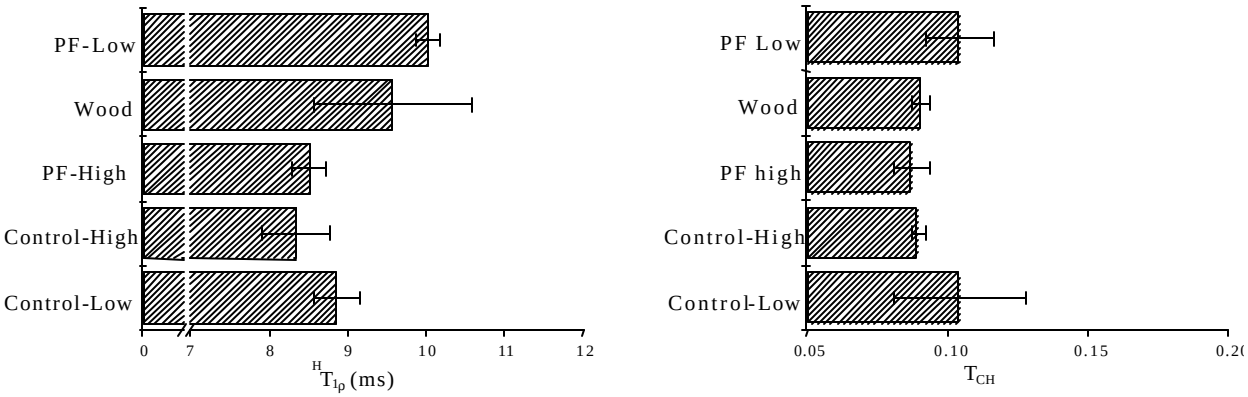

Figure III.3.6. Influence of Treatments on the T_{CH} and $^{H}T_{1r}$ Relaxation Times of Amorphous Cellulose C_4 (85 ppm)

The effect of the treatments on the amorphous cellulose C_4 is similar to that on lignin methoxyl carbon. No significant differences were found among the treatments for the cross-polarization time of the amorphous cellulose C_4 ($p=0.31$). For $^{H}T_{1\rho}$ relaxation, significant differences were detected. Specifically, the control treatments had little or no influence on the amorphous C_4 $^{H}T_{1\rho}$ ($p=0.14$). In addition, a highly significant difference in $^{H}T_{1\rho}$ was detected between the PF-Low and the control-Low ($p=0.004$). No significant difference was detected between the PF-High and Control-High treatments ($p=0.71$).

III.3.3.4 Crystalline Cellulose C_4

The fit of Equation (III.3.1) to the signal versus contact time curve for the crystalline C_4 carbon was comparable to that for the amorphous C_4 signal (Figure III.3.5). Therefore relaxation times could be determined with confidence (Figure III.3.7). As before, none of the treatments altered the CP behavior ($p=0.43$). And again as before, $^{H}T_{1\rho}$ was decreased by the control and PF-High treatments. Little or no significant difference ($p= 0.13$) was found for the $^{H}T_{1\rho}$ in the control treatments and in untreated wood. The PF-High and the control-High treatments exhibited no significant difference in $^{H}T_{1\rho}$ ($p= 0.61$). On the other hand, the PF-Low significantly increased the $^{H}T_{1\rho}$ compared to the control-Low ($p=0.005$).

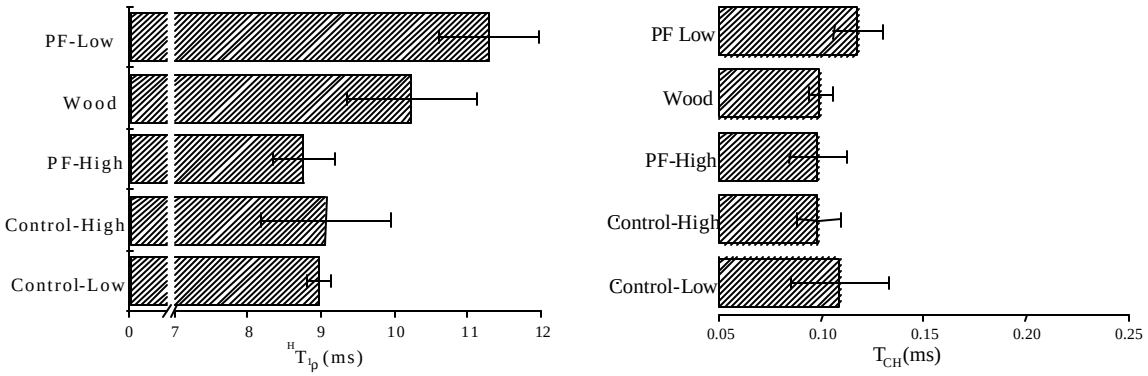

Figure III.3.7. Influence of Treatments on the T_{CH} and $^{H}T_{1r}$ Relaxation Times of Crystalline C_4 (90 ppm)

III.3.3.5 Carbohydrates C_1

The signal vs. contact time curve of carbohydrates C_1 was also very satisfactory for determining the relaxation times according to Equation (III.3.1). The fit was found equivalent to that illustrated in Figure III.3.5.

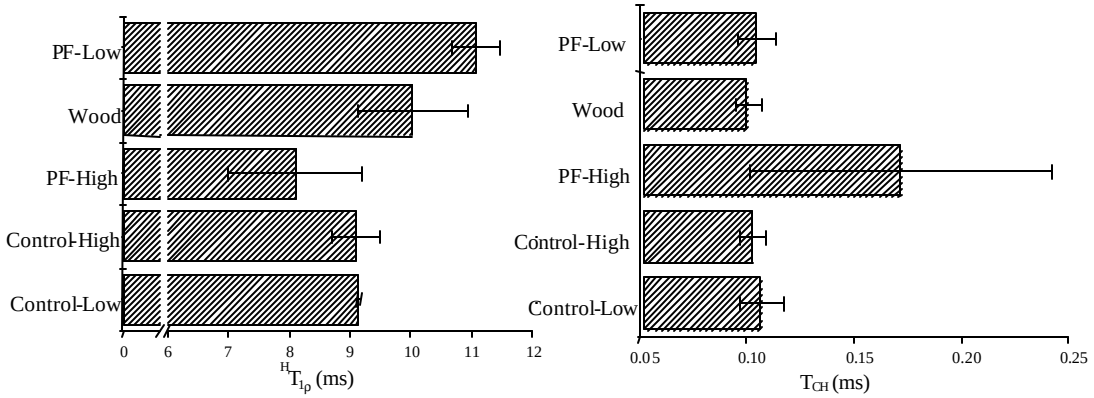

Figure III.3.8. Influence of Treatments on the T_{CH} and $^{H}T_{1r}$ Relaxation Times of Carbohydrates C_1 (105 ppm)

In this case, the PF-High resin was found to affect the T_{CH} compared to the other data sets (p=0.04). For the $^{H}T_{1\rho}$ data significant differences were also detected. As before, the control treatments decreased $^{H}T_{1\rho}$; $T_{1\rho}$ decrease had little or no significance (p=0.16). The PF-High resin decreased $T_{1\rho}$ in a similar way as the control-high (p=0.22). As before also, the PF-Low resin increased $T_{1\rho}$. The difference between the PF-Low and control-Low treatment was highly significant (p=0.04).

III.3.4 Discussion

Table III.3.1 summarizes the $^{H}T_{1\rho}$ data for the previously mentionned samples. Table III.3.2 presents the respective T_{CH} relaxations. In addition, the nanometer scale homogeneity of wood components within each treatment is assessed. Similar values of the $^{H}T_{1\rho}$ for all signals may indicate nanometer scale homogeneity through efficient spin coupling. On the other hand, nanometer scale heterogeneity will be reflected by different $^{H}T_{1\rho}$'s. Therefore Anova analysis was also performed within each treatment to determine whether the different signals of wood have similar $^{H}T_{1\rho}$. Significant differences among

the signal $^{H}T_{1\rho}$'s are indicated in the table by the p-value in the last row. For this analysis, the lignin methoxyl carbon was not included since a side group may not be efficiently spin coupled regardless of phase morphology. For untreated wood, no significant difference (p=0.69) was evidenced between the $^{H}T_{1\rho}$ measured through different carbons. While it is known that wood is a phase-separated material, the uniformity of the $^{H}T_{1\rho}$ relaxations indicates a degree of intimate phase association that promotes coupling via spin coupling. This type of spin coupling in wood is well known [2]. In the control-Low, control-High and PF-High samples, no significant difference is found between the $^{H}T_{1\rho}$ of the different carbons. Again this indicates spin coupling between wood components. The control and PF-High treatments do not seem to disrupt the arrangement of wood components. On the other hand, the PF-low resin alters the spin coupling among wood components, since a highly significant difference is found between the $^{H}T_{1\rho}$ of wood signals (p=0.03). The amorphous C_4 becomes significantly different from its crystalline counter-part. The carbohydrate C_1 signal, which comprises both crystalline and amorphous regions has a $^{H}T_{1\rho}$ intermediate of the crystalline and amorphous carbons. Here we see that the PF-Low inhibits spin diffusion among wood components.

Table III.3.1. $^{H}T_{1r}$ for Wood Polymers under the Influence of PF resins and Control Treatments (Standard Deviation in Parenthesis)

	Yellow-poplar	***Control-Low***	***PF-Low***	***Control-High***	***PF-High***
Lignin methoxyl	***11.1***	***10.3***	***12.0***	***10.3***	***10.7***
(57 ppm)	***(0.6)***	***(0.6)***	***(0.6)***	***(1.0)***	***(1.5)***
Amorphous Cellulose C_4	***9.6***	***8.9***	***10.0***	***8.4***	***8.5***
(85 ppm)	***(1.0)***	***(0.3)***	***(0.1)***	***(0.4)***	***(0.2)***
Crystalline Cellulose C_4	***10.3***	***9.0***	***11.3***	***9.1***	***8.8***
(90 ppm)	***(0.9)***	***(0.2)***	***(0.7)***	***(0.9)***	***(0.4)***
C_1 carbohydrates	***10.0***	***9.1***	***11.1***	***9.1***	***8.1***
(105 ppm)	***(0.9)***	***(0.4)***	***(0.4)***	***(0.4)***	***(1.1)***
p-value	***0.69***	***0.28***	***0.03***	***0.32***	***0.54***

Table III.3.2. T_{CH} for Wood Polymers under the Influence of PF resins and Control Treatments (Standard Deviation in Parenthesis)

	Yellow-poplar	*Control-Low*	*PF-Low*	*Control-High*	*PF-High*
Lignin methoxyl	***0.15***	***0.15***	***0.19***	***0.13***	***0.13***
(57 ppm)	***(0.02)***	***(0.02)***	***(0.07)***	***(0.02)***	***(0.01)***
Amorphous Cellulose C_4	***0.09***	***0.11***	***0.11***	***0.09***	***0.09***
(85 ppm)	***(0.01)***	***(0.02)***	***(0.01)***	***(0.01)***	***(0.01)***
Crystalline Cellulose C_4	***0.10***	***0.11***	***0.12***	***0.10***	***0.10***
(90 ppm)	***(0.01)***	***(0.02)***	***(0.01)***	***(0.01)***	***(0.01)***
C_1 carbohydrates	***0.10***	***0.12***	***0.10***	***0.10***	***0.18***
(105 ppm)	***(0.01)***	***(0.01)***	***(0.01)***	***(0.01)***	***(0.07)***

In general, the nominal values of the $^{H}T_{1\rho}$'s are not dramatically changed by the treatments. While the changes are small, they are significant. In fact, three changes have been systematically observed when comparing the $^{H}T_{1\rho}$ relaxation of all the wood signals monitored in this study.

1. *The control treatments had little or no effect ($p \gg 0.15$) on the $^{H}T_{1r}$ relaxation of wood signals. They consistently decreased the $^{H}T_{1r}$.*

   Sodium hydroxide is known to change the crystal structure of crystalline cellulose. In addition, sodium hydroxide is known to degrade hemicelluloses and can also causes some depolymerization of lignin, especially when combined with heat treatment [4]. Recall however that the alkali treatments were very mild (pH=9.1) and therefore little change is observed on wood polymer $^{H}T_{1\rho}$ upon control treatment.

2. *The PF-Low had a significant effect on the $^{H}T_{1r}$ relaxation of wood components ($p \leq 0.05$). PF-Low consistently increased the $^{H}T_{1r}$ relaxation of wood polymers.*

   The PF-Low resin does affect the nanometer scale environment of wood polymers. One may hypothesize that nanometer scale interactions between wood polymers and PF-Low are responsible for these changes in dynamics. It is reasonable on

thermodynamic grounds to believe that PF-Low can penetrate wood amorphous polymers on a nanometer scale. However, crystalline regions are inaccessible. It is therefore unlikely that the crystalline regions of cellulose can be disrupted by nanometer scale penetration of PF-Low. Rather, the dynamics of the crystalline region may simply be altered as a result of the supramolecular connectivity of wood polymers as suggested by previous studies [5], [6].

3. *The PF-High resin had similar effect than the control treatments on wood polymer ${}^{H}T_{1r}$. Differences between control-high and PF-High were not significant. The cross-polarization rate, T_{CH}, of the carbohydrate C_1 (at 105 ppm) was highly affected by the presence of the PF-High. This was not the case for the cellulose C_4 signals.*

PF-High does not substantially alter the nanometer scale environment of wood polymers. This observation does not rule out that some degree of nanometer scale penetration occurs. In fact, cell wall penetration has been previously suggested by microscopy (see chapter III-1), indicating that penetration on the order of 50 nanometers occurs to some extent with the PF-High resin. However, nanometer scale penetration is not important enough for the average dynamics of wood polymers to be significantly altered on this scale of motion.

The significant effect of PF-High on the cross-polarization rate measured at the 105 ppm signal indicates that the near static molecular motions of the underlying carbons are substantially enhanced upon treatment with PF-High. Generally, the signal at 105 ppm is ascribed to the C_1 of both cellulose and hemicellulose. In addition, a close inspection of isolated lignin spectra indicates that the C_2 and C_6 of lignin syringyl units have a chemical shift of 104.5 ppm. Therefore the 105 ppm resonance bears a contribution from lignin [4]. Because the cellulose C_4 are not affected by PF-High (signals at 85 and 90 ppm), it is possible that the change in CP rate for the 105 ppm resonance stems essentially from lignin and hemicellulose. The slower T_{CH} indicates enhanced near static mobility for these polymers upon impregnation of yellow-poplar with PF-High.

Figure III.3.9 represents the $^{H}T_{1\rho}$ measured through the distinct wood resonances as a function of the treatments. In addition, the PF resin $^{H}T_{1\rho}$ is represented in Figure III.3.9 for the PF-Low and the PF-High composites. The PF signal at 130 ppm was utilized for measuring the resin $^{H}T_{1\rho}$ in the composite spectra.

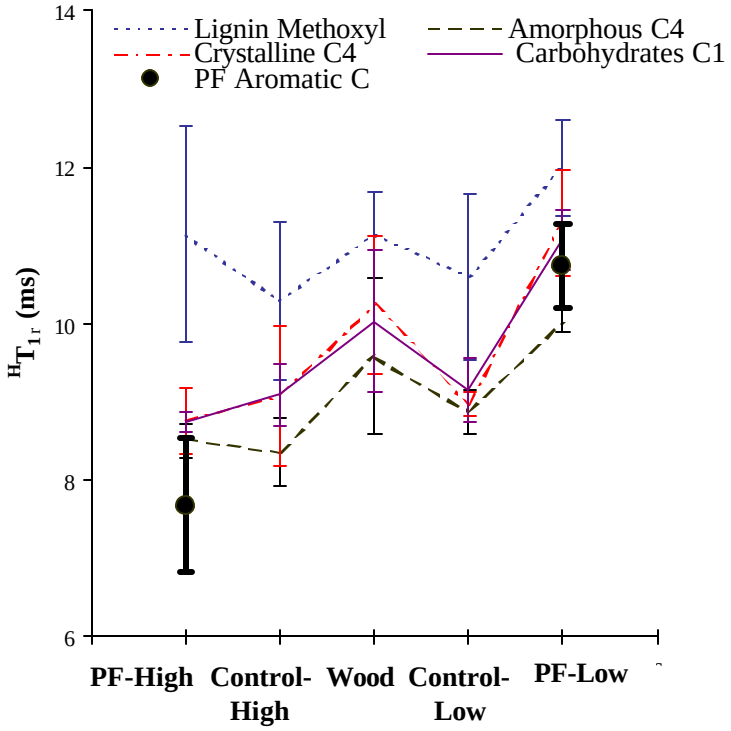

Figure III.3.9. Wood Polymer and PF Resins $^{H}T_{1r}$ as a Function of Treatment (Demonstrating Dynamic Connectivity and Comparing the PF resins $^{H}T_{1r}$)

Interestingly, for the PF-Low, $^{H}T_{1\rho}$ lies within the range of the wood relaxations. On the other hand, in the PF-High composite, the $^{H}T_{1\rho}$ of the resin lies below the range of the wood polymers. This observation suggests that wood and PF-Low resin kilohertz motions may be similar. More importantly, it suggests that resin and wood may be coupled via spin diffusion. On the other hand spin coupling between PF-High and wood

polymers appears less efficient. These observations are consistent with the hypothesis that on average, PF-Low interacts more intimately with wood polymers than PF-High.

Furthermore, the two PF resins have substantially different $^{H}T_{1\rho}$. For the PF-Low the $^{H}T_{1\rho}$ averages 10.8 ± .5 ms while the PF-High has a $^{H}T_{1\rho}$ of 7.7 ± .9 ms. Specific wood/PF interactions pertaining to the PF-Low and PF-High composites likely induce distinct motional characteristics for the two PF networks. These differences in network dynamics are a consequence of the molecular weight dependence of wood/adhesive interactions.

III.3.5 Conclusions

^{13}C CP/MAS NMR relaxation measurements indicated that PF-Low increases significantly the $^{H}T_{1\rho}$ of wood polymers. Although not statistically significant, PF-High systematically lowered the $^{H}T_{1\rho}$ of wood polymers. Control treatments were also found to decrease the $^{H}T_{1\rho}$ of wood polymers. This opposite trend suggests that one PF tends to enhance wood mid-kilohertz motions while the other PF tends to inhibit these motions. Furthermore, PF-Low was found to disrupt the spin coupling that is typical of wood. PF-High left spin coupling between wood components intact. Finally, the PF-Low $^{H}T_{1\rho}$ was within the range of wood relaxation while the PF-High was not. These observations suggest that the PF-Low resin interacts more intimately with wood that the PF-High resin.

III.3.6 References

[1] Mehring M., Principles of High Resolution NMR in Solids, 2nd ed. Springer-Verlag, Berlin, 1983.

[2] Willis J.M. and F. G. Herring, Effect of Water in the ^{13}C CP/MAS NMR Spectrum of White Spruce Wood, Macromolecules, 20, 1554, 1987.

[3] Newman R.H., Nuclear Magnetic Resonance Study of Spatial Relationships Between Chemical Components in Wood Cell Walls, Holzforschung, 46 (3), 205, 1992.

[4] Kosikova B., M. Hricovini and C. Cosentini, Interaction of Lignin and Polysaccharides in Beech Wood (Fagus Sylvatica) during Drying Process, Wood Science and Technology, 33, 373, 1999.

[5] Argyropoulos D. S., and F.G. Morin, Probing the Macromolecular Structure of Wood and Pulps with Proton Spin-Lattice Measurements in the Solid State, Wood Science and Technology, 29, 19, 1995.

[6] Ahvazi A. and D. S. Argyropoulos, Proton Spin-Lattice Relaxation Time Measurements of Solid Wood and its Constituents as a Function of pH. Part I, Wood Science and Technology, 34, 45, 2000.

IV CONCLUSIONS

A novel approach is visited to investigate the morphology of the wood/adhesive interphase. The approach mimics dynamic investigations that are commonly utilized in polymer blend studies. Among the most common dynamic techniques, CP/MAS NMR and DMA are selected for probing molecular motions from the nanometer to the angstrom scale. This dynamic approach is implemented to investigate the molecular weight dependence of the wood/ phenol-formaldehyde adhesive interphase morphology.

The first section addresses potential CP/MAS NMR and DMA methods for characterizing wood polymer dynamics in bulk wood and in wood/PF composites. It is shown that intermolecular CP/MAS NMR experiments with doubly labeled PF-^{13}C-d resin are not suitable for detecting angstrom scale miscibility in wood/thermosetting adhesive systems. This is because differences in molecular rigidity between the two components obscure morphological information. However a more suitable dynamic approach for wood/thermoset composites consists of monitoring the influence of the PF resin on wood polymer relaxation times. This is true because, if on average the adhesive interacts with wood components, then their molecular scale dynamics shall be modified on the scale of the wood/adhesive interaction.

In chapter-II-2, it is shown that DMA can be utilized for monitoring the *in-situ* lignin alpha relaxation both in bulk wood and in wood/PF composites. In this work, *in-situ* lignin alpha relaxation refers mainly to lignin segmental motion while it is recognized that wood carbohydrates largely influence this glass transition. Pertinent to the fundamental understanding of wood viscoelasticity, it is demonstrated that the cooperativity analysis as derived from the Ngai coupling model of relaxation provides a good description of intermolecular coupling above the *in-situ* glass transition of lignin in two species yellow-poplar and spruce. A protocol is developed for quantifying intermolecular cooperativity above lignin glass transition temperature. For the two species, no significant difference in intermolecular cooperativity is evidenced. The Ngai coupling model affords however a novel research tool for probing wood systems.

In order to implement the DMA and CP/MAS NMR approaches for the morphological investigation of the wood/PF interphase, it is necessary to control the *in-*

situ cure of the thermosetting resin. In that purpose, A DMA protocol is presented in chapter-II-3 that allows monitoring the *in-situ* cure of thermosetting adhesives on wood flakes.

In section III, CP/MAS NMR and DMA approaches are implemented in order to investigate the wood/adhesive interphase morphology with two PF resins. PF-Low is a low molecular weight, relatively monodisperse resin. PF-High is highly condensed and has a broad distribution of molecular weights. PF-Low and PF-High composites are manufactured so as to yield similar microscopic penetration and resin loading on wood. They are also cured in compliance with the *in-situ* cure characterization. Microscopic inspection of the composites suggests for both composites some degree of cell wall penetration. Control specimens accounting for the alkali and the heat treatment applied on wood during the composite manufacture are also prepared.

Characterizing the softening behavior or glass transition of the samples before and after PF treatment provides insight on the interphase morphology. In the case of the composite samples, the main softening is as before ascribed to the *in-situ* lignin glass transition but also likely encompasses contributions from the PF resins. In the PF-Low composite no change in glass transition temperature is observed compared to untreated wood. Fortunately, the feasibility of TTSP and of the cooperativity in the PF-Low composite provides additional insight. The cooperativity analysis reveals that the PF-Low resin enhances the temperature dependence of relaxation above the glass transition. Greater intermolecular cooperativity suggests that a more constrained state of the softening polymers in the PF-Low composite. Enhanced intermolecular coupling is also consistent with concentration fluctuations in miscible polymer blends (at least on a nanoscale as measured by DMA). On the other hand, simple DMA measurements indicate a dramatic depression of the sample glass transition temperature in the PF-High composite. This observation is ascribed to the low molecular weight PF fraction acting as external plasticizer (as uncured species) or internal plasticizer (as pendant groups) of wood polymers. This hypothesis is consistent with the very small low molecular weight tail of the PF-High resin being capable to interact with wood polymers on a nanometer scale but being too dispersed for forming an *in-situ* network. By contrast, the highly condensed fraction may form a separate phase from the woody material. This hypothesis

is supported by the poor success of TTSP in the PF-High composites, as is typically observed in phase-separated polymer blends.

The viscoelastic study therefore reveals substantial differences between PF-Low and PF-High composites. In both systems, nanometer scale penetration occurs to some extent. However, opposite trends are observed.

With CP/MAS NMR the influence of PF-Low and PF-High on the spin lattice relaxation time in the rotating frame, proton $T_{1\rho}$, and the cross-polarization time (T_{CH}) is investigated. None of the resins significantly affect T_{CH} , suggesting that angstrom scale penetration does not occur. However, the PF-Low resin substantially modifies wood polymer $T_{1\rho}$, indicating that the nanometer scale environment of wood polymers is altered. In fact, PF-Low is found to significantly increase wood component $^{H}T_{1\rho}$. On the other hand, the PF-High resin tends to decrease wood component $^{H}T_{1\rho}$. Statistically however, the effect of PF-High on wood $^{H}T_{1\rho}$ is not significant, suggesting that PF-High does not on average penetrate wood on a nanometer scale. Interestingly, when wood is treated with the PF-Low resin the spin coupling that is typical among wood components is disrupted. PF-High has no effect on the spin coupling between wood components. Finally, it is noteworthy that the two PF-resins have significantly different $T_{1\rho}$. In fact, the PF-low resin $T_{1\rho}$ lies within the range of wood polymer $T_{1\rho}$, suggesting some degree of spin coupling and therefore nanometer scale interactions. On the other hand, the *in-situ* PF-High resin $^{H}T_{1\rho}$ appears at the periphery of wood polymer $T_{1\rho}$ suggesting no spin coupling between the resin and wood components and therefore nanometer scale phase separation.

In accordance with the viscoelastic and CP/MAS NMR studies, distinct interphase morphologies are proposed for the PF-Low and PF-High composites.

The formation of the PF-High interphase is illustrated in Figure IV.1.1. Upon application of the PF-High resin to wood, the dominant high molecular weight fraction does not penetrate wood on a nanometer scale. However, a small fraction of PF-High is of low enough molecular weight for penetrating wood on a nanometer scale. Upon cure of the composite the high molecular weight species form a crosslinked three dimensional

network. The rare species dispersed in wood on a nanoscale may act as internal or external plasticizers whether they react or remain uncured in the woody matrix.

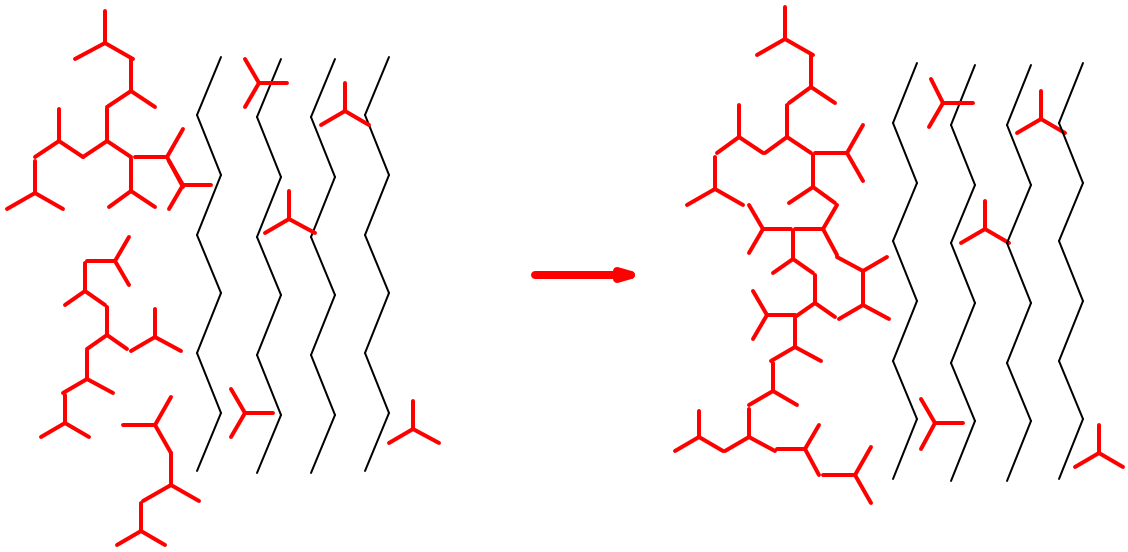

Figure IV.1.1. Nanometer Scale Phase Separation in the Wood/PF-High Interphase

For the PF-Low composite on the other hand, the density of nanometer scale penetration is much greater and it may be possible for the entirety of the PF species to polymerize *in-situ.* This scenario for PF-Low is depicted in Figure IV.1.2. In this system, the cured network interacts with wood on a nanometer scale.

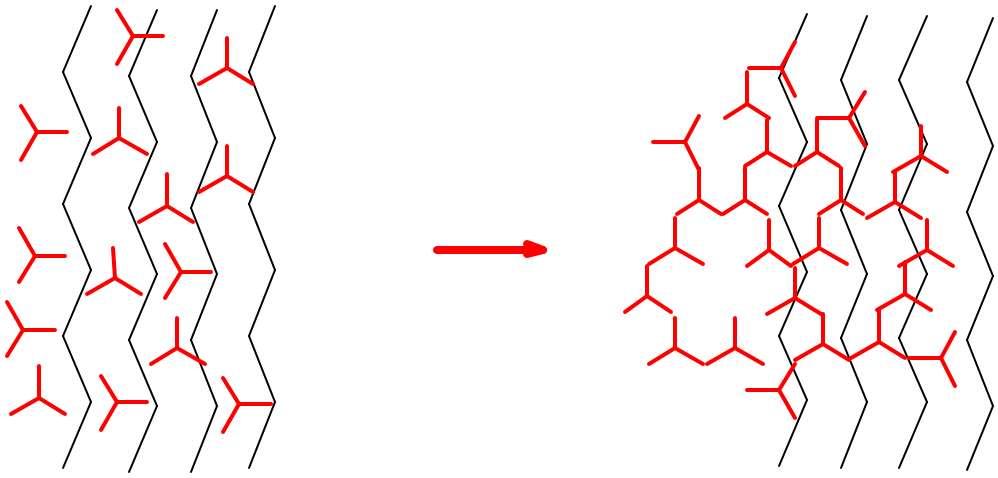

Figure IV.1.2. Nanometer Scale Penetration in the Wood/PF-Low Interphase

The present research has only focused on methods development and implementation for one particular wood adhesive and one particular variable. However it is obvious that such methods may be applied to any other wood/polymer systems and to investigate the influence of any other polymer variable or processing variable. It is also worthwhile pointing out that while microscopic investigation has suggested some degree of cell wall penetration for both adhesives on the micron scale, the dynamic investigations provide a much more informative perspective of the wood/PF interphase with the two PF-resins utilized in this particular study. A flourishing follow-up for this research would consist of relating the wood/adhesive interphase morphology with performance.

VITA

Marie-Pierre G. Laborie

Marie-Pierre G. Laborie was born in Montpellier (France) in June 1972 from parents Marie-José Laborie and Jean-Michel Laborie. After high school she joined the Classes Préparatoires Math-Sup-Bio at the Lycée Ozenne in Toulouse. She subsequently entered l'Ecole Nationale Supérieure des Technologies et Industries du Bois (E.N.S.T.I.B, University of Nancy I) where she graduated in June 1996. During her engineering studies, she obtained summer internships at the Universidad del Bio-Bio (Chile) and at a particleboard manufacturer (Czech Republic). She then worked as a quality engineer in a laminated wood frame manufacturer in France for 9 months. She joined the Ph.D. program in the Department of Wood Science at Virginia Polytechnic Institute and State University in the fall of 1997 where she worked under the guidance of Dr. Charles Frazier. Her Ph.D. dissertation focused on the fundamental investigations of wood/Phenol-Formaldehyde adhesive interactions. During her Ph.D. she has been a fellow of the Center for Adhesive and Sealant Science (CASS) at Virginia Tech University. She conducted part of her research at the Swedish Research Institute for Pulp and Paper (STFI) under the guidance of Dr. Lennart Salmén. She completed her Ph.D. in February 2002.